

**Growth-factor-induced, persistent fibroblast
migration is mediated by mechanical insulation
of cell front and back**

Inauguraldissertation

zur

Erlangung der Würde eines Doktors der Philosophie
vorgelegt der
Philosophisch- Naturwissenschaftlichen Fakultät
der Universität Basel

von

Katrin Martin

aus Österreich

Basel, 2014

Genehmigt von der Philosophisch-Naturwissenschaftlichen Fakultät auf Antrag von:

Prof. Dr. Olivier Pertz

Prof. Dr. Markus Affolter

Prof. Dr. Gerhard Christophori

Basel, den 12.11.2013

Prof. Dr. Jörg Schibler

Dekan

Table of Contents

1.	Abstract.....	3
2.	Introduction	6
2.1.	Cell Migration.....	7
2.1.1.	General Principles of Cell Migration	7
2.1.2.	Cell Migration Strategies	7
2.1.3.	How Cell Migration is Influenced	8
2.1.4.	Functional Units of Migrating Cells	11
2.1.5.	The Leading Edge: Lamellipodium and Lamella	11
2.1.6.	F-actin Stress Fibers Transmit Tensile Forces.....	14
2.1.7.	Adhesion Structures: Composition and Dynamics	20
2.1.8.	Myosin II Generates Tensile Forces.....	26
2.2.	Receptors in Hapto- and Chemokinesis.....	27
2.2.1.	Integrin Signaling.....	27
2.2.2.	Receptor Tyrosine Kinases (RTKs).....	30
2.3.	Rho-GTPases Orchestrate Cell Migration.....	33
2.3.1.	The Rho-GTPase Cycle	35
2.3.2.	The Role of RhoA, Rac1 and Cdc42 in Cell Migration	36
2.3.3.	Questioning the Dogma of Rho-GTPase Signaling.....	38
2.3.4.	Latest Concepts of Rho-GTPase Signaling.....	39
3.	Main Results	41
3.1.	Abstract.....	43
3.2.	Visual Abstract.....	44
3.3.	Introduction	45
3.4.	Results.....	47
3.5.	Discussion	53
3.6.	Experimental Procedures	56
3.7.	Acknowledgements	56
3.8.	Main Figures	57
3.9.	References	65
3.10.	Supplemental Information.....	67
3.10.1.	Extended Experimental Procedures.....	67
3.10.2.	Supplemental Figures.....	71
3.10.3.	Supplemental Movie Legends	77
3.10.4.	Supplemental References	77
4.	Additional Results.....	78
4.1.	PDGF Chemotaxis.....	79

4.1.1.	Introduction	79
4.1.2.	Results	80
4.2.	Immunofluorescence Stainings	82
4.2.1.	Introduction	82
4.2.2.	Results	83
4.3.	Fluorescence Live Cell Imaging	92
4.3.1.	Introduction	92
4.3.2.	Results	92
4.4.	Materials and Methods	101
4.4.1.	Cell Culture ,Stable Cell Lines and Adeno System	101
4.4.2.	Generation of Line Patterns.....	101
4.4.3.	Gradient Generator.....	102
4.4.4.	PDGF Gradient	103
4.4.5.	Immunofluorescence Stainings	104
4.4.6.	Live cell imaging and image analysis	106
5.	Discussion	108
6.	References	120
7.	Acknowledgements	130
8.	Curriculum Vitae	1322

1. Abstract

Cell migration is a crucial process during development, the immune response and wound healing. As a consequence, aberrant cell migration can lead to tumor metastasis or autoimmune disorders. In order to migrate directionally, cells have to orchestrate a complex machinery of cytoskeletal, adhesion and signaling components to reach their place of destination. During directional migration, cells maintain a polarized state, which means that cell front and back have to be co-ordinated in a robust way. This complex process is not yet fully understood and gaining mechanistic information in model cell migration systems might help to explain regulation of cell migration in vivo.

An important question is how local phenomena such as fine leading edge dynamics, Rho-GTPase signaling or cytoskeletal organization impact on establishment and maintenance of cell polarization to co-ordinate front and back activities during directional cell migration. Current models of global front and back co-ordination mostly originate from highly polarized, rapidly moving cells such as neutrophils or *Dictyostelium*. However, due to the small size of these cells, it is not possible to study local phenomena such as fine leading edge dynamics, happening within time scales of seconds and spatial scales of single micrometers. In order to address questions concerning these fine dynamics, fibroblasts are a widely used model system due to their large and flat morphology. The limitation of this system is that fibroblasts are not highly polarized, precluding the study of front/back co-ordination. An integrated, multi-scale view of directional cell migration view is therefore missing.

To overcome this limitation we engineered a system, which enabled us to study polarized and persistent cell migration on multiple time and length scales. In this experimental set up we allowed rat embryonic fibroblasts (REF52) to migrate on fibronectin coated line substrates. Unstimulated cells (referred to as hapto cells) or platelet derived growth factor (PDGF) treated cells (referred to as chemo cells) were studied in a variety of static or live cell imaging experiments using different spatio-temporal resolution. Hapto cells were found to undergo transient episodes of polarization and therefore characterized by low migration persistence as well as low migration velocity. In contrast, chemo cells showed a drastic increase of migration persistence, enabling them to migrate in one specific direction for hours. At the same time migration velocity was elevated by more than five times. This provides an excellent model system to study polarized cell migration.

In order to explain these drastic changes in migration persistence and velocity as global migration parameters, we examined cytoskeletal, adhesion and signaling dynamics at high spatio-temporal resolution. We found that hapto cells displayed classic features previously observed during mesenchymal cell migration. A protrusive lamellipodium led to the formation of initial adhesions, called focal complexes. Directly behind the lamellipodium, these adhesions then matured in mechanosensitive adhesions, called focal adhesions, through interaction with the contractile lamella. Front adhesions connected to back focal adhesions through stress fibers. Thus, as previously proposed, this front/back linkage coupled with stress fiber tension allows the front to pull the back, leading to tail retraction.

Surprisingly, we observed different actin and adhesion dynamics in persistently migrating chemo cells. These cells remodeled their cytoskeleton and developed two distinct front and back functional modules which are mechanically uncoupled. Specifically, a non-contractile front module, containing a

constant sized zone of podosome-like structures (PLSs) replaced the lamella and precluded contractile, retrograde F-actin flow at this subcellular localization. This allowed the PLS zone to function as mechanical insulator, leading to loss of maturation of focal complexes to focal adhesions. Tail retraction was then mediated by a 2nd contractile module that consists of a myosin cluster positioned directly at the back of the PLS zone. Thus, a front module pushes in direction of cell migration, and a contractile back module directly follows the PLS zone and pulls the cell back allowing for tail retraction.

By evaluating front/back motion co-ordination, and using drug perturbations, we formally showed, that the protrusive front is mechanically uncoupled from the contractile back module. From a signaling point of view, we found that the PLS zone acts by locally inhibiting RhoA mediated contractility at the leading edge, allowing uncoupling of cell front and back.

We propose, that mechanical uncoupling of cell front and back by establishment of the PLS zone enables highly efficient and persistent fibroblast cell migration during exposure to a uniform concentration growth factor. The finding that cells do not necessarily require a chemokine gradient to migrate uni-directionally, but can polarize efficiently by simple exposure of an uniform concentration of growth factor in combination with topological confinement of the ECM, might have significance in vivo too. For example, neural crest cells can migrate directionally during collective cell migration in absence of a gradient. During cancer metastasis, a macrophage-tumor cell paracrine loop allows for collective cell streaming in one specific direction on collagen fibrils. While this was suggested to involve chemotaxis, it is conceivable that chemokinesis might therefore be sufficient to induce directional cell migration on the collagen fibril.

Our finding of mechanical uncoupling of cell front and back during chemokinesis on line substrates might provide a mean for generation of directional cell migration.

2.Introduction

2.1. Cell Migration

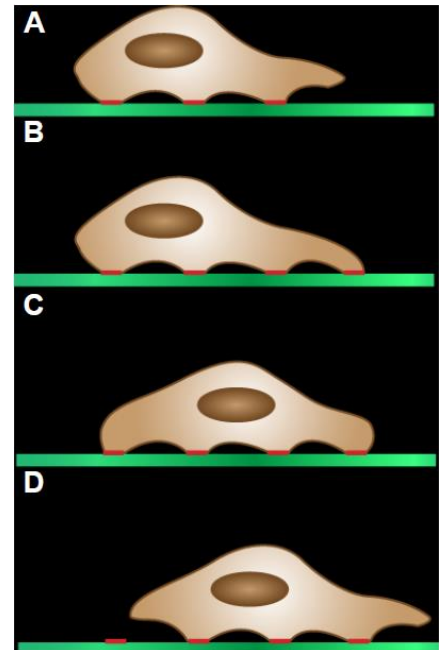
In this chapter general principles including morphological features and their role during cell migration are discussed. I explain the variety of cell migration modalities and how properties of extracellular matrix (ECM) and other factors impact on this process

2.1.1. General Principles of Cell Migration

The process of cell migration can be splitted in several steps:

Firstly, cells protrude their leading edge and probe their environment (Figure 1A). If then, cells encounter permissive substrates, nascent adhesions are formed at the very leading edge. While adhesions at the front mature, the cell cortex gets under tensions (Figure 1B) leading to delocalization of the nucleus (Figure 1C). Mature focal adhesions at the front allow the cell to apply sufficient tension forces to pull forward. At the same time adhesions at the cell rear disassemble and the tail is retracted (Figure 1D).

Figure 1: Steps of cell migration. (A) Leading edge protrusion. (B) Nascent adhesions at the leading edge mature into focal, while tension is applied to the cell cortex. (C) Delocalization of the nucleus. (D) Adhesion disassembly and tail retraction.



2.1.2. Cell Migration Strategies

Cell migration was classified by means of morphology, migration patterns and molecular parameters. During cell migration, the cytoskeleton is reorganized, cell matrix interactions undergo changes and even tissue can be modified.

In principle, one has to distinguish between single and collective cell migration of cohesive multi cellular units (Friedl 2004) (Figure 2).

Amoeboid cell migration can either proceed by formation of blebs, where pushing and propulsive forces are exerted while cells move in a non-adhesive manner. However, amoeboid cell migration is also found in slightly elongated cells forming weak adhesions to the ECM and generating pseudopods and filopodia (Friedl & Wolf 2010). In Contrary, during mesenchymal cell migration strong transient adhesions to the ECM are formed and cells exhibit elongated shape. For example, fibroblasts are typical representatives of mesenchymal migrating cells (Grinnell & Petroll 2010).

Cell streaming occurs as an intermediate of individual and collective cell migration, where single cells transiently form and resolve cell-cell contacts (Teddy & Kulesa 2004).

Collective cell migration on the other hand shows characteristics, such as formation of tubes, strands, sheets or irregular shaped masses with the common feature of stringent cell-cell interactions. During

collective cell migration, the migration activity within the collective is silenced, however at outward edges or cell-ECM contacts cytoskeletal activities are enhanced (Friedl et al. 1995).

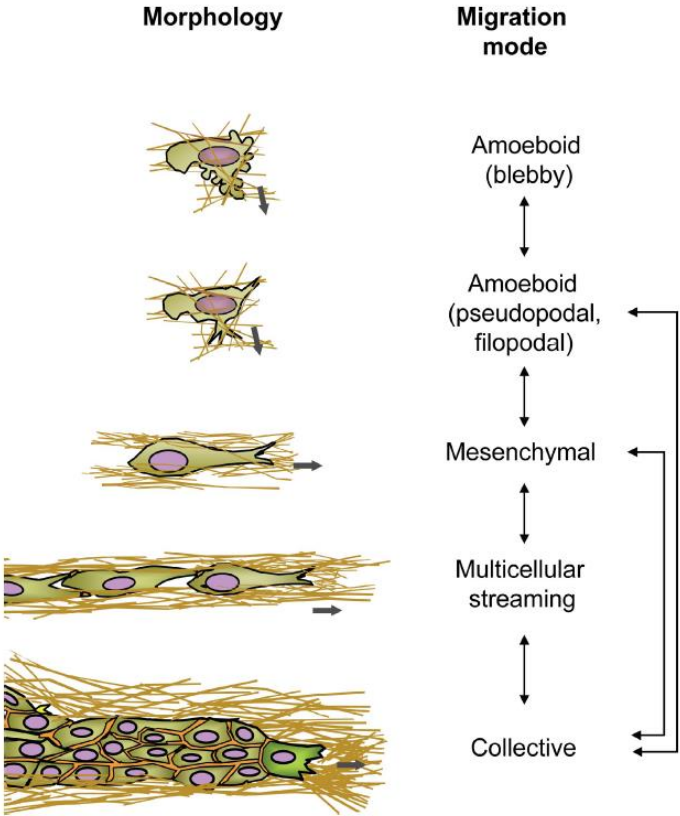


Figure 2: Plasticity of cell migration. Cell morphologies are inter-changeable depending cell type and environmental condition. (Friedl & Wolf. 2010)

2.1.3. How Cell Migration is Influenced

Directed cell migration demands tight regulation of the cytoskeleton, adhesion dynamics and signaling components in order to guide cells efficiently to their destination. Indeed, directionality of cell migration is triggered by different factors either immobilized at the ECM, soluble cues or by matrix rigidity. Additionally, matrix topology can influence cell migration.

2.1.3.1. Gradients Induce Directed Cell Migration

Cell migration in response to immobilized cues (Weber et al. 2013) is termed haptotaxis. Thereby, directed cell migration occurs towards a higher concentration of matrix or immobilized cue. However, if cells migrate on uniform substrates, without being exposed to any other stimuli, this process is called haptokinesis.

In order to direct cells to their destination, soluble cues are often involved such as chemokines or growth factors. Directed cell migration triggered by a gradient of soluble cues, named chemotaxis, is performed by different types of cells from bacteria such as *E.coli* (Kirby 2009) over a variety of eucaryotic cell lines. In eukaryotic cells chemotaxis is frequently studied in fast migrating cells like *dictyostelium*, neutrophils and a variety of transformed mammalian cells (Schneider & Haugh 2006; Stephens et al. 2008).

When cells are stimulated with a uniform concentration of soluble cue, and therefore random migration is induced, this process is referred to as chemokinesis.

But not only matrix concentration or soluble cues can stimulate cell migration or directed migration respectively. Cells also respond to stiffness of ECM they are attached to. Sensing this property of the ECM and consequently performing directed cell migration towards stiffer matrix regions is termed durotaxis. Durotaxis shows high impact on development, immune response or cancer metastasis. Recently the mechanism, how cells are directed by a gradient of matrix stiffness was elucidated: Cells use individual focal adhesions autonomously and exhibit either stable or dynamically fluctuating (“tugging”) traction in order to sense matrix rigidity (Plotnikov et al. 2012).

Different kinds of gradients can induce cell polarization and thus directional cell migration.

2.1.3.2. Matrix Geometry Impacts on Cell Migration

Surrounding tissue or ECM respectively, not only influences gene expression patterns, but also influences cell migration tremendously. Even cells showing malignant phenotypes with gross genomic abnormalities can be prevented from metastasizing when they are embedded in tissue with non-malignant dimensionality (Nelson & Bissell 2006). Since tissue and organs are three dimensional (3D), many standard cell culture approaches on two dimensional (2D) substrates might be misleading (Nelson & Bissell 2006). On the other hand, animal models are not always suitable to reproduce features of human tumors, autoimmune diseases or stem cell differentiation. A bridge between classic 2D tissue culture and animal models is comprised of 3D tissue culture approaches. Here synthetic substrates, such as matrigel or collagen gels can provide environments exhibiting certain pore sizes, stiffness or display a variety of ECM components (Griffith & Swartz 2006). Moreover, 3D environments trigger cell polarization, which is crucial for tissue organization, where endothelial cells have to define their apical and basal surfaces or the organization of mammary glands. Seeding cells on a plane substrate often disturbs organization and may further lead to aberrations in secretory functions (Griffith & Swartz 2006; Nelson & Bissell 2006).

Directionality of mesenchymal cell migration is also strongly dependent on matrix topology. In 2001 it was shown by the group of Kenneth Yamada, how fibroblasts increase their migration velocity by the factor of 1.5 while migrating unidirectional on a 3D substrate consisting of ligand-dense ECM fibers (Cukierman et al. 2001). This further led to the hypothesis that fibrillar matrix topology provides a physical basis for this persistent migration behavior. This concept was extrapolated and cells were allowed to migrate on a so called one dimensional (1D) micro fabricated matrix with diameters (1.5 μm) corresponding to those of collagen fibers. Thereby, the authors demonstrated that a 1D matrix topology can mimic a 3D environment (Figure 3). Cells increase their migration velocity compared to 2D substrates reaching velocities comparable to 3D cell migration. Moreover, migration velocity of cells on 1D substrate is independent from ECM concentrations (Doyle et al. 2009).

Collagen fibers, the substrates fibroblasts are surfing on in physiological conditions (Figure 3B), exhibit a substructure comprised of collagen fiberills with diameters ranging from 20 to 200 nm. It was found that these substructures influence polarization of cells and migration velocity (Wang et al. 2002; Meshel et al. 2005; Perentes et al. 2009). Though, less is known about synergistical or antagonistical effects of matrix topology and chemical stimuli opening a challenging field of research.

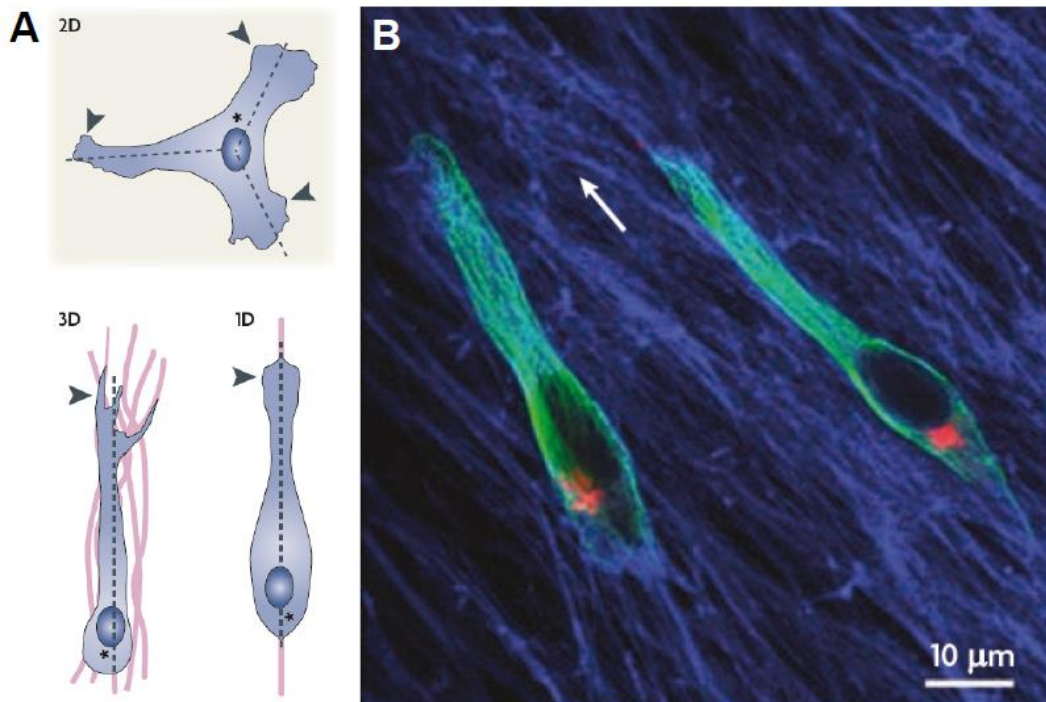


Figure 3: Cell morphologies depend on matrix topology. (A) Schematic cells plated on different matrix topologies. **(B)** Confocal image of NIH3T3 fibroblasts migrating on cell derived matrix (Fibronectin in blue, microtubules in green and golgi in red). (Petrie et al. 2009)

2.1.4. Functional Units of Migrating Cells

Cells are composed of different functional units. These units exhibit specific cytoskeletal composition and need to be well orchestrated in order to allow efficient cell migration. The coordination of these functional units underlies again diverse regulatory networks functioning in space and time.

In this chapter, I discuss the organization and function of the lamellipodium and lamella as functional units at the leading edge of migrating mesenchymal cells. Further, there are explanations how cells manage to exert tensile forces to retract their rear. Different strategies how cells adhere to the ECM are discussed as well as how adhesion dynamics are implemented in the process of cell migration.

2.1.5. The Leading Edge: Lamellipodium and Lamella

The lamellipodium locates 3 - 5 μm from the cell edge (Figure 4A, Area1) and is directly followed by the lamella (Figure 4A, Area2). Structurally, lamellipodium and lamella differ from each other: While the lamellipodium consists of a dendritic F-actin network (Figure 1B, Area1) (Koestler et al. 2008), the lamella is composed of bundled actin filaments (Figure 1B, Area2) (Burnette et al. 2011).

On molecular level, lamellipodium and lamella distinguish themselves as well: The Lamellipodium exhibits high concentrations of Arp2/3 and ADF/cofilin, contrary to the lamella, where myosin II and tropomyosin are highly abundant (Ponti et al. 2004).

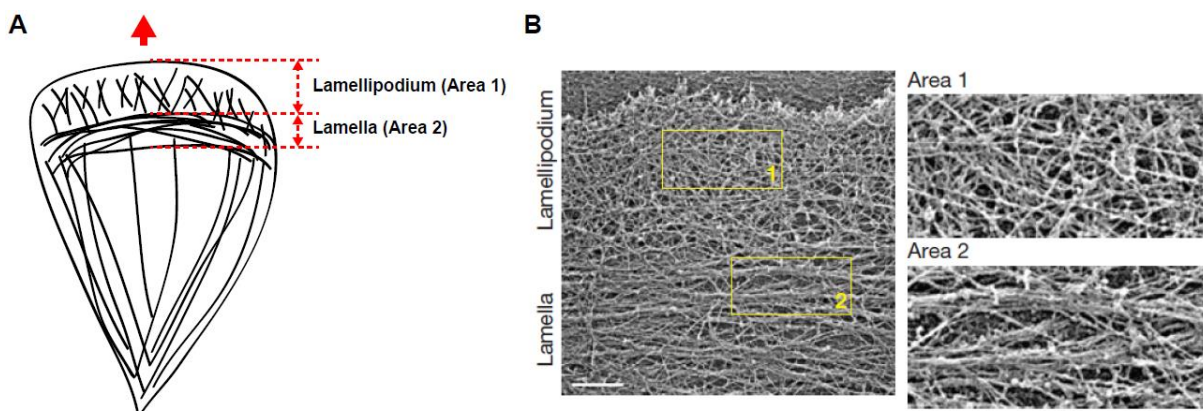


Figure 4: Lamellipodium and Lamella. (A) Scheme of a migrating cell displaying lamellipodium and lamella at the leading edge; red arrow points in direction of cell migration. (B) Electron micrograph of a rotary-shadowed cell after life-cell extraction. Areas 1 and 2 show actin-filament organization in the lamellipodium and lamella, respectively. Scale bar, 1 μm . Adapted from (Burnette et al. 2011)

2.1.5.1. Zooming Into the Lamellipodium

Using speckle microscopy, it was shown that the lamellipodium consists of two distinct, but overlapping zones with characteristic F-actin dynamics (Ponti et al. 2004). Approximately one μm from the cell edge, elevated levels of actin polymerization occur, while in the last μm of the lamellipodium actin depolymerization prevails (Figure 5).

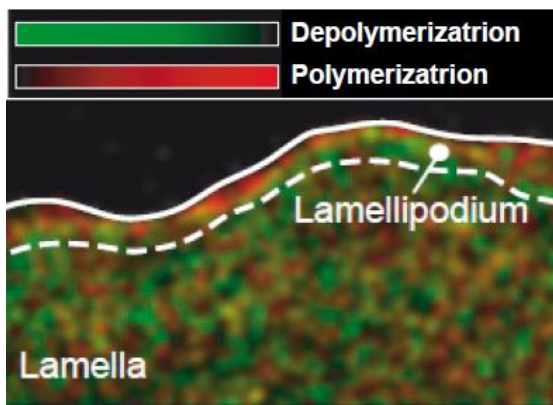


Figure 5: The lamellipodium consists of two zones. Speckle microscopy demonstrated that the lamellipodium exhibits two distinct zones. The zone proximal to the cell edge shows an increased rate of actin polymerization, while one μm behind depolymerization prevails. **Adapted from (Ponti et al. 2004)**

2.1.5.2. Wave-Like Motion of the Lamellipodium Drives Edge Progression

An important question asked was how actin polymerization, myosin activity and adhesion formation is linked. Theoretical models describing cell edge progression in the context of efficient cell migration did not fully explain this process so far (Mogilner 2006). It was suggested, that actin polymerization, force transmission and adhesion maturation are interdependent functions (Gupton & Waterman-Storer 2006). Further investigations showed that myosin II is in charge of pulling back the lamellipodial network resulting in upward bending, followed by edge retraction and finally leads to initiation of new adhesion sites (Giannone et al. 2007).

This model explains from a mechanical point of view why wave-like motions and ruffling of the lamellipodium are crucial for efficient cell migration of mesenchymal cells (Figure 6).

Elevated actin polymerization rates in the lamellipodium, which overlaps with the lamella, causes upward bending of the anterior cell edge. At the same time the lamellipodium is expanding and myosin contraction pulls back the lamella, resulting in a wave-like structure. Adhesion maturation can now be explained by flattening this wave-like structure, when nascent adhesions have been formed: During this process, tensile forces are applied on nascent adhesions, which lead consequently to their maturation.

Considerable, cells exhibiting low contractility show elevated number of ruffling events. This can be explained by the fact, that the total bond energy connecting lamellipodial actin to the edge is higher than the bond energy to nascent adhesions (Giannone et al. 2007).

Wave-like motion of the lamellipodium explains mechanics of edge progression.

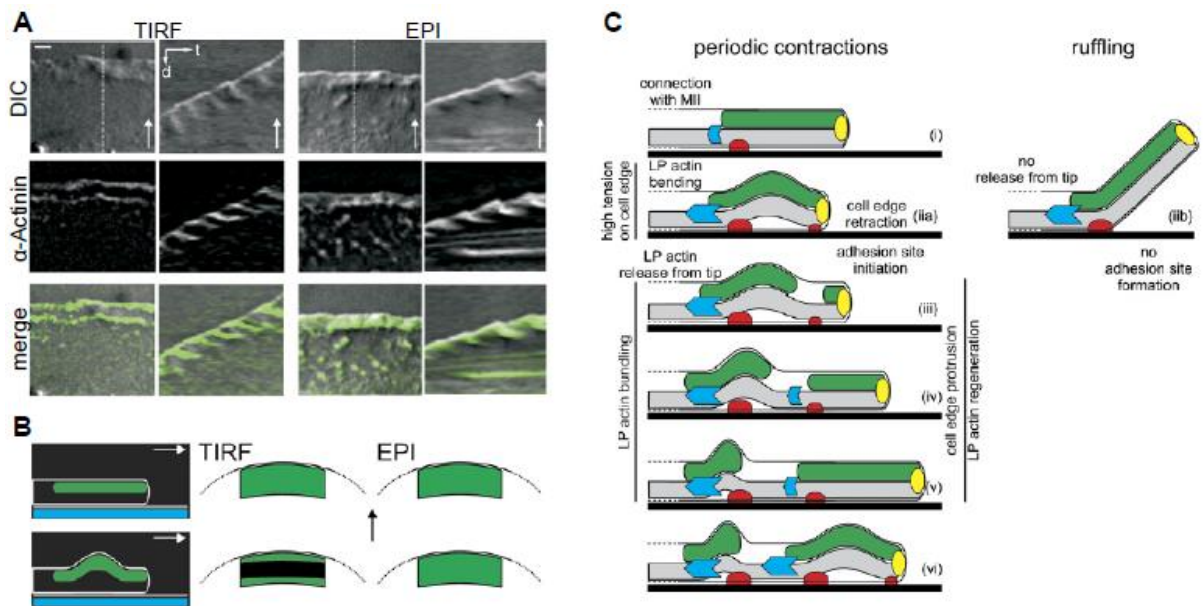


Figure 6: Mechanics of membrane protrusion. (A) Micrographs (left) and kymographs (right) of DIC (top), α -actinin TIRF (middle), and merge (bottom). The dashed line depicts the region used to generate the kymographs. Left, scale bar, 2 μ m. Right, $t = 30$ s; $d = 2$ μ m. (B) Identical to (A) except with α -actinin EPI (middle). (C) Kymographs of DIC (top) and α -actinin TIRF (bottom). Dashed lines mark the start of edge retraction. Note that LP-actin bending, visualized in TIRF by the loss in α -actinin-GFP fluorescence, initiates simultaneously with the start of edge retraction. $t = 30$ s; $d = 2$ μ m. (Giannone et al. 2007)

2.1.5.3. Arc Formation Explains How Lamellipodial Turns into Lamellar F-actin

Lamellipodium and lamella do not change their relative location to each other during cell migration. This fact raises questions about dynamics at the interface and transition from lamellipodial to lamellar F-actin respectively.

The hypothesis of F-actin arc formation provides an explanation how lamellipodial F-actin turns into lamellar F-actin bundles.

This model proposes, that myosin II locates in the middle of the lamellipodium, between polymerization and depolymerization zone and condenses the dendritic F-actin network. Finally, periodic edge retraction causes the formation of F-actin arcs, which move further away from the cell edge. This dynamic process is referred to as retrograde F-actin flow. Through coupling of F-actin arcs to nascent adhesions and retrograde F-actin flow, traction forces are applied to adhesion structures, leading to their maturation (Figure 7) (Burnette et al. 2011).

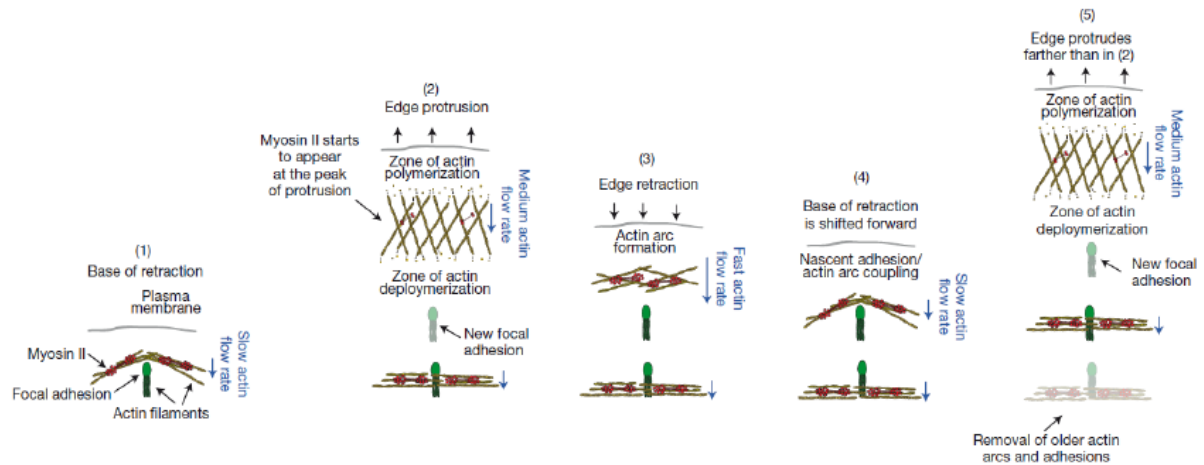


Figure 7: Formation of F-actin arcs. (1) Shows the base of a previous retraction where a newly created actin arc is coupled to a focal adhesion. (2) Actin-lament polymerization during protrusion occurs behind the plasma membrane and depolymerization occurs a few micrometres away from the edge. Actin laments treadmill through the lamellipodium during protrusion, and nascent adhesions form. At the peak of protrusion (2), myosin II laments form in the lamellipodium and a local network contraction occurs that drives actin-arc formation and edge retraction (3). In cells that show net advance, the new actin arc slows at the nascent adhesion (4). The base of the retraction in (4) is shifted forward when compared with (1). As a consequence, the start of the new protrusion in (5) is also shifted forward and the edge protrudes farther than in (2). In cells that do not show net advance, the actin arc and adhesion slip rearward during edge retraction. Actin-arc addition to the front of the lamella is balanced by actin-arc removal at the back of the lamella (5). Lamellipodial and arc actin laments are yellow. Focal adhesions and associated actin laments are green. Myosin II laments in red. Relative actin-rearward-flow rates are represented by blue arrows. (Burnette et al. 2011)

Maintenance of the lamellipodium at the cell edge during cell migration demands transition of lamellipodial to lamellar F-actin. This process is explained by the formation of F-actin arcs travelling from the lamellipodium to the lamella.

2.1.6. F-actin Stress Fibers Transmit Tensile Forces

The actin cytoskeleton is a dynamic scaffold, keeping the cell in shape during various processes like cytokinesis or cell migration. While cell shape changes drastically, the actin cytoskeleton has to remodel rapidly to allow cell motion.

Actin stress fibers play an important role in force and signal transmission and are diverse in molecular composition, shape and function. In the early 1980s the sarcomere-like character of stress fibers was emphasized (Kreis 1960). A sarcomeric stress fiber is composed of several parallel F-actin filaments with opposite polarity (barbed and pointed end orientation), cross-linked through α -actinin and connected by myosin II filaments (Figure 8A). Movement of myosin II towards barbed ends of actin filaments causes contraction of the sarcomeric stress fibers (Ono 2010). However, studies revealed, that also uniform polar arrangements of F-actin stress fibers exist, pointing at functional diversity of these structures (Cramer et al. 1997).

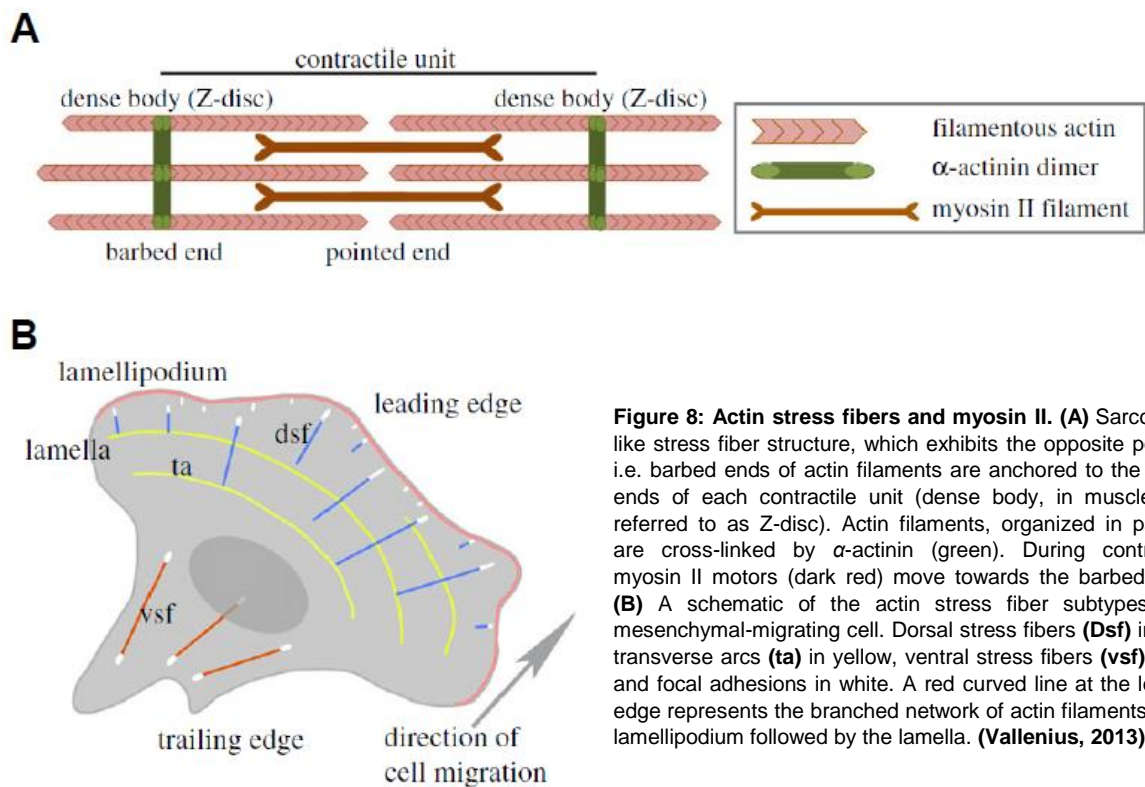


Figure 8: Actin stress fibers and myosin II. (A) Sarcomere-like stress fiber structure, which exhibits the opposite polarity, i.e. barbed ends of actin filaments are anchored to the lateral ends of each contractile unit (dense body, in muscle cells referred to as Z-disc). Actin filaments, organized in parallel, are cross-linked by α -actinin (green). During contraction myosin II motors (dark red) move towards the barbed ends. (B) A schematic of the actin stress fiber subtypes in a mesenchymal-migrating cell. Dorsal stress fibers (Dsf) in blue, transverse arcs (ta) in yellow, ventral stress fibers (vsf) in red and focal adhesions in white. A red curved line at the leading edge represents the branched network of actin filaments at the lamellipodium followed by the lamella. (Vallénius, 2013)

Dorsal Stress Fibers

Dorsal stress fibers (Figure 8B) elongate primarily from FAs at the leading edge towards the cell center (Pellegrin & Mellor 2007). Actin filaments are arranged in uniform orientation with barbed ends pointing towards the plasma membrane. At the same time uniform polarity of actin filaments points at the non-contractile character of these structures. Dorsal stress fibers are required for the formation of tensin rich fibrillar adhesions (Oakes et al. 2012). Formation of these structures is reported to be mDia1 driven (Hotulainen & Lappalainen 2006), while recent work additionally point at function of mDia1 to sense matrix rigidity.

It was shown, that mDia increases filament elongation rates up to two-fold when traction forces are sensed. Simultaneously, mDia1 itself is able to apply mechanical tension on actin filaments (Jégou et al. 2013). Instead of tensile forces solely generated by myosin II, this work presents an alternative strategy of force application.

Transverse Arcs

Transverse F-actin arcs (Figure 8B) appear in a curved shape parallel to the leading edge. Arc formation is initiated by condensation of dendritic actin filaments during lamellipodial edge retraction and myosin II force application. These condensed and parallel actin filaments travel further back towards cell center and disassemble before reaching it (Burnette et al. 2011). Transverse arcs are rich in myosin IIA and polymerization is driven by the Arp2/3 complex (Hotulainen & Lappalainen 2006) as well as by mDia2 (Tojkander et al. 2011).

Ventral Stress Fibers

Ventral stress fibers (Figure 8B) elongate from lamellar FAs towards FAs at the trailing edge and are located at the ventral part of the cell (Vallénius 2013). Fusion of preexisting dorsal stress fibers and transverse arcs might lead to formation of ventral stress fibers (Hotulainen & Lappalainen 2006). Another mechanism proposed is the stress fiber elongation triggered by the disheveled-associated activator of morphogenesis 1 (DAAM1) formin, which has been found to induce myosin IIB enriched ventral stress fiber assembly (Ang et al. 2010).

To allow polarized cell migration, protrusion can only take place at the cell front, while the back of the cell is retracting. Decoration of ventral stress fibers with myosin IIB leads to suppression of membrane protrusion at the back (Vicente-Manzanares et al. 2008) and enforces thereby directionality of cell migration.

2.1.6.1. F-actin: A Polymer with Polar Properties

Actin is the most abundant protein in a cell and occurs in two states: Monomeric, as globular actin (G-actin) and polymerized in form of filamentous actin (F-actin).

Three main isoforms are known to be expressed in vertebrate cells, namely α -, β - and γ -actin. α -actin is mainly found in skeletal, cardiac and smooth muscle cells, however β - and γ -actin are expressed in non-muscle and muscle cells (Dominguez and Holmes, 2011). G-actin occurs mainly in an ATP-bound state because of its low intrinsic GTPase activity.

F-actin forms a double helix allowing in this arrangement every new incoming monomer to bind to two subunits in the filament. Binding of a monomer to an already existing filament is a highly exothermic reaction rendering spontaneous actin filament polymerization and providing energy for the cell. A special feature of F-actin is its polar structure (Figure 9): The barbed end is favored for assembly of ATP-bound G-actin, and points preferentially to the plasma membrane, whereas the pointed end is most prone to ADP-bound actin dissociation. F-actin is a polymer out of equilibrium, meaning polymerization and depolymerization are constantly taking place, which leads to treadmilling. Treadmilling can be explained by two different critical concentrations of G-actin for each end of the actin filament. F-actin treadmilling enables the cell to rapidly adjust length of actin filaments and hence react to extracellular stimuli by altering cell shape (Carlsson 2010).

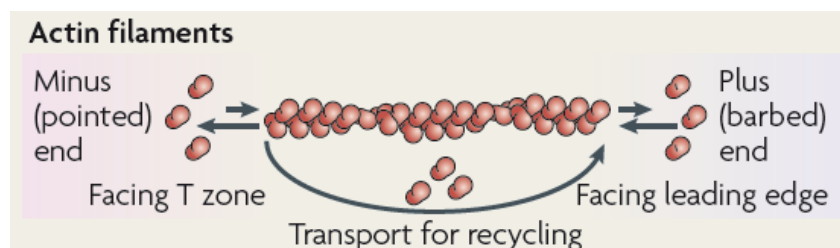


Figure 9: Polar Actin filament: Actin filaments exhibit polar properties. The minus (pointed) end is prone to actin disassembly, while F-actin polymerization occurs preferentially at the plus (barbed) end. (Lowery & Van Vector 2009)

2.1.6.2. Binding Proteins Regulate F-actin Dynamics

More than 100 proteins bind actin in order to regulate its polymerization or depolymerization in a spatio-temporal manner, depending themselves on different input signaling cascades (dos Remedios et al. 2003).

Actin polymerization can occur spontaneously with the caveat, that spontaneously formed actin filaments are less stable compared to filaments formed with the help of actin binding proteins. In the process of actin assembly and disassembly more than 60 classes of proteins and complexes are involved rendering strict control of this process (Pollard, 1999). A dendritic nucleation/ array treadmilling hypothesis describes distinct processes and involved factors (Figure 10) (Pollard and Borisy 2003):

(1) Extracellular cues induce via receptors activation of (2) GTPases and PIP_2 which in turn activate WASP/ SCAR proteins. (3) Active WASP/ SCAR trigger interaction of the (4) Arp2/3 complex with an actin monomer on one side and an actin filament on the other side to form a new branch. (5) The free barbed end elongates rapidly and (6) pushes plasma membrane forward. (7) Within seconds, filament elongation can be stopped by capping proteins. (8) When ATP gets hydrolyzed as a hallmark for filament aging, γ -phosphate is released. (9) F-actin severing and depolymerization of aged filaments is facilitated by actin depolymerizing factor (ADF)/cofilin. (10) Further, profilin binds to monomeric ADP-bound actin and catalyzes phosphorylation from ADP to ATP. (11) The pool of ATP bound monomeric actin is consequently used to elongate available barbed ends. (12) Actin depolymerization by ADF/cofilin is stopped through PAK and LIMK signaling which in turn is initiated by activated Rho-GTPases.

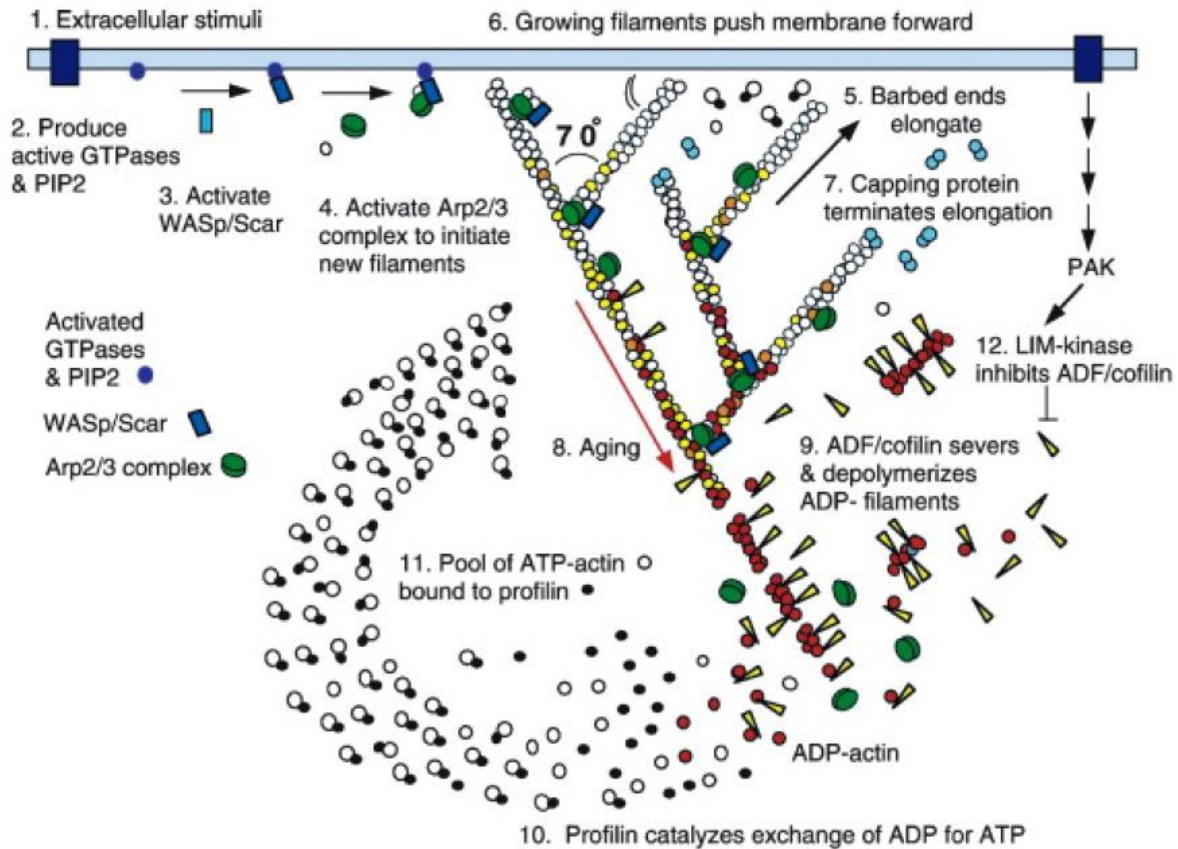


Figure 10: Actin turnover. Actin polymerization and depolymerization as described in main text. (Pollard & Borisy 2003)

Profilin

Profilin binds to monomeric actin and provides most of the unpolymerized actin used for F-actin polymerization. A minor pool of G-actin consists of the free ATP-bound form or bound to Thymosin- β 4. Profilin contributes in many ways to an increased actin polymerization rate (Dominguez and Holmes, 2011): Firstly, profilin catalyzes exchange of ADP for ATP on G-actin. Secondly, it inhibits F-actin nucleation if no nucleator is involved and thirdly prevents actin from associating with the pointed end of the actin filament. Additionally, profilin competes effectively with Thymosin β 4 for G-actin and binds with higher affinity to proline-rich sequences, which are abundant among cytoskeletal proteins. Thus, recruitment of profilin-bound G-actin by nucleation factors is promoted and actin polymerization enhanced.

Actin-Depolymerizing Factor (ADF)/ Cofilin

Actin-depolymerizing factor (ADF) and cofilin depolymerize or sever actin filaments and are responsible for recycling of actin monomers. This class of proteins is expressed in all eucaryotic cells and enable rapid cytoskeletal turnover, important for membrane ruffling and during cytokinesis (Bernstein & Bamburg 2010). ADF/cofilin binds in contrast to profilin preferentially to ADP-bound G-actin.

Actin Related Protein 2/3 (Arp2/3) Complex

The Arp2/3 complex is responsible for actin polymerization by binding a pre-existing actin filament and consequently initiates generation of a filament branch in a characteristic angle of 70° from the mother filament (Figure 11). This implies the importance of the Arp2/3 complex in generation of actin networks composing the lamellipodium, endocytotic vesicles or podosomes. The Arp2/3 complex itself needs to be activated by nucleation promoting factors (NPFs). Two classes of NPFs exist, differing in their structure and function:

Type I NPFs include among others the WASP family verprolin-homology proteins (WAVE or also known as SCAR), Wiskott-Aldrich syndrome protein (WASP), neural WASP (N-WASP), the WASP and SCAR homologue (WASH) and junction-mediating and regulatory protein (JMY). Moreover, type I NPFs contain a characteristic verprolin-homology domain (VCA or also known as WH2), a cofilin homology domain and an acidic domain which allows for binding to G-actin and Arp2/3.

Type II NPFs in contrast lack these VCA domains, but display acidic domains responsible for Arp2/3 binding, while tandem repeats bind to F-actin. A representative of type II NPFs is cortactin, which itself comprises relatively weak ability to activate the Arp2/3 complex, but on the other hand prevents Arp2/3 nucleated filaments from debranching (Weaver et al. 2001).

However, there is also negative regulation of the Arp2/3 complex, executed by proteins like glia maturation factor (GMF) (Gandhi et al. 2010), coronin1B (Cai et al. 2009), gadkin (Maritzen et al. 2012) and protein interacting with protein C kinase 1 (PICK1) (Rocca et al. 2008).

Formins

Formins are multidomain proteins, evolutionary conserved among eucaryotes, and exert effects on actin and microtubule networks. Elongated, straight actin filaments as found in filopodia, stress fibers or the cytokinetic contractile ring are produced by formins (Glotzer 2005; Naumanen et al. 2008).

Common features of formins, are the formin homology (FH) domains FH1 and FH2, while the FH3 domain is not as abundant among formins. While binding and recruitment of profilin is the mayor role of FH1 domains, FH2 domains associate with the barbed end of actin filaments and consequently nucleate actin filaments. Both domains are flanked by the regulatory domains diaphanous inhibitory domain (DID) and diaphanous auto regulatory domain (DAD), which are driving activation and localization (Goode & Eck 2007). Several formins are auto inhibited and get activated upon binding to GTP-loaded Rho-GTPases (Goode & Eck 2007). Remaining bound to the barbed end of F-actin, formins prevent capping and stimulate the addition of FH1 domain-bound profilin-actin (Harris et al. 2004; Kovar et al. 2006). The N-terminal GTPase binding domain (GBD) releases upon binding to GTP-loaded Rho-GTPases auto inhibition of the two regulatory domains and activates filament assembly (Lammers et al. 2005). Prominent representatives of formins are diaphanous-related formins mDia1, mDia2 and mDia3 promoting unbranched actin filament elongation (Figure11).

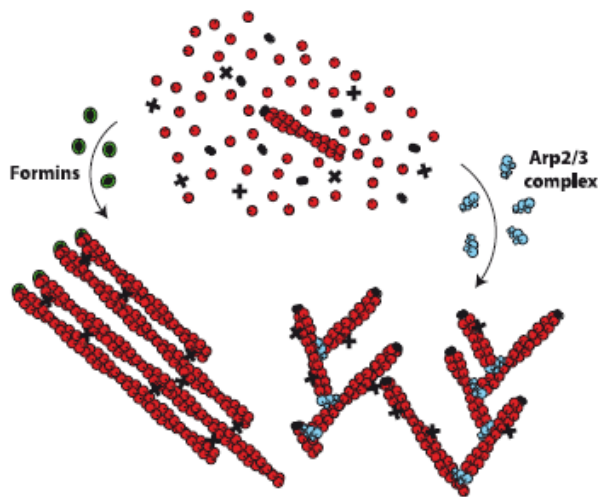


Figure 11: Actin filament nucleation. The Arp2/3 complex generates branched F-actin networks, while formins assemble unbranched filaments. (Bindschadler & McGrath 2004)

2.1.7. Adhesion Structures: Composition and Dynamics

Depending on ECM properties (composition, rigidity, dimensionality, etc.) or other extracellular stimuli such as growth factors or chemokines, cells use a variety of adhesion structures (Figure 12) (Petrie et al. 2009; Plotnikov et al. 2012; Renkawitz et al. 2009). In this chapter, different characteristics of adhesion structures are discussed: Starting with nascent adhesions as first adhesion structure assembled at the lamellipodium. Nascent adhesions further mature into focal complexes, and these turn later upon tensile force application into mature focal adhesions. Besides, podosomes are introduced exhibiting different architecture and dynamics compared to nascent adhesions, focal complexes or focal adhesions.

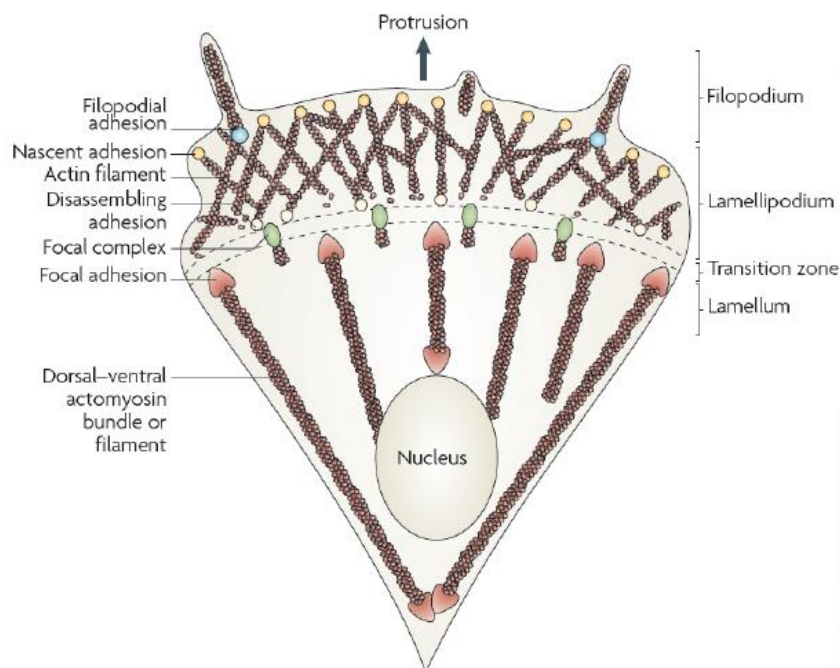


Figure 12: Adhesion and cytoskeletal structures of a mesenchymal cell. (A) Adhesion is closely coupled with the protrusions of the leading edge of the cell. Nascent adhesions initially form in the lamellipodium (although adhesions may also be associated with filopodia) and the rate of nascent adhesion assembly correlates with the rate of protrusion. Nascent adhesions either disassemble or elongate at the convergence of the lamellipodium and lamellum (the transition zone). Adhesion maturation to focal complexes and focal adhesions is accompanied by the bundling and cross-bridging of actin filaments, and actomyosin-induced contractility stabilizes adhesion formation and increases adhesion size. (Parsons et al. 2010)

2.1.7.1. Nascent Adhesions

Formation of focal adhesions is a continuous process and starts with the formation of nascent adhesions at the very leading edge of the cell, at the lamellipodium.

Nascent adhesions (Figure 12) are initiated by integrins, clustering at interaction points of the plasma membrane with the ECM (Giannone et al. 2007) and rapidly turn over within ~60 seconds or mature into larger, dot-like shaped adhesions, named focal complexes (Parsons et al. 2010).

2.1.7.2. Focal Complexes

Upon condensation of dendritic lamellipodial F-actin during periodic edge retraction and thereby application of pulling forces on nascent adhesions, these structures mature into focal complexes (Burnette et al. 2011).

Focal complexes (Figure 12) do not move referred to the substrate and disassemble again within several minutes if dorsal or ventral stress fibers are not pulling on them. However, upon force application, focal complexes mature into focal adhesions (Parsons et al. 2010).

2.1.7.3. Focal Adhesions

Focal adhesions (Figure 13) are made up of clustered integrins, binding to the ECM and cytoplasmic components and are connected to F-actin stress fibers (Zaidel-Bar et al. 2007; Geiger & Zaidel-Bar 2012). Functionally, focal adhesions are playing a role in mechanotransduction and are required for matrix rigidity sensing (Plotnikov et al. 2012), adhesive state or molecular properties of the ECM (Hynes 2002). Typically, focal adhesions are 2 μm wide and 3 to 10 μm long (Zimerman et al. 2004) and persist for a couple of minutes up to several hours.

Integrins on the base of focal adhesions attach to the ECM. These transmembrane proteins are composed of heterodimeric, but non-covalently associated α and β subunits (Hynes 2002). F-actin stress fibers are bound to integrins via a complex, consisting of several components: Talin, interacting with the cytoplasmic tail of integrins (Polecek et al. 1998) (Horwitz et al., 1986) is required to sense matrix rigidity. It was shown, that by mechanical stretching of single talin rods, a cryptic binding domain for vinculin binding gets exposed (Rio et al. 2009).

Besides talin, other proteins like focal adhesion kinase (FAK), α -actinin, paxillin, zyxin or VASP are integrated in the adhesion complex. A nanoscale approach shed more light into the exact organization of this multiprotein complex and revealed that integrins are separated by an about 40-nm adhesion core region. This core region consists of multiple functional layers (Figure 9): (1) In a integrin signaling layer cytoplasmic integrin tails are connected to FAK and paxillin, (2) an intermediate force transduction layer consists of talin and vinculin, while (3) an actin regulatory layer contains zyxin, VASP and α -actinin (Kanchanawong et al. 2010).

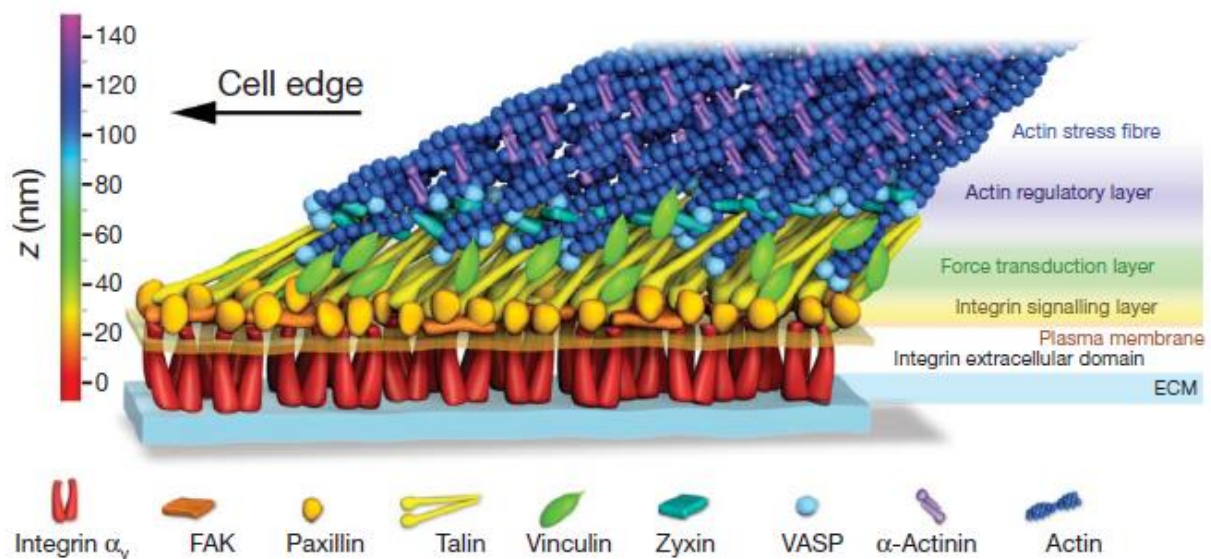


Figure 13: Molecular architecture of focal adhesions. Schematic model of focal adhesion molecular architecture, depicting experimentally determined protein positions. Note that the model does not depict protein stoichiometry. (Kanchanawong et al. 2010)

Adhesion maturation is caused by traction forces, generated by myosin II (Parsons et al. 2010) and mDia1 (Jégou et al., 2013) and transmitted via F-actin stress fibers, but also adhesion disassembly is influenced by tension (Puklin-Faucher & Sheetz 2009; Vicente-Manzanares et al. 2008). Well balanced cell contractility is crucial for efficient cell migration, considering that too low myosin II activity leads to adhesion disassembly and on the other hand too high contractility inhibits leading edge protrusion and formation of nascent adhesions (Vicente-Manzanares et al. 2008).

Disassembly of focal adhesions at the trailing edge of migrating cells is accompanied by a sliding motion of adhesions and thus dispersion (Broussard et al. 2008). The protease calpain is involved in disassembly of focal adhesions at the trailing edge (Franco et al. 2004). Interestingly, integrin residues remain on substrates, but no cytosolic components of focal adhesions (Polecek et al. 1998).

Focal adhesions perform sliding motions in direction of retrograde F-actin flow due to applied traction forces. A clutch-like mechanism was proposed in 1999 to explain this phenomenon:

The affinity of integrins to the ECM is modulated in response to substrate properties (Smilenov 1999). That means anchoring of cells to the ECM via focal adhesions is no all-or-nothing decision. Depending on the efficiency of shunting traction forces to the substratum, slippage of focal adhesions occurs to a certain degree. Is the clutch engaged, slippage is minor and leading edge protrusion most efficient (Parsons et al. 2010).

2.1.7.4. Podosomes and Invadopodia

Initially, podosomes were discovered in 1980 by David-Pfeuty and Singer. Chicken embryonic fibroblasts were infected with Rous sarcoma virus (RSV) containing the oncogene *v-src*. The following observation showed cytoskeletal remodeling and actin rearrangement in rosette-like structures. In 1985 podosomes got their name reminding of „feet of the cell“ (Tarone et al., 1985). Some years later, the ability of podosomes to degrade the ECM was discovered (Chen et al., 1989), leading to the introduction of the name invadopodia. Since that, nomenclature of these structures is of debate and not consistent throughout literature. Although, podosomes and invadopodia share molecular composition and architecture, invadopodia seem to be more efficient in matrix degradation. They preferentially localize below the nucleus and occur mainly in transformed cells (Murphy & Courtneidge 2011).

Podosomes are important for different functions in diverse cell types: Osteoclasts for example, take advantage of the ECM degradation by podosomes to degrade bone. Lymphocytes use podosomes to palpate the vascular endothelium (Carman et al. 2007).

Podosomes are not solely used to degrade ECM. It was also reported, that due to formation of podosomes, the cell is able to co-ordinate motility and matrix degradation in order to facilitate cell migration through tissue microenvironments (Murphy & Courtneidge 2011).

Podosome Architecture

Pillar-like shaped podosomes are composed of an F-actin core, oriented perpendicular to the ECM, and surrounded by adhesion proteins such as integrins, α -actinin, talin, vinculin or paxillin (Figure 14D). Actin polymerization is accomplished by the Arp2/3 complex and actin regulators WASP, N-WASP, WIP, tyrosin kinase SRC and cortactin, while matrix is degraded by transmembrane membrane type 1 matrix metalloprotease (MT1MMP) (Buccione et al. 2009; Desai et al. 2008). Podosomes contain as well the scaffold proteins tyrosine kinase substrate four SH3 domains (TKS4) and tyrosine kinase substrate five SH3 domains (TKS5). These proteins are known to play a role in formation of reactive oxygen species (ROS) (Diaz et al. 2009).

Podosome Dynamics

Podosomes form at the ventral surface of cells, appear as dot-like structures which are not moving referred to the ECM and persist for 2 up to 30 minutes (Albiges-Rizo et al. 2009).

During podosome assembly integrins and other yet unidentified receptors bind to the ECM (Figure 14A), leading to clustering of receptors into PtdIns(4,5)P₂-enriched regions of the plasma membrane. Next, Src is recruited and phosphorylates a variety of proteins like cortactin, WASP, FAK and regulators of Rho-GTPases. Continuous actin nucleation is required for the formation of podosomes and is achieved by synergistic action of cortactin and WASP-family proteins (Figure 14B). The formin mDia1 is responsible for columnar actin filament elongation protruding from the initially formed branched F-actin network (Figure 14C). Podosomes are mechanically connected among each other

via a network of radial actin filaments that are arranged in parallel to the ECM (Figure 14D) (Albiges-Rizo et al., 2009).

Dorsal ruffles or waves contain similar molecular components as podosomes and contribute to cytoskeletal reorganization. Formation of dorsal ruffles, waves as well as podosomes can be induced by growth factor stimulation. Thereby Arp2/3 complex gets activated via phosphatidylinositol 3-kinase (PI3K) or Src phosphorylating the effector P21-associated kinase (PAK1) (Buccione et al. 2004). Dorsal ruffles or waves are necessary to sequester and internalize receptor tyrosine kinases (RTKs) in macropinosomes in order to recycle them (Suetsugu et al. 2003). These membrane distortions might also be important in transition from a non-motile to motile state of cells (Soranno & Bell 1982).

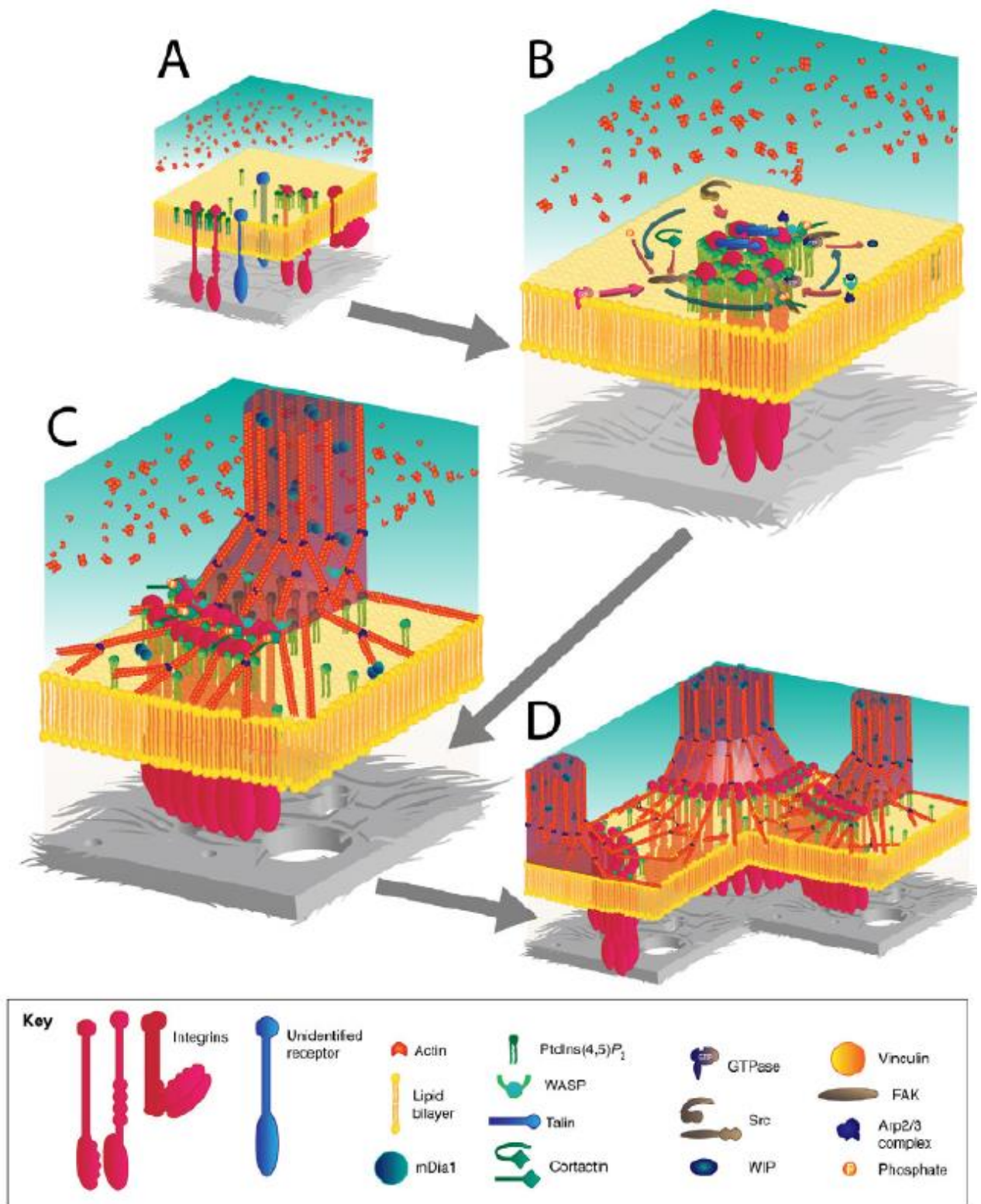


Figure 14: Assembly and organization of podosomes and invadopodia. (A) At the initial stage of adhesion formation, integrins or other unidentified receptors bind to components of the ECM (grey), leading to clustering of receptors into PtdIns(4,5)P₂-enriched areas of plasma membrane. (B) Recruitment of Src to adhesion sites leads to phosphorylation of several proteins such as cortactin, WASP, FAK and regulators of small GTPases. (C) mDia1 elongates actin filaments into columnar structures from the branched actin network that was previously induced by N-WASP, the Arp2/3 complex and cortactin. (D) Podosomes or invadopodia are mechanically connected through a network of radial actin filaments that lie parallel to the substratum. (Albiges-Rizo et al. 2009)

2.1.8. Myosin II Generates Tensile Forces

The motor protein myosin II is composed of two heavy chains, two regulatory and two essential light chains. In mammalian cells three non-muscle myosin isoforms are expressed, namely myosin IIA, IIB and IIC.

These isoforms differ in enzymatic properties, although considerable homologies exist (Kovács et al. 2003). Indeed, different myosin isoforms fulfill different functions: Myosin IIB for example is involved in stabilizing cell polarity (Lo et al. 2004), while myosin IIA is linked with Rho kinase-dependent functions (Sandquist et al. 2006) and myosin IIC might be important in cancer (Vicente-Manazares et al., 2009). Myosin is activated by phosphorylation of Tyr18 and Ser19 of the regulatory light chain and generates tensile forces by pulling actin filaments against each other (Figure 15A).

In migrating cells, myosin II acts in many ways: Starting at the lamellipodium, myosin II is responsible for condensation of dendritic F-actin networks in order to form transverse F-actin arcs and propel leading edge protrusion. In order to allow cell migration, tensile forces are demanded to mature adhesion structures and to retract the trailing edge (Figure 15B) (Parsons et al., 2010). Additionally, antiparallel movement of actin filaments causes bundling into F-actin Stress fibers (Vicente-Manazares et al., 2008; Vicente-Manazares et al., 2009).

To study acute effects upon loss of myosin II activity, the inhibitor blebbistatin is a potent tool. The compound interferes with the adenosine triphosphatase (ATPase) and prevents therefore gliding motility activities of myosin II without inhibiting myosin light chain kinase (MLCK), resulting in tail retraction phenotypes or impaired edge protrusion (Straight et al. 2003).

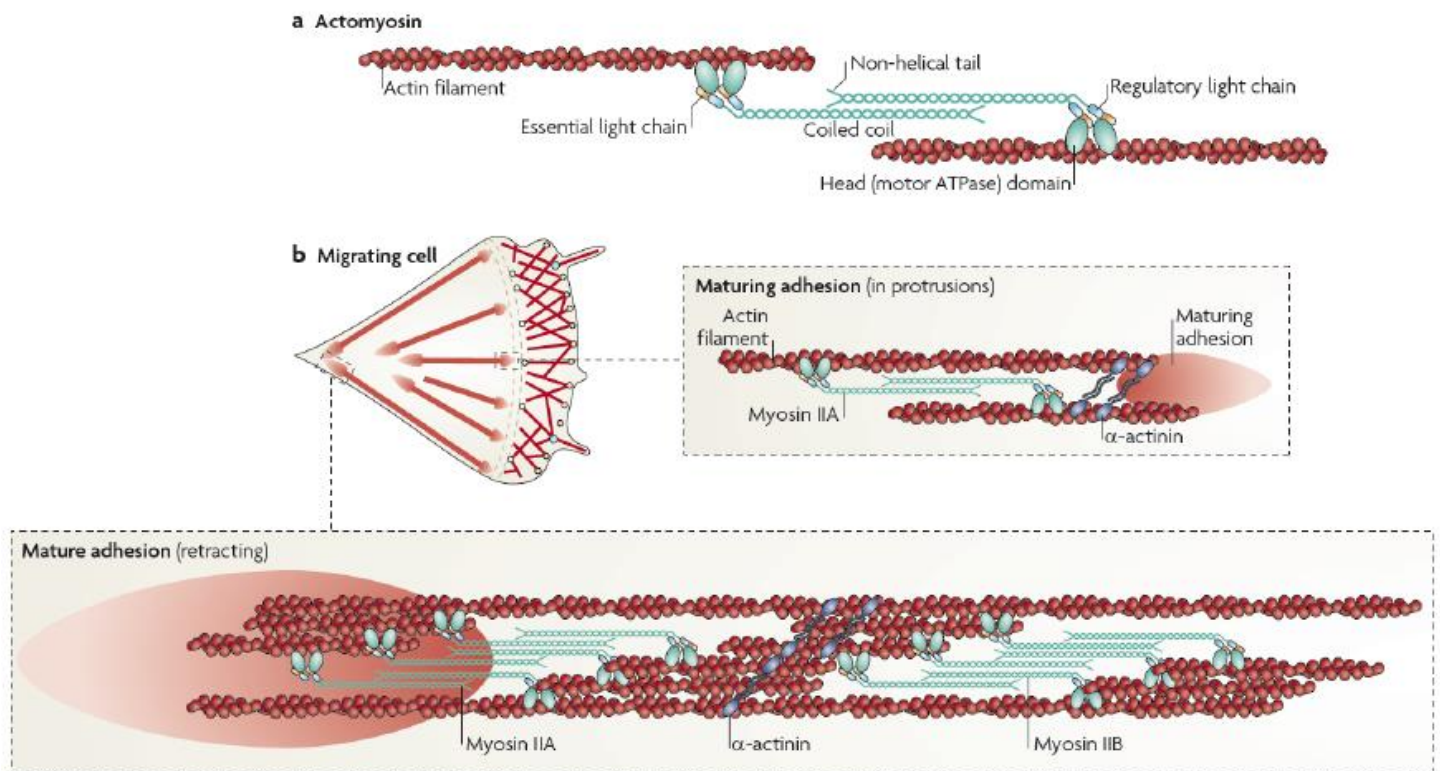


Figure 15: Myosin II, adhesion maturation and turnover. (A) Adhesions elongate along actin filaments that contain myosin II A, which cross links the actin filaments and exerts tension on them. This leads to tension on the conformational sensitivity, and clustering of, adhesion molecules that are directly or indirectly associated with actin. Myosin II activity is regulated by phosphorylation on the regulatory light chain at Thr18 and Ser19, although other regulatory sites in the heavy chain are also implicated in its activities. **(B)** In a migrating cell, myosin IIA acts at a distance to regulate adhesion maturation and turnover as it is juxtaposed to, but not directly associated with, the maturing adhesion at the cell front. α -actinin cross links actin filaments. Adhesions at the rear are associated with large actin filament bundles that contain both myosin IIA and myosin IIB. Their activity mediates rear retraction and adhesion disassembly. (Parsons et al. 2010)

2.2. Receptors in Hapto- and Chemokinesis

Cell signaling, driving efficient cell migration, involves a variety of receptors to sense the environment and diverse signaling network trigger adaptations according to extracellular stimuli. During haptokinesis/ haptotaxis, integrin signaling is crucial to sense ECM composition. In this mode of cell migration, matrix composition is the main input signal influencing migration dynamics, while receptor tyrosine kinase (RTK) signaling is demanded to drive PDGF chemokinesis/ chemotaxis.

2.2.1. Integrin Signaling

Integrins compose the base of focal adhesions, anchoring the ventral plasma membrane to the ECM and show at the same time tissue specificity due to distinct binding affinities to particular ligands (Humphries et al. 2006). This class of receptors belongs to heterodimeric type 1 transmembrane glycoproteins and consists of non-covalently associated α and β subunits (Hynes, 2002).

In total 18 different types of α integrin and 8 β integrin subunits are encoded in the mammalian genome, allowing the formation of 24 different combinations.

For binding of integrins to fibronectin, the heterodimers $\alpha5\beta1$ and all αv -class integrins are used (Leiss et al. 2008). Recently, it was shown how $\alpha1$ and αv integrins cooperate to regulate myosin activity

during mechanotransduction (Schiller et al. 2013). It was demonstrated that αv - class integrins are coupled to a GEF-H1-RhoA -mDia1 pathway but not to myosin II, while $\alpha 5 \beta 1$ integrins signal to a RhoA-ROCK-myosin pathway. This indicates that $\alpha 5 \beta 1$ integrins accomplish force generation, while αv - class integrins are used for structural adaptation to forces.

2.2.1.1. Integrin Conformations and Clustering

α and β subunits consist of a large extracellular domain, a transmembrane domain and a short cytoplasmic domain. Changing their conformation can either be caused by outside-in or inside-out signaling.

A „bent“ conformation causes low substrate affinity, while an intermediate extended conformation with a closed head-piece represents the activated state. Upon ligand engagement integrins are situated in an extended conformation with open head-piece (Shattil et al. 2010a).

An increased binding affinity of integrins to the ECM can be accomplished either by conformational changes or by integrin clustering (Figure 14A). During clustering, integrins form hetero-oligomers and increase thereby receptor valency (Carman & Springer 2003). Further, integrin clustering is important for triggering outside-in signaling, integrin recycling (Caswell & Norman 2006) and mechanotransduction (Puklin-Faucher & Sheetz 2009).

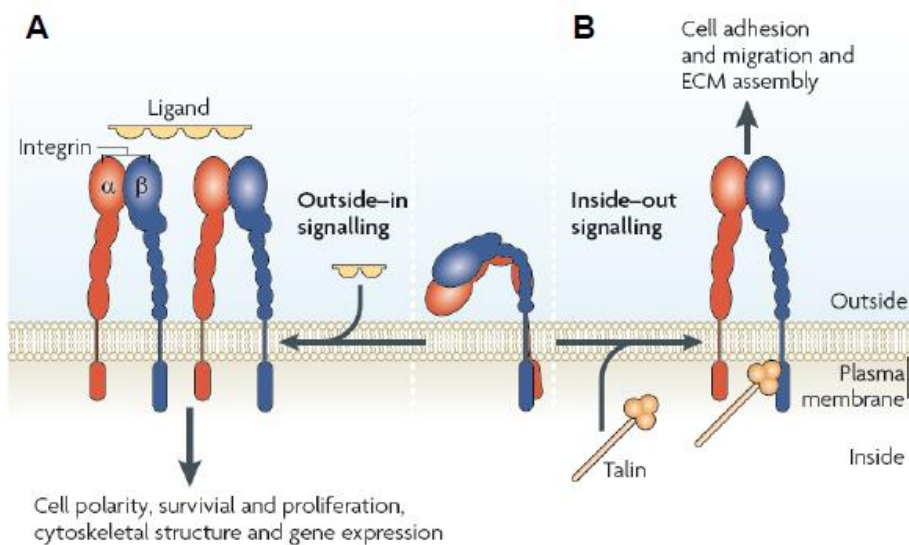


Figure 14: Bidirectional integrin signaling. (A) Integrins transmit information into cells by 'outside-in' signaling. Binding of integrins to their extracellular ligands causes conformational changes and induces integrin clustering. **(B)** During 'inside-out' signaling integrin binding proteins induce conformational changes resulting in modulation of binding affinity to the. **(Shattil et al. 2010)**

2.2.1.2. Outside-in Signaling

Outside-in signaling is needed to modulate cytoskeletal and adhesion morphodynamics according to ECM properties.

Signals from the outside are transmitted across the membrane via transmembrane domains of α and β subunits (Figure 14A). Ligand binding to the extracellular domain induces separation of the α and β transmembrane domains and cytoplasmic tails, which in turn promotes integrin clustering, conformational changes and thus signal transmission across the membrane. Cytoplasmic proteins are recruited to the cytosolic domain of integrins (Du et al. 1991; Miyamoto et al. 1995; Zhu et al. 2007; Kim et al. 2011). Next, adaptors and scaffold proteins link integrins to downstream kinases, such as focal adhesion kinase (FAK) or Src (Giancotti 1999). Through conformational changes and clustering of integrins ligand information is transmitted and binding affinity to the ECM modulated.

2.2.1.3. Inside-out signaling

Inside-out signaling is needed to control adhesion strength to the ECM and contributes by modulating of this interaction to the generation of traction forces needed for cell migration (Figure 14B) (Shattil et al. 2010b).

Both, inside-out and outside-in signaling mutually influence each other as for instance ligand binding to extracellular domains can enforce integrin engagement caused by binding of cytoplasmic proteins such as talin or kindlins and lead further to conformational changes.

Talin

Talin is composed of two domains, a 50 kDa N-terminal head (THD) and a 220 kDa rod domain. The FERM (band 4.1, ezrin, radixin, moesin) domain, as part of THD, shows high affinity to the cytoplasmic domain of β integrin (Calderwood 1999). However, the talin rod domain is able to bind F-actin, vinculin and the β integrin cytoplasmic tail (Hemmings et al. 1996; Gingras et al. 2008; Gingras et al. 2010)

Talin exhibits the ability to activate integrins and forms a physical linkage between integrins and the actin cytoskeleton (Calderwood 1999; Critchley 2009).

A special property of talin is its function in mechanosensitivity: By mechanical stretching of single talin rods a cryptic binding domain is exposed, which leads to vinculin binding (Del Rio et al., 2009).

Alpha-actinin

Alpha-actinin belongs to the spectrin protein superfamily and has an anti-parallel rod-shaped dimeric structure including one actin binding domain at each end. In non-muscle cells α -actinin is found along F-actin filaments (Pavalko & Otey 1991). Apart from its role in bundling actin filaments (Sjöblom et al. 2008) and adhesion maturation (Choi et al. 2008) recent studies demonstrated the impact of α -actinin on mechanotransduction: In the proposed model α -actinin competes with talin for the binding to β_3 integrin tails and consequently transmits cytoskeletal forces triggering mechanotransduction (Roca-Cusachs et al. 2013).

Kindlins

Kindlins are 76 kDa proteins occurring in three different orthologs expressed in mammalian cells: Kindlin-1, -2 and 3.

Kindlins are able to bind to the cytoplasmic tail of β integrin subunits via their FERM domain. The FERM domain of kindlins can be divided in three sub domains namely F1, F2 and F3. A pleckstrin homology (PH) domain separates the F2 from F1 and F3 domain (Kloeker et al. 2004). However, it was shown, that kindlins, unlike talin, are not able to activate integrins directly (Harburger et al. 2009). A possible mechanism of kindlins regulating integrin activation may involve kindlin-binding proteins, such as integrin linked kinase (ILK) or migfilin (Moser et al. 2009; Shattil et al. 2010a)

2.2.2. Receptor Tyrosine Kinases (RTKs)

A large family of transmembrane receptors is represented by receptor tyrosine kinases (RTKs). RTKs exhibit intrinsic protein tyrosine kinase activity and catalyze the transfer of γ -phosphate from ATP to hydroxyl groups of tyrosines on target proteins (Hunter 1998). They play a crucial role in diverse cellular processes including cell cycle, cell migration, proliferation, differentiation and survival (Schlessinger 2000). Structurally, RTKs consist of an extracellular, glycosylated, ligand binding domain which is connected to the cytoplasmic domain via a single transmembrane helix. Moreover, the cytoplasmic domain carries a protein tyrosine kinase (PTK) core with additional regulatory sequences. These regulatory sequences are exposed to auto phosphorylation by heterologous protein kinases (Hunter 1998; Hubbard, 2002).

2.2.2.1. Activation of Receptor Tyrosine Kinases

Most RTKs occur monomeric in the cell membrane when no ligand has bound, although some subsets of RTKs including the insulin and IGF1 receptor, are expressed as disulfide-linked ($\alpha\beta$)₂ dimers (Ward et al. 2007). Further, it was reported, that subsets of RTKs, such as the angiopoietin receptor (Tie2) or Ephrin receptors (Eph) require the formation of larger oligomers in order to get activated (Barton et al. 2006; Himanen & Nikolov 2003). Concisely, inactive RTKs can occur as dimers and oligomers, although binding of ligands is demanded to stabilize a specific relationship between individual receptor molecules, in order to activate the receptor. Once, a ligand has bound, the association of the extracellular domains lead to dimerization of the cytoplasmic domains and consequently activates their tyrosine kinase domains (Figure 15). Thus, an activated receptor dimer/ oligomer phosphorylates neighboring RTKs and serves itself as site for assembly/ activation of intracellular signaling proteins (Lemmon & Schlessinger 2010).

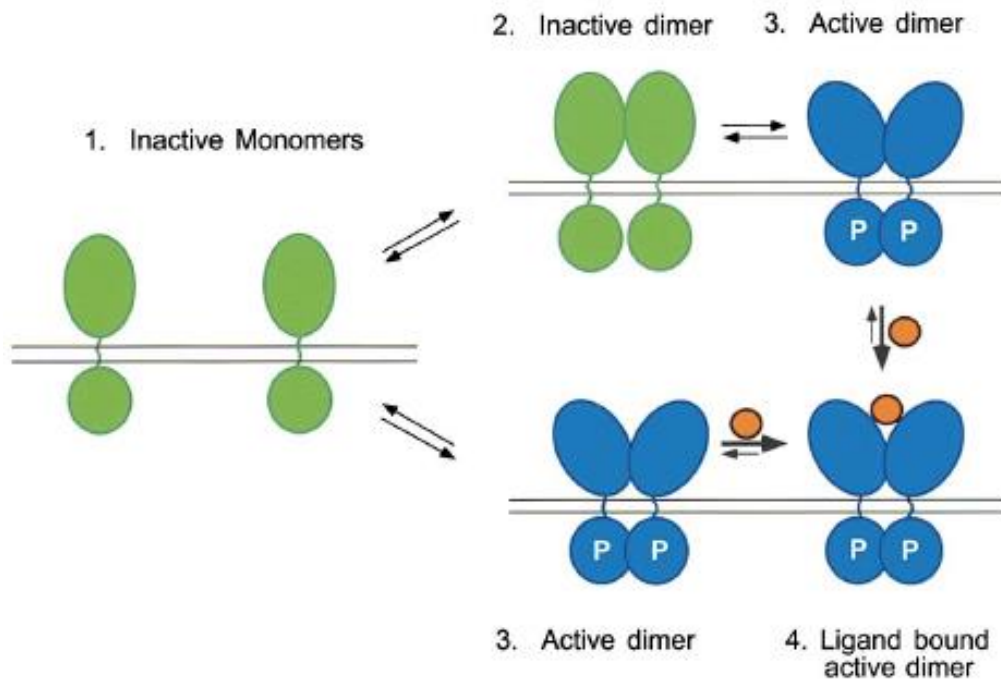


Figure 15: Ligand binding stabilizes the formation of activated integrin dimers. (A) Inactive receptor monomers (green) are in equilibrium with inactive (green) or active (blue) receptor dimers. The active receptor dimers exist in a conformation compatible with trans-autophosphorylation and stimulation of PTK activity (blue). Ligand binding stabilizes active dimer formation and hence PTK activation. (Schlessinger 2000)

2.2.2.2. Receptor Tyrosine Kinase Downstream Signaling

Activated RTKs act as transmitter of outside-in signals across the plasma membrane. Since there are a variety of interactions with activated RTKs possible, specificity of protein interaction and signal transduction is achieved by multidomain interactions. Directly after autophosphorylation of the PTK domains, RTKs recruit downstream effectors containing either phosphotyrosine-binding domains (PTB) (Figure 16A) or Src homology-2 (SH2) domains (Figure 16B) (Lemmon & Schlessinger 2010). These molecules bind directly or via docking proteins to the cytoplasmic domain of RTKs (Pawson 2004; Schlessinger & Lemmon 2003).

An important role in receptor degradation plays the ubiquitination, which depends on receptor activation and serves as important negative feedback mechanism (Hunter 2007).

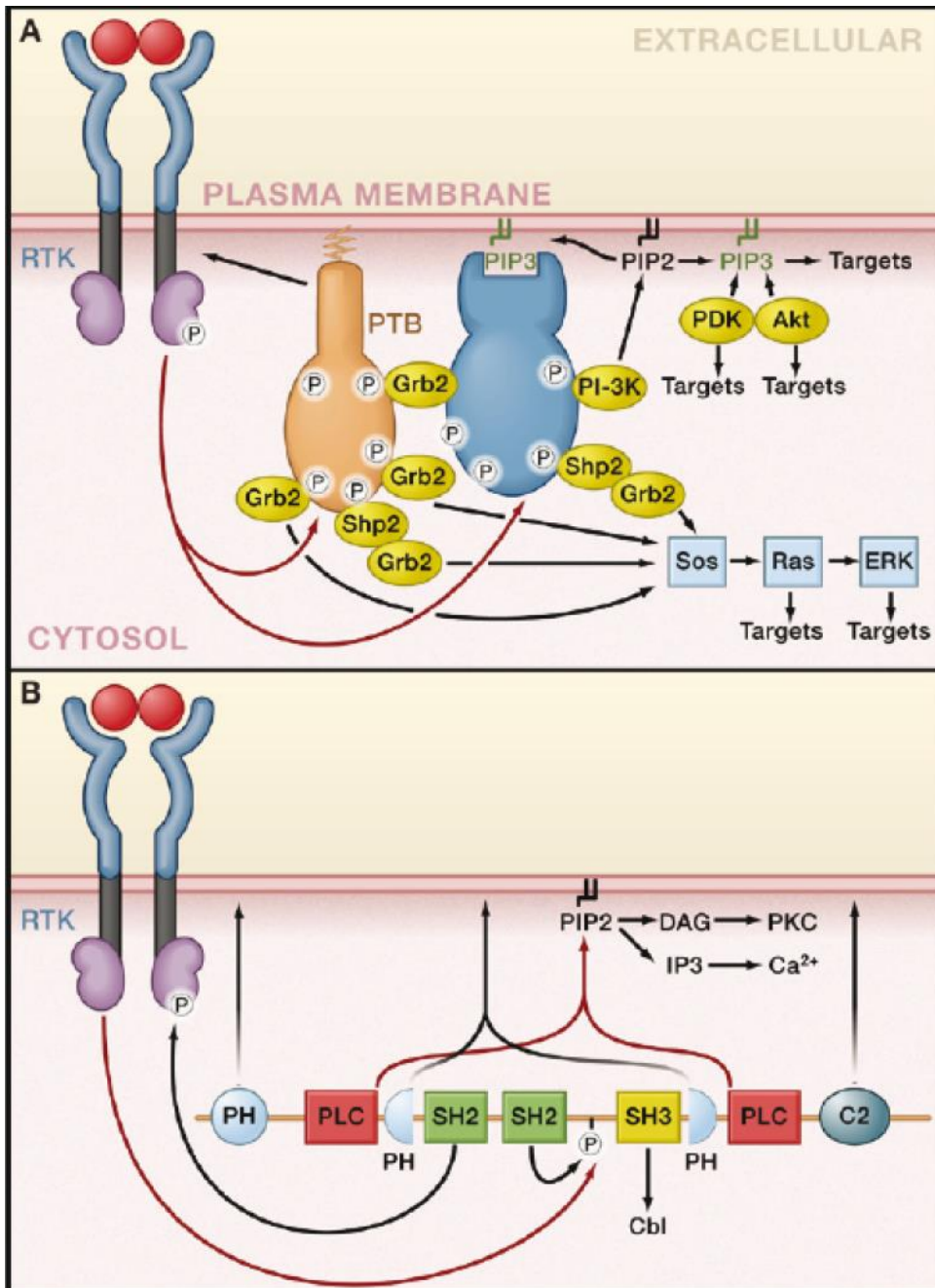


Figure 16: Network Branching in RTK Signaling. (A) Coordinated assembly of multiprotein complexes in receptor tyrosine kinase (RTK) signaling provides branching points in a signaling network. The ligand forms a complex with activated RTK via its phosphotyrosine-binding domain (PTB). The activated RTK autophosphorylates on multiple tyrosines, and the resulting phosphotyrosines recruit multiple Grb2 and Shp2 molecules, which bring a second docking protein, Gab1, into the complex. Gab1 is tyrosine phosphorylated and recruits additional signaling proteins, including phosphoinositide 3-kinase (PI-3K). PI-3K initiates a positive feedback loop in which PtdIns(3,4,5)P₃ (PIP₃), generated by PI-3K, recruits more Gab1, leading to further PI-3K activation. **(B)** The multiple domains of phospholipase C-γ (PLCγ) cooperate to integrate multiple signals at the plasma membrane. The N-terminal SH2 domain is responsible for complex formation with activated RTKs. The C2 and PH domains cooperate with the SH2 domain to target PLCγ to the plasma membrane. One or both of the PH domains may also specifically recognize products of RTK-activated PI-3K. RTK-mediated tyrosine phosphorylation of PLCγ leads to intramolecular binding of the C-terminal SH2 domain to phosphotyrosine 783. This stimulates enzymatic activity of PLCγ, leading to hydrolysis of PtdIns(4,5)P₂ (PIP₂), and consequently leads to the formation of Ins(1,4,5)P₃ (IP₃) and diacylglycerol (DAG). (Lemmon & Schlessinger 2010)

2.3. Rho-GTPases Orchestrate Cell Migration

Rho-GTPases are involved in a variety of cellular processes including cytoskeletal and dynamics or establishment of cell polarity (Etienne-Manneville & Hall 2002) 20 genes encode mammalian Rho-GTPases, which can be divided in five subgroups:

1.) Rho-like, 2.) Rac-like, 3.) Cdc42-like, 4.) Rnd and 5.) Rho-BTB.

However, the Rho-GTPases RhoD, Rif and RhoH/TTF are not part of any of these subgroups (Figure 17) (Burrige et al. 2004).

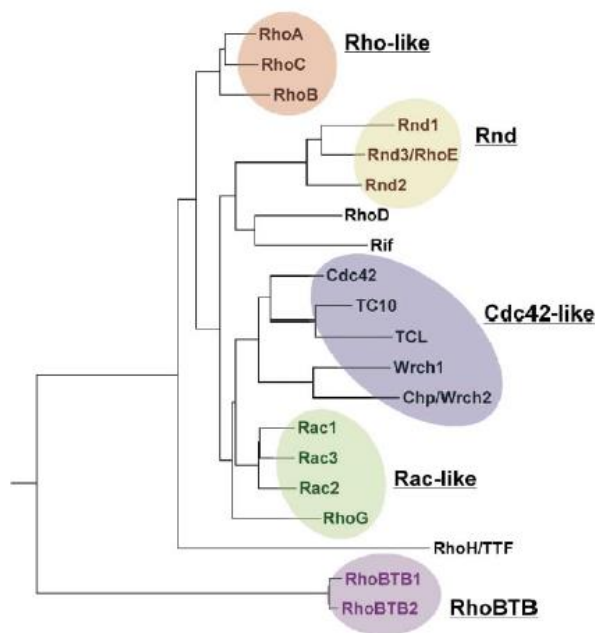


Figure 17: Rho family GTPases. Dendrogram representing relationships between the 20 Rho family members. The five subfamilies, Rholike, Rnd, Cdc42-like, Rac-like, and RhoBTB, are highlighted by circles. (Burrige et al. 2004)

The dogma of Rho-GTPase signaling assigns in a Rho-GTPase centralistic view specific functions and localizations to certain members of this protein family: Accordingly, Rac1 is responsible for membrane protrusion, Cdc42 for generation of filopodia and RhoA establishes contractility and stress fibers (Burrige et al. 2004; Sahai & Marshall 2002; Ridley et al. 1992; Kozma et al. 1995; Nobes & Hall 1995)

Although in the last years it has turned out that Rho-GTPase signaling is more complex, this dogma still persists in literature (Figure 18).

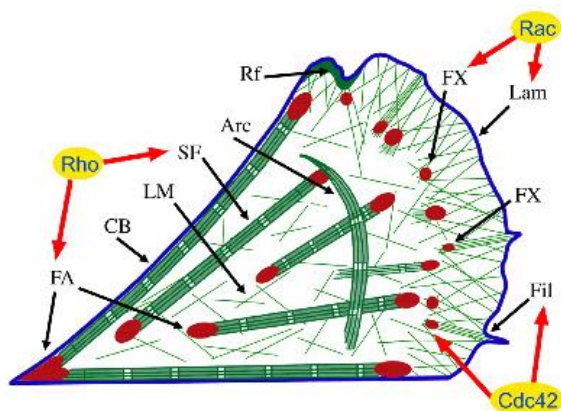


Figure 18: Scheme of a fibroblast, indicating the Rho-family members involved in signaling according to (Ridley et al. 1992).

Abbreviations: FX, focal complexes; FA, focal adhesions, Lam, lamellipodium; Fil, Filopodium; SF, stress fibre bundle; CB, Concave bundle (essentially stress fibre bundle at non-motile cell edges); Arc, arc shaped bundles sometimes observed under the dorsal cell surface; LM, loose meshwork of actin filaments; Rf, adapted from (Kaverina et al. 2002).

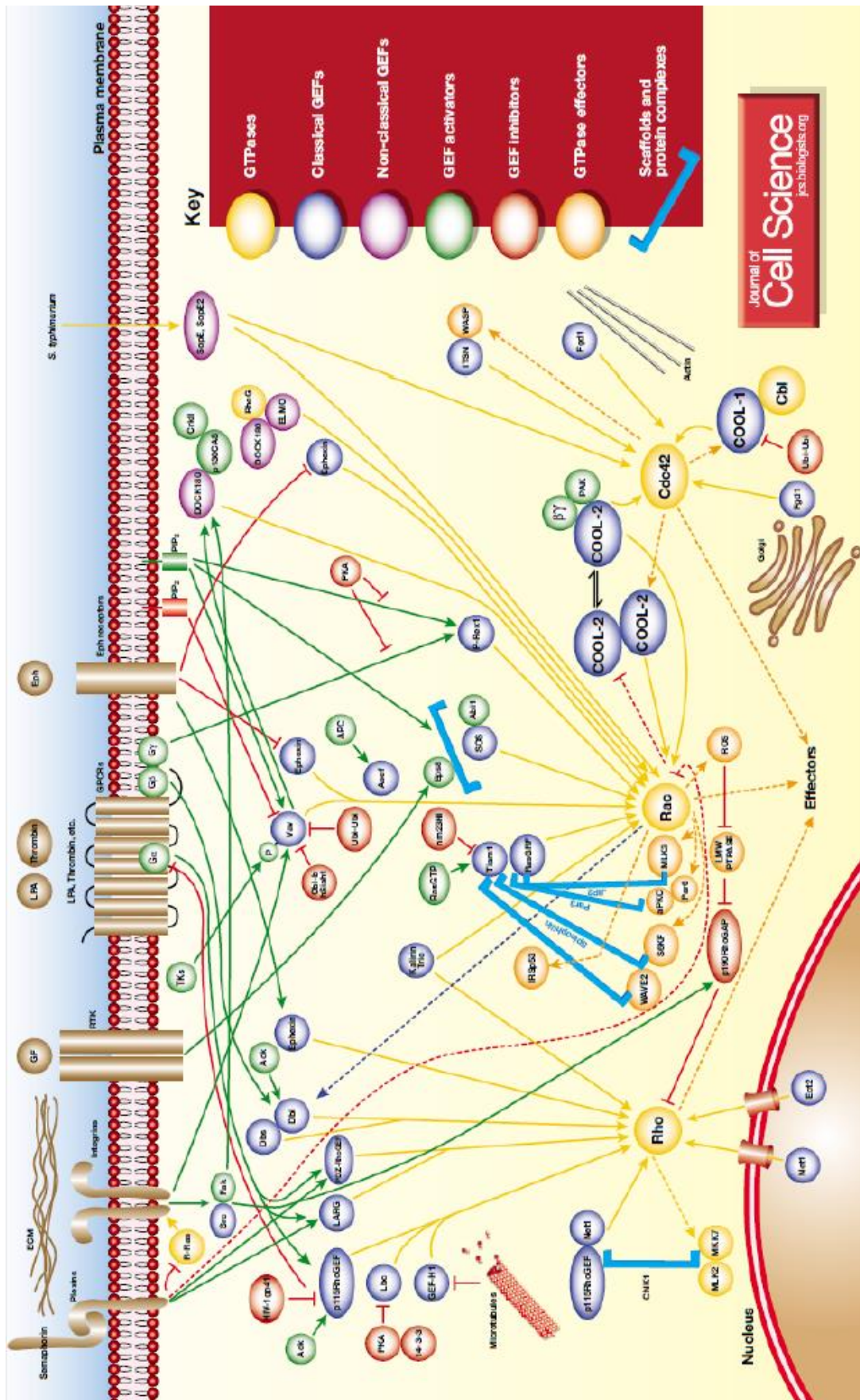


Figure 20: Rho GTPase activation. Excerpt of pathways and proteins involved in Rho-GTPase activation. (Buchsbaum 2007).

2.3.1. The Rho-GTPase Cycle

Rho-GTPases act as molecular switches and cycle between an active (GTP-bound) and inactive (GDP-bound) form (Figure 19). This process is crucial for transient signaling to their downstream effectors including kinases, enzymes and cytoskeletal regulatory proteins and is thus strictly controlled through a variety of upstream regulators.

Rho-GTPases are regulated according to signaling inputs by three classes of proteins:

- 1) Guanine nucleotide exchange factors (GEFs)
- 2) GTPase activating proteins (GAPs)
- 3) Rho GDP dissociation inhibitors (Rho GDIs)

1.) Active GTP-bound Rho-GTPases interact with over 60 GEFs exchanging GTP by GDP. These effector proteins mediate their catalytic activity via Dbl homology (DH) domains, which stabilize GTP free intermediates and trigger exchange of GDP to GTP. Adjacent to the DH domain, GEFs contain a pleckstrin homology (PH) domain C-terminally. The PH domain has regulatory functions in respect to the DH domain, including modulation and exchange activity, protein and phospholipid interactions or membrane targeting (Figure 20) (Buchsbbaum 2007).

2.) Over 70 different GAPs are involved in hydrolysis of GTP to GDP and thereby inactivate Rho-GTPases.

3.) Rho GDIs stabilize the GDP-bound state, maintaining an inactive pool of Rho GTPases in the cytoplasm.

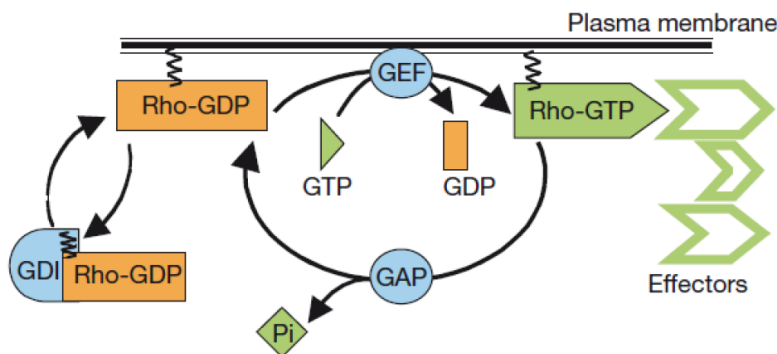
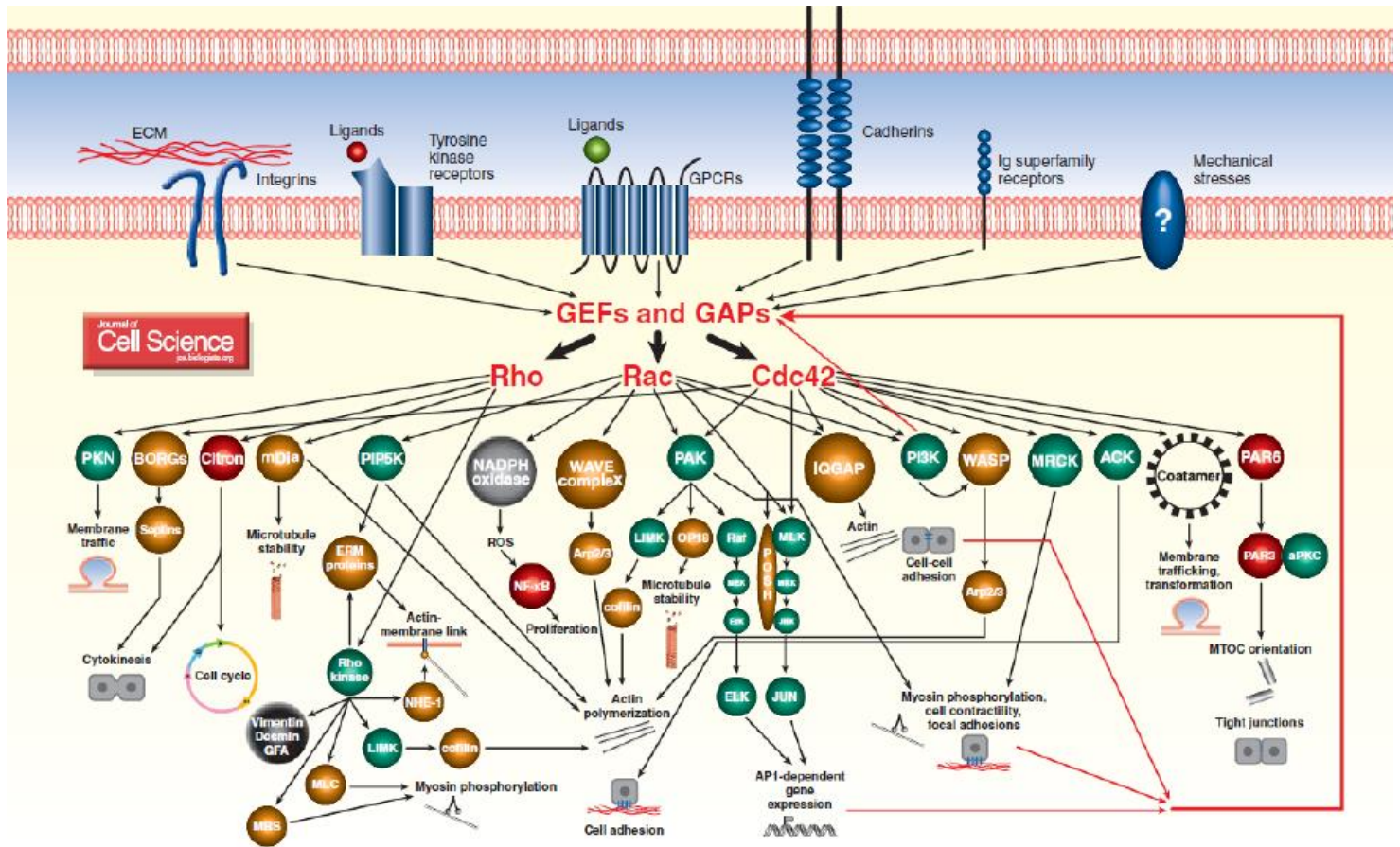


Figure 19: The Rho-GTPase cycle. Active Rho-GTPase (green) is bound to GTP and phosphorylates effectors. Next, it gets hydrolyzed by GAPs into the GDP loaded inactive form (orange). GDIs extract GDP loaded GTPases from the plasma membrane and keep them in the cytoplasm. GEFs exchange GDP by GTP and thereby activate the GTPase. (Etienne-Manneville & Hall 2002).

2.3.2. The Role of RhoA, Rac1 and Cdc42 in Cell Migration

Since, there is such a variety of Rho-GTPase signaling events (Figure 21), just a small selection can be discussed at that point. The illustration below should give an idea about the complexity of Rho-



GTPase signaling

Figure 21: Rho-GTPase signaling. Excerpt of downstream pathways targeted by Rho-GTPases. (Schwartz 2004)

2.3.2.1. RhoA

One primary target of RhoA is the protein Rho associated protein kinase (ROCK). ROCK phosphorylates other downstream targets including LIM kinase (LIMK), myosin light chain (MLC) and MLC-phosphatase.

LIMK is directly activated by ROCK and in turn inactivates the downstream actin depolymerization factors ADF/cofilin by phosphorylation (Maekawa 1999). Thus, LIMK is counteracting F-actin disassembly. Phosphorylation of MLC by ROCK leads to activation resulting in myosin contractility (Chrzanowska-Wodnicka & Burridge 1996; Amano et al., 1996). At the same time phosphorylation of MLC-phosphatase by ROCK positively influences myosin activity (Rho-kinase et al. 1996).

Furthermore, RhoA directly activates the nucleator mDia in order to generate unbranched actin filaments (Watanabe et al. 1999).

2.3.2.2. Rac1 and Cdc42

Rac1 triggers actin polymerization by activating the WAVE complex in two different ways:

The nucleation promoting factor WAVE associates with two Rac1 binding proteins (Nap125 and PIR121) and the adaptor proteins Abi1 and HSPC300 in a complex. Rac1 activity causes dissociation of this complex, leaving active WAVE and HSPC300 remain. Thus, activated WAVE triggers Arp2/3-actin polymerization. Additionally, Nck promotes by binding to Nap125 the dissociation of the complex and therefore positively effects WAVE activation (Eden et al. 2002). Alternatively, WAVE can be activated by Rac1 via interaction with IRSp53 (Miki et al. 2000). Furthermore, Rac1 as well as Cdc42 signal via PAK1 and regulate several downstream effectors. Several PAK1 substrates are known, including the actin binding protein filamin, LIMK, myosin, the paxillin/PIX/PKL complex and the adaptor protein Nck (Burridge et al. 2004).

Filamin acts as major actin binding protein in the cell cortex and in ruffles respectively (Vadlamudi et al. 2002) and represents a key element in versatile cytoskeletal remodeling (Ohta et al. 2006).

Another downstream target of PAK1 is LIMK (Edwards et al. 1999). LIMK in turn inactivates the actin severing protein cofilin by phosphorylation, leading to stabilization of F-actin filaments.

Moreover, PAK1 is associating with PIX, which is known to be a GEF for Rac1 and Cdc42, suggesting a positive signaling feedback loop (Turner et al. 2001). PAK1 interacts as well with the adaptor protein Nck, which recruits PAK1 to RTKs and promotes actin polymerization as mentioned previously (Bokoch 2003).

Rac1 is also positively influencing generation of reactive oxygen species (ROS) (Gianni et al. 2008): Binding of Rac1 to p67 PHOX activates NADPH oxidases, while generated ROS further mediates activation of NF- κ B-dependent gene expression (Schwartz 2004). Both, Rac1 and Cdc42 are important in activation of Jun N-terminal kinase (JNK) and p38 and thus stimulate AP-1-dependent gene expression.

Further Rac1 and Cdc42 activate PI3-kinase resulting in production of 3'-phosphorylated lipids, which stimulate again Rac1-GEFs and induce therefore a positive feedback loop (Schwartz 2004).

2.3.3. Questioning the Dogma of Rho-GTPase Signaling

Early studies led to a Rho-GTPase centralistic model, where each Rho-GTPase was assigned to a specific structure and function. For instance, Cdc42 was supposed to be solely responsible for filopodia formation, Rac1 for membrane protrusion and RhoA for control of contractility at the cell rear (Burridge and Wennerberg, 2004). This concept has emerged from observations based on global experimental manipulations such as over expression of dominant negative or dominant positive Rho-GTPase mutants. These Global manipulations ignore the fact that Rho-GTPase signaling cascades are interconnected and cross-talk at various levels. Therefore, a dominant positive mutant of a certain Rho-GTPase can shift the balance of a whole network and lead to artificial phenotypes and signaling phenomena.

After establishment of biosensors used to study Rho-GTPases on a single cell basis in live cell imaging experiments, the obtained results were inconsistent with previous findings based on population based biochemical measurements.

What causes this inconsistency between biosensor data and global manipulation approaches?

- Rho-GTPases regulate cytoskeletal dynamics in cells happening in spatial scales of microns and in timescales of seconds, while Rho-GTPase signaling happen in similar spatio-temporal scales. Considering the spatio-temporal function of Rho-GTPases, it is obvious that global measurements are not able to capture these signaling events. Thus, tools meeting these requirements need to be applied to resolve spatio-temporal Rho-GTPases activity fluctuations. Considering, that Rho-GTPase activities can vary tremendously within a cell depending location and morphodynamic state, biochemical assays such as pull down experiments on a population basis have to be questioned critically. However, it was even shown that robust phenotypical changes caused by stimulation led at most to an increase of 5% of the total pool of RhoA at a certain time (Ren et al., 1999). For Rac1 and Cdc42 was reported to be activated at similar proportions as RhoA within cells (Bernard et al., 1999)
- Rho-GTPase signaling comprises highly complex networks involving 20 Rho family GTPases, 80 GEFs, 80 GAPs and a plethora of downstream effectors. These proteins are ubiquitously expressed in a cell and consequently need to be tightly regulated in a spatio-temporal manner to act at the right time and space. So far, most approaches dealt with single components studying them one by one, while precluding interactions among them. As well, these studies used a variety of different cell systems hampering fair comparisons. Only systems biology approaches can account for this network complexity.

2.3.4. Latest Concepts of Rho-GTPase Signaling

In 2006 confusion in the Rho-GTPase signaling community was created by results obtained with a RhoA biosensor (Pertz et al. 2006). In contrary to the dogma of Rho-GTPase signaling, RhoA was not solely found at the back of migrating fibroblasts, but also at the leading edge. Surprisingly, several morphodynamic structures such as membrane ruffles, macropinosomes, membrane protrusions and retracting tails showed high RhoA activity too (Figure 22A). These results could not be explained anymore by a Rho-GTPase centralistic model. In a revised hypothesis, Rho-GTPases are considered to interact with a variety of GEFs and GAPs at different time points and locations in the cell. This hypothesis, organizing Rho-GTPase signaling events in spatio-temporal signaling modules, explains how one Rho-GTPase can be activated during diverse morphodynamic events. Supporting this model, it was shown using the technique of FRET and fluorescence lifetime imaging (FLIM) that one specific GTPase interacts with two different downstream effectors (Figure 22B) (Parsons et al. 2005).

This spatio-temporal Rho-GTPase signaling hypothesis was even extended by the finding that distinct Rho-GTPases co-operate in order to fine tune cytoskeletal dynamics. Taking advantage of computational multiplexing approaches, it was shown that RhoA, Rac1 and Cdc42 are activated in defined zones along the leading edge at different time points (Figure 22C) (Machacek et al. 2009).

Further complexity was introduced due to the finding, that similar morphodynamic events show diverse Rho-GTPase signaling characteristics. Upon PDGF stimulation, the leading edge showed no RhoA activity in contrast to unstimulated cells, where RhoA activity was elevated at the cell edge (Figure 22D) (Pertz et al. 2006). This leads to the assumption, that different Rho-GTPase signaling dynamics are involved in similar dynamic processes like edge protrusion. Presumably at the same time these morphodynamic structures are different in architecture and fine dynamics.

A complex interplay of Rho-GTPase signaling dynamics was observed during wound healing in single *Xenopus* oocytes (Benink & Bement 2005). Mutually exclusive activation zones of RhoA and Cdc42 moved inwards following the actin array during wound closure (Figure 22E)

During maturation of phagocytic cups, very specific Rho-GTPase signaling patterns were identified. Monitoring Cdc42 activity, activation during the first phase of particle binding was shown, followed with a time delay by activation of Rac1 at the same location. While, during onset of phagosome closure Rac1 gets another time activated along the inner phagosomal membrane, Rac2 is only active at the base of this structure (Figure 22F) (Hoppe & Swanson 2004).

Within the last ten years and technological inventions such as FRET based biosensors, it has emerged that Rho-GTPase signaling comprises high complexity. It was found that Rho-GTPase signaling and morphodynamic events are linked and therefore of Rho-GTPase signaling events need to be studied in a spatio-temporal context. Furthermore, cross-talk between Rho-GTPases via GAPs and GEFs increase this complexity pointing out that a conceptual view of signaling networks instead of separated pathways is needed in order to draw valid conclusions.

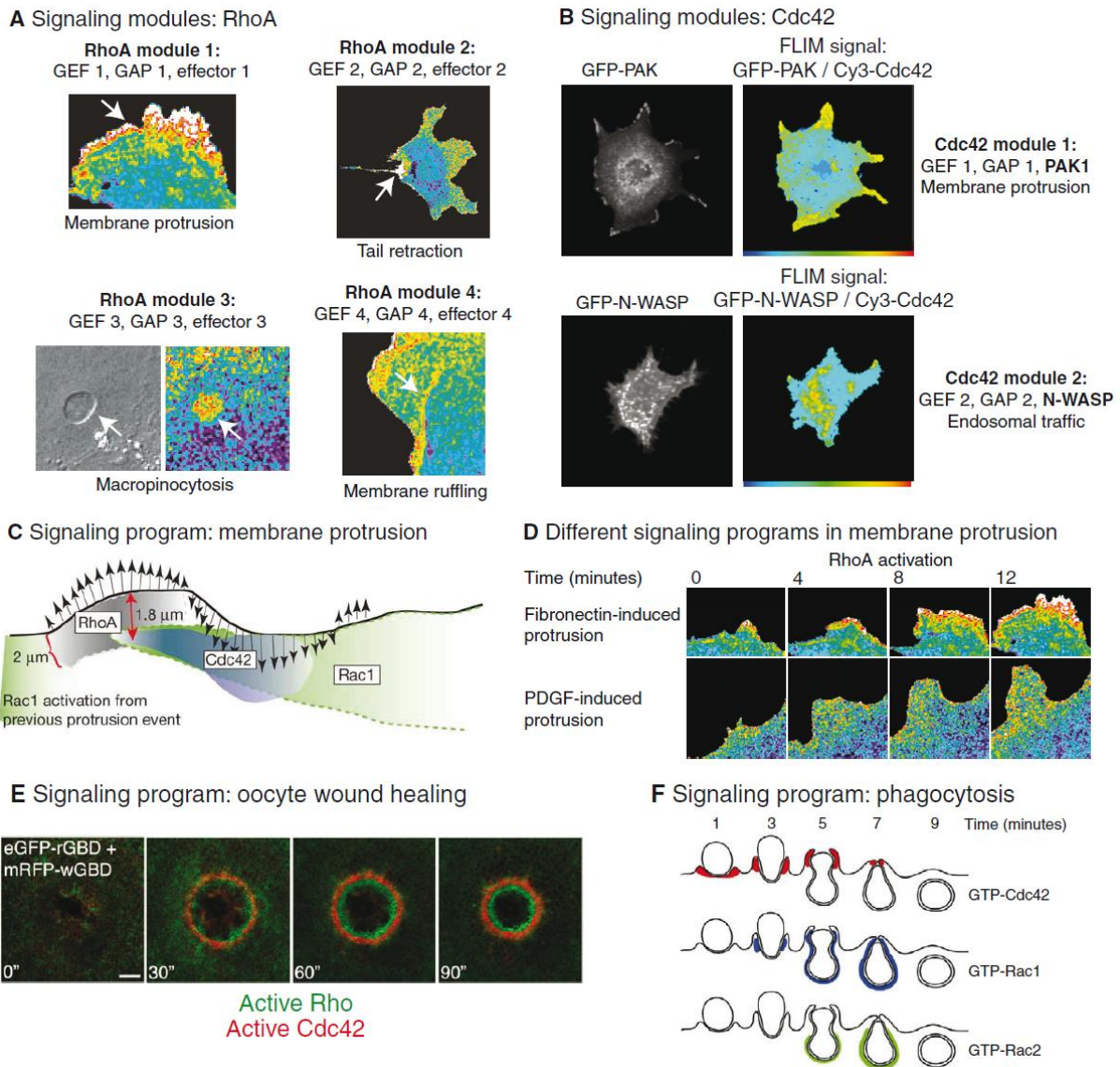


Figure 22: Visualizing spatio-temporal Rho GTPase signaling. (A) RhoA activation patterns during cell migration, as visualized with a FRET RhoA sensor (Pertz et al., 2006). Different morphogenetic behaviors are shown. The RhoA activation signal is coded so that 'warm' and 'cold' colors represent regions of high and low activation, respectively. White arrows point to the specific subcellular zones at which RhoA is activated. Image reproduced from Pertz et al. (Pertz et al., 2006) with permission. (B) Differential coupling of Cdc42 with different effectors at different subcellular locations. The interaction of a GFP-tagged effector and Cy3-labeled Cdc42 is measured using FLIM (Parsons et al., 2005). The images are color coded so that warm colors represent regions where each effector interacts with Cdc42 (red and yellow, interaction with effector; blue, no interaction). Image reproduced from Parsons et al. (Parsons et al., 2005) with permission. (C) Model of the dynamic spatio-temporal activation profiles of Rac1, Cdc42 and RhoA during leading-edge membrane protrusion (Machacek et al., 2009). The black line represents the leading-edge boundary, and arrows indicate membrane protrusion and retraction behavior. Different-colored zones represent RhoA (grey), Cdc42 (blue) and Rac1 (green) activation. Image reproduced from Machacek et al. (Machacek et al., 2009) with permission. (D) Different RhoA GTPase signaling patterns during membrane protrusion induced by fibronectin or PDGF stimulation (Pertz et al., 2006). Images are color coded as in A. Image reproduced from Pertz et al. (Pertz et al., 2006) with permission. (E) Cdc42 and RhoA activation zones during wound healing of a *Xenopus* oocyte. eGFP-rRBD, GFP fusion to the effector domain of rhotekin; mRFP-wGBD, mRFP fusion to the effector domain of WASP. Image reproduced from Benink and Bement (Benink and Bement, 2005) with permission. (F) Model of Cdc42, Rac1 and Rac2 activation during phagocytic uptake of an IgG-opsonized erythrocyte (Hoppe and Swanson, 2004). Each different-colored zone represents the activation pattern of one specific GTPase. Image reproduced from Hoppe and Swanson (Hoppe and Swanson, 2004) with permission. **Pertz, 2010**

3. Main Results

Growth-factor-induced, persistent fibroblast migration is mediated by mechanical insulation of cell front and back

Katrin Martin¹, Marco Vilela², Noo Li Jeon³, Gaudenz Danuser², Olivier Pertz¹

¹ Institute for Biochemistry and Genetics, Dept. Biomedicine, University of Basel, Mattenstrasse 28, 4058 Basel, Switzerland

² Department of Cell Biology, Harvard Medical School, 240 Longwood Avenue, LHRB, 301B Boston, MA 02115, USA

³ School of Mechanical and Aerospace Engineering, Seoul National University, Seoul, 151-742, Republic of Korea

*To whom correspondence should be addressed:

Olivier Pertz, Dept. of Biomedicine, University of Basel, Mattenstrasse 28, 4058 Basel, Switzerland

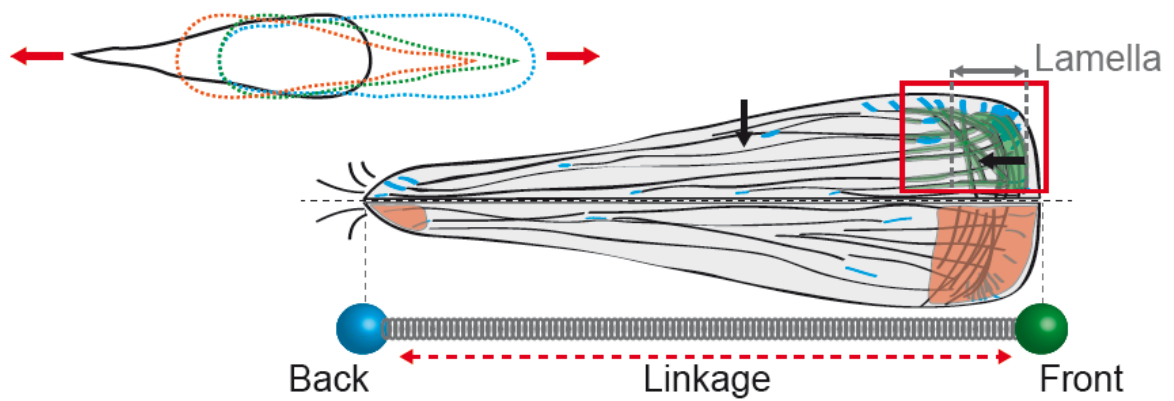
Phone: +41 61 267 22 03; Fax: +41 61 267 35 66; E-mail : olivier.pertz@unibas.ch

3.1. Abstract

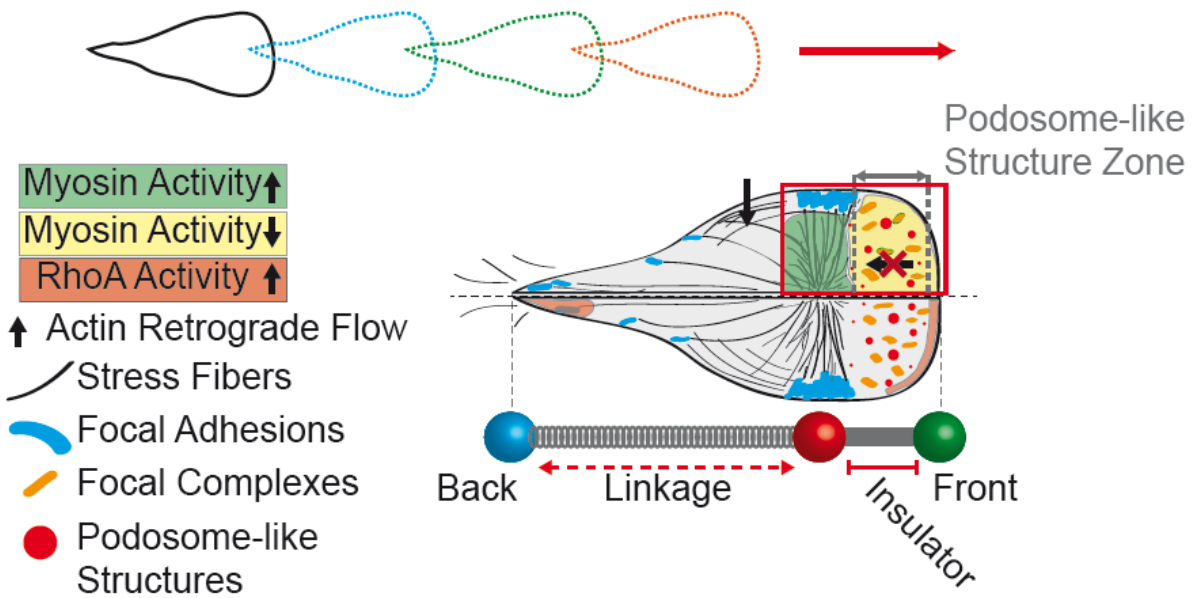
Directional migration requires robust front/back polarity. We find that fibroblasts treated with platelet-derived growth factor (PDGF) and pre-polarized by plating on a fibronectin line substrate, exhibit persistent migration for hours. This does not occur in the absence of PDGF, or on uniformly-coated fibronectin substrates. Persistent migration arises from establishment of two functional modules at cell front and back. At the front, membrane protrusions trigger the formation of a zone containing podosome-like structures (PLS), which locally inhibits RhoA-dependent activation of myosin, and formation of a contractile lamella. At the back, myosin contractility controls tail retraction with minimal crosstalk to the front module. The PLS zone is maintained in a dynamic equilibrium that preserves size and position relative to the cell front, allowing long term coordination of front and back modules. We propose that front/back mechanical insulation achieved by the PLS zone is crucial for persistent migration in absence of directional cues.

3.2. Visual Abstract

Haptokinesis



Chemokinesis



3.3. Introduction

Cells directionally migrate in response to gradients of immobilized (haptotaxis) or diffusible (chemotaxis) cues (Parsons et al., 2010). Extracellular matrix (ECM) rigidity or dimensionality can also modulate this process (Petrie et al., 2009). Combinations of these cues will affect parameters such as cell speed, shape, and directionality, producing a continuum of cell migration modalities (Friedl and Wolf, 2010). While the diversity of cell migration modalities is well accepted, they have been described in a wide variety of different model systems making fair comparisons difficult. Accordingly, our understanding as to how the dynamics of the migration machinery is modulated to establish particular migration modes is still limited.

Fibroblasts are large mesenchymal cells that are mostly involved in tissue repair. Due to their well-defined cytoskeleton organization, they have been a popular model system to study actin and adhesion dynamics during cell migration. At the front, two cytoskeletal modules are coupled with integrin-based adhesion structures to allow cell propulsion (Ponti et al., 2004). The lamellipodium uses Arp2/3 mediated assembly of an actin dendritic meshwork to propel the leading edge forward (Pollard and Borisy, 2003). Nascent adhesions are formed and can mature into focal complexes (FCs). Behind the lamellipodium, the lamella consists of bundled actin and non-muscle myosin II filaments that provide a contractile network for traction. Here, FCs mature into stress fiber-linked, elongated focal adhesions (FAs), that exhibit sliding motions (Parsons et al., 2010). Linkage of front and back FAs through stress fibers, coupled with propulsion of the leading edge, moves the cell forward, and leads to disassembly of back FAs and tail retraction. Podosomes are an additional type of adhesions that consist of a central actin core associated with integrins and other proteins (Murphy and Courtneidge, 2011). They are observed in a wide variety of immune and cancer cells (Calle et al., 2006), and are also found in Src-transformed fibroblasts (Oikawa et al., 2008). Podosome substrate interaction leads to localized protease secretion and local ECM degradation, enabling invasion.

One important limitation of fibroblasts is their moderate capability to robustly polarize during random migration on uniform ECM fields (haptokinesis) or in response to global growth factor stimulation (chemokinesis). Thus, on planar ECM substrates, unrestricted membrane protrusion leads fibroblasts to adopt a wide variety of cellular shapes with various degrees of polarization. While this is sufficient to study the fine dynamics of membrane protrusion and tail retraction, it precludes the analysis of how both processes are coordinated to produce net movement. In vivo, fibroblasts interact with ECM structures of specific geometries and length scales that influence cell polarization (Kim et al., 2012). Hence, fibroblasts migrating on micrometric ECM line patterns exhibit increased migration speed and directionality (Doyle et al., 2009). Mimicking the anisotropic ECM organization observed in vivo therefore provides an opportunity to induce robust fibroblast polarization.

Rho family GTPases are key regulators of the spatio-temporal organization of actin and adhesion dynamics during cell migration. While initial models suggested that Rac1 and Cdc42 operate at the front to regulate membrane protrusion, and RhoA functions at the back to control tail retraction

(Burridge and Wennerberg, 2004), recent studies using fluorescence resonance energy transfer (FRET)-based biosensors have indicated a higher level of signaling complexity (Machacek et al., 2009; Pertz et al., 2006). Most importantly, RhoA signaling is also active at the cell front, where during fibroblast haptokinesis, two distinct activities are observed: Adjacent to the leading edge, a focused region of RhoA activity is coupled to the initiation of edge protrusion (Machacek et al., 2009). This is followed by a broader gradient of RhoA activity reaching 10 – 15 μ m into the lamella (Pertz et al., 2006). Rac1 and Cdc42 are also activated at the front, however, with a delay relative to protrusion onset (Machacek et al., 2009). This organization is fundamentally altered when fibroblasts are acutely stimulated with platelet derived growth factor (PDGF), which leads to heightened cell edge protrusion and membrane ruffling. Here, RhoA activity is displaced from the leading edge (Pertz et al., 2006), and supposedly replaced by heightened Rac1 and Cdc42 activity. Hence, dependent on the cue, different Rho GTPase signaling programs are activated to induce distinct modes of cell migration.

In this paper, we dissect the mechanisms underlying the differences of fibroblast haptokinesis and PDGF-induced chemokinesis on micropatterned fibronectin (FN) line substrates. We find that PDGF-treated fibroblasts exhibit persistent cell migration for hours. This is not observed during haptokinesis. PDGF chemokinesis correlates with the formation of a zone containing podosome-like structures (PLSs) directly behind the lamellipodium. PLSs inhibit RhoA-dependent myosin contraction and preclude the formation of a lamella. Instead, myosin activity is concentrated behind the PLS zone to promote tail retraction. Thus, PLSs mediate the formation of two mechanically insulated modules, one for membrane protrusion, and one for tail retraction, enabling persistent migration.

3.4. Results

PDGF induces persistent migration of pre-polarized fibroblasts

To compare the haptokinetic (hapto) and PDGF-induced chemokinetic (chemo) cell migration modes, we used REF52 rat embryonic fibroblasts, a classic model system to study actin and adhesion dynamics (Zamir et al., 1999). Throughout this work, we used the following conditions: serum-starved REF52 fibroblasts were plated on 10 μ g/ml FN-coated coverslips in absence (hapto) or presence of 40 ng/ml PDGF (chemo). On uniformly coated plane substrates, both hapto and chemo fibroblasts migrate randomly with instantaneous velocities of \sim 10 μ m/hour (Figure 1A, B). Although not significant at the population level, a fraction of chemo cells displayed increased directional persistence (Figure 1B). To normalize cell shape and mimic the anisotropic nature of the ECM observed in vivo, we used plasma etching to construct 20 μ m wide 10 μ g/ml FN lines separated by the non-adhesive compound poly-L-Lysine-polyethylene glycol (PLL-PEG) (Figure S1A). This allowed FN coating at a density identical to the coat on the plane substrate (Figure S1B, C). Fibroblasts on line substrates adopted an elongated morphology (Figure 1A and C). Hapto cells exhibited similar velocity and persistence to hapto cells on plane substrates (Figure 1B and D). In contrast, chemo cells gradually sped up on line substrates, reaching a 5-fold increase in cell velocity within hours after plating in presence of PDGF. At this time point, a steady state was reached, with chemo cells stably migrating in one direction (Figure 1B-E, Movie S1). Both steady state speed and persistence scaled inversely with the FN coating density (Figure S1D and E). The differences between hapto and chemo cells in terms of migration properties was accompanied by acquisition of distinct cell morphologies. Hapto cells were elongated and flat, and displayed a wide variety of spreading and morphological states (Figure 1A,C,F). Chemo cells, on the other hand, displayed a persistent polarized shape that consisted of a flat leading edge, a thick cell body and an obvious trailing edge (Figure 1F). Together, these results show that PDGF stimulation of fibroblasts, that are pre-polarized on a FN line substrate, induces rapid, persistent and unidirectional cell migration for hours.

Polarization of chemo cells involves a morphological transition with uncoupling of front and back motions

The cell shape normalization on the line substrate enabled us to unambiguously define cell front and back and thus to study how front and back are coordinated. For that purpose, we acquired timelapse sequences of fibroblasts stably expressing the F-actin marker Lifeact-green fluorescent protein (GFP) (Riedl et al., 2008) with a 20x objective. We then designed an automated segmentation algorithm to evaluate the dynamics of front, centroid and back parts (Figure 2A,B, Movie S2, Supplemental Information). Hapto cells continuously exhibited left and right motions, impeding cell polarization (Figure 2C). In contrast, few hours after spreading, chemo cells displayed a stably polarized state of persistent migration (Figure 2C). This correlated with increased velocity and decreased cell length, whereas these parameters remained constant throughout time in hapto cells (Figure 2D).

We then evaluated the coordination between cell front and back movements by performing time-dependent cross-correlation analysis of velocity fluctuations (Figure 2E,F; Supplemental information and Figure S1F). Hapto cells displayed transient episodes of strongly positive and strongly negative cross-correlations, where front and back move coordinately in identical or opposite directions. This indicates that at least during episodes of co-movement, front and back are mechanically-linked. In contrast, chemo cells did not exhibit robust positive or negative cross-correlations, suggesting that front and back movements are uncoordinated and mechanically uncoupled. Thus, establishment of the steady state of persistent migration in chemo cells occurs on time scales of hours, and involves a morphological transition that correlates with increased velocity. Furthermore, the polarized steady state of chemo cells correlates with uncoupling of front and back motions.

Chemo cells display podosome-like structures at the leading edge

The distinct cell morphologies suggest that hapto and chemo cell migration modes are mediated by different cytoskeletal and adhesion dynamics. To test this we employed high-resolution immunostaining and live cell imaging by epifluorescence (EPI) and total internal reflection fluorescence (TIRF) microscopy. Transiently polarized hapto cells displayed asymmetric distributions of front-enriched, stress fibers and FAs (Figure 3A). A network of transverse stress fibers connected leading edge and lateral FAs, while a lower amount of FAs was observed at the trailing edge. FAs at front and back were connected by lateral stress fibers. In contrast, stably polarized chemo cells overall had less stress fibers (Figure 3B). A large region at the leading edge displayed dotted F-actin structures reminiscent of podosomes (PLSs, Figure 3B, red arrowheads). Although PLSs did not display the bona fide F-actin core surrounded by a ring containing adhesion structures (Albiges-Rizo et al., 2009), they displayed proteolytic activity on a gelatin line substrate (Figure S2A), and contained very low amounts of adhesion components as visualized by expression of vinculin-GFP (Figure S2B). Within the PLS zone, we also observed vinculin-containing adhesions not connected to stress fibers (Figure 3B, yellow arrowheads) reminiscent of FCs, but FAs were absent. Immediately behind the PLS zone, TIRF microscopy revealed a network of ventrally localized transverse actin fibers (Figure 3B, white arrowhead). The network was not connected to any adhesion structure in the cell center, but associated with elongated FAs confined to the lateral edges and the back of the cell (Figure 3B, blue arrowheads). Overall, such organization with a PLS zone was observed in 70 % of chemo cells on lines (Figure S2C). These results indicate the existence of different actin and adhesion structures in hapto and chemo cells.

Chemo cells lack a contractile lamella

We subsequently monitored actin dynamics in both cell migration modes using the F-actin marker Lifeact-GFP (Movie S3). In hapto cells, the lamellipodium remained continuously attached to the substrate leading to a highly adherent mode of membrane protrusion (Figure 3C, right panels). Formation of actin arcs (Hotulainen and Lappalainen, 2006) indicated robust actin retrograde flow in the lamella as well as on the lateral sides (Figure 3C, kymographs 1 and 2, quantitated in Figure 3E).

In marked contrast, in chemo cells, the lamellipodium was characterized by rapid bursts of filopodial and membrane protrusions that escaped the TIRF illumination field. This indicates a low adhesive protrusion mode as these structures extend in Z before contacting the substrate (Figure 3D, right panels). Directly behind the lamellipodium, the lamella was replaced by the PLS zone (Figure 3D, kymograph 1). Neither TIRF, nor epifluorescence imaging of the leading edge indicated the presence of actin arcs or actin retrograde flow at this location. Live cell imaging also revealed that PLSs specifically originate in the lamellipodium that extends on the permissive FN substrate, remain immobile with respect to the substrate (Figure 3D, kymograph 1, white arrowheads) and display a lifetime of about 10' (Figure 3I). Accordingly, the PLS zone remained constant in size (Figure 3D, dotted white lines in kymograph 1). Robust actin retrograde flow persisted on the sides as observed by inward flow of lateral arcs (Figure 3D, kymograph 2, quantitated in Figure 3E).

We then visualized adhesion dynamics (Figure 3F-I, Movie S4), and noticed that chemo cell polarization and formation of the PLS zone was highly sensitive to exogenous expression of GFP-tagged cytoskeletal or adhesion proteins, even when stably expressed at low level. This required two-color imaging experiments, in which we first produced stable cell lines using a lentiviral system for the expression of GFP-tagged proteins, then used an adenovirus system to co-express Lifeact-mCherry for identification of polarized chemo cells. We tested a number of different constructs, and found that VASP-GFP was the adhesion marker that was least perturbing. In hapto cells, FCs immediately converted to FAs after interaction with stress fibers (Figure 3F-H, Hapto, blue arrowheads). These FAs displayed typical centripetal sliding behavior (Figure 3H) with a lifetime of approximately 30' (Figure 3I). Chemo cells displayed both PLSs and FCs at the leading edge. Non-motile PLSs grew and shrunk in lateral extension-contraction cycles (Figure 3G,H, red arrowheads). Within the PLS zone, VASP-GFP revealed that FCs also remained immobile relative to the substrate (Figure 3G,H, yellow arrowheads) and almost never matured into FAs. Thus, they display identical lifetimes as PLSs (Figure 3I). Elongated FAs were only observed on the lateral edges and at the back of the cells, and exhibited sliding motions (Figure 3H, chemo, blue arrowheads) when pulled on by the stress fiber array emanating from the cell center (Movie S4). Together, these results indicate that the contractile lamella observed in hapto cells, is replaced by the PLS zone in chemo cells. Absence of a contractile lamella inhibits FC maturation to FA within the PLS zone, leads to their turnover, and restricts FAs to the back and lateral sides of the cell.

The PLS zone also occurs in PDGF-treated fibroblasts on plane substrates

We wondered whether PDGF stimulation would also promote PLS formation in fibroblasts migrating on unrestricted plane substrates. Chemo cells displayed PLS containing regions also in this case, but these were intermixed with stress fibers and FA arrays (Figure S2D). In contrast, hapto cells displayed prominent concentric stress fiber arrays throughout their periphery (Figure S2D). This demonstrated, that on plane substrates, chemo cells develop a hybrid morphology consisting of features prominently present in chemo cells on line substrates and hapto cells on plane substrates. Chemo cells displayed a lower aspect ratio compared to hapto cells (hapto: 0.27 ± 0.06 , $n = 13$ cells; chemo: 0.17 ± 0.04 , $n = 16$ cells, $***P < 0.0001$) indicating a higher level of polarization. Evaluation of the ratio of adhesive over

total cell surface (TIRF over EPI signal of a plasma-membrane localized GFP-CAAX construct) showed that chemo cells had less substrate contact than hapto cells on both the plane and line substrate (Figure S2E and F). Live imaging revealed that these PLS zones exhibited lateral scanning motions throughout the chemo cell on a timescale of hours (Figure S2G).

Robust actin retrograde flow in hapto cells led to rapid FA maturation; however these FAs displayed shorter lifetimes than on the line substrate (Figures S2H-K, hapto). In chemo cells, PLS zones were surrounded by regions of high actin retrograde flow with robust FA maturation (Figure S2H,I, chemo). Within the PLS zone, non-motile PLSs displayed much shorter lifetimes than on the line substrate and FCs did not mature to FAs (Figure S2I-K). These results show that on the plane substrate, the PLS zone performs scanning motions throughout the cell, but promotes mild cell polarization because it inhibits contractile networks only locally. On the line substrate, PLSs scanning is geometrically confined, allowing the PLS zone to efficiently inhibit lamella formation at the leading edge, and establish robust front/back polarization.

Hapto and chemo cells display different leading edge dynamics

We next investigated the dynamics of the leading edge in high resolution time lapse sequences sampled at 5 seconds per frame. We quantified the dynamics of edge protrusion and retraction as previously described (Machacek and Danuser, 2006). Protrusion velocity maps were generated for hapto and chemo cells both on plane and line substrates (Figure 4A-D) and statistically evaluated (Figure 4E-G). Hapto cells on the plane substrate displayed poorly protrusive edges, with low velocities and no obvious persistence (Figure 4A). Spatial clustering of locally measured edge velocities revealed two populations of edge dynamics in chemo cells on the plane substrate. Remarkably, they specifically associated either with the PLS zone (red edge) or contractile networks (blue edge) (Figure 4B). While the velocity of the PLS-associated edge was enhanced, it displayed low protrusive persistence, but still promoted efficient net protrusion. The contractile edge displayed similar properties as those observed for edges in hapto cells (which had only one type of protrusion dynamics). On the line substrate, hapto cells displayed a slight enhancement of edge velocity and protrusion persistence (Figure 4C). Chemo cells displayed enhancement of both protrusion persistence and velocity, resulting in a higher net protrusive activity (Figure 4D, red edges). These results indicate that the non-contractile PLS zone associates with a highly protrusive leading edge, prominently on line substrates, but present also locally on plane substrates.

Chemo cells assemble a myosin cluster directly behind the PLS zone for trailing edge retraction

The absence of a contractile lamella in chemo cells raised the question of their migration dependence on non-muscle myosin II (myosin) based contractility. To address this, we evaluated the subcellular localization and dynamics of myosin light chain 2a (MLC2a), and of its active Ser19 phospho-state (pMLC). In hapto cells, MLC2a prominently decorated stress fibers (Figure 5A, Hapto), while pMLC additionally labeled the lamella (Figure S3A, Hapto, red arrow). Identical patterns were observed on plane substrates (Figure S3B, Hapto). In contrast, in chemo cells, both MLC2a and pMLC were absent

from the cell front, and localized to a cortical cluster positioned behind the PLS, that coincided with the transverse stress fiber array that connects to FAs at the lateral sides and back of the cell (Figure 5A and Figure S3A, Chemo, red arrow). Outside the cluster, faint MLC2A staining remained present on these stress fibers. On the plane substrate, chemo cells displayed mixed pMLC patterns: pMLC localized both as a cluster adjacent to the PLS zone, as well as to peripheral contractile arrays (Figure S3B, Chemo). Live imaging of MLC2a-GFP and Lifeact-mCherry dynamics revealed constant association between MLC2a and stress fibers in hapto cells (Figure 5B and C, Hapto). In chemo cells, apposed but mutually exclusive PLS and MLC2a zones of constant size occurred throughout cell migration (Figure 5B and C, Chemo).

To test the functional significance of myosin-based contractility, we used blebbistatin to acutely inhibit myosin ATPase activity (Straight et al., 2003). Whole cell kymograph analysis showed that hapto cells lost their transient polarized state by extending uncontrolled membrane protrusions in all directions (Figure 5D, Movie S7), which correlated with a decrease in front/back coordination (Figure 5F). Chemo cells were specifically impaired in tail retraction, but displayed almost unaffected leading edge membrane protrusion (Figure 5E). This confirms that in these cells, PLSs establish functionally distinct cytoskeleton structures, one without (front), and one with (back) myosin-driven contractility. In agreement with these observations, blebbistatin treatment led to loss of the pMLC cluster in chemo cells without affecting PLSs (Figure S4A). On a time scale of 12 hours, loss of myosin-based contractility decreased chemo cell migration persistence without affecting velocity (Figure 5G-H). This occurred because of extreme stretching of chemo cells that ultimately led to their turning. Blebbistatin-treated hapto cells displayed a decrease in velocity (Figure 5G-H). These results show that myosin activity occurs in the lamella and stress fiber network of hapto cells, and its inhibition deregulates overall edge protrusion and migration. In contrast, myosin activity in chemo cells is focused behind the PLS zone. Its inhibition only affects tail retraction while the lamellipodial machinery in front of the PLS remains intact.

The PLS zone specifically inhibits leading edge myosin contractility in chemo cells

The lack of myosin activity at the leading edges of chemo cells prompted us to explore if the PLS zone directly inhibits contractile function. To this end, we tested a panel of drugs, and identified the CK666 Arp2/3 inhibitor (Nolen et al., 2009) as the most potent compound to perturb PLSs. In both hapto and chemo cells, treatment with 200 μ M CK666 led to the appearance of spiky protrusions as previously described (Wu et al., 2012), indicative of the inhibition of the Arp2/3 pool necessary for lamellipodial protrusion (Movie S7). As expected, this correlated with decreased actin retrograde flow in the lamellipodium of hapto cells (Figure S4B), but only minimally affected adhesion dynamics (Figure 6A, Movie S8), as well as pMLC signals (Figure S4C, Hapto). In chemo cells, CK666 treatment led to rapid removal of PLSs, which was concomitant with immediate appearance of stress fibers and FAs at the leading edge (Figure 6A, Movie S8). pMLC signals relocated from the back of the PLS zone to the leading edge, in a pattern reminiscent of the lamella of hapto cells. CK666 treatment did however not revert chemo cells to a contractile state as intense as in hapto cells. At a global level, CK666 did not affect hapto cell morphodynamics with temporal cross-correlation analysis still indicating the presence

of front/back coordination (Figure 6B,C, Movie S7). Chemo cells however only remained polarized for approximately 1 hour after CK666 treatment, and then lost persistent migration (Figure 6C, Movie S7). During this polarized cell migration episode, strong front/back motion correlations were observed, suggesting that abrogation of the PLS permitted establishment of a mechanical link between the cell front and back (Figure 6C,D). These results indicate that the PLS inhibits lamella formation and mechanically insulates cell front and back.

PLSs locally inhibit RhoA to hinder lamella formation in chemo cells

Our previous findings of distinct RhoA signaling programs in hapto and chemo cells (Pertz et al., 2006) prompted us to explore RhoA activation dynamics in both cell migration modes, and to test whether perturbation of PLSs would affect the distribution of this signal. We employed RhoA2G, a novel FRET-based biosensor of RhoA activation (Fritz et al., 2013), and found again that acute stimulation with PDGF induced membrane protrusion concomitant with decreased RhoA activity (Figure S5A) (Pertz et al., 2006). In hapto cells, RhoA was activated as a broad gradient spanning the entire lamella with activity decreasing from the leading edge to the cell center (Figure 7A). A similarly broad RhoA activation gradient was observed in hapto cells on the plane substrate (Figure S5B). In chemo cells, RhoA activation was low in the PLS zone, with very low RhoA activity observed directly in the vicinity of PLSs (Figure 7B). A highly focused region of RhoA activity was however observed directly at the leading edge. In chemo cells on plane substrates, low RhoA activity dynamically correlated with PLS motion (Figure S5C). These evidences strongly suggest that PLSs locally inhibit RhoA activity. We then inhibited PLSs using the CK666 compound. In hapto cells, this treatment did not affect the broad gradient of lamellar RhoA activity (Figure 7C). In contrast, concomitant with CK666-induced PLS inhibition, we observed a broadening of the RhoA activation zone in chemo cells (Figure 7D). These results formally show that PLSs locally inhibit RhoA activation in chemo cells, allowing inhibition of myosin activity, ultimately impeding formation of a contractile lamella.

3.5. Discussion

PLSs serve as a spatially organizing module to polarize cells

Fibroblast migration has classically been studied on planar substrates with uniform coating that do not allow strong cell polarization. Here, we show that PDGF stimulation of pre-polarized fibroblasts in the absence of any gradient leads to persistent migration for hours. This is accompanied by a robust increase in migration velocity. Our results show that PDGF induces the formation of a PLS zone, which functions as a spatially organizing module that inhibits myosin contractility at the cell front. While the PLSs are not bona fide podosomes as described in macrophages (Calle et al., 2006) or in Src-transformed fibroblasts (Oikawa et al., 2008), similar structures have been observed before in NIH 3T3 fibroblasts (Collin et al., 2006). These PLSs have most likely remained elusive because they require hours to appear after PDGF stimulation. Moreover, on plane substrates, leading edge PLS zones (with an adjacent myosin activity zone) exhibit lateral "wave" scanning motions. This allows only moderate cell polarization, most likely because these zones inhibit the contractile networks observed throughout the cell periphery only in local subsectors. On line substrates, sustained persistent migration can be explained by two emergent properties of the system. First, fibroblast pre-polarization geometrically constrains the PLS zone proximal to the leading edge to inhibit lamella formation and to restrict contraction to the back of the cell. The establishment of a non-contractile, protrusive front, and a contractile back allows for front/back mechanical insulation and efficient cell symmetry breaking. Second, the dynamic properties of PLSs (Figure 3D,H) maintain the size of the PLS zone constant throughout time, making it a stable, spatially organizing module that coordinates front lamellipodium protrusion with back myosin retraction throughout the cell migration process. Similar spatially organizing cytoskeletal structures have already been proposed to regulate cytoskeletal polarity in neutrophils (Weiner et al., 2007). In the latter cells, the higher cytoskeletal plasticity, and the intrinsically asymmetric cell shape might explain the absence of a requirement for pre-polarization. It is worth mentioning that in absence of PDGF, persistent fibroblast migration also occurs on 1 μ m wide FN line substrate, which mimic 3D ECM dimensionality (Doyle et al., 2009). The 20 μ m wide line substrate studied in this work does not mimic physiological ECM dimensionality. Thus, both pre-polarization and PDGF stimulation, are required for persistent migration in our system. This suggests that persistent migration can be mediated by multiple, complementary pathways.

Unlike in neutrophil chemokinesis, acquisition of steady state chemo cell migration takes hours. While the sequence of events leading to formation of a self-sustained PLS zone at one of the two cell poles is not clear, we envision that the PLSs function as part of a stochastic symmetry breaking process. Upon PDGF stimulation, PLSs might gradually scan through the cell and locally inhibit the contractile cytoskeletal network observed in hapto cells, until the symmetry breaking process produces a steady state non-contractile lamellipodium in the front and a contractile tail retraction module in the back. The requirement of a structural scaffold, the PLS zone, for growth factor-induced cell polarization has important consequences for experimental analysis of this system. First, signaling events that regulate cytoskeletal dynamics during persistent migration cannot be perturbed before acquisition of a

polarized steady state. Instead, acute perturbations by pharmacological inhibition have to be used to study these pathways. Second, the outcome of acute growth factor stimulation is not informative before the polarized steady state is achieved. This is illustrated by the finding that leading edge RhoA activity decreases upon acute PDGF stimulation, but then is robustly activated directly in the lamellipodium in the steady-state of persistent cell migration.

Functional consequences of front/back mechanical insulation

An important feature of persistent chemo cell migration is the mechanical insulation of front and back. The current model for front/back coordination of fibroblast migration posits that contraction of stress fibers connected to FAs at the front generate forces on FAs in the rear, promoting disassembly and tail retraction (Parsons et al., 2010). In pre-polarized haptotactic cells, stress fiber arrays along the cell length indeed induce mechanical coupling between FAs in the lamella and FAs at the cell rear. However, this mechanical linkage admits only transient polarization episodes, and is insufficient to establish persistent migration. In chemo cells, the PLS zone inhibits the formation of a contractile lamella, and prevents FCs from maturation into FAs, which results in decoupling of front and back. Perturbation of the PLS zone using the CK666 compound leads to rapid rise of myosin activity at the cell front, which is accompanied by FA maturation. This translates into front/back mechanical coupling and ultimately to loss of persistent migration. This formally shows the need for a mechanical insulation of cell front and back for maintenance of cell polarity and persistent migration.

One consequence of front/back mechanical insulation is a concentration of myosin activity behind the PLS zone allowing tail retraction without affecting the protrusive activity of the cell front. This is supported by our finding that myosin inhibition leads to loss of tail retraction without affecting leading edge protrusion. Surprisingly, stress fibers emanating from behind the PLS are not anchored to any adhesion structure within the myosin cluster. Most likely the concentrated myosin zone generates tension through attachment to cortical actin. Importantly, chemo cells display lower levels of stress fibers and focal adhesions, as well as less substrate contact than haptotactic cells. Therefore, adhesion and contraction strength in these cells are adjusted, so that lower rear contractility is still sufficient to promote rear FA disassembly. Similar myosin clusters have been observed at the back but not at the front of neutrophils (Pestonjamasp et al., 2006) and fish keratocytes (Svitkina et al., 1997), which both migrate rapidly and highly persistently. Hence, we speculate that a rear-concentrated myosin module may be a general feature of rapid, persistent migration.

An additional consequence of front/back mechanical insulation is the appearance of a highly efficient mode of membrane protrusion at the cell front of chemo cells. This is characterized by a potent increase in protrusion velocity and persistence, enabling highly processive leading edge advancement. Here, the absence of a contractile lamella might optimize the functional output of the lamellipodial actin treadmill at the leading edge. Our data implies that the Arp2/3 complex is involved but not required for this membrane protrusion mode. Together, these observations suggest that front/back mechanical insulation leads to fast cell migration by promoting efficient lamellipodial protrusion without inhibitory lamellar contraction at the front, and by forming a loosely anchored myosin module, just strong enough to dissolve rear FAs.

PLSs inhibit RhoA/myosin activity necessary for lamella formation

Our analyses of RhoA signaling suggest that a broad gradient of RhoA in hapto cells from the leading edge regulates myosin contractility in the lamella, most likely through Rho kinase-mediated control of MLC (Burrige and Wennerberg, 2004). In chemo cells, the PLS zone displays reduced RhoA activity, which correlates with absence of phosphorylated MLC, stress fibers and FAs. Inhibition of the PLS zone restores the broad RhoA activity gradient, MLC phosphorylation and contractile structures, strongly suggesting that PLSs provide a structural scaffold that locally inhibits RhoA activity. By inhibiting front contractility, PLSs might switch off a positive feedback, in which RhoA-specific GEFs such as LARG or GEF-H1 (Guilluy et al., 2011), translate mechanical activation of integrins by contractile forces into RhoA activation upstream of myosin II. Alternatively, PLSs might locally generate reactive oxygen species as shown for invadopodia (Diaz et al., 2009), which inhibit RhoA through control of the RhoA-specific GAP p190 RhoGAP (Nimnual et al., 2003). An interesting result is that, in absence of front contractility, chemo cells still display a highly focused zone of active RhoA directly in the lamellipodium not visible in hapto cells. Our previous work has already established two pools of RhoA activity at the leading edge: A broad gradient, and a focused band directly at the edge that correlates specifically with the onset of robust membrane protrusion (Machacek et al., 2009; Pertz et al., 2006). We propose that in chemo cells the former is switched off in conjunction with the inhibition of the lamella by the PLS, leaving the edge-focused RhoA activity pool to regulate membrane protrusion, e.g. through the effectors mDia1/2 (Palazzo et al., 2001). As already documented before (Pertz et al., 2006), additional RhoA activation pools can be observed in retracting tails (Figure 7B,D), but not at the myosin cluster observed behind the PLS zone in chemo cells. These results reveal a complex spatio-temporal RhoA activation landscape that correlates with the induction of specific cytoskeletal structures. This also suggests the existence of multiple signaling pathways that regulate different subcellular myosin pools.

Significance of chemokinesis in directional cell migration

Our results show that growth factor-induced, persistent fibroblast migration does not necessarily require a chemotactic gradient. Chemokinesis is sufficient to lock the cell in a polarized state of persistent migration. This has important consequences for the regulation of directed cell migration in vivo. During development, this might be useful during collective, directional migration of neural crest cells, in which chemokinesis and contact inhibition cooperate to generate an overall polarity to the cell population (Theveneau and Mayor, 2012). During cancer metastasis, a macrophage-tumor cell paracrine loop, that involves secretion of growth factors from the two different cell types, allows for collective cell streaming in one specific direction on collagen fibrils (Roussos et al., 2011). Although this was proposed to involve chemotaxis, it is conceivable that chemokinesis might be sufficient to induce directional cell movement on the highly asymmetric collagen fiber. In both cases, the ability of a chemokinetic stimulus to hardwire directionality of pre-polarized cells might therefore provide a mean for generation of persistent, directional cell migration.

3.6. Experimental Procedures

Cell culture and generation of stable cell lines

Rat embryonic fibroblasts (REF52), a kind gift from Alan Howe, were cultured in Dulbecco's modified eagle medium (DMEM; Sigma) supplemented with 10% fetal bovine serum (FBS; Sigma), 100 U/ml penicillin/ streptomycin (Sigma) and 4mM L-Glutamine (Sigma). For serum starving conditions, DMEM was supplemented with 0.5 % FBS and 0.5 % bovine serum albumin (BSA; Sigma), 100 U/ml penicillin/ streptomycin, 4 mM L-Glutamine. Stable cell lines expressing Lifeact-GFP, VASP-GFP, Vinculin-GFP and the RhoA biosensor RhoA2G were generated by lentiviral transduction. For simultaneous imaging of F-actin dynamics, stable cells were infected with an adenovirus encoding Lifeact-mCherry (extended experimental procedures).

Line substrate microfabrication

Glass coverslips containing line substrates were generated by plasma etching using polydimethylsiloxane (PDMS)-based stamps (Figure S1A, extended experimental procedures). For most live cell imaging experiments, a PDMS-based live cell chamber (100 μ m high roof) was grafted on top of the line substrate. For drug perturbations, PDMS chambers with an open roof were employed (500 μ l imaging medium) to prevent drug absorption by PDMS. See extended experimental procedures for detailed information.

3.7. Acknowledgements

We are grateful to Johan De Rooij, Alan Howe, Matthias Kaeser and Ana-Maria Lennon-Dumenil for sharing reagents, and to Eugene Tkachenko and Bernhard Wehrle-Haller for comments on the manuscript. This work was supported by grants from the Swiss National Science Foundation to O.P., and from the Human Frontier Science Program to O.P, G.D, N.L.J. M.V. was supported by the Institutional Training Grant NIH/NRSA 1F32GM103278-01.

3.8. Main Figures

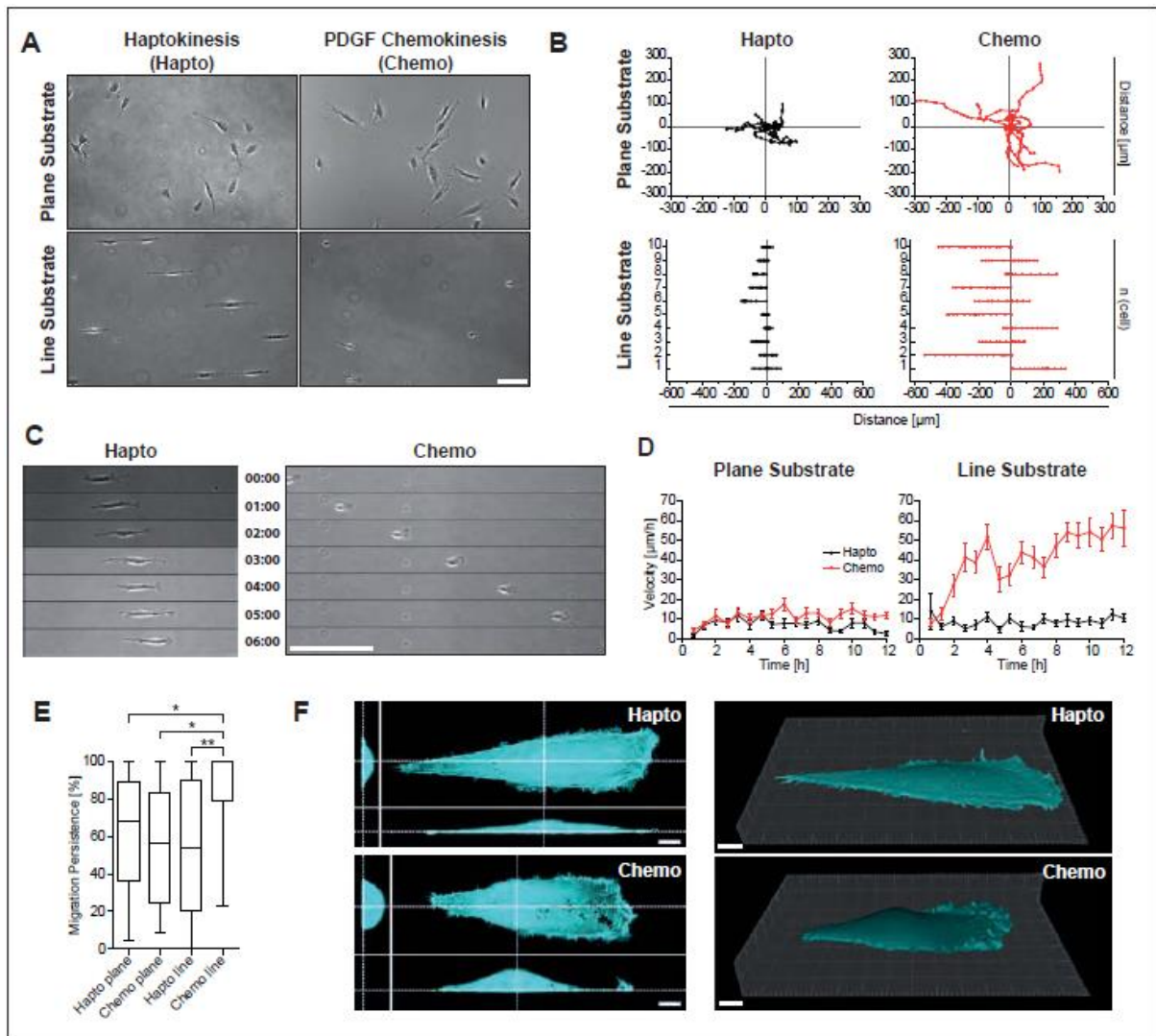


Figure 1. PDGF stimulation of fibroblasts on line substrates leads to rapid and directional cell migration.

(A) Phase contrast images of cells performing haptokinetic (Hapto) and chemokinetic (Chemo) migration on plane and line substrates. (B) Cell trajectories. Points indicate 40' timesteps. (C) Representative phase contrast time-series of hapto and chemo cell migration on line substrates. (D) Time course of instantaneous cell velocities. Average velocity \pm SEM of at least 20 cells are shown. (E) Cell migration persistence. Net over total travel distance during steady state migration (6h until 12h post PDGF stimulation). * $P < 0.005$, ** $P < 0.001$; (n = at least 19 cells; Dunn's multiple comparison test). (F) Confocal imaging of phalloidin stained hapto and chemo cells. Left panels: xy, xz and yz cross-sections. Right panels: 3D reconstructions of fibroblasts. Scale bars: (A), (C) 100 μm ; (F) 10 μm .

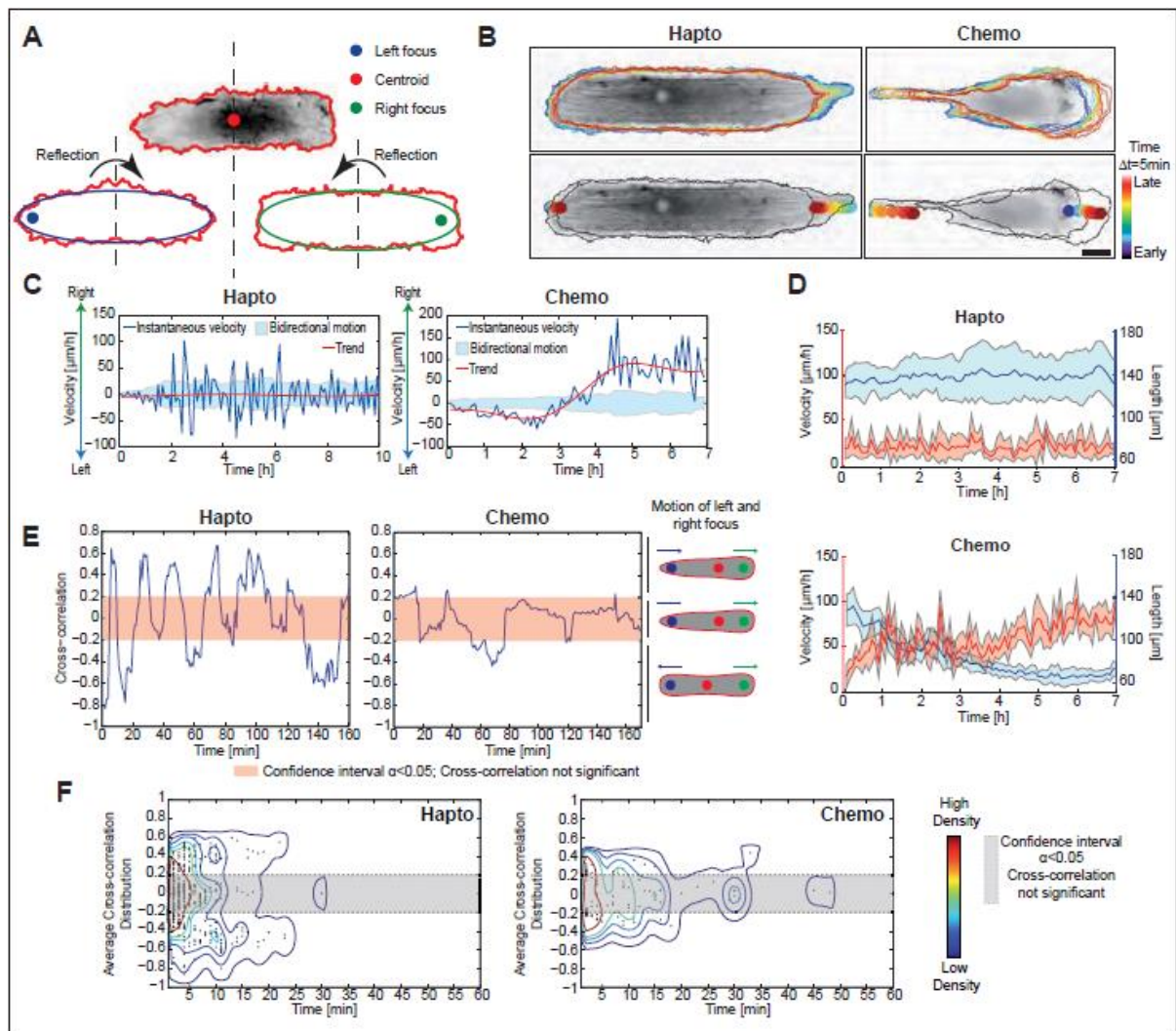


Figure 2. Analysis of global morphodynamics of hapto and chemo cells.

Cells were plated in absence or presence of 40 ng/ml PDGF, and timelapse analysis was started 1 hour post-plating. **(A)** Strategy for identification of centroid and left and right foci. Cell centroid is first identified using the segmented outline of the cell. Ellipse fitting to reflected (left and right) halves defines left and right foci, representing independent cell motions at both cell edges. **(B)** Examples of cell segmentation of hapto and chemo cells. Cell outlines (upper panel); and movements of left and right foci (lower panel) are color-coded according to time. **(C)** Representative time courses of centroid velocities for hapto and chemo cells (dark blue line). Red line, low variation trend velocity. Light blue bands indicate 95% confidence intervals of bidirectional motion. In phases in which the trend velocity is outside the band, the cell transiently establishes directed motion. See supplement for complete description of time course decomposition in high and low variation components. **(D)** Average time courses of cell velocities (red) and lengths (blue), $n=21$ chemo cells, $n=16$ hapto cells. Light blue and red intervals represent the 95% confidence interval around the mean value. Note that different cell trajectories were aligned in time so as to faithfully represent the transition to a polarized phenotype. **(E)** Motion coordination between left and right foci as quantified by cross-correlation. Cartoons indicate possible states of focus motion yielding positive, null, and negative cross-correlation. See extended experimental procedures for the time-dependent cross-correlation algorithm. **(F)** Two-dimensional distribution of the average cross-correlation (y-axis) - duration of all instances of uniform qualitative behavior (x-axis). See extended experimental procedures for a more detailed description. **(D,F)** Data from $n=13$ cells (hapto), $n=10$ cells (chemo). Scale bars: **(B)** 10 μm .

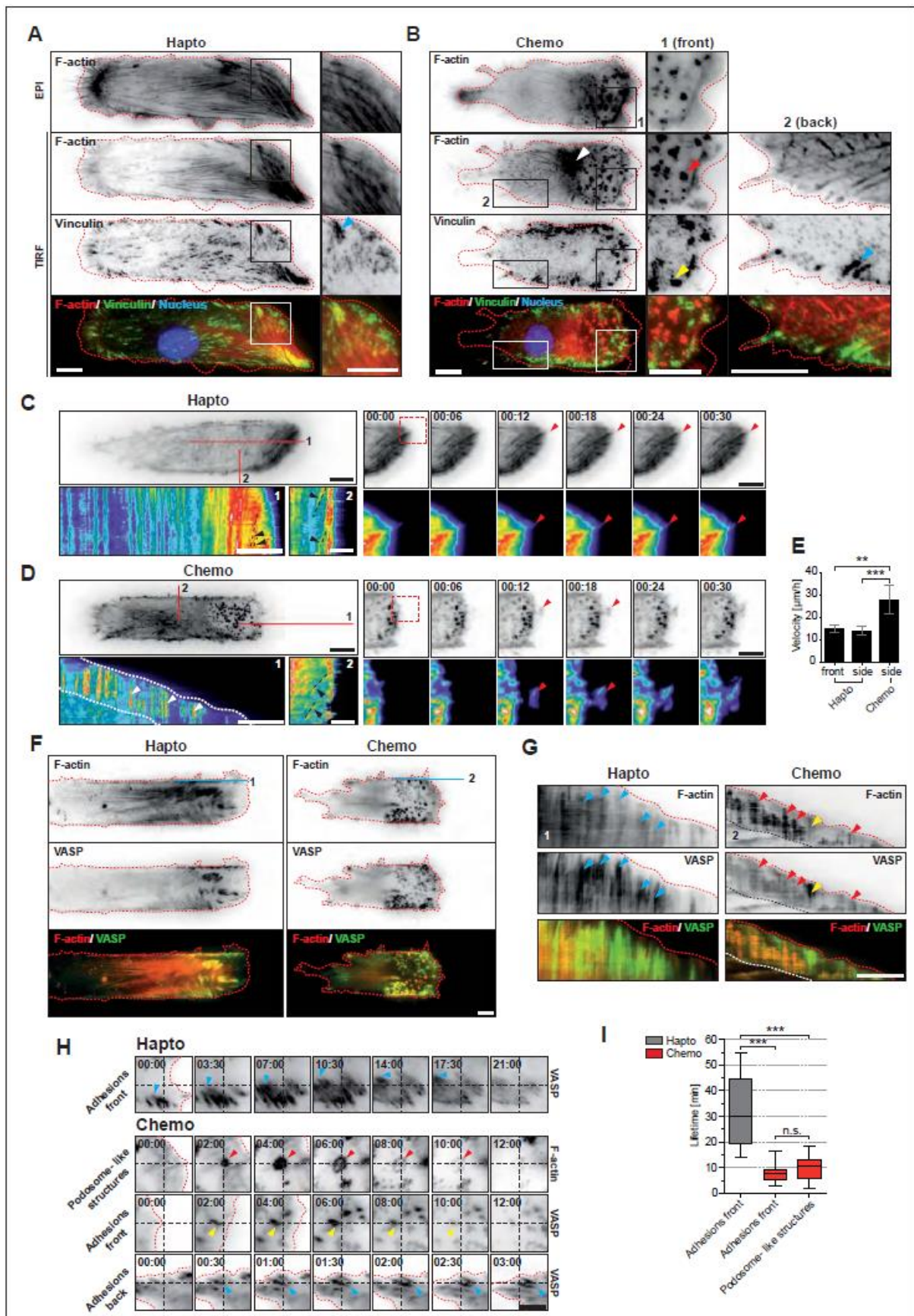


Figure 3. Actin and adhesion dynamics in hapto and chemo cells.

Micrographs and kymographs are shown in inverted black and white contrast (ibw), as color composites, or are color-coded to indicate fluorescence intensity. **(A,B)** Representative F-actin and vinculin stainings in hapto (A) and chemo (B) cells. Cells were fixed 6 hours post-plating, stained with phalloidin-Alexa546 and anti-vinculin antibody, and imaged using EPI or TIRF

microscopy. A DAPI nuclear stain was also included. **(C,D)** Representative micrographs, time-series, and inset zooms of Lifeact-GFP signals using TIRF in hapto **(C)** and chemo **(D)** cells. Kymographs are used to analyze actin dynamics at the leading (1) and lateral edges (2). Black arrowheads indicate actin arcs used to measure actin retrograde flow velocity. Red arrowheads indicate membrane protrusions. White arrowheads indicate PLSs lifecycles. White dotted lines delineate PLS zone. **(E)** Quantification of actin retrograde flow velocity by kymograph analysis. Hapto: n= 9 cells, chemo: n= 5 cells, error bars indicate SEM, **P<0.001, ***P<0.0001; Dunn's multiple comparison test. **(F)** Representative micrographs of VASP-GFP and Lifeact-mCherry signals in hapto and chemo cells. **(G)** Kymographs of lines drawn in **(F)**. Blue arrowheads point to FAs, yellow arrowheads point to FCs, red arrowheads point to PLSs. **(H)** Representative time series of front and back adhesions and podosomes. Dashed crosshair provides reference for virtual inspection of motile behaviors of the adhesions. Arrowheads are color-coded as in **(G)**. **(I)** Quantification of lifetimes of leading edge adhesions and PLSs, n ≥ 5 cells each, ≥ 20 adhesions per cell, 87 PLSs, ***P<0.0001; Dunn's multiple comparison test. Scale bars: **(A-C), (E), (F)** 10µm; **(G)** 5µm.

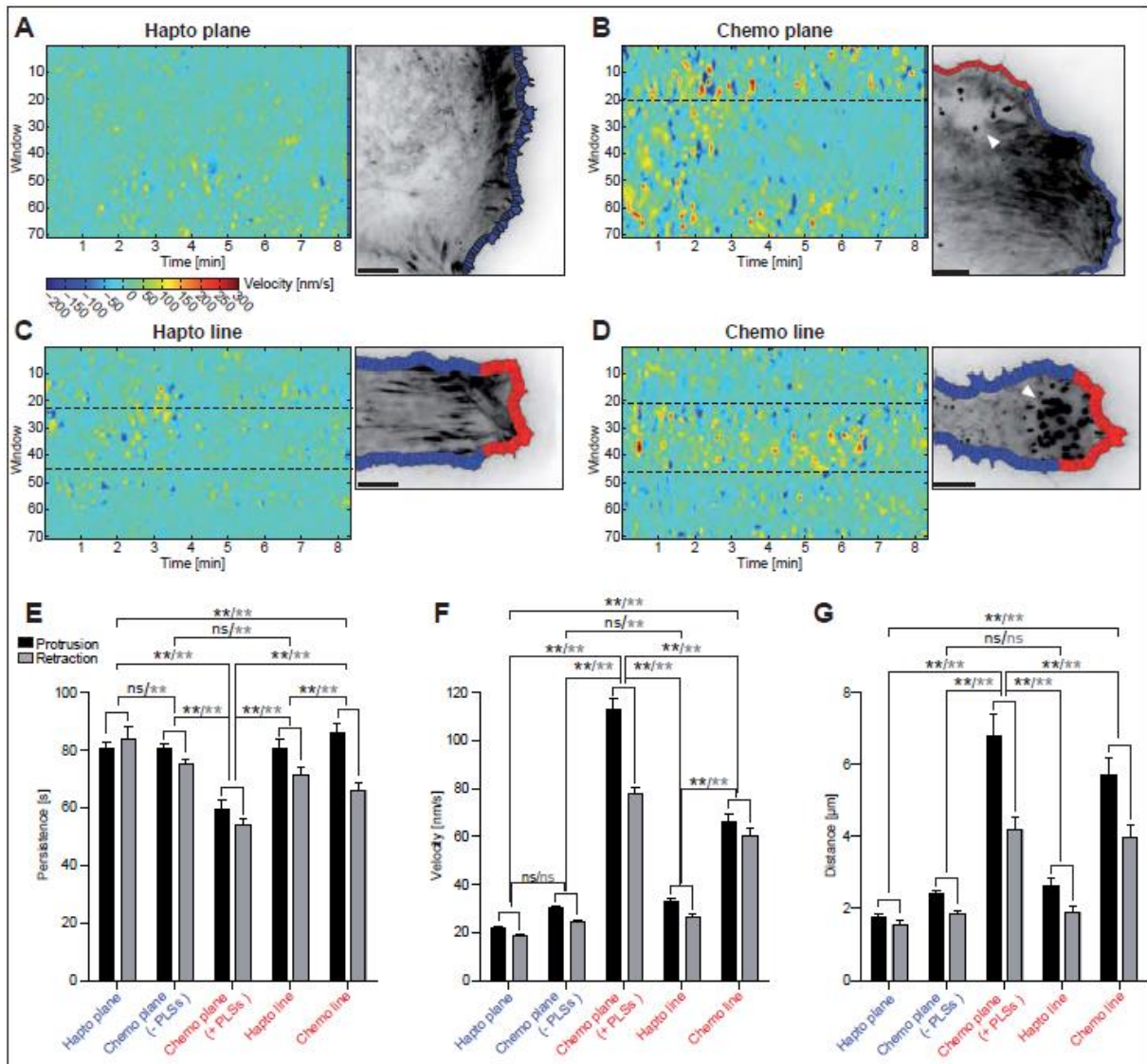


Figure 4. Dynamics of leading edge in hapto and chemo cells.

Micrographs are shown in ibw contrast. **(A-D)** Space-time maps of edge velocities and representative cell edges indicating segments used for the analysis. Edge velocities are color-coded according to scale with protrusions displayed in warm and retractions displayed in cold colors. **(C,D)** Dotted lines indicate edge dynamics on the permissive substrate. **(B)** Dotted lines indicate edge segments containing PLSs. **(E-G)** Quantification of different metrics characterizing membrane protrusion dynamics. Average persistence times **(E)**, velocities **(F)** and traveled distance **(G)**. Scale bars: **(A-D)** 10μm.

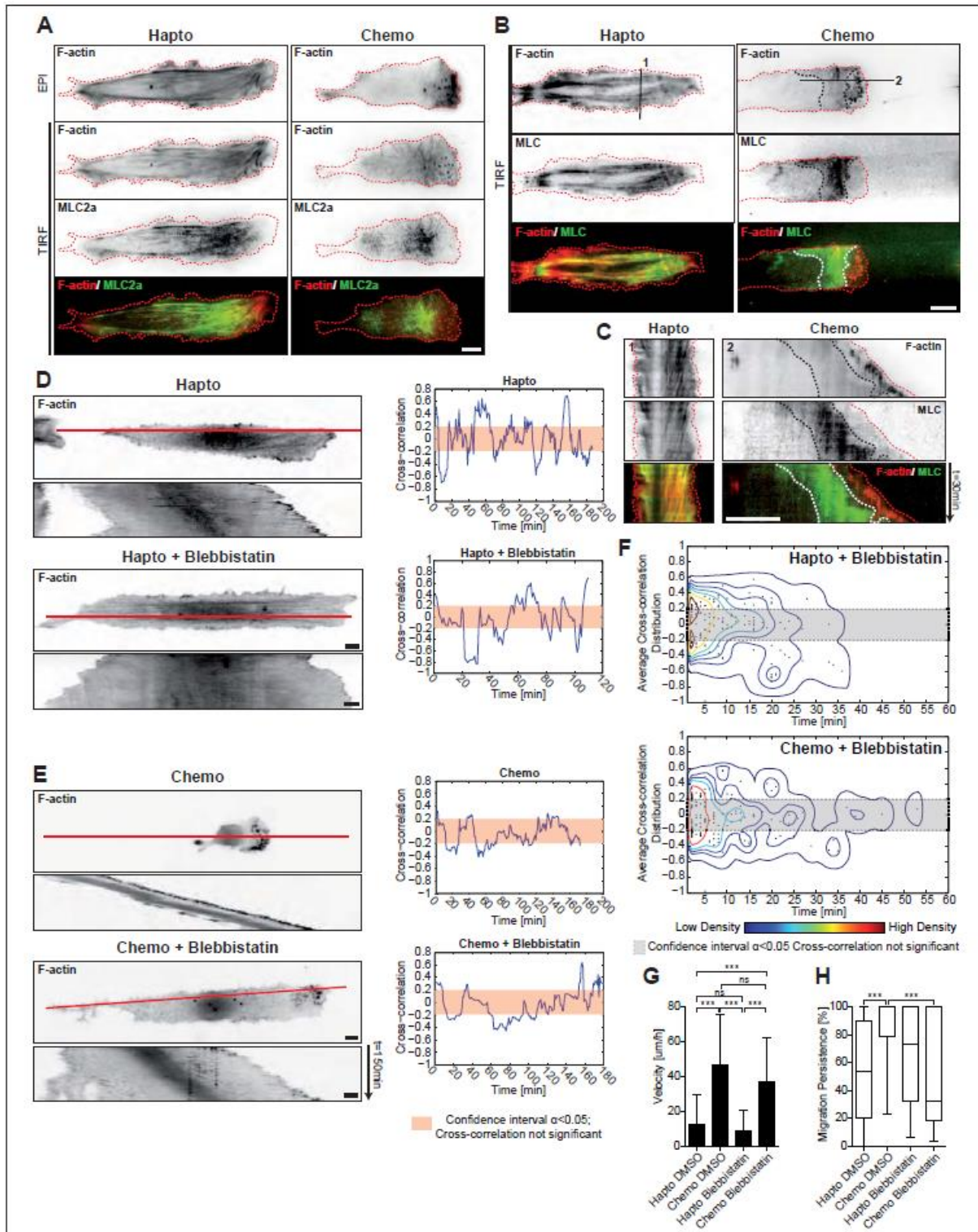


Figure 5. Characterization of myosin function in hapto and chemo cells.

Micrographs and kymographs are shown in ibw contrast or as color composites. **(A)** Representative high-resolution micrographs of F-actin and MLC2a stainings. **(B)** Representative micrographs of Lifeact-mCherry and MLC2a-GFP signals using TIRF. Dotted black lines delineate PLS and myosin zones. **(C)** Kymograph analysis of F-actin and MLC2a dynamics along profiles shown in **(B)**. **(D,E)** Global morphodynamics of hapto **(D)** and chemo **(E)** cells in response to acute myosin inhibition. Fibroblasts expressing Lifeact-GFP were incubated with carrier or 10 μM blebbistatin and immediately imaged using a 20x air objective. Whole cell kymograph and time-dependent foci motion cross-correlations. **(F)** Two-dimensional distribution of the average cross-correlation - duration of all instances of uniform qualitative behavior. $n=10$ cells (hapto) and $n=11$ cells (chemo). **(G,H)** Instantaneous cell velocity **(G)** and persistence **(H)** averaged between 6h and 12h after drug application. Scale bars: **(A-C)**, **(D)**, **(E)** 10 μm .

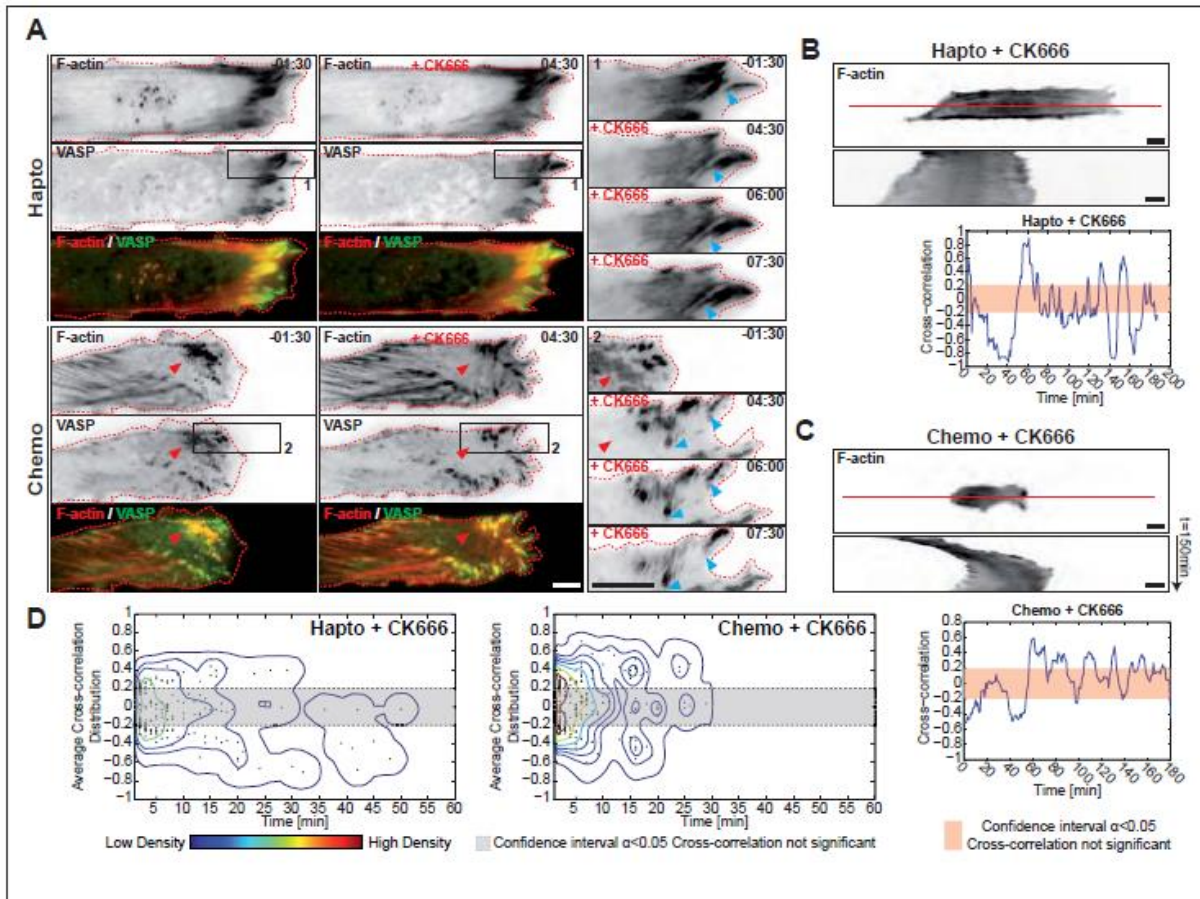


Figure 6. The PLS zone inhibits contractility at the front of chemo cells.

Micrographs and kymographs are shown in ibw contrast or as color composites. **(A)** Representative TIRF micrographs (Lifeact-mCherry and VASP-GFP) and time-series (VASP-GFP) of hapto and chemo cells before and after PLSs disruption by Arp2/3 inhibition. Cells were incubated with 200 μ M CK666 at time 0:00. Red arrowheads indicate PLSs, blue arrowheads indicate FAs. **(B-D)** Global morphodynamics of cells in response to acute Arp2/3 inhibition. Whole cell kymograph and cross-correlations of foci motion in hapto **(B)** and chemo **(C)** cells. Cells were imaged as in Figure 5D. **(D)** Two-dimensional distribution of the average cross-correlation - duration of all instances of uniform qualitative behavior. $n=12$ cells (hapto) and $n=8$ cells (chemo). Scale bars: **(A-C)** 10 μ m

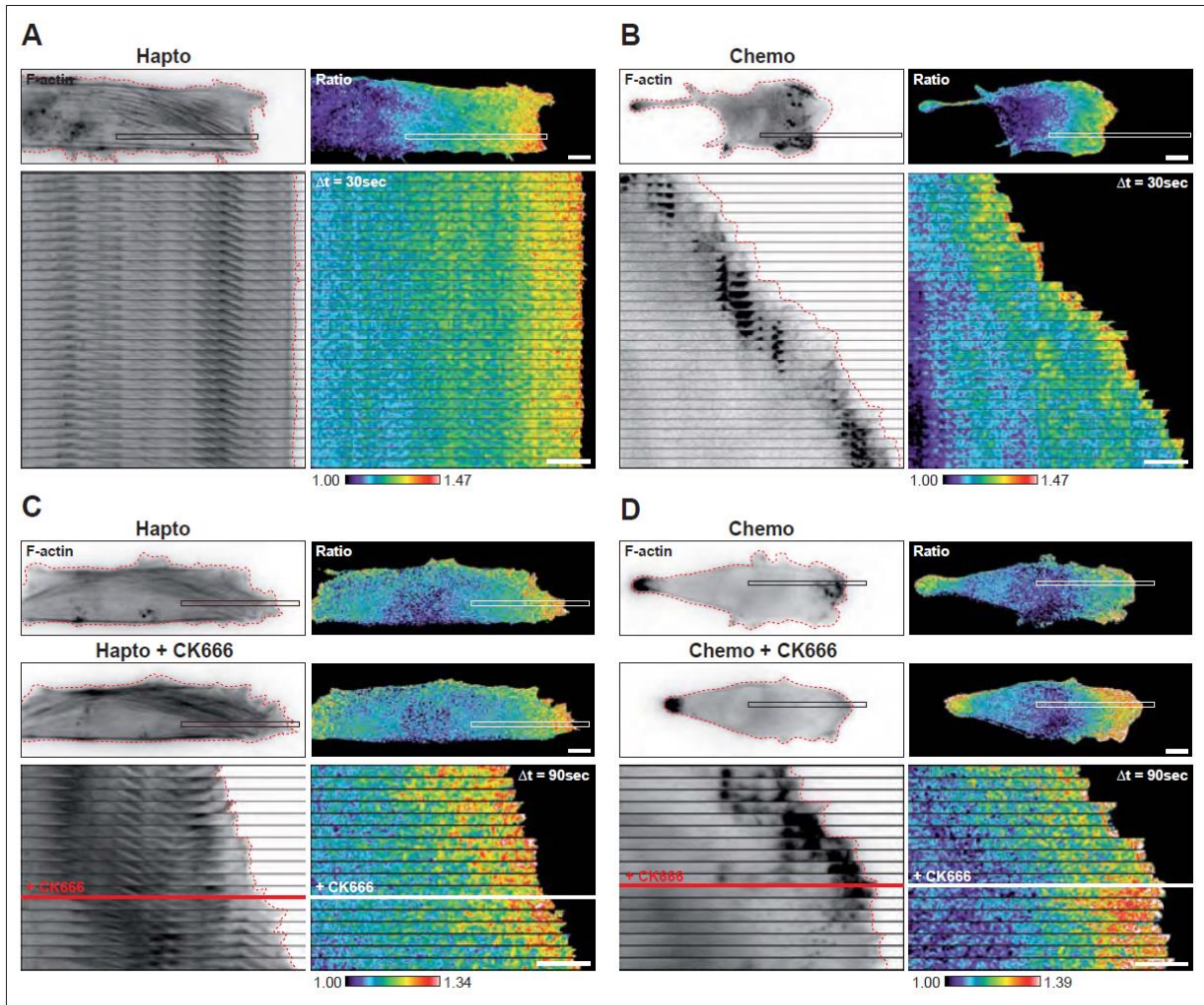


Figure 7. RhoA activation dynamics in hapto and chemo cells.

RhoA activation ratio images are color-coded according to scale bars. Lifeact-mCherry micrographs are shown in ibw contrast. **(A,B)** Representative micrographs and kymographs of hapto and chemo cells expressing RhoA2G and Lifeact-mCherry. **(A)** Hapto, **(B)** Chemo. **(C,D)** Representative micrographs and kymographs of hapto and chemo cells before and after Arp2/3 inhibition. At the indicated time, cells were incubated with 200 μ M CK666. **(C)** Hapto, **(D)** Chemo. Scale bars: **(A-D)** 10 μ m.

3.9. References

- Albiges-Rizo, C., Destaing, O., Fourcade, B., Planus, E., and Block, M.R. (2009). Actin machinery and mechanosensitivity in invadopodia, podosomes and focal adhesions. *Journal of cell science* 122, 3037-3049.
- Burridge, K., and Wennerberg, K. (2004). Rho and Rac take center stage. *Cell* 116, 167-179.
- Calle, Y., Burns, S., Thrasher, A.J., and Jones, G.E. (2006). The leukocyte podosome. *European journal of cell biology* 85, 151-157.
- Collin, O., Tracqui, P., Stephanou, A., Usson, Y., Clement-Lacroix, J., and Planus, E. (2006). Spatiotemporal dynamics of actin-rich adhesion microdomains: influence of substrate flexibility. *Journal of cell science* 119, 1914-1925.
- Diaz, B., Shani, G., Pass, I., Anderson, D., Quintavalle, M., and Courtneidge, S.A. (2009). Tks5-dependent, nox-mediated generation of reactive oxygen species is necessary for invadopodia formation. *Science signaling* 2, ra53.
- Doyle, A.D., Wang, F.W., Matsumoto, K., and Yamada, K.M. (2009). One-dimensional topography underlies three-dimensional fibrillar cell migration. *The Journal of cell biology* 184, 481-490.
- Friedl, P., and Wolf, K. (2010). Plasticity of cell migration: a multiscale tuning model. *The Journal of cell biology* 188, 11-19.
- Fritz, R.D., Letzelter, M., Reimann, A., Martin, K., Fusco, L., Ritsma, L., Ponsioen, B., Fluri, E., Schulte-Merker, S., van Rheenen, J., *et al.* (2013). A Versatile Toolkit to Produce Sensitive FRET Biosensors to Visualize Signaling in Time and Space. *Science signaling* 6, rs12.
- Guilluy, C., Swaminathan, V., Garcia-Mata, R., O'Brien, E.T., Superfine, R., and Burridge, K. (2011). The Rho GEFs LARG and GEF-H1 regulate the mechanical response to force on integrins. *Nature cell biology* 13, 722-727.
- Hotulainen, P., and Lappalainen, P. (2006). Stress fibers are generated by two distinct actin assembly mechanisms in motile cells. *The Journal of cell biology* 173, 383-394.
- Kim, D.H., Provenzano, P.P., Smith, C.L., and Levchenko, A. (2012). Matrix nanotopography as a regulator of cell function. *The Journal of cell biology* 197, 351-360.
- Machacek, M., and Danuser, G. (2006). Morphodynamic profiling of protrusion phenotypes. *Biophysical journal* 90, 1439-1452.
- Machacek, M., Hodgson, L., Welch, C., Elliott, H., Pertz, O., Nalbant, P., Abell, A., Johnson, G.L., Hahn, K.M., and Danuser, G. (2009). Coordination of Rho GTPase activities during cell protrusion. *Nature* 461, 99-103.
- Murphy, D.A., and Courtneidge, S.A. (2011). The 'ins' and 'outs' of podosomes and invadopodia: characteristics, formation and function. *Nature reviews Molecular cell biology* 12, 413-426.
- Nimnual, A.S., Taylor, L.J., and Bar-Sagi, D. (2003). Redox-dependent downregulation of Rho by Rac. *Nature cell biology* 5, 236-241.
- Nolen, B.J., Tomasevic, N., Russell, A., Pierce, D.W., Jia, Z., McCormick, C.D., Hartman, J., Sakowicz, R., and Pollard, T.D. (2009). Characterization of two classes of small molecule inhibitors of Arp2/3 complex. *Nature* 460, 1031-1034.
- Oikawa, T., Itoh, T., and Takenawa, T. (2008). Sequential signals toward podosome formation in NIH-src cells. *The Journal of cell biology* 182, 157-169.
- Palazzo, A.F., Cook, T.A., Alberts, A.S., and Gundersen, G.G. (2001). mDia mediates Rho-regulated formation and orientation of stable microtubules. *Nature cell biology* 3, 723-729.
- Parsons, J.T., Horwitz, A.R., and Schwartz, M.A. (2010). Cell adhesion: integrating cytoskeletal dynamics and cellular tension. *Nature reviews Molecular cell biology* 11, 633-643.
- Pertz, O., Hodgson, L., Klemke, R.L., and Hahn, K.M. (2006). Spatiotemporal dynamics of RhoA activity in migrating cells. *Nature* 440, 1069-1072.
- Pestonjamas, K.N., Forster, C., Sun, C., Gardiner, E.M., Bohl, B., Weiner, O., Bokoch, G.M., and Glogauer, M. (2006). Rac1 links leading edge and uropod events through Rho and myosin activation during chemotaxis. *Blood* 108, 2814-2820.
- Petrie, R.J., Doyle, A.D., and Yamada, K.M. (2009). Random versus directionally persistent cell migration. *Nature reviews Molecular cell biology* 10, 538-549.

- Pollard, T.D., and Borisy, G.G. (2003). Cellular motility driven by assembly and disassembly of actin filaments. *Cell* 112, 453-465.
- Ponti, A., Machacek, M., Gupton, S.L., Waterman-Storer, C.M., and Danuser, G. (2004). Two distinct actin networks drive the protrusion of migrating cells. *Science* 305, 1782-1786.
- Riedl, J., Crevenna, A.H., Kessenbrock, K., Yu, J.H., Neukirchen, D., Bista, M., Bradke, F., Jenne, D., Holak, T.A., Werb, Z., et al. (2008). Lifeact: a versatile marker to visualize F-actin. *Nature methods* 5, 605-607.
- Roussos, E.T., Condeelis, J.S., and Patsialou, A. (2011). Chemotaxis in cancer. *Nature reviews Cancer* 11, 573-587.
- Straight, A.F., Cheung, A., Limouze, J., Chen, I., Westwood, N.J., Sellers, J.R., and Mitchison, T.J. (2003). Dissecting temporal and spatial control of cytokinesis with a myosin II Inhibitor. *Science* 299, 1743-1747.
- Svitkina, T.M., Verkhovskiy, A.B., McQuade, K.M., and Borisy, G.G. (1997). Analysis of the actin-myosin II system in fish epidermal keratocytes: mechanism of cell body translocation. *The Journal of cell biology* 139, 397-415.
- Theveneau, E., and Mayor, R. (2012). Neural crest delamination and migration: from epithelium-to-mesenchyme transition to collective cell migration. *Developmental biology* 366, 34-54.
- Weiner, O.D., Marganski, W.A., Wu, L.F., Altschuler, S.J., and Kirschner, M.W. (2007). An actin-based wave generator organizes cell motility. *PLoS biology* 5, e221.
- Wu, C., Asokan, S.B., Berginski, M.E., Haynes, E.M., Sharpless, N.E., Griffith, J.D., Gomez, S.M., and Bear, J.E. (2012). Arp2/3 is critical for lamellipodia and response to extracellular matrix cues but is dispensable for chemotaxis. *Cell* 148, 973-987.
- Zamir, E., Katz, B.Z., Aota, S., Yamada, K.M., Geiger, B., and Kam, Z. (1999). Molecular diversity of cell-matrix adhesions. *Journal of cell science* 112 (Pt 11), 1655-1669.

3.10. Supplemental Information

3.10.1. Extended Experimental Procedures

Supplemental Information includes Extended Experimental Procedures, five Supplemental Figures and eight Supplemental Movies.

Extended Experimental Procedures

Plasmids

PCR was used to flank the N-terminus of GFP with the Lifeact coding sequence. The lifeact-GFP fragment was then shuttled into the lentiviral plasmid pRRL-SV40(puro)_CMV(mcs) (a kind gift from Matthias Kaeser) by homologous recombination (InFusion[®] technology, Clontech). PCR was used to amplify VASP and vinculin, derived from peGFP-VASP-C2 and peGFP-vinculin-C3 (kind gifts from Johan de Rooij), and MLC2a-GFP from pDEST-eGFP-MLC (a kind gift from Ana-Maria Lennon-Dumenil). These were then shuttled into pRRL-SV40 (puro)_CMV(mcs) using InFusion recombination.

Immunofluorescence

After 1 wash in phosphate buffered saline (PBS), cells were fixed with 4 % paraformaldehyde (PFA) and blocked for 1 h at room temperature in PBS containing 0.1 % Triton-X-100 (PBS-T) and 5 % BSA. Cells were incubated for 1 hour with antibodies in PBS-T and 2 % BSA. Cells were washed 3 times for 10 minutes in PBS-T. Polyclonal rabbit anti-myosin2a (1:50; Cell Signaling), polyclonal rabbit anti-phosphoSer19-myosin-light chain 2 (1:50; Cell Signaling), monoclonal mouse anti-vinculin (1:400; Abcam) antibodies in PBS-T were used. Secondary detection was performed using Alexa fluor 488 goat anti rabbit IgG (1:1000; Invitrogen) or Alexa fluor 488 goat anti mouse (1:1000; Invitrogen). DAPI (1:1000) and phalloidin-alexa fluor 555 (1:50; Invitrogen) was applied to unmounted samples while imaging, to visualize F-actin. TIRF imaging of these stainings was performed in a live cell chamber in presence of PBS in order to provide the glass-water interface necessary for incident light reflection.

Viral Transduction and Generation of Stable Cell lines

Stable cell lines were generated by infection of REF52 cells with lentiviral vectors. Lentiviral particles were produced by transfection of pRRL-SV40(puro)_CMV carrying the gene of interest, with the pVSV, pMDL and pREV packaging plasmids using FuGENE[®] HD (Promega) transfection reagent into human embryonic kidney 293 FT cells (HEK293FT). Culture supernatants were harvested 72 and 96 hours post transfection and purified using a Lenti-X[™] concentrator (Invitrogen). To achieve optimal expression levels of the respective construct, REF52 cells were transduced with different amounts of purified lentivirus in the presence of 5 µg/ml polybrene. Cells exhibiting minor morphology alterations and best possible expression levels of fluorescently tagged protein were chosen and selected with 1 µg/ml puromycin.

The adenovirus encoding Lifeact-mCherry was generated by recombination into the pAd/CMV/V5-DEST[™] Gateway[®] Vector Kit according to the manufacturers instructions (Invitrogen). To determine

the viral titer necessary to achieve optimal expression levels, REF52 were infected with different amounts of virus supplemented with 5 µg/ml polybrene. Lifeact-mCherry adenovirus infected cells were then imaged 48 h post infection.

Line substrate microfabrication

PDMS ridge stamps were used as a template to produce the line substrate (20 µm wide ridge structures separated by 100 µm wide gaps) on glass coverslips (Figure S1A). PDMS was mixed well in a ratio of 10:1 with curing agent (Sylgard[®] 184 Silicone Elastomere KIT; Dow Corning) and poured onto a silicon wafer produced by soft lithography. Vacuum was applied to remove enclosed air bubbles and PDMS was cured by incubation for 2 h at 70 °C. The polymer was then peeled off the silicon wafer and cut into pieces with adequate dimensions. PDMS-based live cell chambers consisting of a square chamber (5 mm width, 6mm length, 100 µm high roof) connected to an inlet and an outlet, were constructed the same way using specific silicon wafers.

Glass coverslips (24 x 50 mm) were extensively cleaned with anhydrous ethanol and demineralized water and were coated with 0.5 mg/ml poly-L-Lysine - poly-ethylene-glycol, (PLL-PEG; SUSOS) for 30 min at room temperature. Next, the glass coverslip was once washed with water and dried. In the meanwhile, the PDMS ridge stamp and PDMS live cell chamber were cleaned with tape at the structured surface. The PDMS ridge stamp was then aligned on the PLL-PEG coated surface of the glass coverslip and exposed to plasma etching at 100 % power for 90 seconds using a CUTE[®] plasma oven (Femto Science). The glass coverslips (with PDMS ridge stamp), as well as the PDMS-based, live cell imaging chamber (structured side up) were treated with plasma for an additional 30 seconds. The PDMS ridge stamp was then removed and the PDMS-based live cell imaging chamber was grafted on the glass coverslip on top of the line substrate. Once the PDMS-based live cell imaging chamber was covalently bound to the glass coverslip, fibronectin was coated overnight at 4°C at 10 µg/ml. Line substrates were then washed 1x with PBS and 1x with imaging medium. 5 µl of a suspension containing 2×10^5 cells/ml was loaded into the microfluidic device. Loading cells in such a small volume minimized flow and improved cell attachment. After 30 min, when cells had adhered, the inlet and outlet of the microfluidic device were filled with imaging medium and the devices were kept in an incubator until live cell imaging.

Live cell imaging

EPI and TIRF images were acquired on a Nikon TI Eclipse inverted fluorescence microscope equipped with a motorized stage, hardware based autofocus, a CoolLED light source, and controlled using Metamorph imaging software. For TIRF imaging, 491 nm and 561 solid-state laser diodes integrated in a TIRF system were used (Roper Scientific). All static images were acquired with a PlanApo TIRF 60x objective.

For live cell imaging, REF52 cells were seeded into microfluidic devices after at least 8h serum starvation. At least 6 hours prior to imaging, chemo cells were exposed to 40 ng/ml PDGF in phenol red free DMEM, 0.5 % BSA, 0.5 % FBS to allow establishment of steady state persistent migration.

Hapto cells were treated identically, but imaged in HAM's F12 medium, 0.5 % BSA, 0.5 % FBS 2 hours post-seeding at the earliest. Cells were kept at 37 °C and supplied with 5 % CO₂ throughout imaging. Phase contrast experiments were performed with a PlanFluor air 10x objective. Low resolution imaging of REF52 stably expressing Lifeact-GFP was performed using a PlanApo air 20x objective. TIRF imaging was performed using a PlanApo TIRF 60x oil objective. FRET experiments were performed using a 60x PlanApo oil objective as described elsewhere (Fritz et al., 2013). Most images were acquired using a Hamamatsu Orca R2 CCD camera. A Photometrics Evolve EMCCD camera was used when high sensitivity was needed (MLC-GFP).

Image analysis

Basic image analysis and processing was performed using MetaMorph software. FRET data was analyzed as described elsewhere (Fritz et al., 2013). Cell edge dynamics as shown in Figure 4 were quantified using in-house matlab-based software. This software calculates the velocities by tracking the displacement of all pixels at the cell edge from one frame to the next (Machacek and Danuser, 2006). The pixel-wise velocities were averaged within sampling windows of approximately 1µm width placed along the cell edge. This averaging step gave rise to the final velocities used for analysis. We further analyzed the edge dynamics by clustering regions of the cell edge with similar velocity magnitude. A fuzzy k-means algorithm was used for this purpose (Nock and Nielsen, 2006).

Analysis of global fibroblast morphodynamics

To analyze global properties of fibroblasts migrating on the line substrate, a computer vision algorithm was developed to measure the kinematic parameters from different cell regions. These analyses were all performed on timelapse movies of fibroblasts stably expressing Lifeact-GFP, which provide adequate contrast for the segmentation of the cell boundary using intensity-based thresholding. The basic idea behind this algorithm is to separately capture the motion from the left, central and right regions of the cell by reducing these areas to single points. After segmentation, the algorithm calculates the cell centroid. The centroid point is then used to divide the cell in half where the dividing plane is perpendicular to the long axis of the migration path. Once divided, each cell half is reflected over the same dividing plane to form a closed symmetric object. An ellipse is then inscribed to both objects and the foci coordinates are calculated (Figure 2A). The right and left ellipse foci from the right and left mirrored halves, respectively were used to quantify the motion for the right and left regions. The motion of the center region was quantified by the centroid. Two important aspects are achieved with this approach: independence between right/left measurements and the ability to include local cell morphology from the right/left regions to capture their respective motions. Additionally to the velocities described above, the algorithm also calculates the cell length (Figure 2D).

Cell velocity analysis. Visual inspection of hapto and chemo cells revealed a clear difference of cell displacement over time. In order to quantify the different migration modes, we implemented an algorithm based on a time series analysis technique called empirical mode decomposition (Wu et al., 2007). This algorithm locally decomposes the centroid instantaneous velocity into two frequency components: a fast component (including quick changes in velocity direction) and a slow component

(including the overall trend in velocity). The fast component was used to estimate an interval that represents the distribution of magnitudes for the fast, quasi-random changes in velocity. The interval was locally estimated using a sliding window of 10 points with reflective boundaries in order to accommodate temporal variations of the fast component. The range values were calculated from the spread of the fast component within the 10 points window (± 3 standard deviations centered in 0).

We defined as bidirectional migration, periods in which the slow component of the centroid velocity was contained in the fast component interval. That means the cell changes direction from one frame to the next, having little or no displacement. Unidirectional migration mode was defined as periods in which the slow component is outside the fast component interval. Although there is a possibility of change in direction, this scenario indicates that the cell has an overall displacement in one direction. We used left-to-right as the direction of positive migration. The front region of the cell was defined as the side corresponding to the direction of centroid motion and left/right foci velocities were labeled as front/back accordingly (Figure 2C).

Front/back coordination quantification. We used time-dependent cross-correlation to test the coordination between the front and back regions of the cell. Given two time series $x(t)$ and $y(t)$, the time-dependent cross-correlation is defined as:

$$\rho(t) = \frac{1}{W + 1} \sum_{i=t-W/2}^{t+W/2} \frac{(y_i - \bar{y})(x_i - \bar{x})}{\sigma_y \sigma_x}$$

, where $W + 1$ is the length of the sliding window and $\sigma_x, \sigma_y, \bar{x}, \bar{y}$ denote the standard deviations and means for x and y within the sliding window. The coupling between front and back regions was estimated by replacing x and y with front/back instantaneous velocities. Positive values indicate front and back moving in the same direction. The confidence interval about zero correlation was estimated based on asymptotic distribution analysis for the cross-correlation of two random gaussian processes (Box et al., 1994). Correlations values inside this interval are statistically insignificant.

Average cross-correlation distributions. The time-dependent cross-correlation plots showed a transient nature of the front/back coordination with time periods of negative, insignificant and positive cross-correlation. To better summarize this variability in behavior for the entire dataset, we plotted the 2D distribution of the interval length and its respective average cross-correlation for three qualitative behaviors (Figure S1F).

3.10.2. Supplemental Figures

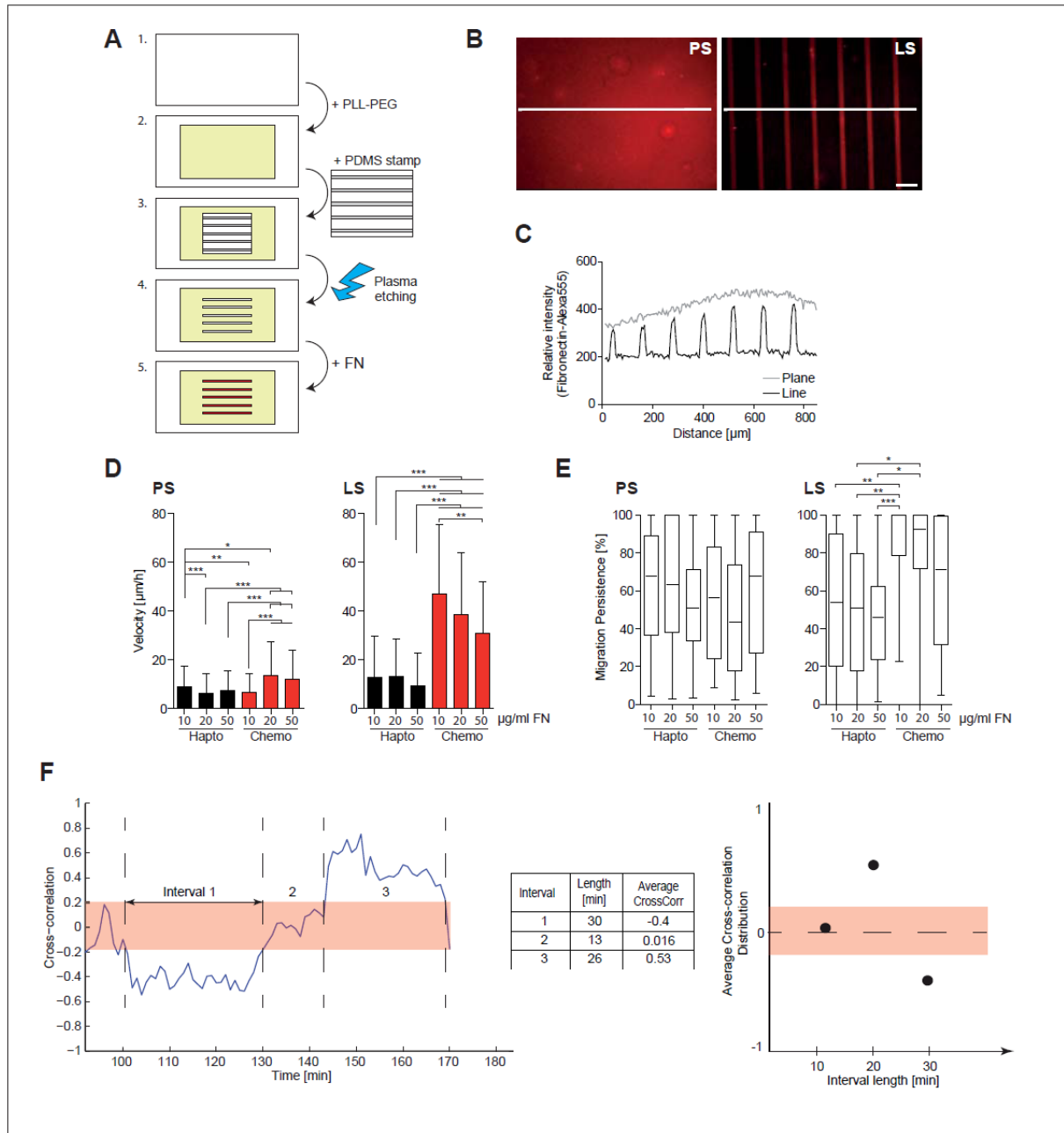


Figure S1. Production and quality control of FN line substrates, quantitation of effect of FN coating density on cell migration and rationale for cross-correlation analysis of left-right motion coordination. Related to Figures 1 and 2.

(A) Manufacturing of FN line substrate. 1. Coverslips were coated with PLL-PEG. 2. A polydimethylsiloxane (PDMS) stamp containing 100 μm -wide, 30 μm thick ridges separated by 20 μm -wide valleys was placed on the coverslip. 3. Plasma was applied to the coverslip to etch out PLL-PEG and the stamp was removed. 4. PDMS stamp was removed. 5. The coverslip was coated with FN, which could only adsorb at locations at which PLL-PEG was etched out. **(B)** Representative micrographs of alexa fluor 555 labeled FN adsorbed on a line substrate and a plane substrate. **(C)** Linescan of fluorescence intensities of alexa fluor 546 labeled FN shown in **(B)**. **(D,E)** Quantification of cell velocities **(D)** and migration directionality **(E)** of hapto and chemo cells on plane and line substrates at different ECM coating concentrations. * $P < 0.005$, ** $P < 0.001$, *** $P < 0.0001$; Dunn's multiple comparison test. **(F)** Average cross-correlation distributions. Time intervals with homogeneous front/back behavior were selected and their corresponding average cross-correlation was calculated to form measurement pairs (average cross-correlation versus time interval length). These pairs were used to estimate the local density.

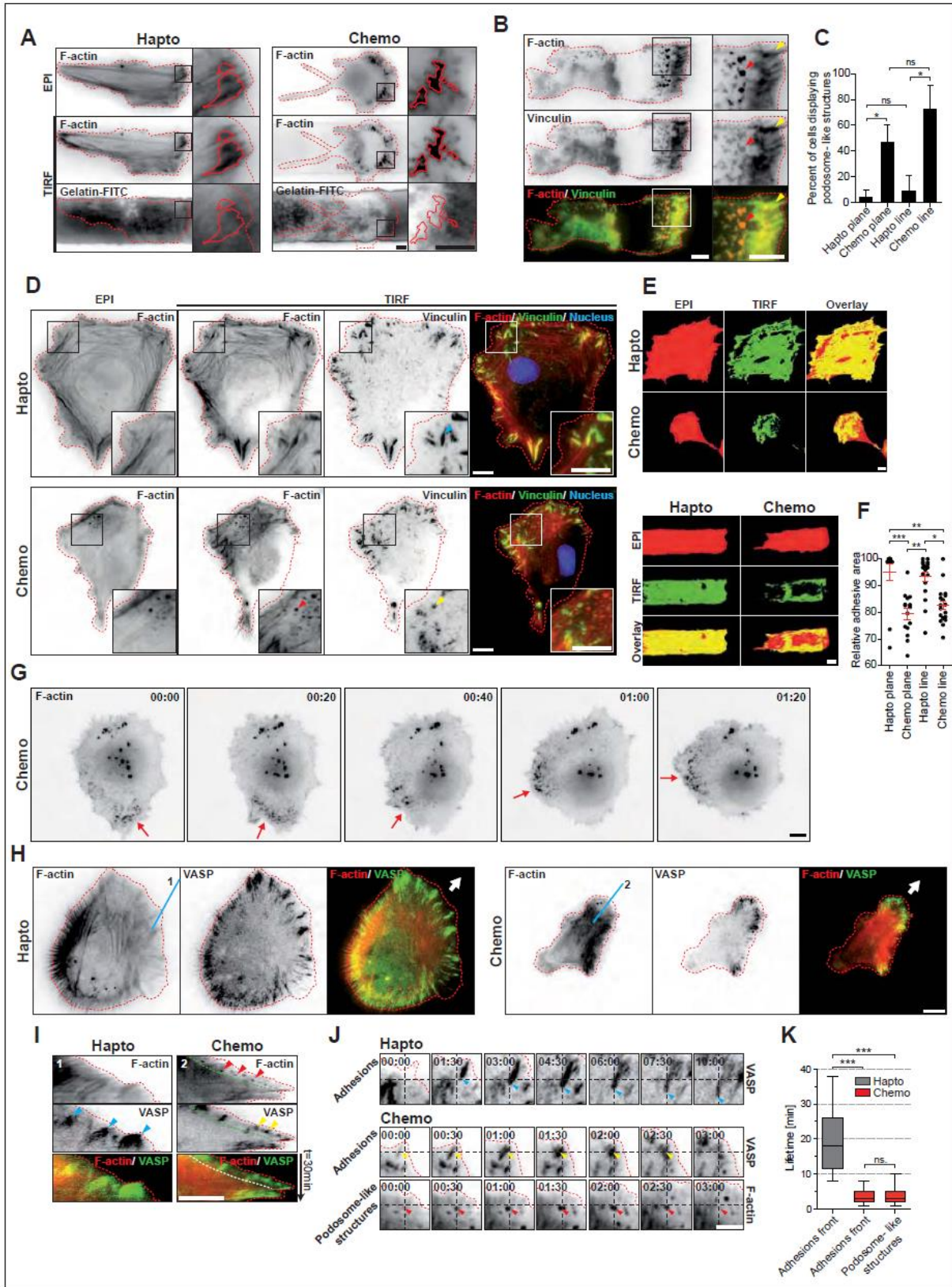


Figure S2. Further characterization of actin and adhesion structures in hapto and chemo cells, related to Figure 3. (A) PLSs have gelatin degradation activity. Fibroblasts were plated on a FITC-labeled gelatin (1 mg/ml) line substrate. Cells were subsequently stained with phalloidin-alexa fluor 546, and imaged using TIRF or EPI. Note the loss of FITC fluorescence in chemo but not in hapto cells. Red lines in insets indicate FITC-gelatin degradation at PLSs at the leading edge of chemo but not hapto cells. (B) Vinculin colocalizes with F-actin at PLSs. TIRF images of cells expressing vinculin-GFP and Lifeact-mCherry. Note the colocalization of vinculin-GFP with F-actin containing PLSs (red arrowheads). Also note the prominent enrichment of vinculin-GFP at FCs (yellow arrowheads). (C) Quantification of number of cells containing PLSs scored visually on 135 cells per condition. Statistical analysis was performed using Dunn's Multiple Comparison test, $*P < 0.005$. (D) Representative F-actin and vinculin stainings of fibroblasts on the plane substrate. Cells were fixed 6 hours post-plating and PDGF stimulation. Micrographs

are shown in *ibw* contrast and as color composites. Insets indicate regions with prominent FAs (blue arrowhead) in hapto cells, and, FCs (yellow arrowheads) and PLSs (red arrowheads) in chemo cells respectively. **(E,F)** PDGF lowers cell-substrate adhesion in chemo cells. **(E)** Representative fluorescence signals of a GFP-K-Ras4b CAAX peptide fusion as visualized by EPI or TIRF microscopy. Cell regions with fluorescence signal in both channels were binarized and color-coded. **(F)** Ratio of adhesive to total cell surface were calculated for at least $n=13$ cells in each condition. Statistical analysis was performed using Dunn's Multiple Comparison test, $*P<0.005$, $**P<0.001$, $***P<0.0001$. **(G)** Representative time series of global F-actin dynamics (Lifeact-GFP) in chemo cells on the plane substrate by 20x imaging. Lateral scanning motions of the PLS zone are indicated by a red arrow. **(H-I)** High resolution imaging (60x) of F-actin and adhesion dynamics in hapto and chemo cells on the plane substrate. **(H)** Representative F-actin (Lifeact-mCherry) and adhesion (VASP-GFP) micrographs on the plane substrate. Micrographs are shown in *ibw* contrast and as color composites. **(I)** Kymographs of lines shown in **(H)**. **(J)** Representative time series of PLSs and adhesion dynamics as in **(H)**. **(K)** Lifetime quantification of leading edge adhesions and PLSs, $n \geq 4$ cells each, ≥ 5 adhesions or PLSs per cell, Dunn's Multiple Comparison test, $***P<0.0001$. Scale bars: **(A), (B), (D), (E), (H), (I)** = 10 μm ; **(J)** = 5 μm .

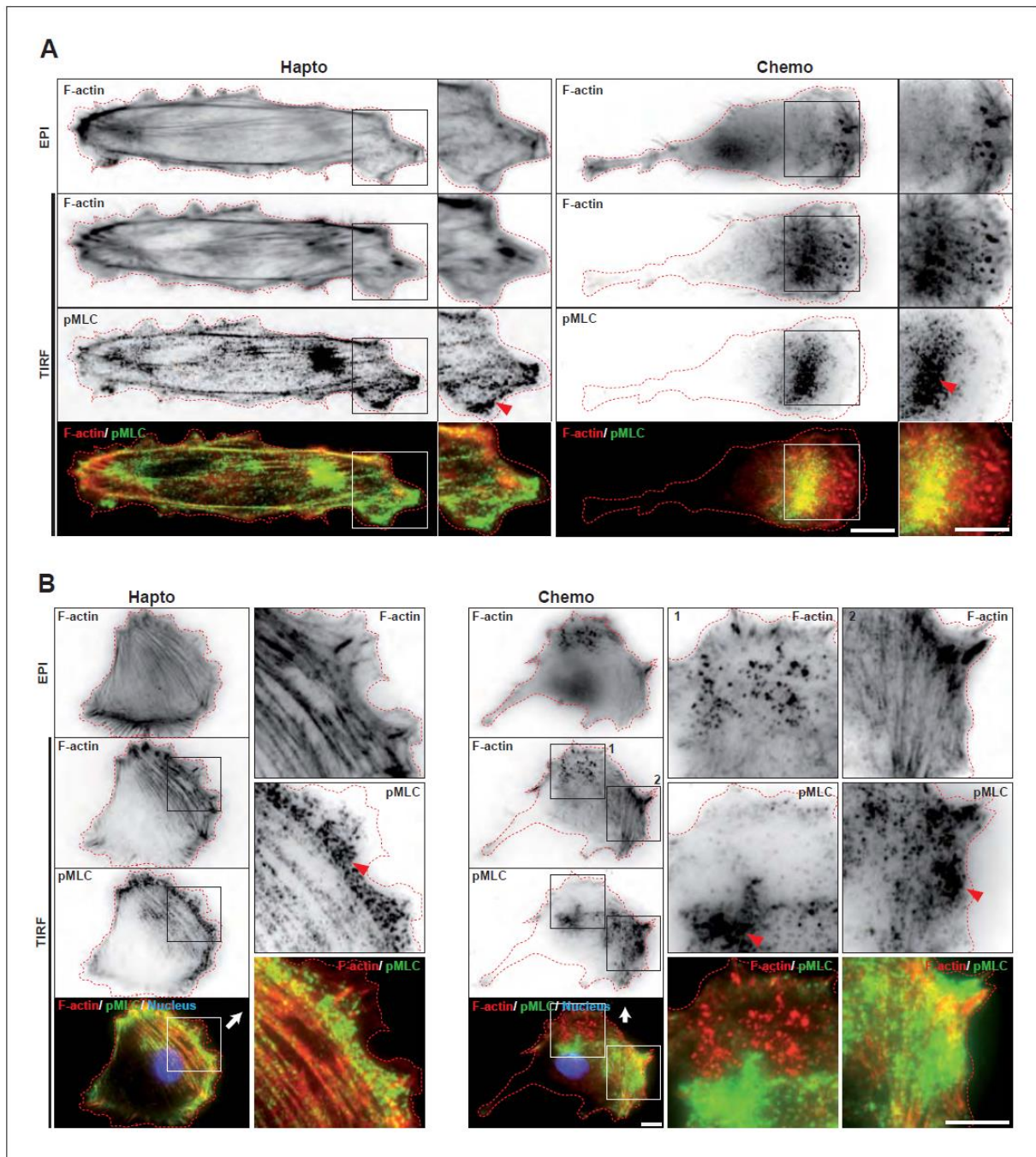


Figure S3. Subcellular localization of pMLC, related to Figure 5.

Representative micrographs of F-actin and pMLC are shown in ibw contrast, and as color composites. White arrows indicate cell migration direction. **(A)** pMLC signals on the line substrate. Hapto cells: red arrowhead indicates pMLC enrichment at the leading edge. Chemo cells: red arrowhead indicates pMLC in the myosin cluster behind the PLS zone. **(B)** pMLC signals on the plane substrate. Hapto: inset shows a closeup of peripheral pMLC signal at the leading edge (red arrowhead). Chemo: inset 1 shows a closeup of pMLC region not associated to peripheral stress fibers adjacent to a PLS region; inset 2 shows a closeup of pMLC signal associated with a peripheral stress fiber array (red arrowhead). Scale bars: **(A)**, **(B)** = 10 μ m.

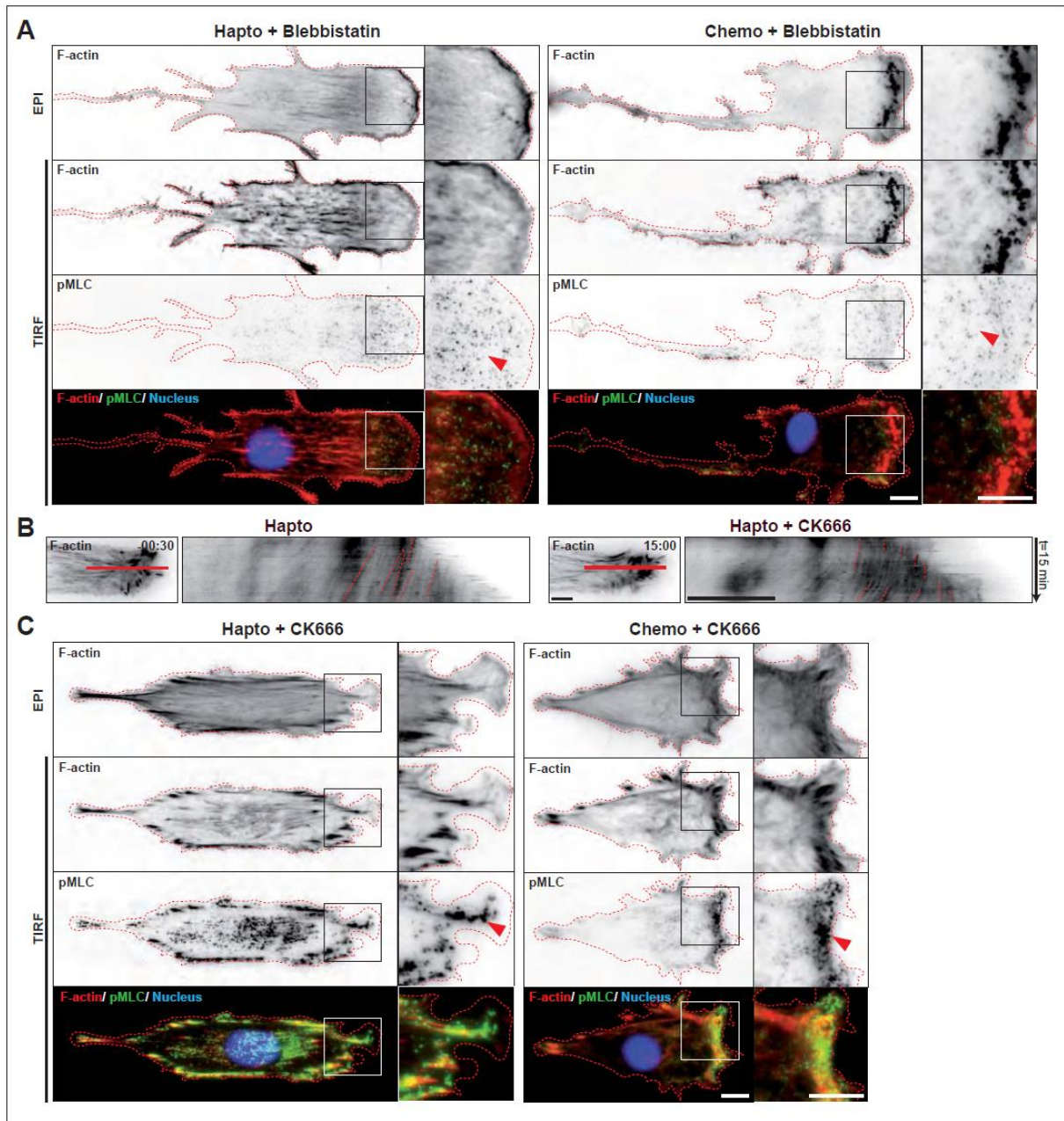


Figure S4. Subcellular localization of pMLC in response to myosin and Arp2/3 inhibition. Quantitation of actin retrograde flow in response to Arp2/3 inhibition. Related to Figures 5 and 6.

Representative micrographs are shown in ibw contrast, and/or as color composites. **(A)** pMLC signals after 1 hour treatment with 10 μ M blebbistatin. Red arrowhead indicates loss of pMLC signal at the leading edge in hapto cells, and loss of pMLC signal behind the PLS zone in chemo cells. **(B)** Representative TIRF micrographs and kymographs of F-actin dynamics (Lifeact-GFP) in hapto cells before and after 200 μ M CK666 incubation. Red dotted lines in kymographs represent actin arc dynamics indicative of actin retrograde flow. **(C)** pMLC signals of hapto and chemo cells after 1 hour treatment with 200 μ M CK666. Red arrowhead indicates pMLC signal in spindly protrusions of hapto cells, and rescue of leading edge pMLC directly at the leading edge in chemo cells. **(A,C)** Images have been scaled relatively to their untreated counterparts in Figure S3. Scale bars: **(A-C)** = 10 μ m.

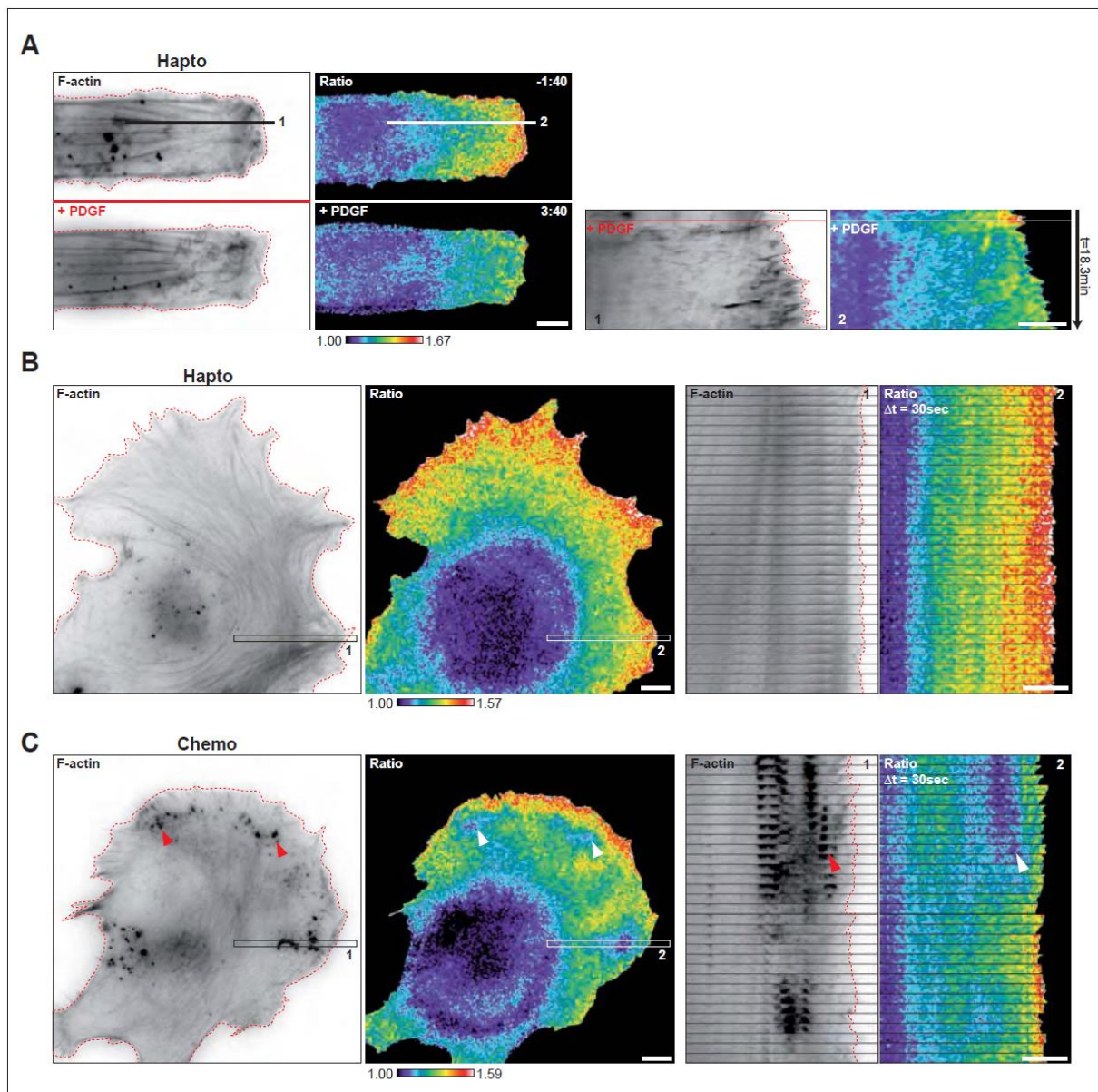


Figure S5. Additional RhoA activation experiments, related to Figure 7.

RhoA activity ratio images are color-coded according to the scale. F-actin (Lifeact-mCherry) images are shown in ibw contrast. **(A)** Representative RhoA activation dynamics in response to acute stimulation with 40 ng/ml PDGF on the line substrate. Representative micrographs pre- and post PDGF stimulation, as well as kymograph analysis are shown. **(B)** RhoA activation dynamics of hapto and chemo cells on the plane substrate (treated with 40 ng/ml PDGF for 5 hours). Representative micrographs as well as kymographs are shown. Note the broad RhoA activity gradient at the leading edge of hapto cells. White arrows indicate low RhoA activity in the vicinity of PLSs in chemo cells. Scale bars: **(A), (B)** = 10 μm .

3.10.3. Supplemental Movie Legends

Movie S1 Phase contrast movies of fibroblasts on plane and line substrates. Fibroblasts were plated in presence or absence of PDGF and imaging was started about 1 hour post plating. Scale bar = 100 μm . Timescale = hours:minutes. Related to Figure 1.

Movie S2 Global cell morphodynamics of Lifeact-GFP expressing hapto and chemo cells on the line substrate. Scale bar = 10 μm . Timescale = minutes:seconds. Related to Figure 2.

Movie S3 High resolution TIRF movies of hapto and chemo cells expressing Lifeact-GFP on the line substrate. Scale bar = 10 μm . Timescale = minutes:seconds. Related to Figure 3.

Movie S4 High resolution movies of Lifeact-mCherry/VASP-GFP signals of hapto and chemo cells on the line substrate. Scale bar = 10 μm . Timescale = minutes:seconds. Related to Figure 3.

Movie S5 High resolution movies of Lifeact-mCherry/MLC-GFP movies of hapto and chemo on the line substrate. Scale bar = 10 μm . Timescale = minutes:seconds. Related to Figure 5.

Movie S6 Global cell morphodynamics of Lifeact-GFP expressing hapto and chemo cells on the line substrate in response to blebbistatin or CK666 compounds. Scale bar = 10 μm . Timescale = minutes:seconds. Related to Figures 5 and 6.

Movie S7 High resolution movies of Lifeact-mCherry/VASP-GFP signals of hapto and chemo cells on the line substrate in response to acute Arp2/3 perturbation using the CK666 drug. Scale bar = 10 μm . Timescale = minutes:seconds. Related to Figure 6.

Movie S8 High resolution movies of Lifeact-mCherry/RhoA activation dynamics of hapto and chemo cells. Scale bar = 10 μm . Timescale = minutes:seconds. Related to Figure 7.

3.10.4. Supplemental References

Box, G.E.P., Jenkins, G.M., and Reinsel, G.C. (1994). Time series analysis: forecasting and control. 3rd ed Prentice Hall, Englewood Cliffs, NJ.

Fritz, R.D., Letzelter, M., Reimann, A., Martin, K., Fusco, L., Ritsma, L., Ponsioen, B., Fluri, E., Schulte-Merker, S., van Rheenen, J., *et al.* (2013). A Versatile Toolkit to Produce Sensitive FRET Biosensors to Visualize Signaling in Time and Space. *Science signaling* 6, rs12.

Machacek, M., and Danuser, G. (2006). Morphodynamic profiling of protrusion phenotypes. *Biophysical journal* 90, 1439-1452.

Nock, R., and Nielsen, F. (2006). "On Weighting Clustering". *IEEE Trans on Pattern Analysis and Machine Intelligence* 8, 1-13.

Wu, Z., Huang, N.E., Long, S.R., and Peng, C.K. (2007). On the trend, detrending, and variability of nonlinear and nonstationary time series. *Proceedings of the National Academy of Sciences of the United States of America* 104, 14889-14894.

4. Additional Results

Apart from results discussed in the manuscript in this section additional experiments and results are discussed.

4.1. PDGF Chemotaxis

4.1.1. Introduction

Chemotaxis, among other modes of directed cell migration, drives cells to their place of action in an organism. Fibroblasts are not professional chemotaxers and in order to enhance their response to chemotactic cues we engineered a system allowing cells to migrate on LSs during exposure to a PDGF gradient. The idea behind using LSs integrated in a gradient generator was arising from a study, which demonstrated, that 1D substrate can mimic 3D topologies (Doyle et al. 2009). We speculated, when cells migrate on line substrates, mimicking physiological matrix topologies, they might be able to integrate information about chemotactic gradient steepness more efficiently.

Further we hypothesized, that pre-polarization of cells might favor directional migration. On line substrates cells elongate and pre-polarize, meaning they are restricted in their decision which direction to migrate in: They can choose to go either left or right (Figure 23A). This pre-polarization simplifies polarization and enables the cell to migrate directionally while it is exposed to a growth factor (Figure 23B). However, cells on plane substrates are free to move in any direction (Figure 23C) and only transiently polarize, leading to random cell migration (Figure 23D).

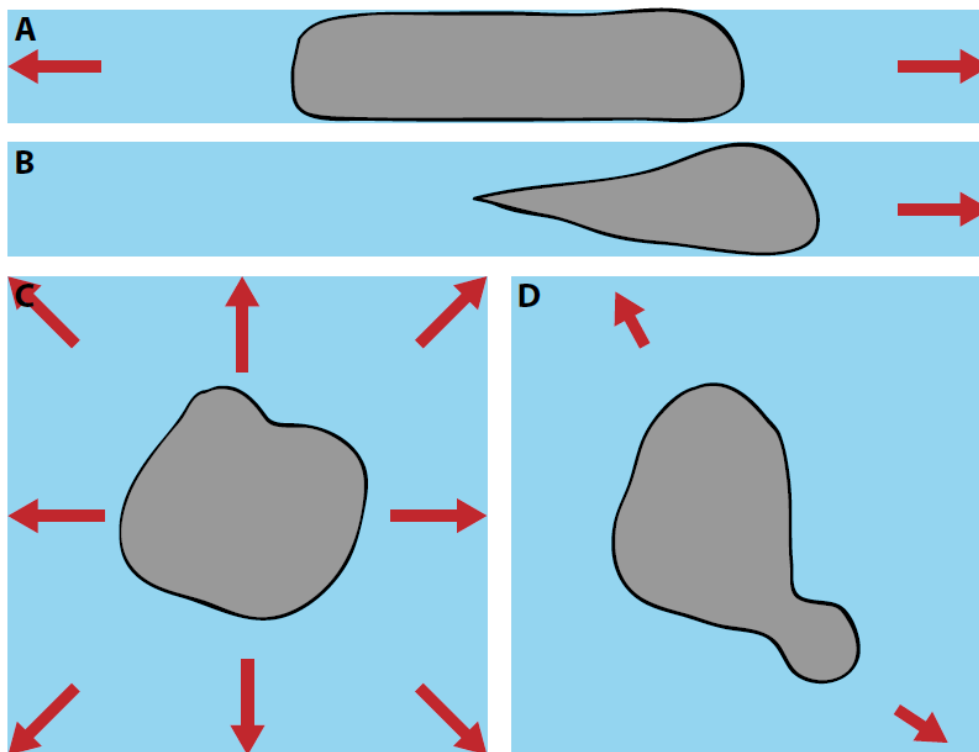


Figure 23: Possible directions of cell migration. (A) A cell in a pre-polarized state on a line substrate elongates and can either migrate left or right. (B) The cell has polarized on the line substrate and has decided for one direction of migration. (C) Cells on plane substrate are not limited in their possible migration directions. Not confined substrates allow any migration direction. (D) A cell on plane substrate transiently polarizes and migrates randomly.

Additionally, we considered, that elongated cells on line substrates (Figure 24A) encounter higher differences in PDGF concentration between leading and trailing edge in contrast to evenly spread cells on plane substrates (Figure 24B). We speculated that this might support cells during gradient sensing.

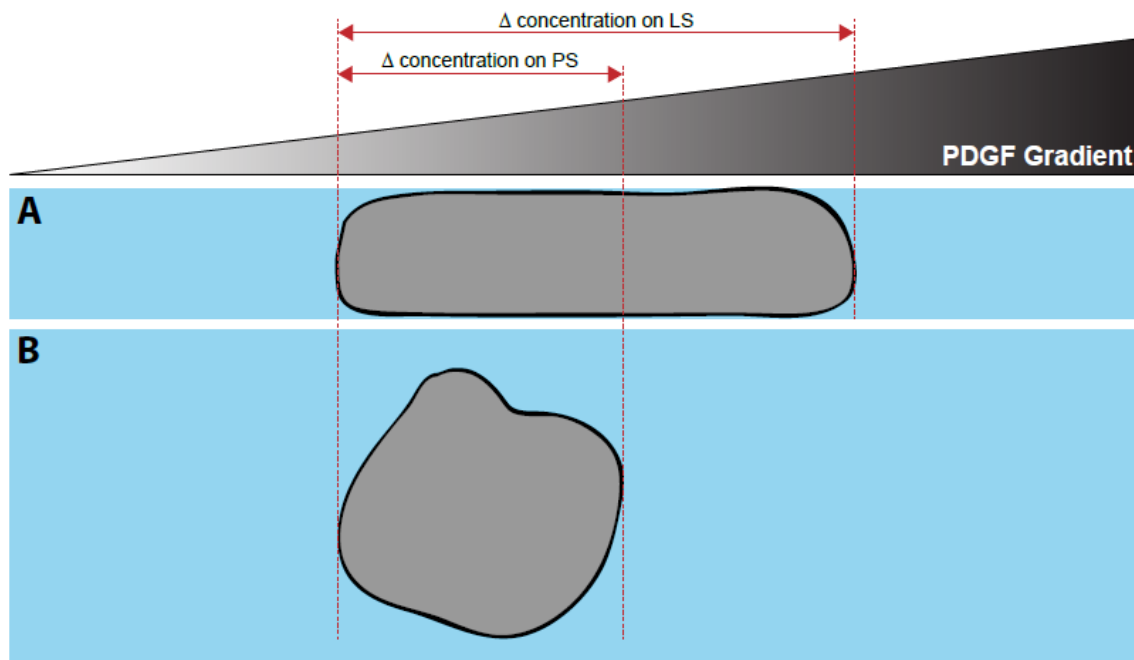


Figure 24: Gradient integration. (A) Cells on line substrates (LS) encounter higher PDGF concentration difference due to elongated shape compared to **(B)** equally spread cell on plane substrate (PS).

4.1.2. Results

Chemotaxis experiments were carried out using a diffusion-based gradient generator during phase contrast live cell imaging experiments. Cells were tracked manually and total travel distance and directionality over 12 hours was determined. Algebraic signs account for the direction: Positive values indicate migration in direction to the PDGF source, while negative values describe total migration distances towards lower PDGF concentrations.

Different cell lines were tested enabling us to select a cell system responding robustly to the PDGF gradient. We aimed to achieve robust chemotaxis in our system in order to reliably identify chemotaxing cells and further study their morpho- and signaling dynamics during directed cell migration.

Cells stimulated with a PDGF gradient (chemotaxis) were therefore compared to uniform stimulated (chemokinesis) and not stimulated cells (haptokinesis) respectively. Using statistical tests (ANOVA) it was determined, whether significant differences in directionality occurred.

4.1.2.1. Mouse Embryonic Fibroblasts (NIH 3T3)

For NIH 3T3 cells, no chemotactic response could be monitored. Direction of cell migration was not significantly different compared to control conditions (haptokinesis or chemokinesis) (Figure 25).

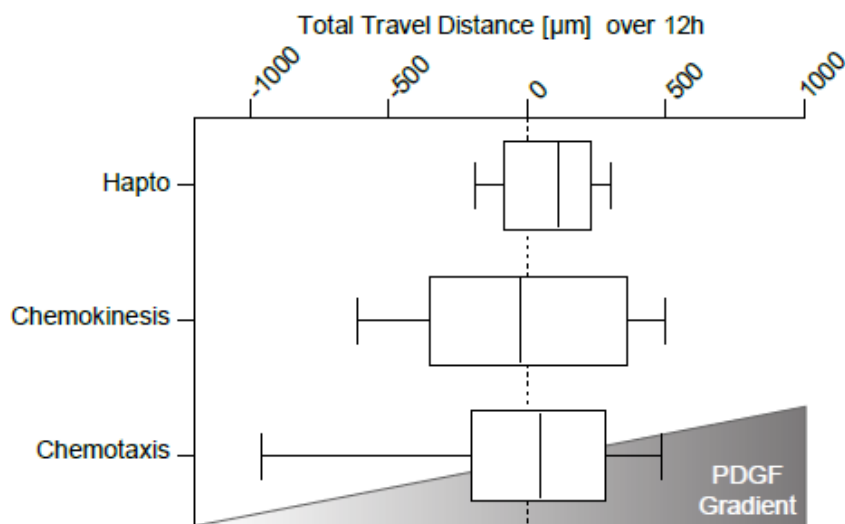


Figure 25: Chemotaxis experiment with NIH 3T3 fibroblasts. No significant difference in migration direction of gradient stimulated cells compared to bulk stimulated cells and not stimulated cells could be detected. N (Hapto) = 16; n (chemokinesis) = 29; n (chemotaxis) = 74; ANOVA (Dunn's multiple comparison test): No significant difference

4.1.2.2. Primary human foreskin fibroblasts (AG1518)

Primary human foreskin fibroblasts were responding to the chemotactic gradient of PDGF. Although, the system appeared to be noisy, meaning that a certain population of cells did not move towards the higher concentration of PDGF (Figure 26).

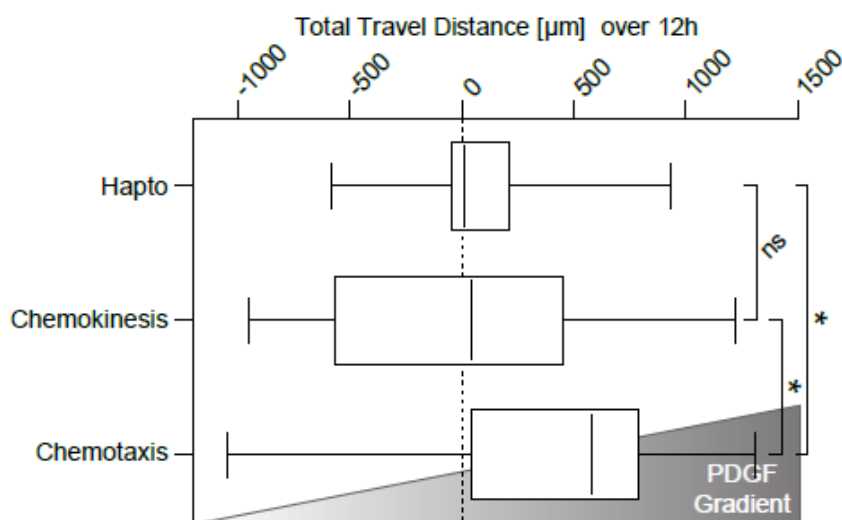


Figure 26: Chemotaxis experiment with primary human foreskin fibroblasts. Significant difference in migration direction of gradient stimulated cells compared to bulk stimulated cells and not stimulated cells could be detected. N (Hapto) = 34; n (chemokinesis) = 22; n (chemotaxis) = 30; ANOVA (Dunn's multiple comparison test), *P < 0.005

4.1.2.3. Rat embryonic fibroblasts (REF52)

Rat embryonic fibroblasts (REF52) did not differ in migration directionality between chemokinesis as control condition, and chemotaxis (Figure 27). However, we observed a trend in migration directionality towards higher concentrations of PDGF.

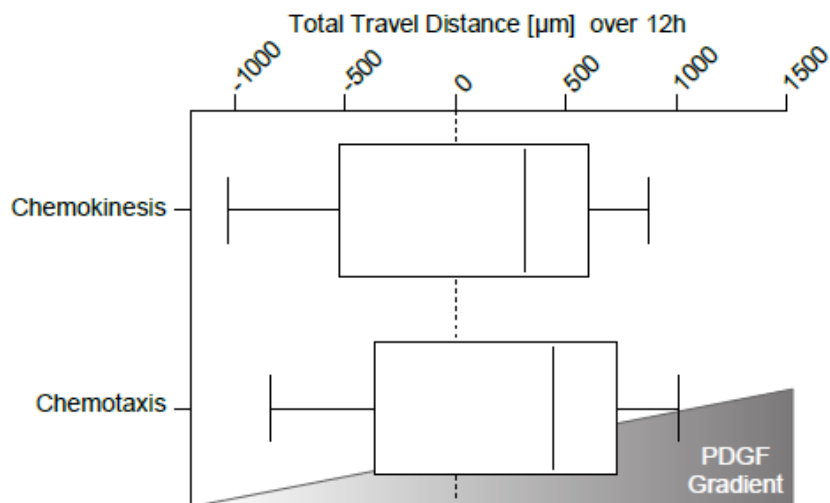


Figure 27: Chemotaxis experiment with REF52 fibroblasts. No significant difference in migration direction of gradient stimulated cells compared to bulk stimulated cells could be detected. N (chemokinesis) = 28; n (chemotaxis) = 31; ANOVA (Dunn's multiple comparison test): No significant difference

4.2. Immunofluorescence Stainings

4.2.1. Introduction

In order to gain more information about the system of hapto and chemo cells migrating on plane or line substrates we performed a variety of immunofluorescence staining of cells fixed. Here, hapto as well as chemo cells in a steady state of polarized migration on line and plane substrates were imaged. F-actin was stained beside each other target in order to relate observations to cytoskeletal structures.

4.2.2. Results

4.2.2.1. Paxillin

Paxillin, an adhesion structure component, was visualized by immunofluorescence stainings in fixed cells together with an F-actin staining using phalloidin-Alexa546 with TIRF microscopy. A DAPI staining was imaged with epifluorescence microscopy to show the nuclear localization (Figure 28). Strong paxillin signal appears at FAs, connected to SFs and at FCs, respectively. Hapto cells on PS and LS show a higher degree of elongated FAs enriched at the leading edge of the cell. However, chemo cells on LS do not display FAs but focal complexes at the leading edge without connection to SFs. While FCs exhibit prominent paxillin staining, only faint paxillin is detected at PLSs. Since chemo cells on PSs are more adhesive caused by the lack topological restriction, PLS zones are embedded in SF arrays. PLSs of chemo cells on PSs show, similar to those on LSs, only traces of paxillin staining.

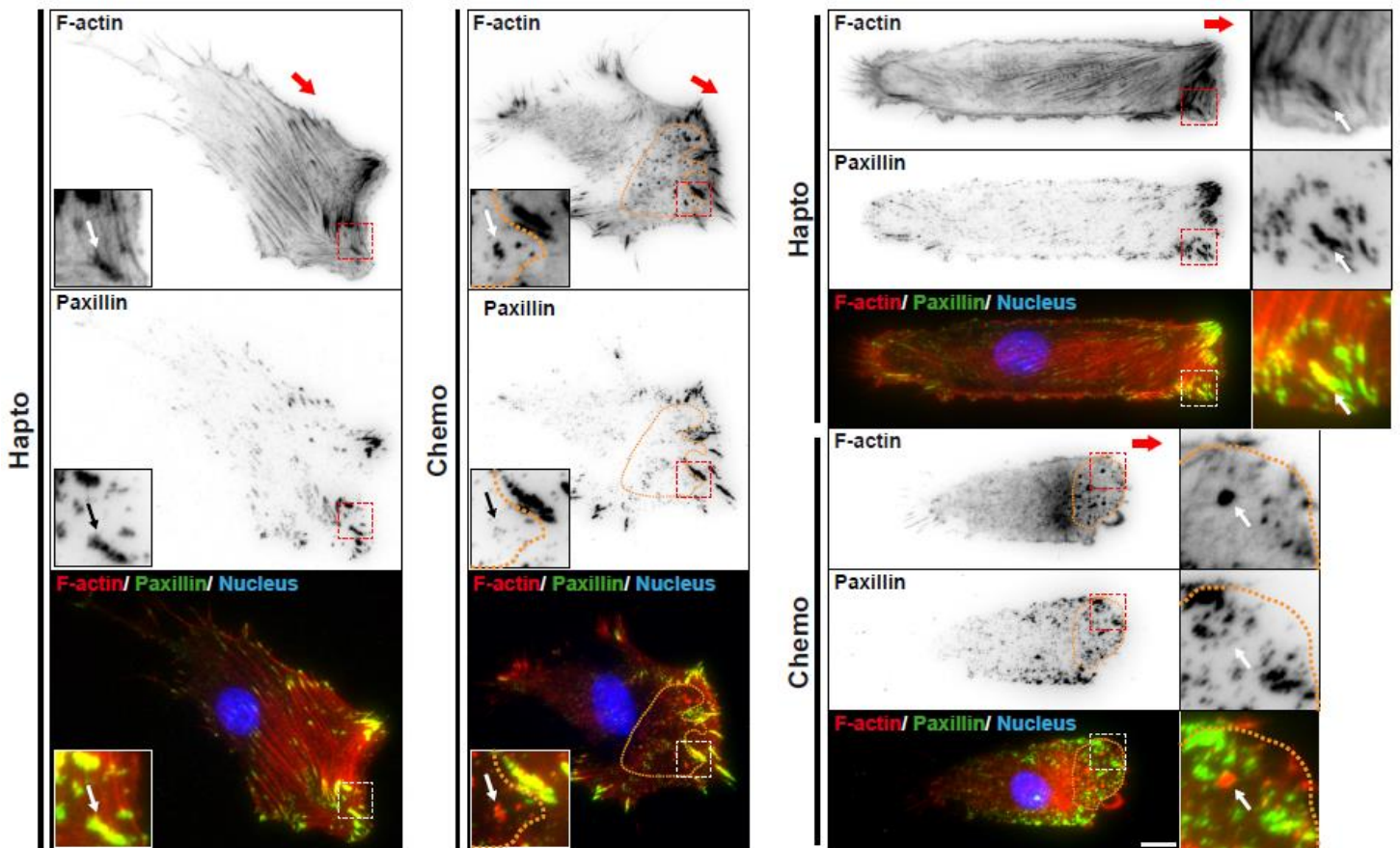


Figure 28: Actin and adhesion structures in hapto and chemo cells on PS and LS. Representative micrographs of immunofluorescence paxillin stainings together with phalloidin-Alexa 546 stained F-actin are shown in ibw contrast and as color composites. Insets originate from regions confined by either red or white dashed boxes. White/ black arrows point at FA, FCs or PLSs; Red arrow points in putative direction of cell migration; Orange boarder highlights PLS zones in chemo cells. Scale bars = 10µm

4.2.2.2. Talin

Fixed hapto and chemo cells on LS were stained with an antibody against talin and phalloidin-Alexa546 to co-visualize F-actin structures using TIRF microscopy (Figure 29). Nuclear localization was detected by epifluorescence imaging of a DAPI staining. In hapto cells, talin is enriched at elongated FAs as well as on FCs in chemo cells. Additionally, PLSs exhibit robust talin signals compared to other adhesion markers.

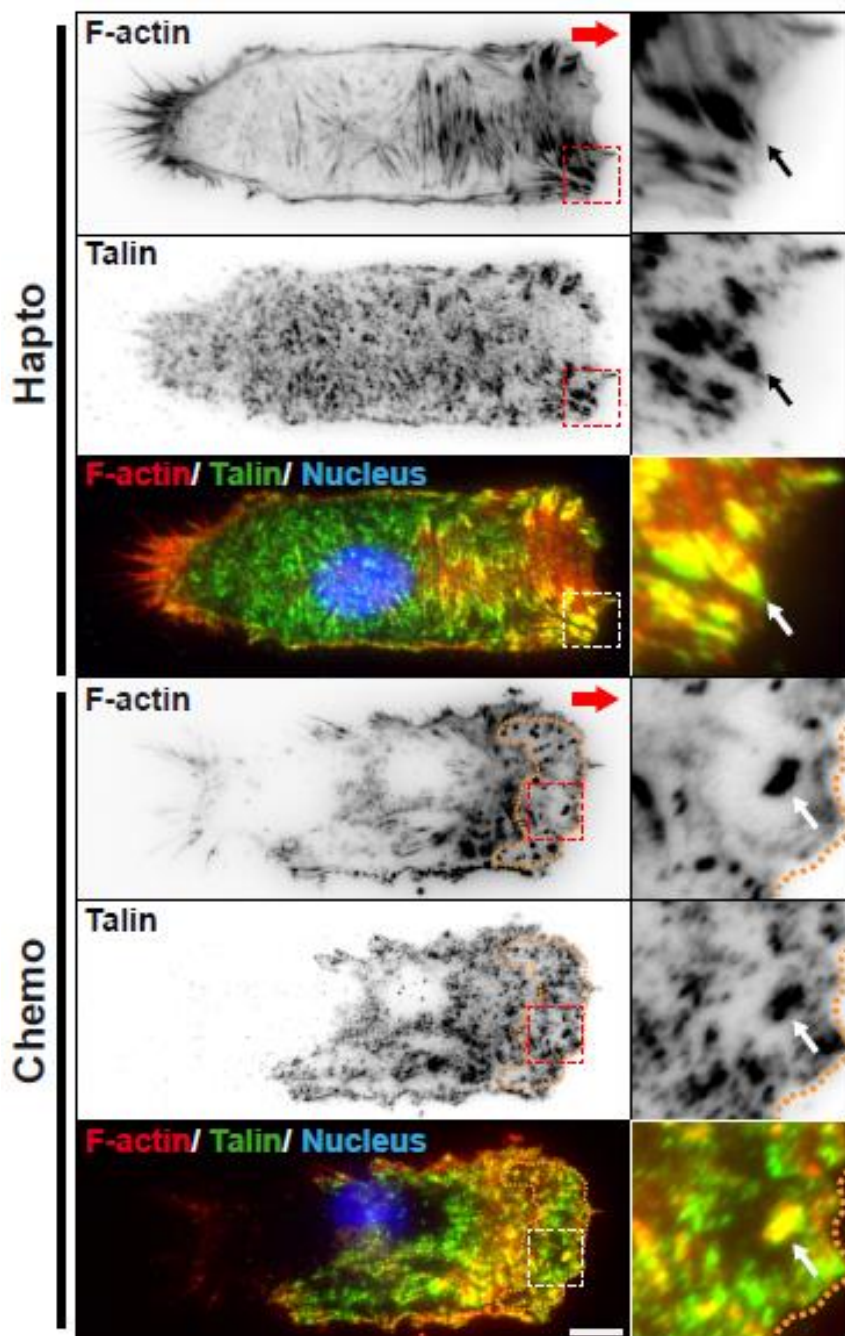


Figure 29: Actin and adhesion structures in hapto and chemo cells on PS and LS. Representative micrographs of immunofluorescence talin stainings together with phalloidin-Alexa546 stained F-actin are shown in ibw contrast and as color composites. Insets originate from regions confined by either red or white dashed boxes. White/ black arrows point at FA, FCs or PLSs; Red arrow points in putative direction of cell migration; Orange boarder highlights PLS zones in chemo cells. Scale bars = 10µm

4.2.2.3. Phospho Tyrosine

Tyrosine phosphorylation is a major step in signal transduction and also accompanies adhesion formation on substrates such as fibronectin (Sun et al. 2012; Burridge et al. 1992). In order to detect sites of adhesion assembly, fixed cells were stained with an antibody specific to phospho tyrosine together with F-actin and imaged using TIRF microscopy (Figure 30). Phospho tyrosine as marker for adhesion assembly is enriched at the cell leading edges at places of FAs, FCs as well as PLSs.

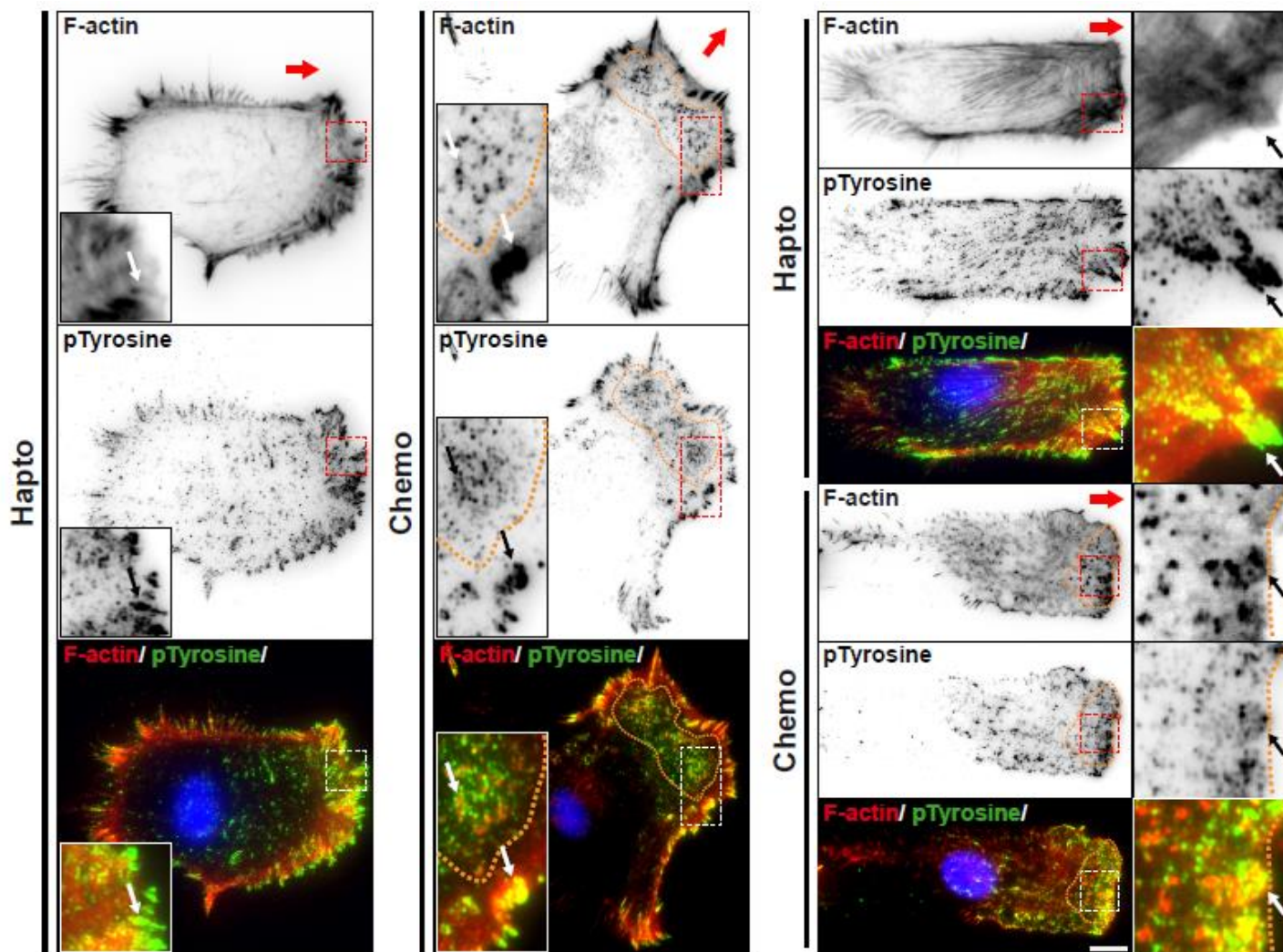


Figure 30: Actin and newly assembled adhesion structures in hapto and chemo cells on PS and LS. Representative micrographs of immunofluorescence p-tyrosine stainings together with phalloidin-Alexa546 stained F-actin are shown in ibw contrast and as color composites. Insets originate from regions confined by either red or white dashed boxes. White/ black arrows point at FA, FCs or PLSs; Red arrow points in putative direction of cell migration; Orange boarder highlights PLS zones in chemo cells. Scale bars = 10µm

4.2.2.4. Actin Related Protein 2 (Arp2)

Arp2, a component of the Arp2/3 complex, was visualized in fixed cells by immunofluorescence stainings, together with F-actin and a nuclear DAPI staining. TIRF imaging reveals enriched Arp2 abundance at the leading edge in both, hapto and chemo cells on either PS or LS (Figure 31). Arp2 was found in hapto cells at the lamellipodium as well as at the lamella. However, in chemo cells, strong Arp2 staining appears at PLSs consistent with literature (Albiges-Rizo et al. 2009; Murphy & Courtneidge 2011). Membrane ruffles at the leading edge extend in z and escape the TIRF field, and were therefore only captured in epifluorescence images.

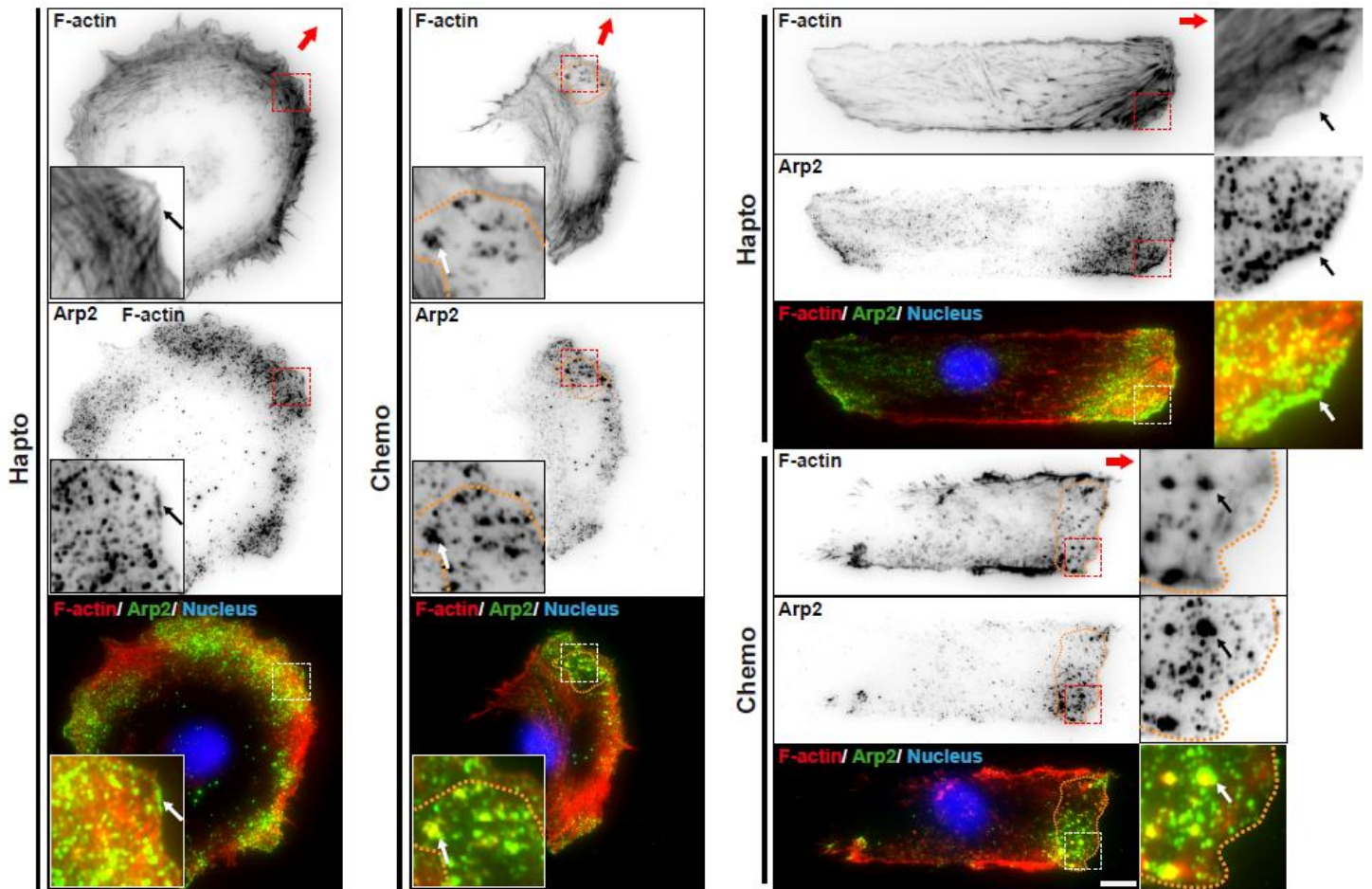


Figure 31: Immunofluorescence staining of Arp2 and F-actin. Arp2 together with F-actin was stained and TIRF imaged. A nuclear DAPI staining was imaged by epifluorescence microscopy. Micrographs are shown in ibw contrast as well as color composites. Insets originate from regions confined by either red or white dashed boxes. White/ black arrows point at the lamellipodia of hapto cells or PLSs in chemo cells; Red arrow points in putative direction of cell migration; PLS zones are highlighted by orange boarder. Scale bars = 10 μ m

4.2.2.5. β -PIX (Arhgef7)

The Rac1 GEF β -Pix, plays a role in Rac1 promoted destabilization of focal adhesions and enforces lamellipodial protrusion. Bound to actomyosin stress fibers, β -Pix is not available to activate Rac1 activation (Lee et al. 2010). However, at FCs and FAs β -Pix is enriched although myosin IIA activity is, leading to destabilization of adhesion structures (Kuo et al. 2011).

Fixed hapto and chemo cells on PS and LS were stained with an antibody against β -Pix were imaged simultaneously with a phalloidin-Alexa546 staining of F-actin in TIRF mode. Immunofluorescence staining reveals enrichment of β -Pix at the leading cell edge of polarized cells (Figure 32), specifically at adhesion sites and SFs. In contrast, β -Pix is not enriched at PLSs (Figure 32, chemo), which were shown prior to lack Myosin IIA activity. This proposes a different regulation of PLSs in contrast to FCs or FAs, in presumably mechanoinsensitive manner not directly involving β -Pix.

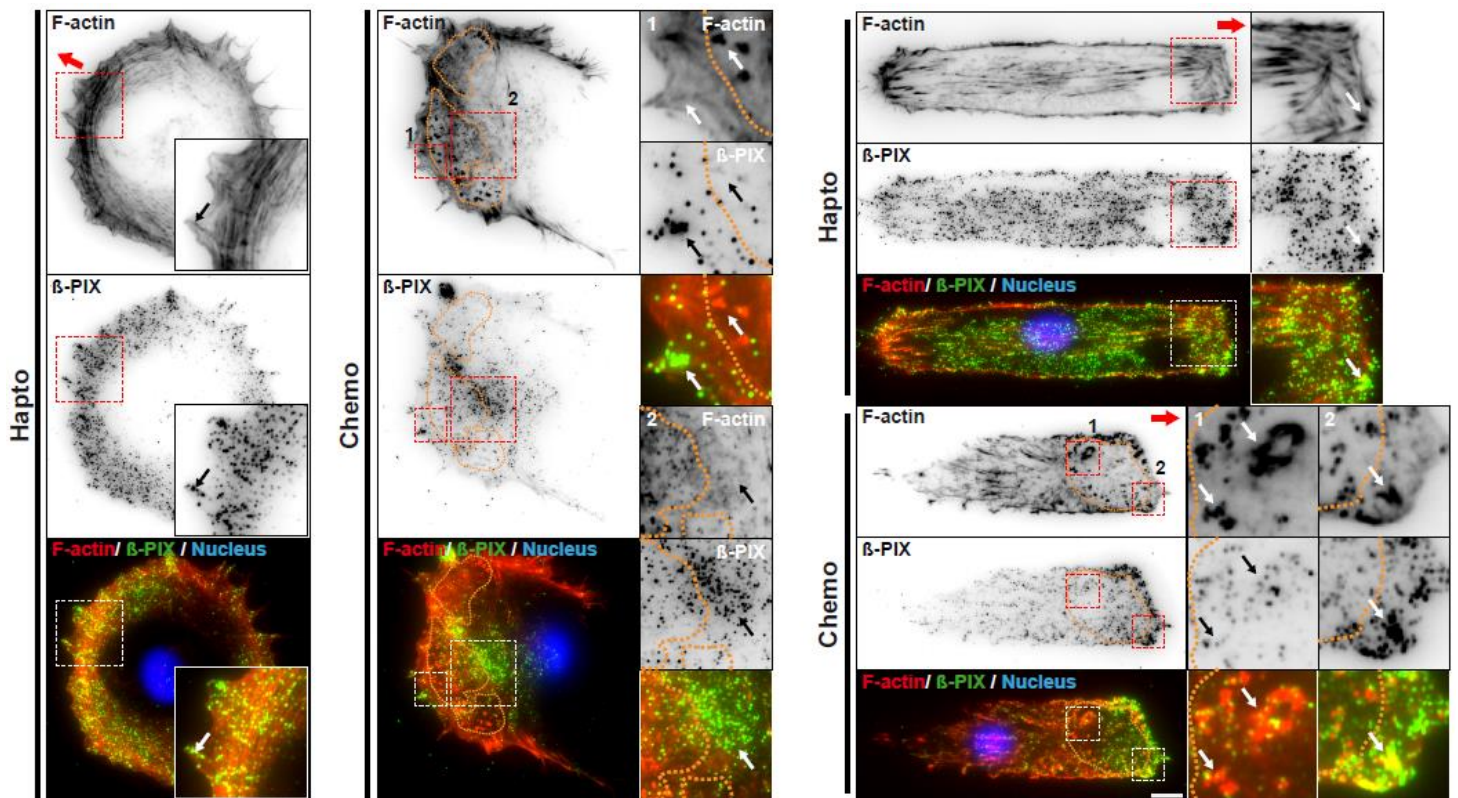


Figure 32: Immunofluorescence stainings of β -PIX and F-actin. β -PIX together with F-actin was stained and imaged using TIRF microscopy. A nuclear DAPI staining was imaged by epifluorescence microscopy. Micrographs are shown in ibw contrast as well as color composites. Insets originate from regions confined by either red or white dashed boxes. Black or white arrows point at adhesion structures co-localizing with β -PIX in hapto cells. In chemo cell on PS arrows in inset 1 point at FCs and PLS, in inset 2 at β -PIX cluster behind PLS zone. Arrows in inset 1 of chemo cell on LS point at PLS, in inset 2 at FCs; Insets originate from red/ white squared region; Red arrow points in putative direction of cell migration; PLS zones are highlighted by orange boarder. Scale bars = 10 μ m

4.2.2.6. TIAM1 (T-cell Lymphoma Invasion and Metastasis 1)

The Rac1 GEF TIAM1 is, among other functions, involved in establishment of cell polarity by interaction with the PAR complex, a major player in cell polarization. TIAM1 was visualized using TIRF microscopy after antibody staining simultaneously with phalloidin-Alexa546 stained F-actin structures and a DAPI nuclear stain.

Consistent with literature, TIAM1 is more abundant at the leading edge of polarized cells, specifically at FAs, FCs and SFs (Figure 33) (Wang et al. 2012). However, TIAM1 levels were low at PLS.

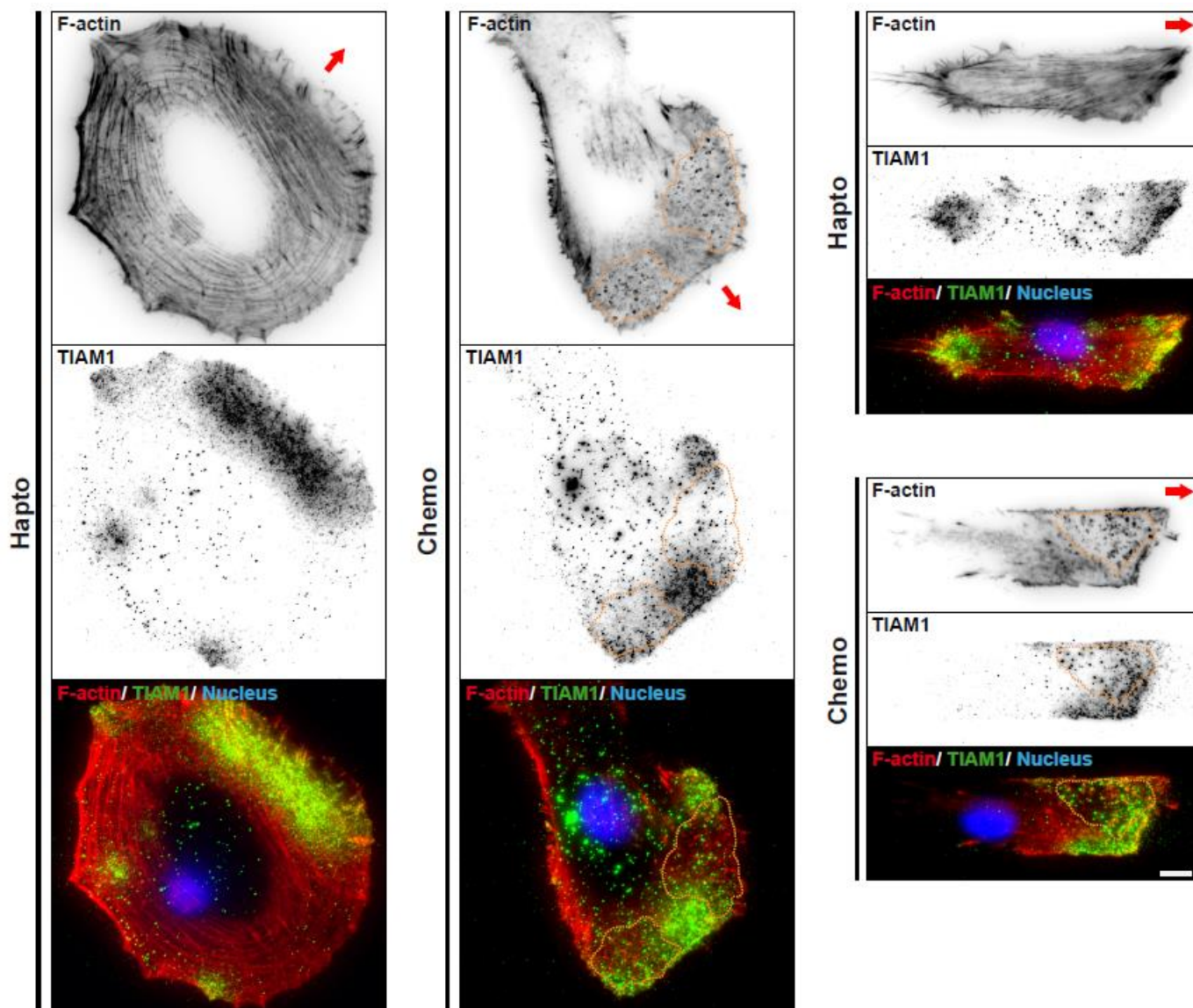


Figure 33: Immunofluorescence stainings of TIAM1 and F-actin. TIAM1 was stained together with F-actin and imaged using TIRF microscopy. A nuclear DAPI staining was imaged in epifluorescence mode. Micrographs are shown in ibw contrast as well as color composites. Red arrow points in putative direction of cell migration and PLS zones are highlighted by orange border. Scale bars = 10µm

4.2.2.7. α -Tubulin

Microtubules exhibit a heterodimeric structure, composed of α and β tubulin subunits, arranged - head to tail - in a hollow tube. Additionally to the F-actin cytoskeleton, microtubules play an important role in many processes such as cell division, cell migration or intracellular cargo transport. Microtubules are polar filaments containing an α -tubulin exposing, slow-growing, so called minus end (-end) and a β -tubulin exposing fast-growing plus end (+end) (Nogales & Wang 2006). Since microtubules, adhesion structures and cytoskeleton are mutually influencing each other it was as well of interest to investigate microtubule organization in our cell system of hapto and chemo cells on either PS or LS (Stehbens & Wittmann 2012). Stainings of fixed cells with an antibody specific to α -tubulin and phalloidin-Alexa546 to co-visualize F-actin structures were imaged using TIRF and epifluorescence microscopy (Figure 34). TIRF microscopy reveals, that α -tubulin is enriched at the ventral part of the leading edge in hapto cells and at the same time aligns with SF orientation. In contrast, chemo cells on PS and LS display no co-localization of α -tubulin with PLSs at the ventral part of the cell. However, in epifluorescence images microtubules are recognizable, telling that microtubules are located above PLSs but obviously do not physically interact with them. Though, in vicinity to the PLS zone, microtubules appear again in the TIRF field. Interestingly, chemo cells, exhibiting bursting lamellipodial protrusions, do not show α -tubulin stainings in these dynamic structures presumably, because no focal contact was established yet.

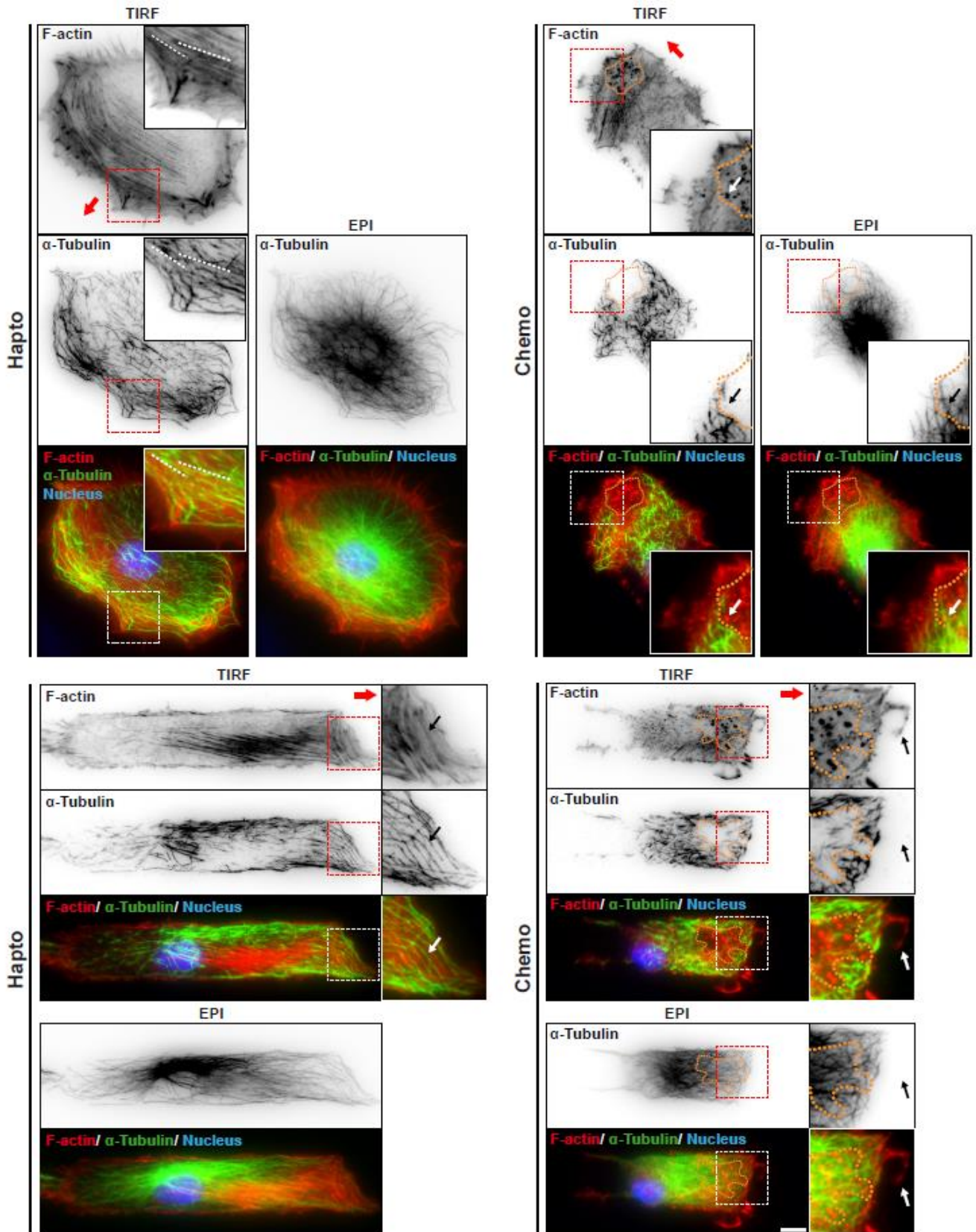


Figure 34: Immunofluorescence stainings of α -Tubulin and F-actin. α -Tubulin together with F-actin was stained and imaged using TIRF and epifluorescence microscopy. A nuclear DAPI staining, imaged using epifluorescence microscopy, was included. Representative micrographs are shown in ibw contrast as well as color composites. Insets originate from regions confined by either red or white dashed boxes. White dashed lines in insets of hapto cells on PS and black/ white arrows in insets of hapto cells on LS indicate alignment of SFs and microtubules prominent in TIRF images. Note, in PLSs zone of chemo cells on PS and LS no α -tubulin was detected in the TIRF field, but in EPI. Black/ white arrows point at PLSS in chemo cell on PS, where microtubules are located above. In chemo cells on LS black/ white arrows indicate a lamellipodial protrusion lacking MTs. Red arrow points in putative direction of cell migration; PLS zones are highlighted by orange border. Scale bars = 10 μ m

4.2.2.8. EB3 (End Binding Protein 3)

While microtubule -ends are in most cases stably anchored, +ends are highly dynamic and undergo phases of growth and shrinkage. A variety of so called microtubule plus-end tracking proteins (+TIPs), which are structurally and functionally very diverse associate specifically with growing microtubule +ends (Mimori-Kiyosue et al. 2000; Schuyler & Pellman 2001). Therefore, the end binding protein (EB3) can be used as indicator of microtubule +ends (Komarova et al. 2009).

In order to determine the orientation of microtubule polymerization or distribution of +ends respectively, fixed hapto and chemo cells on PS and LS were stained with an antibody against EB3. EB3, together with phalloidin-Alexa546 stained F-actin, was visualized using TIRF microscopy (Figure 35). Consistent with α -tubulin stainings (Figure 34) enrichment of EB3 is not co-localizing with PLSs at the ventral part of the cell, but however appears in vicinity to the PLSs. Moreover, hapto cells, on either PS or LS, display EB3 enriched at the leading edge.

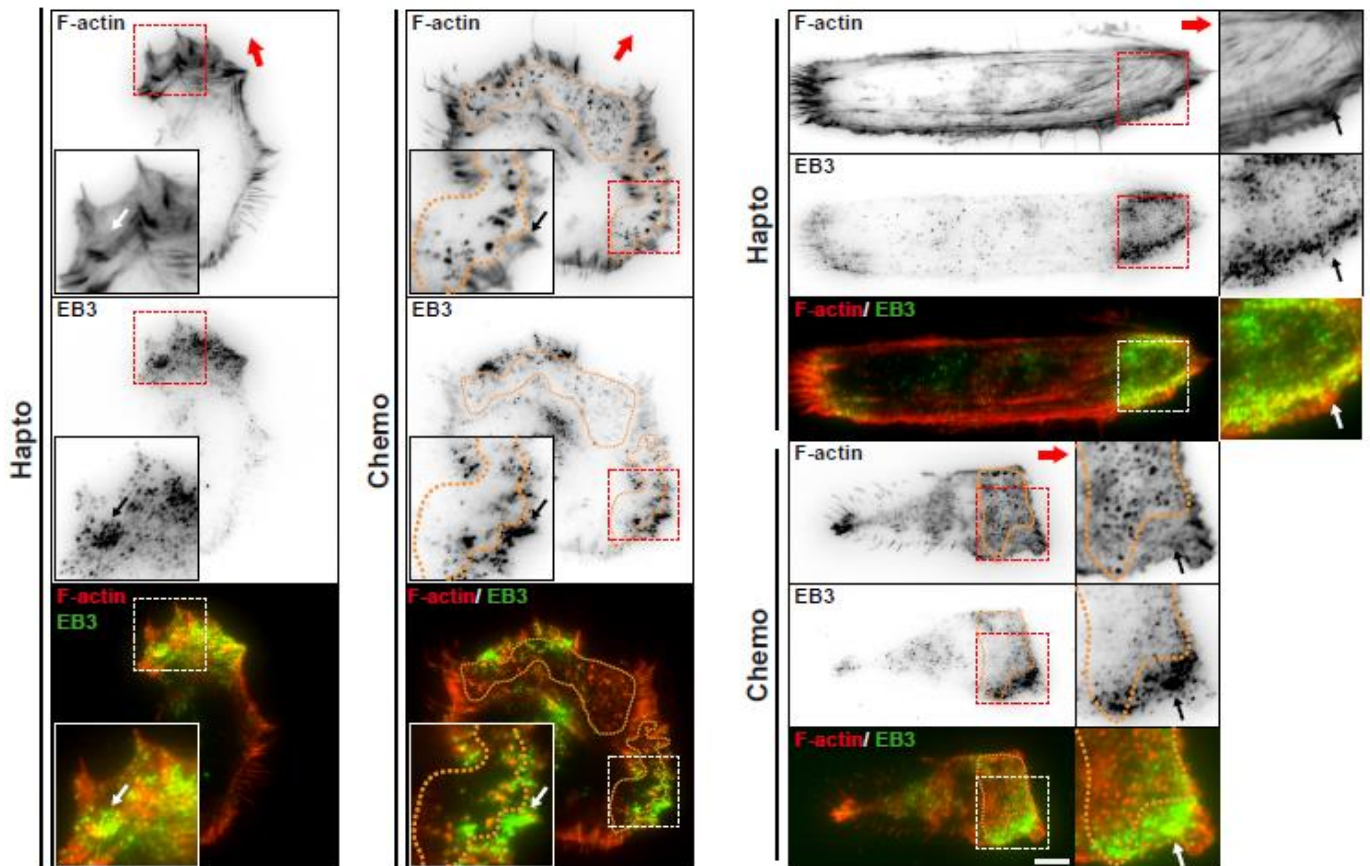


Figure 35: Immunofluorescence stainings of EB3 and F-actin. EB3 together with F-actin was stained and imaged using TIRF microscopy. A nuclear DAPI staining was imaged by epifluorescence microscopy. Micrographs are shown in ibw contrast as well as color composites. Insets originate from regions confined by either red or white dashed boxes. Black/ white arrows in insets of hapto cells on PS point at EB3 enrichment in vicinity to FAs at the ventral part of the leading edge. Similarly, EB3 is enriched at the leading edge of hapto cells on LS at the leading edge close to SF arrays and FAs (indicated by black/ white arrows in insets). In chemo cells on PS and LS EB3 is absent at the ventral part of PLS zones, but appears in their vicinity at the very leading edge (indicated by black/ white arrows in corresponding insets). Red arrow points in putative direction of cell migration; PLS zone is highlighted by orange border. Scale bars = 10 μ m

4.3. Fluorescence Live Cell Imaging

4.3.1. Introduction

A variety of fluorescently tagged proteins were tested during this work. This section summarizes observations which are not included in the paper. During these tests we realized that not all fluorescently tagged proteins expressed in the REF52 cell system led to satisfying quality of data sets. Primarily, problems we encountered involved abnormal cell morphology for majority of the cells although we generated stable cell lines expressing the target protein at low levels. Aberrations in phenotype and motility became especially obvious, when cells were grown on line substrates. There it seemed, that cells are in general more sensitive to any perturbations (sheer stress, drugs,...data not shown).

However, I discuss in this section dynamics of fluorescently tagged adhesion markers and caveolin-1(Y14F) during live cell imaging experiments. In most cases Lifeact-mCherry was co-expressed to relate to F-actin dynamics. Finally, I report on preliminary results derived from FRET live cell imaging experiments using Rac1 and Cdc42 biosensors in relation to F-actin dynamics.

4.3.2. Results

4.3.2.1. β_3 -Integrin

β_3 -integrin dynamics were monitored during live cell imaging experiments (Figure 36). At the time these imaging experiments were performed there was no TIRF system available and therefore images were acquired in epifluorescence mode. The Adenovirus used for transient transduction of Lifeact-mCherry was at that stage of the project not established and thus unfortunately F-actin dynamics are missing. Despite these limitations, it was possible to observe maturation of β_3 -integrin containing FCs and FAs in hapto as well as sliding retrograde motion of FAs during migration. Chemo cells showed fast turnover of FCs and lateral FAs with low sliding motion. Interestingly, we observed in chemo cells transport of endocytotic vesicles containing recycled β_3 -integrin.

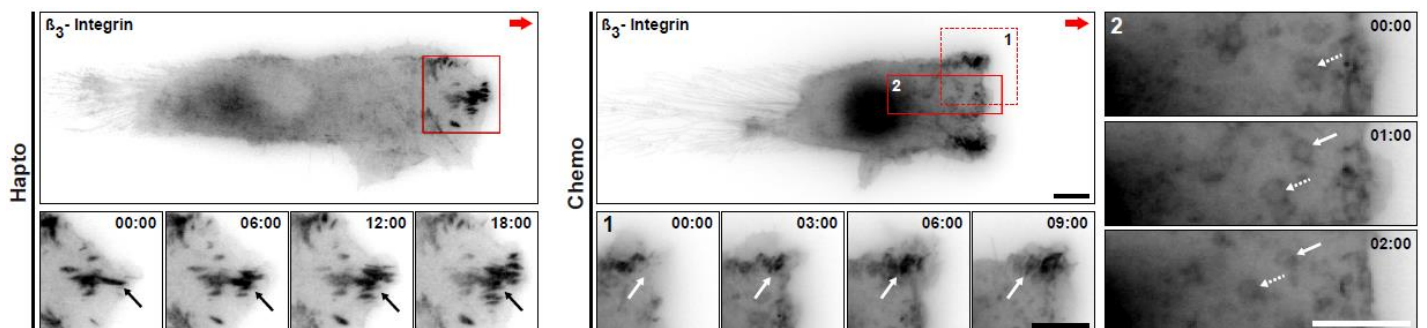


Figure 36: Epifluorescence live cell imaging of β_3 -integrin dynamics in hapto and chemo cells on LS. β_3 -integrin was imaged in living cells using epifluorescence microscopy. Micrographs are shown in ibw contrast. Insets of time series originate from regions confined by red/ red dashed boxes in hapto and chemo. Black arrows in insets of hapto follow FA assembly and maturation. White arrows in inset 1 of chemo follow turnover of lateral FA in chemo. White/ white dashed arrows in inset 2 of chemo point at endocytotic vesicles traveling from the leading edge towards cell center. Red arrow points in direction of cell migration; PLS zone is highlighted by orange boarder. Time indicated in minutes:seconds; Scale bars = 10 μ m

4.3.2.2. β_1 Integrin

β_1 -integrin, forming heterodimers with the α -integrin subunit, is involved in adhesion of fibroblasts to the matrix fibronectin. In order to image β_1 -integrin in living cells, the construct β_1 AK80GFP was stably expressed in REF52 and simultaneously imaged with the F-actin marker Lifeact-mCherry using TIRF microscopy (Figure 37). In the construct β_1 AK80GFP the N- and C-terminus of β_1 integrin were preserved to obtain wild-type like β_1 integrin properties.

β_1 -integrin was found to localize at FAs, FCs and PLSs throughout time lapse experiments. Interestingly, β_1 -integrin dynamics show, that in hapto cells on LS, distinct motions of adhesions occur at the same time. At the lamellipodium, formation of FCs is initiated, which mature immediately to FAs due to the highly contractile nature of REF52 cells. SFs attached to FAs pull on these and cause their further maturation and retrograde sliding motion, driven by retrograde F-actin flow. Retrograde F-actin flow appears as well at lateral cell edges. However, a region in the central part of the cell exhibit anterograde flow of F-actin and β_1 -integrin.

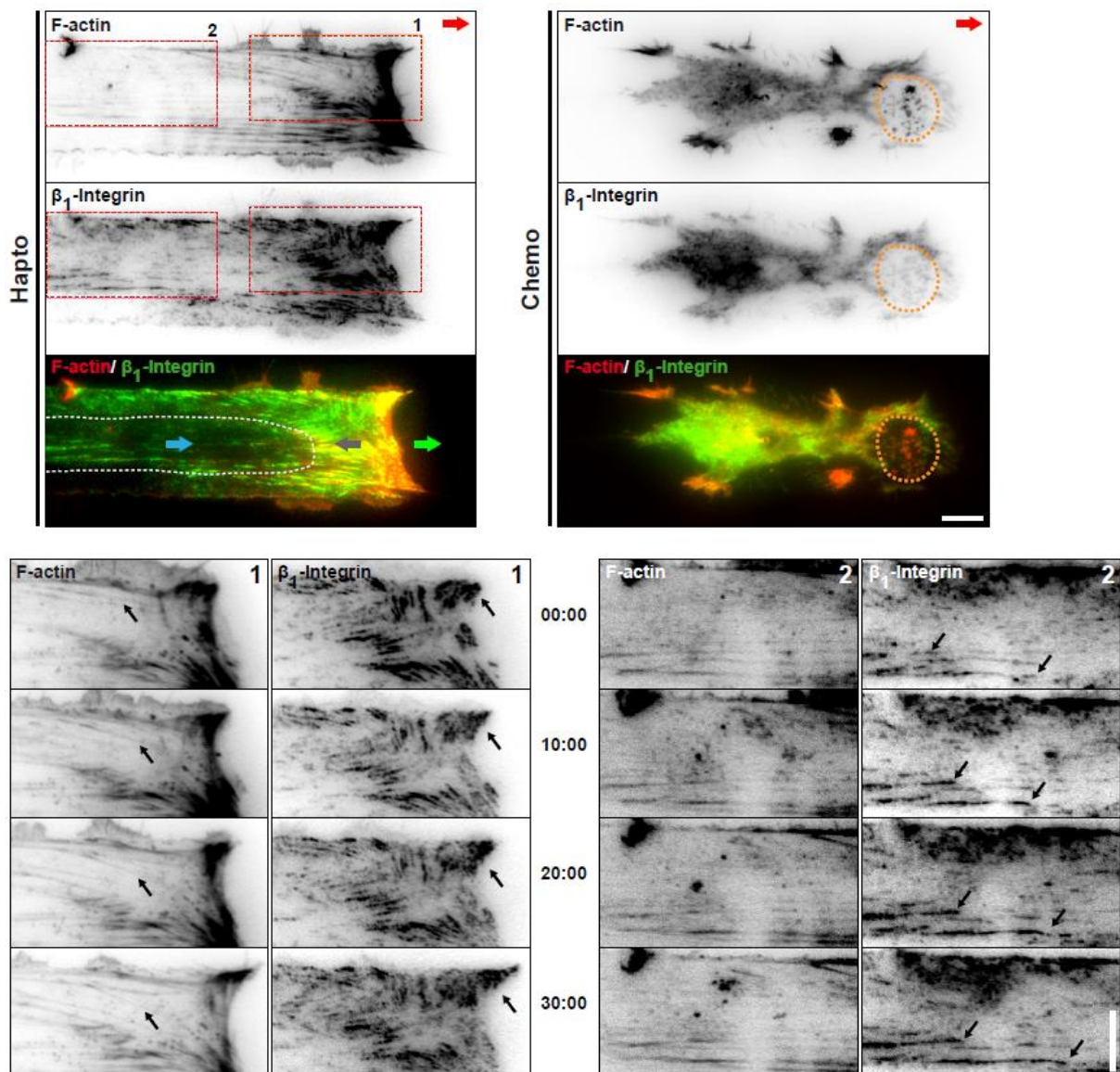


Figure 37: TIRF live cell imaging of β_1 -integrin and F-actin dynamics in hapto and chemo cells on LS. β_1 -integrin were imaged together with Lifeact-mCherry in living cells using TIRF microscopy. Micrographs are shown in ibw contrast and color composites. Insets of time series originate from regions confined by red dashed boxes in hapto. Black arrows in inset 1 (F-actin) follow retrograde F-actin flow; black arrows in inset 2 (β_1 -integrin) point at maturing FA. Black arrows in inset 3 (β_1 -integrin) point at β_1 -integrin moving in anterograde fashion. Blue arrow shows direction of anterograde flow in the proximal cell body (confined by white dashed line), while grey arrow follows the direction of retrograde F-actin flow. Green arrow points into direction of leading edge progression. Orange dashed line confines PLS zone in chemo cell. Red arrow points in direction of cell migration; PLS zone is highlighted by orange boarder. Time indicated in minutes:seconds; Scale bars = 10 μ m

4.3.2.3. Vinculin

The adhesion component vinculin was imaged simultaneously with Lifeact-mCherry (Figure 38) using TIRF microscopy. Monitoring of vinculin and F-actin dynamics showed that F-actin and adhesion flow occurs in various directions. At the leading edge of hapto cells retrograde flow was observed, while in proximal parts of the cell anterograde flow of F-actin and vinculin was noticed. However, chemo cells exhibited mainly anterograde flow of vinculin, consistent with the observation, that retrograde F-actin flow and therefore adhesion maturation is abolished at the leading edge.

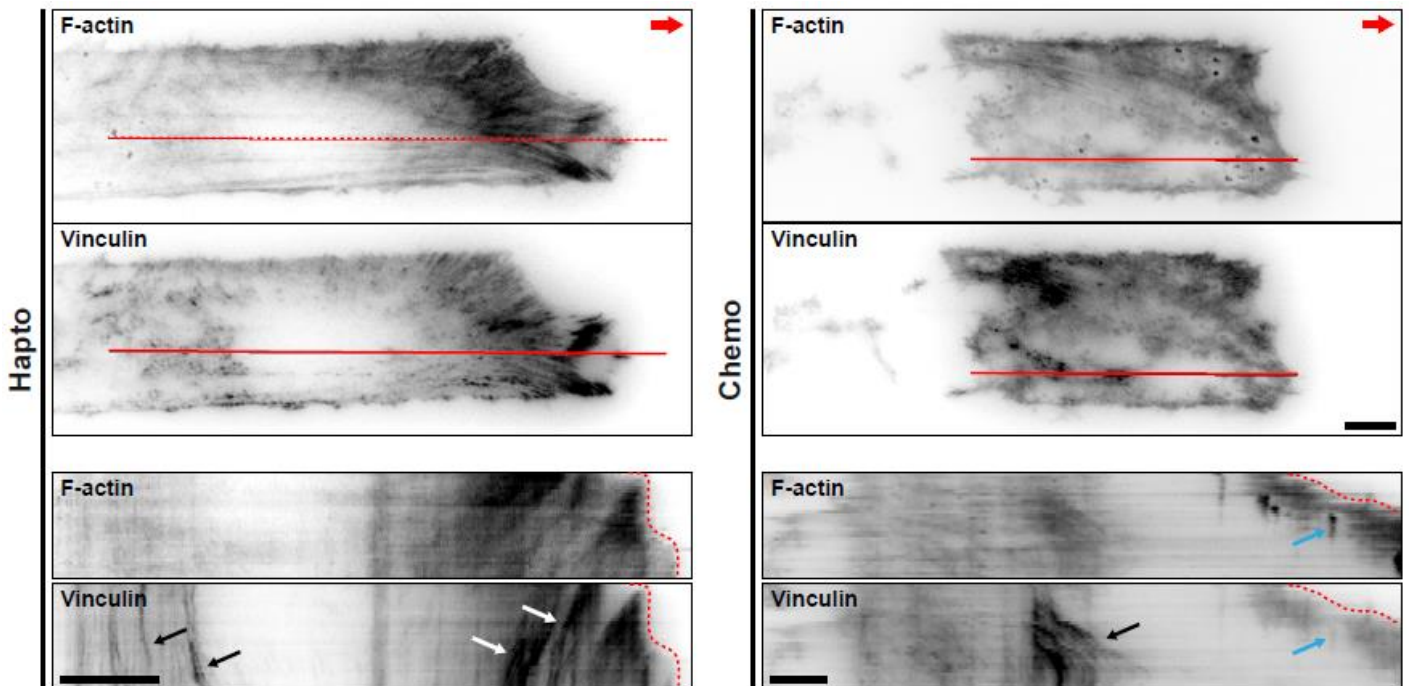


Figure 38: TIRF live cell imaging of Vinculin and F-actin dynamics in hapto and chemo cells on LS. Vinculin and F-actin dynamics have been imaged simultaneously during live cell imaging experiments in TIRF mode. Micrographs are shown in ibw contrast. Kymograph analysis along red line reveal retrograde flow (white arrows) at the leading edge and anterograde flow (black arrows) in proximity of the cell body in hapto. In chemo cells mainly anterograde flow occurs (black arrow), while PLS (blue arrows) show static contact to the substrate. Red dashed line in kymographs follow leading edge progression; Red arrow points in direction of cell migration; Scale bars = 10 μ m

4.3.2.4. Caveolin-1 (Y14F) (Dominant Negative Mutant)

Caveolin is one of the major components of caveolae, which are bulb-like membrane structures getting finally invaginated to perform cargo transport. Despite transport functions, caveolae seem to be involved in mechanotransduction too: Due to mechanical stress, caveolae flattening is induced leading to various downstream effects, while serving as buffer of membrane supply to prevent membrane rupture. Caveolin-1 localizes to the plasma membrane or caveolae and was shown to heterogeneously distribute in migrating cells with enrichment at the trailing edge (Parat et al. 2003). While it was reported that over expression of wild type caveolin-1 increases caveolae density, the over expression of the dominant negative form, caveolin-1 (Y14F), does not change caveolae abundance (Shatz et al. 2010). This leads to the consideration, that caveolae homeostasis is not altered, when endogenic expression of caveolin-1 remains unchanged. Similar to this study, caveolin-1 (Y14F) was enriched at the trailing edge in hapto and chemo cells. Since caveolin-1 locates to the plasma membrane, it can be considered as membrane marker with the special feature of dotted appearance. By following the displacement of these dots it was possible to observe dynamics of membrane flow. In TIRF live cell imaging experiments Lifeact-mCherry and Caveolin-1(Y14F)-GFP were imaged simultaneously in hapto and chemo cells migrating on LS (Figure 39). Micrographs shown in figure 39 illustrate observations qualitatively: Interesting in hapto cells, membrane dynamics of different velocities and directionalities occurred. At the leading edge, membrane was pulled back similar to retrograde F-actin flow, while lateral membrane followed an anterograde F-actin flow. Interestingly, in proximal regions of the cell, vortical dynamics appeared, reminiscent of turbulent flow in fluidic systems. In contrast, membrane flow of chemo cells happened in a more organized fashion. There, direction of membrane flow uniformly pointed into direction of cell migration following anterograde F-actin flow. Consistent with the finding, that PLS zones inhibit retrograde F-actin flow at the leading edge, retrograde membrane flow was absent from the leading edge of chemo cells.

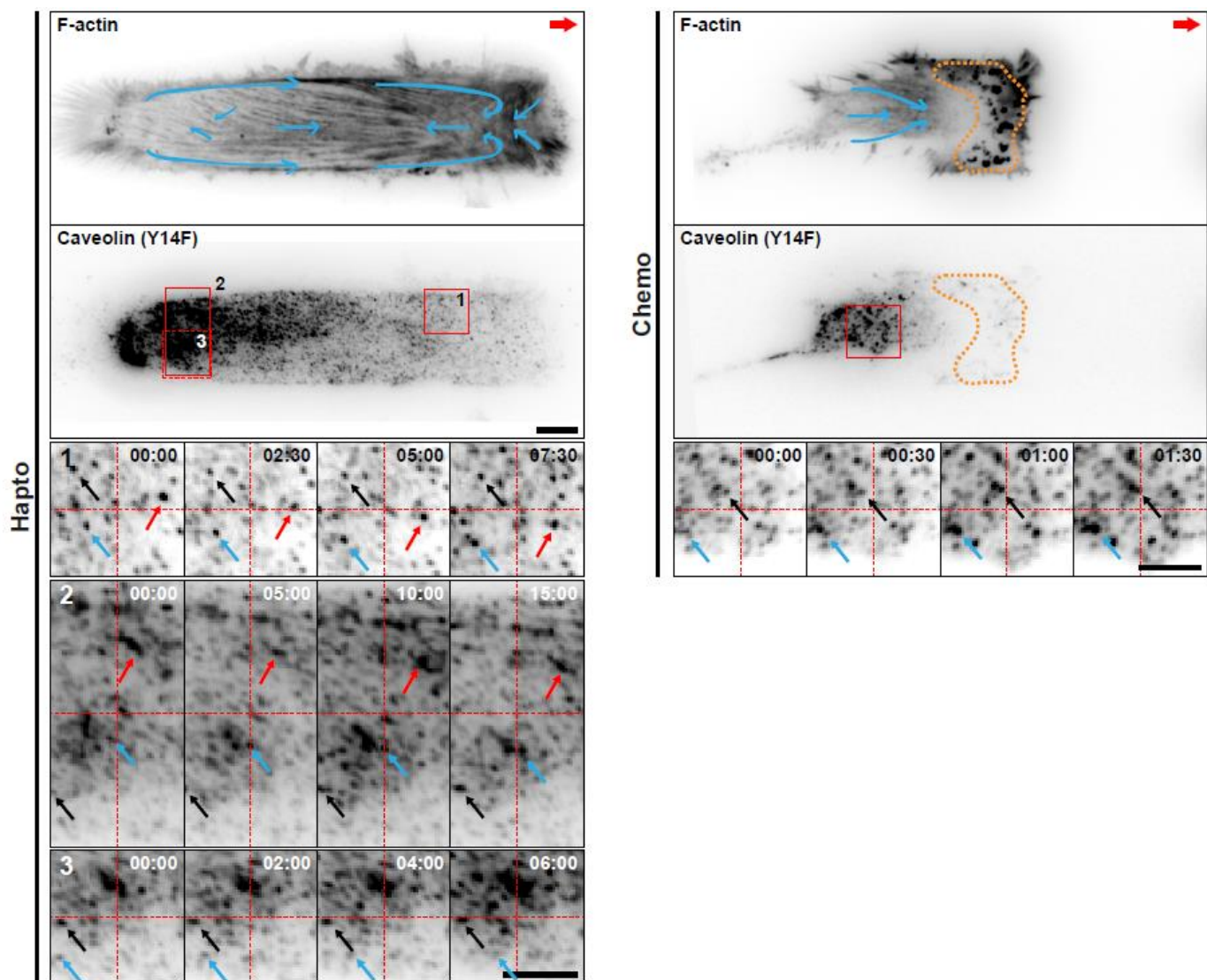


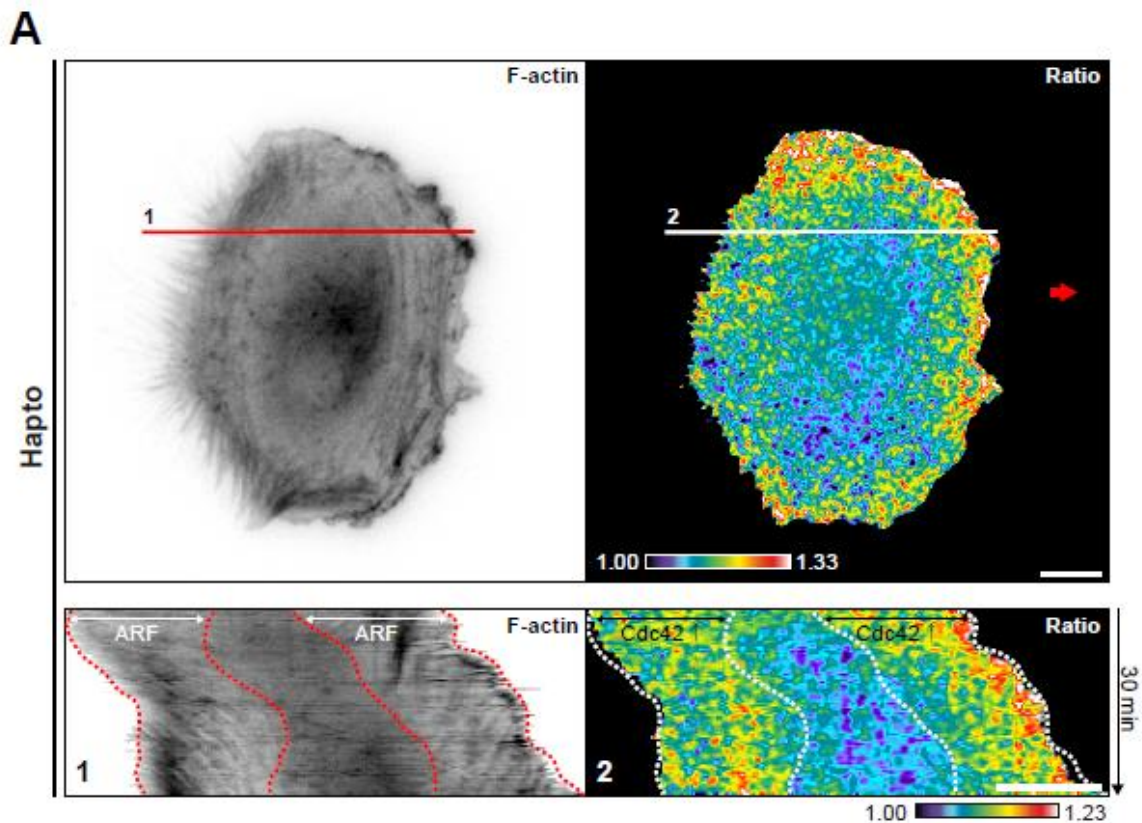
Figure 39: TIRF live cell imaging of caveolin-1 (Y14F) and F-actin dynamics in hapto and chemo cells on LS. Caveolin-1 (Y14F) was imaged together with F-actin in living cells using TIRF microscopy. Micrographs are shown in ibw contrast. blue arrows in the whole cell micrograph represent observations of membrane flow during cell migration. Insets confined by red/ red dashed boxes below present displacement of Caveolin-1 (Y14F)-GFP during time. Arrows in black, red or blue follow particular

4.3.2.5. Cdc42

Activity of the small Rho-GTPase Cdc42 was measured in live cell imaging experiments using a FRET based biosensor constructed using the cpFRET toolkit (Fritz et al. 2013). FRET imaging and image analysis were performed according to Fritz et al., 2013. Simultaneously, Lifeact-mCherry was imaged in order to relate Cdc42 activation state to cytoskeletal dynamics (Figure 40). Data shown below is preliminary and experimental procedures need to be optimized.

In the meanwhile it turned out, that transduction with the biosensor 24h before start of experiments is superior compared to transduction 48h, as it was used to acquire data presented here. Reduction of time in which the biosensor is expressed results in more wild type like cell morphology and improved cell health, which is crucial for live cell imaging. Therefore, data presented below should give a first glance at Cdc42 signaling dynamics during cell migration in hapto and chemo cells on PS and further studies are needed to definitely draw conclusions.

These first observations showed activation of Cdc42 at the leading and trailing edge in hapto and chemo cells. It can also be speculated, that retrograde F-actin flow and Cdc42 activity are related to each other, considering kymograph analysis presented in Figure 39 A. There Cdc42 activity co-localized with regions of retrograde F-actin flow. In chemo cells Cdc42 activity was strongly reduced at regions of PLSs (Figure 40 B).



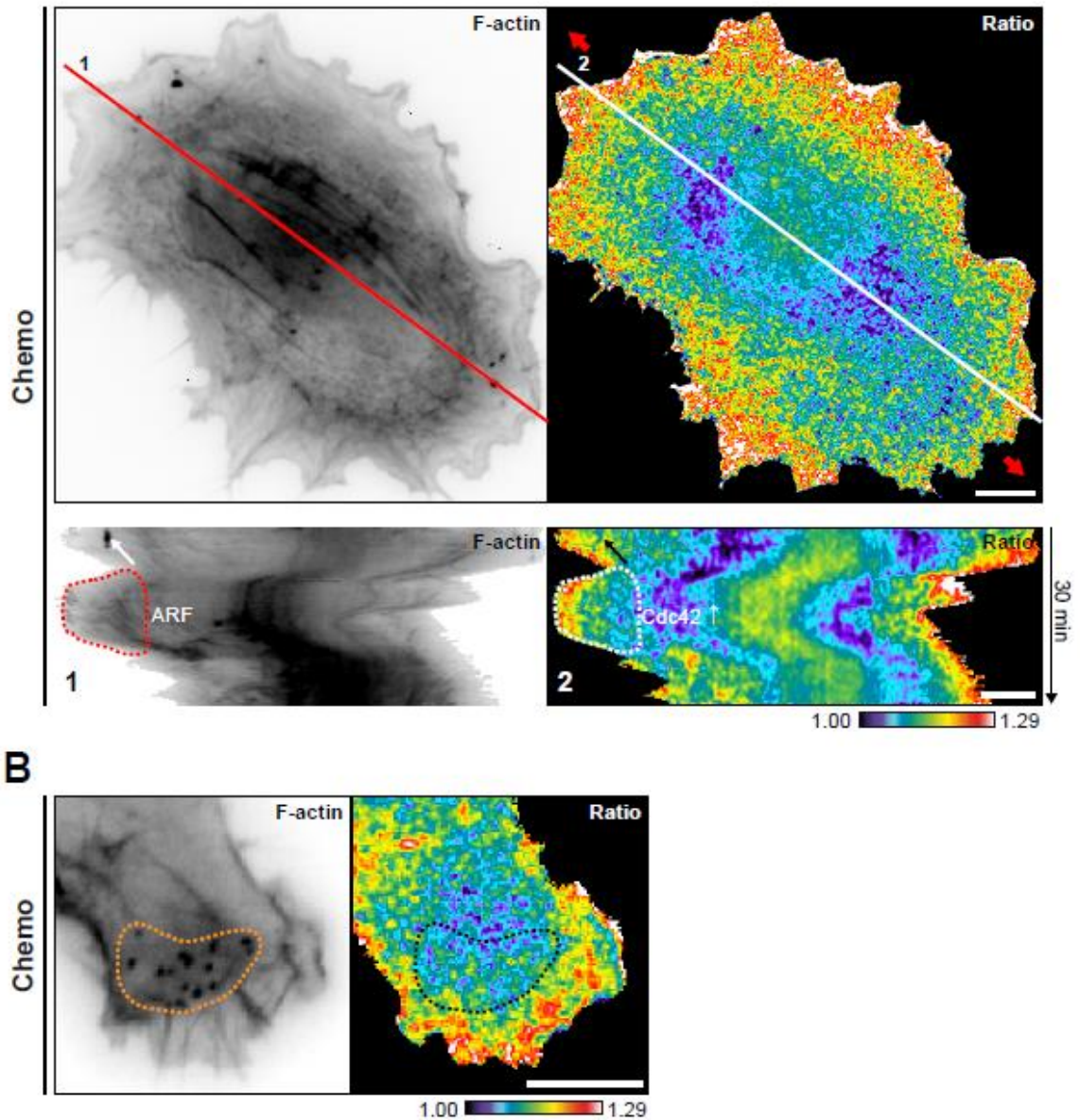


Figure 40: FRET live cell imaging of Cdc42 activity and F-actin dynamics in hapto and chemo cells on PS . (A) Cdc42 activity was measured using a FRET based biosensors transiently expressed simultaneously with Lifeact-mCherry. Micrographs are shown in ibw contrast or in color code. Cdc42 is activated at the leading and trailing edge as in hapto and chemo cells. Comparison of F-actin and ratio (Cdc42 activity) kymograph analysis (along red/ white lines) let assume, that Cdc42 activity and retrograde F-actin flow are coupled. Note, Zone of retrograde F-actin flow confined by red/ white dashed line in kymographs 1 and 2 in hapto and chemo. **(B)** Cdc42 activity is decreased at PLS zones. Orange dashed line confines PLS zone in chemo cell. Red arrow points in direction of cell migration/ protrusion; Scale bars = 10 μ m

4.3.2.6. Rac1

Live cell imaging experiments were performed using a FRET based Rac1 biosensor constructed with the cpFRET toolkit (Fritz et al. 2013). Similar to the Cdc42 sensor, the Rac1 biosensor was transiently transduced together with Lifeact-mCherry implemented in an adenoviral system (Figure 41). Alike data derived from the Cdc42 biosensor discussed prior, Rac1 data should be considered as preliminarily and definite conclusions demand further studies under optimized experimental conditions. This first observations showed elevated Rac1 activity all around a not polarized hapto cell on PS. Focusing at a protruding region displayed in the inset (Figure 41 A, hapto) and the corresponding kymographs, Rac1 activation occurred prior to protrusion, which contradicted the study of Machacek et al. 2009, where Rac1 activation reaches its maximum 40 seconds after protrusion. In chemo cells exhibiting a broad lamellipodium in front of PLSs, Rac1 was activated at the cell edge as well as behind the PLSs throughout protrusion (Figure 41A, chemo). At PLSs themselves, Rac1 was not activated. However, in a chemo cell, with narrow lamellipodium adjacent to PLSs, Rac1 was not activated during protrusion neither at the cell edge, nor at PLSs (Figure 41B). In this case elevated Rac1 activity appeared only behind the PLS zone.

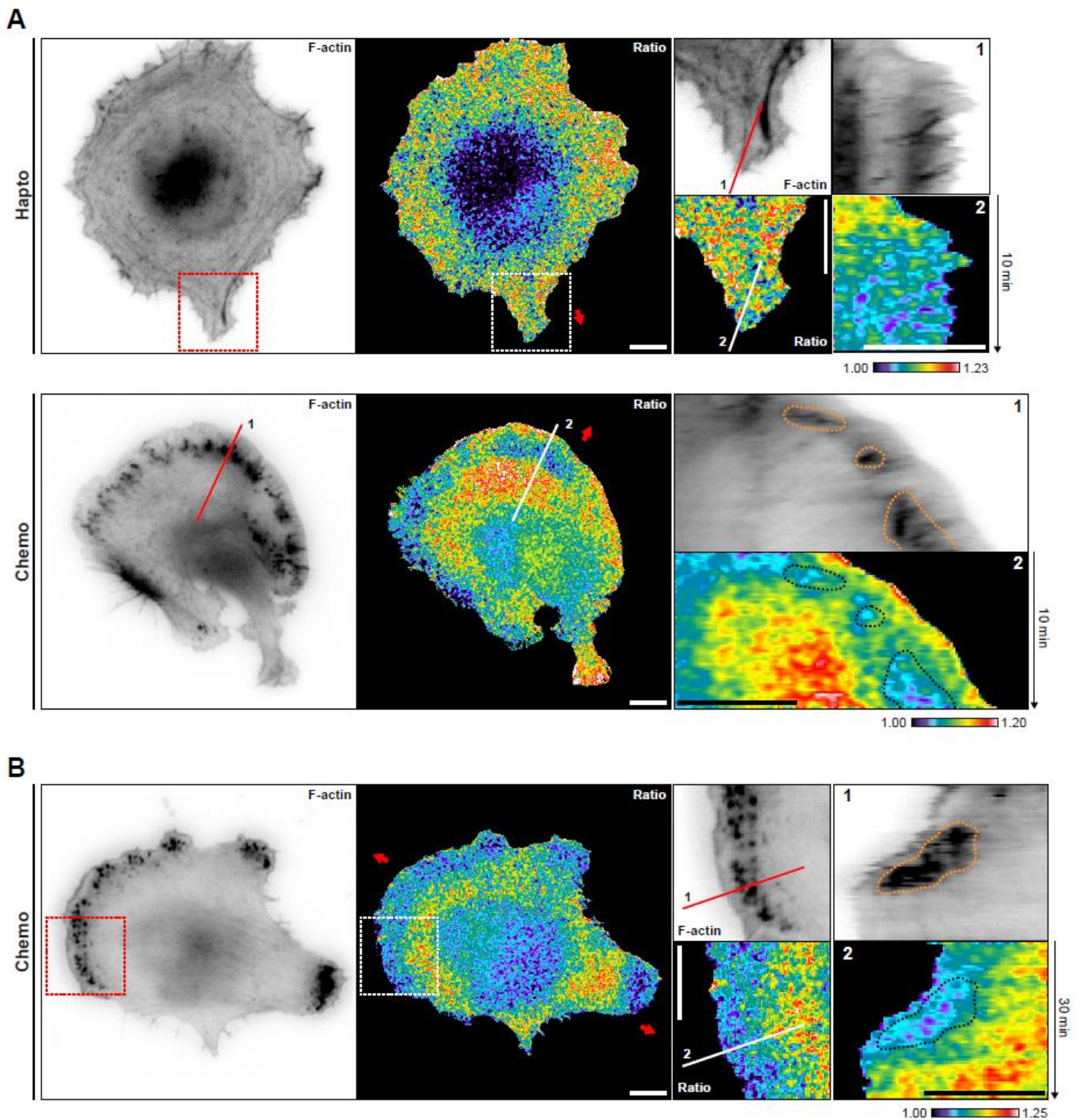


Figure 41: FRET live cell imaging of Rac1 activity and F-actin dynamics in hapto and chemo cells on PS. (A) Rac1 activity was measured using a FRET based biosensor transiently expressed together with Lifeact-mCherry. Micrographs are shown in ibw contrast or in color code. In a not polarized hapto cell Rac1 is active all around the cell, but decreased during protrusion (kymograph 1/ 2 of inset hapto along red/ white line). Chemo cell on PS with broad lamellipodium in front of PLSs shows elevated Rac1 activity in front and behind PLSs, while Rac1 activity is low at PLSs. Kymograph analysis 1/ 2 in chemo along red/ white line illustrates Rac1 activity pattern over time (kymo 2) in reference to F-actin dynamics (kymo 1): Note PLSs confined by orange/ black dashed line correspond to low Rac1 activity. **(B)** Chemo cell with narrow lamellipodium in front of PLSs lacks Rac1 activity at the cell edge (inset). During protrusion directly followed by PLSs, Rac1 activity remains low at the cell edge and PLSs, but is elevated behind the PLS zone. Orange/ black dashed lines confines PLS zone in chemo cell. Red arrow points in direction of cell migration/ protrusion; Scale bars = 10 μ m

4.4. Materials and Methods

4.4.1. Cell Culture ,Stable Cell Lines and Adeno System

Procedures are similar as described in section 3.6.

Stable cell line expressing following target proteins have been generated:

- β_1 -integrin-GFP derived from $\beta 1AK80eGFP$ (a kind gift from Bernhard Wehrle-Haller)
- β_3 -integrin-GFP derived from peGFP- $\beta 3$ -integrin-N1
- Vinculin-GFP derived from peGFP-vinculin-C3
- Caveolin-1(Y14F)-GFP derived from peGFP-caveolin (Y14F)-N1

Similar to Adenovirus carrying Lifeact-mCherry (section 3.7.1.) adenoviral particles carrying the FRET biosensors for Rac1 and Cdc42 have been generated. Transient transduction has been performed 48h before start of imaging experiments.

4.4.2. Generation of Line Patterns

In order to generate line patterns consistent across their whole length, different conditions for plasma treatment were tested. Efficiency of coating depends on total exposure to plasma, which in turn can be modulated by plasma intensity, duration of exposure and confinement of the exposed surface. The coated glass cover slip faces a gradient of plasma, with its minimum in proximity of the pattern-valley (Figure 42A). Finding the optimal conditions for plasma treatment means to find a compromise between sufficient plasma exposure to etch out the prior coated anti-adhesive PLL-PEG and not to exceed a certain level of plasma exposure which leads to destruction of the PDMS substance and consequently impaired line consistency. To test for optimal conditions, the geometry of the PDMS stamp and plasma intensity was kept constant, while the duration of treatment was varied. A glass cover slip coated prior with anti-adhesive PLL-PEG was covered with a PDMS stamp. This PDMS stamp contained 100 μm wide, 30 μm thick ridges separated by 20 μm -wide valleys and was 5mm in width.

It turned out, that durations of plasma etching between one and three minutes gave the best results in line consistency, visualized by epifluorescence microscopy after coating of 10 $\mu\text{g}/\text{ml}$ fluorescently labeled fibronectin.

Longer durations of plasma etching exceeding 10 min led to inconsistent line patterning (figure 42B). Finally, duration of plasma treatment for two minutes was considered as optimal condition and was used throughout all experiments.

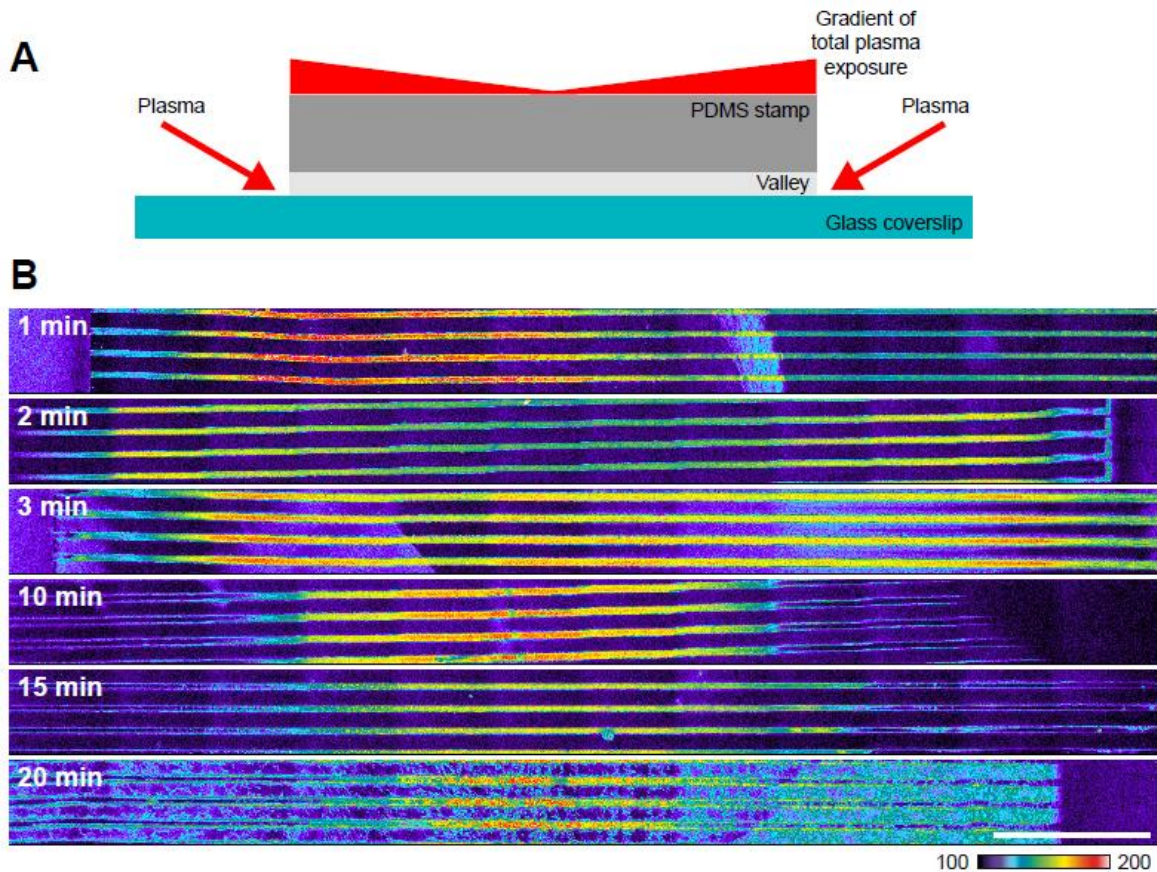


Figure 42: Optimization of line pattern generation. (A) Schematic cross-section through a PDMS stamp on a glass cover slip: Plasma is allowed to enter the valley of the PDMS stamp and the glass surface is gradually exposed to plasma. Maximal plasma exposure occurs at distal regions of the patterned area decreasing towards the proximal region (in red: gradient of total plasma exposure). (B). Different durations of plasma treatment with 100% power have been tested to determine optimal conditions for plasma etching. After plasma etching 10 μ g/ml Fibronectin-Alexa555 has been coated and coating efficiency has been tested by epifluorescence microscopy. Scale bar: (B) 1mm

4.4.3. Gradient Generator

As gradient generator, a similar design as for the neuron device, developed in the group of Noo Li Jeon, was used (Taylor et al. 2005). A gradient of PDGF across the cell compartment is formed by diffusion from the source, via microgrooves into the sink (Figure 43). In order to enhance the chemotactic response of fibroblasts to the PDGF gradient, a fibronectin line pattern, as prior described, was integrated into the cell compartment. Additionally, medium in source and sink was supplemented with 0.5 mg/ml gelatin to increase viscosity, resulting in slower diffusion keeping the PDGF gradient stable over longer time.

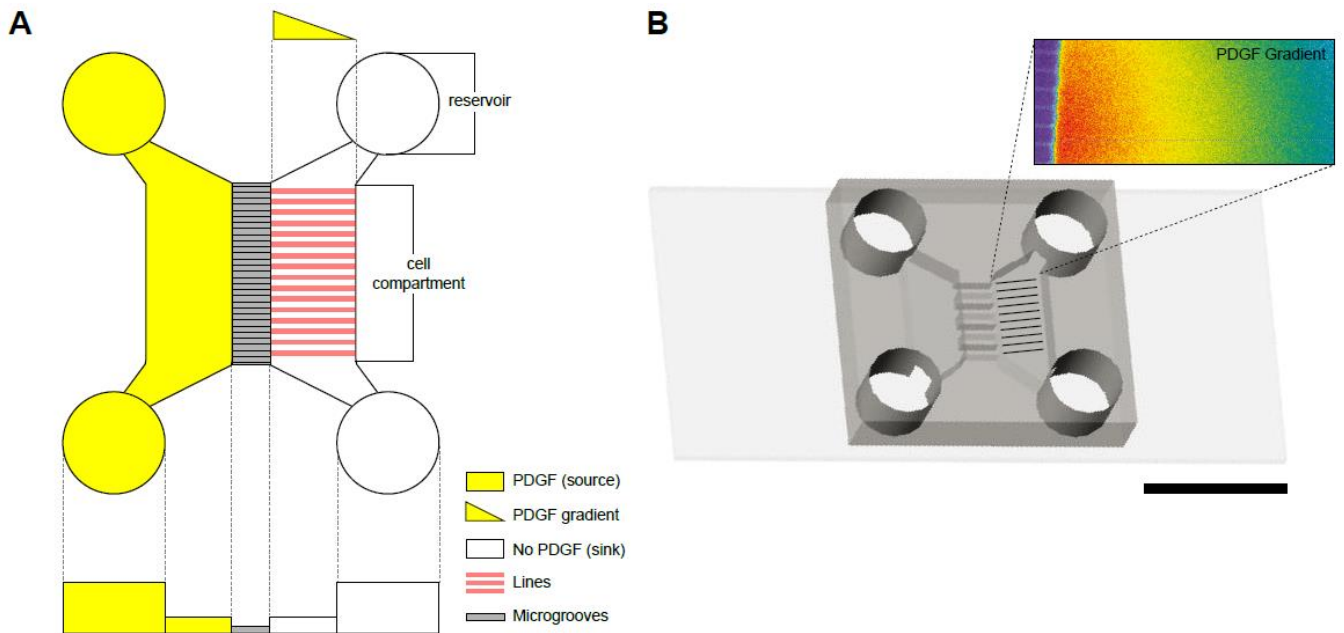


Figure 43: Gradient Generator. (A) Scheme of a gradient generator. PDGF containing medium is applied to the source and by diffusion across microgrooves a PDGF gradient in the cell compartment is established.

4.4.4. PDGF Gradient

To monitor gradient formation and stability approximately, the PDGF containing source medium was supplemented with fluorescently labeled 10 kDa Dextrane-Alexa546. Gradient steepness was determined by measuring fluorescence intensity at the first and the last point of a 430 μ m line scan across the whole field of view. By calculating a ratio of maximum fluorescence intensity of the 10 kDa Dextrane-Alexa546 in proximity to the source over the intensity distal to the source, a trend of gradient progression was determined (Figure 44). Using a supplement of 0.5 % gelatin in source and sink medium improved gradient stability within the first three hours.

A diffusion based gradient generator lacks the possibility to keep a gradient constant over long time, but prior experiments of generating flow based gradients failed due to high shear stresses, which caused cell death. Moreover, at that time these experiments were carried out, more sophisticated gradient generators were not available to us.

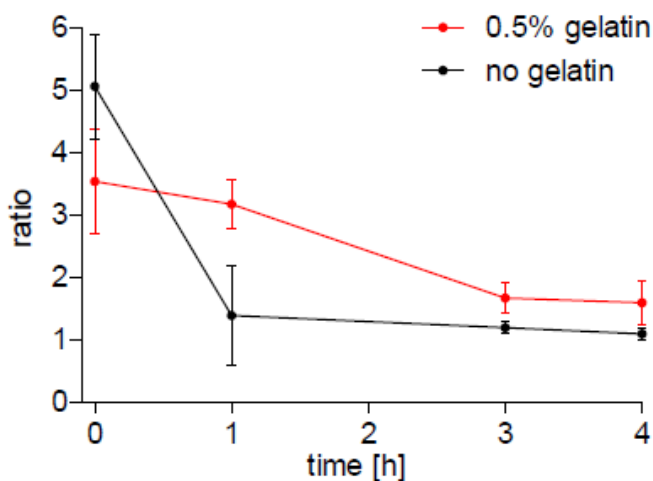


Figure 44: Gradient Stability. Gradient stability was monitored by distribution of fluorescently labeled 10kDa Dextrane-Alexa546 using epifluorescence microscopy.

4.4.5. Immunofluorescence Stainings

LSs were produced according description in section 4.4.2. (generation of line patterns) on round glass cover slips with 24mm diameter. Cells were subconfluent seeded and chemo cells were at the same time stimulated with 40ng/ml PDGF. After six hours of incubation, medium was aspirated and cells immediately fixed with 4% PFA for 10min.

Next, samples were blocked with 5% BSA in PBS with 0.1% Triton-X-100 (Sigma) (PBS-T) for one hour at RT.

Antibody dilutions were prepared in PBS-T + 2 % BSA according table 1, and cells were incubated one hour with the respective antibody at RT. Further, samples were washed three times for 10 min each in PBS-T before secondary detection.

Secondary detection was performed using Alexa-fluor488 goat anti rabbit IgG (1:1000; Invitrogen) or Alexa-fluor488 goat anti mouse (1:1000; Invitrogen). DAPI (1:1000) and phalloidin-alexa-fluor555 (1:50; Invitrogen) was applied to unmounted samples while imaging, to visualize F-actin. TIRF imaging of these stainings was performed in a magnetic live cell chamber in presence of PBS so as to have a glass-water interface necessary for incident light reflection.

Target	Host	Dilution	Company	Catalog number
Vinculin [hVIN-1]	M	1:400	Abcam	ab 11194
Paxillin [Y113]	Rb	1:250	Abcam	ab32084
α -Tubulin [DM1A]	M	1:1000	Sigma Aldrich	T 9026
Talin 1 and 2 [8D4]	M	1:40	Abcam	ab11188
Phosphotyrosine [4G10]	M	1:50	Millipore	05-321
ARP2 [FMS96]	M	1:200	Abcam	ab49674
Beta-PIX, SH3 domain	Rb	1:1000	Millipore	07-1450
TIAM1 [C-16]	Rb	1:50	Santa Cruz	sc-872

Table 1. Primary antibody used for immunofluorescence stainings

Antibodies listed in table 2 did not give proper stainings in REF52 cells:

Target	Host	Dilution	Company	Catalog number
p-Stathmin (Ser38)	Rb	1:50	Cell signaling	#3426
α -Tubulin acetylated	M	1:200	Abcam	ab24610
α -Tubulin detyrosinated	Rb	1:200	Abcam	ab48389
Dia2	Goat	1:50	Santa Cruz	sc-10889
DIAPH2	Rb	1:100	Abnova	PAB20307
PKC-Z	Rb	1:50	Santa Cruz	sc-216
Cortactin (p80/85) [4F11]	M	1:100	Millipore	05-180
TKS5 (SH3#1)	Rb	1:500	Millipore	09-403
Integrin β 1 [EP1041Y] (to C-terminus)	Rb	1:50	Abcam	ab52971
Integrin β 3 [EP2417Y]	Rb	1:100	Abcam	ab75872
Vav2 [F-6]	M	1:50	Santa Cruz	sc-271442
Dock1 (to C-terminus)	Rb	1:150	Sigma Aldrich	D9820
p-Cofilin (Ser3) [77G2]	Rb	1:100	Cell signaling	#3313

Table 2. Primary antibody did not achieve proper immunofluorescence stainings

4.4.6. Live cell imaging and image analysis

TIRF Microscopy

Total internal reflection fluorescence (TIRF) microscopy takes advantage of unique properties of an induced evanescent field in a region immediately adjacent to the interface between glass cover slip and specimen. Required here is that these two components differ in their refractive index to allow total internal reflection above a critical angle of incoming laser light.

The physical basis for the phenomenon of total internal reflection (Figure 45):

Refraction of light occurs as it encounters the interface of two media exhibiting different refractive indices. Thereby the light beam is partly or totally confined to the medium with higher refractive index. A collimated light beam can therefore be refracted upon propagating one medium and reaching the interface, or it gets reflected. This so called total internal reflection is only possible, if the light encounters an interface to a medium with lower refractive index. The angle of incoming light has to exceed a critical angle to be entirely reflected.

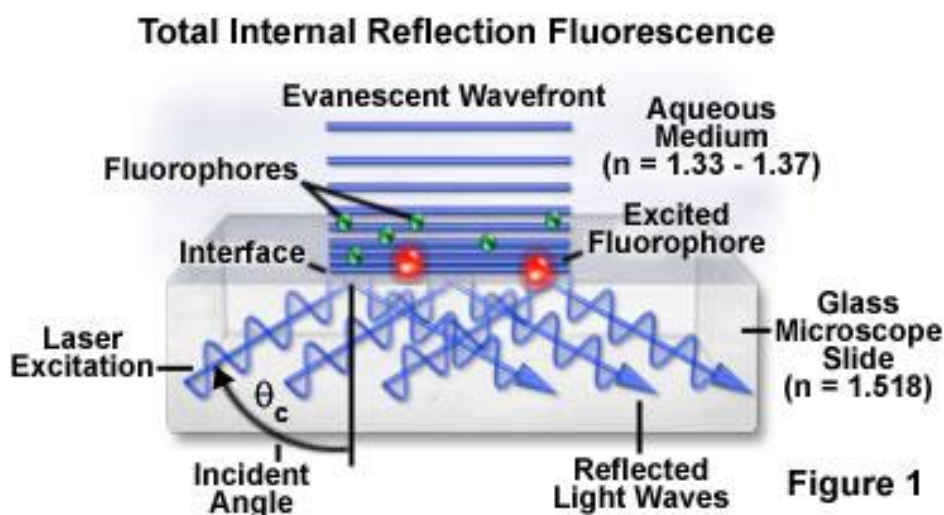


Figure 45: TIRF microscopy. Collimated light propagates a medium with high refractive index (glass) and reaches the interface with a medium (aqueous medium, specimen) exhibiting a lower refractive index. Exceeds the angle of incoming light a critical angle, the light beam gets totally reflected and at the same time an electromagnetic field called evanescent field extends up to 100 nm in z direction. This evanescent field excites only fluorophores adjacent to the glass cover slip resulting in minimization of background signal (**Image from Nikon homepage**).

Upon total internal reflection of a light beam, light no longer passes the second medium. However, this light generates a highly restricted electromagnetic field adjacent to the medium interface. This electromagnetic field is termed evanescent field and appears in the same wavelength as the incoming light and extends at most 100 nm in z-direction into the specimen.

As excitation of fluorophores above 100nm specimen height is avoided, this imaging technique allows acquiring images with very low signal to noise of structures adjacent to the glass cover slip. For live cell imaging TIRF microscopy is a very powerful tool to detect structures at the ventral part of cells. This is crucial to monitor cytoskeletal and adhesion dynamics, which would otherwise disappear within high background signal.

FRET live cell imaging

FRET live cell imaging and image analysis was performed according to Fritz et al., 2013

Epifluorescent live cell imaging

Epifluorescent imaging experiments and image analysis were performed as indicated in section 3.7.1..

5. Discussion

Is Chemotaxis Required for Persistent Cell Migration?

In this project we initially aimed to study in this project cytoskeletal and Rho-GTPase signaling dynamics during PDGF chemotaxis (directional cell migration) versus hapto- and chemokinesis (non-directional cell migration). We assumed cytoskeletal dynamics might change during different modes of cell migration. This assumption based on prior observations, where protrusions were lacking RhoA activity upon PDGF stimulation in contrast to protrusions of not stimulated cells (Pertz et al. 2006).

Hence, we developed a diffusion based gradient generator with integrated line substrates (LSs) to induce chemotaxis and consequently polarized cell migration. The consideration for using LSs was that it was shown by Doyle et al. 2009 how one dimensional matrix can mimic three dimensional environments such as under physiological conditions. We hypothesized that using a similar approach would render the chemotactic response more robust, by various means:

- 1.) Due to topological confinement by LSs cells can only choose to migrate in two directions (Figure 46A, B), whereas on plane substrates (PSs) cells are free to move in any direction (Figure 46C, D). We hypothesized that this pre-polarization might promote ability of cells to migrate directional towards higher PDGF concentrations.
- 2.) Another assumption why LSs might promote gradient sensing in particular concerned cell shape. When cells are seeded on LSs they elongate during spreading. Consequently, leading and trailing edge are farther away from each other compared to circular shaped cells on plane substrates. Further, we hypothesized that this increased distance between cell front and back might be beneficial for gradient integration. We considered here, that the concentration difference of PDGF encountered by front and back is elevated in contrast to not pre-polarized circular cells (Figure 46E, F).

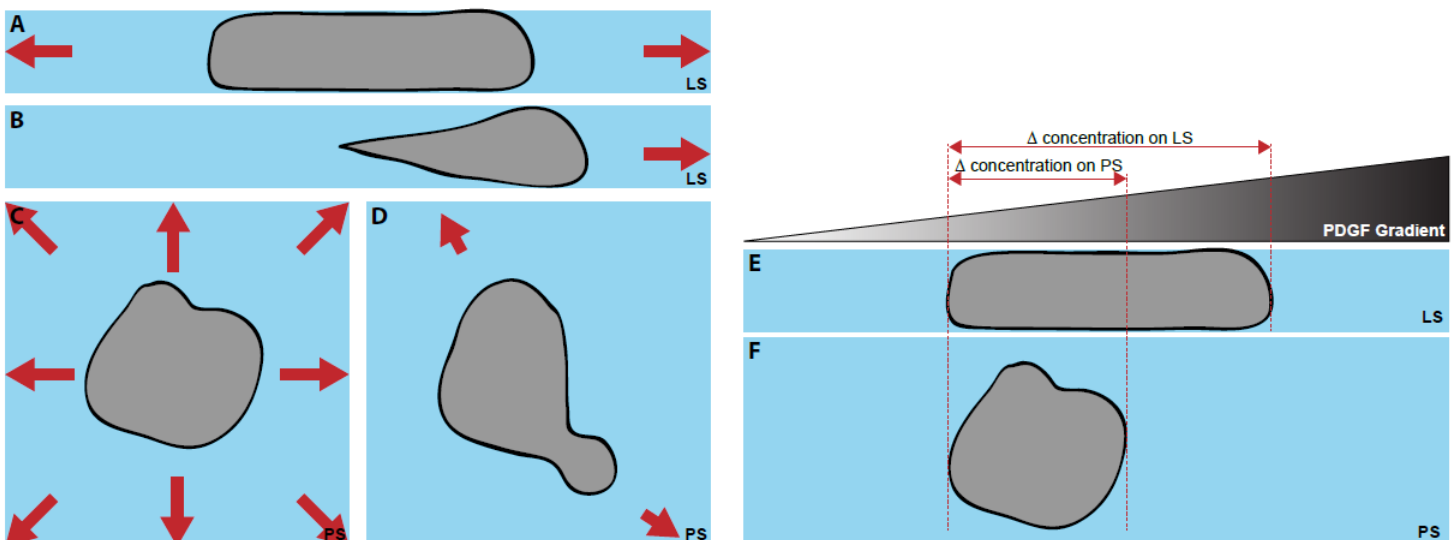


Figure 46: Possible directions of cell migration and gradient sensing. (A) A cell in a pre-polarized state on a line substrate elongates and can either migrate left or right. (B) The cell has polarized on the line substrate and has decided for one direction of migration. (C) Cells on plane substrate are not limited in their possible migration directions. Not confined substrates allow any migration direction. (D) A cell on plane substrate transiently polarizes and migrates randomly. (E) Cells on line substrates (LS) encounter higher PDGF concentration difference due to elongated shape compared to (F) equally spread cell on plane substrate (PS).

However, we could only obtain significant chemotactic response for primary human foreskin fibroblasts (AG1518). Furthermore, in this cell system, a huge degree of noise remained, e.g. a certain population did not migrate towards the PDGF source. The immortalized cell line NIH3T3 did not respond to the PDGF gradient, while for REF52 cells a trend of directional migration towards higher PDGF concentration was observed.

The reason why our approach failed might be due to multiple facts:

1. The system used here to generate chemotactic gradients was a very simple approach with the drawback that the gradient could not be kept at constant levels throughout the experiment. Using a more sophisticated approach, which was not available to us at the time the chemotaxis experiments were carried out, could improve the chemotactic response.
2. After cell proliferation, which is induced by PDGF, most daughter cells moved into opposite directions and were not responsive for gradient sensing in our system.
3. Cells have a higher probability to collide on a line substrate and were often observed to move afterwards into opposite directions, while sometimes evading each other and thereby maintaining their direction of migration. Therefore, cell-cell contacts seem to strongly influence cells in their decision for a direction of migration.
4. Similar to cell-cell collision, cell-device collision also led to cell turning and consequently to more noise in the system.

Chemokinesis on Line Substrates Leads to Persistent and Cell Migration

Although this approach to establish robust PDGF chemotaxis of fibroblasts failed, it nevertheless indicated that chemokinesis is sufficient for cells migrating on line substrates to obtain unidirectional cell migration persistent over several hours. This brought us already a huge step further and simplified the experimental setup at the same time.

Striking advantages of this system are firstly that gradient stimulation is not required to induce unidirectional and persistent cell migration when cells migrate on line substrates upon growth factor stimulation. Secondly, persistence and unidirectionality standardizes the process of cell migration. This means precisely, that leading and trailing edge always remain in the same orientation (Figure 47A). A process persistent for hours can be observed at different timescales and magnifications (Figure 76) rendering it possible to draw inferences from local phenomena on global dynamics allowing us to bridge the gap between fine migration dynamics and global observations. For example, impact of edge motion (timescales of seconds; spatial resolution of micrometers) on front/back co-ordination (timescales of hours; spatial resolutions of several hundred of micrometers) can be explored.

We show in this work, that persistent fibroblast migration do not demand a chemotactic gradient, but is mediated by global growth factor stimulation in combination with topological confinement keeping cells in a polarized state. Permanent polarization in turn is required to mediate persistent and unidirectional cell migration.

This could be relevant for the regulation of directed cell migration in vivo. For instance, during collective cell migration of neural crest cells in development the combination of chemokine exposure and contact inhibition might cooperate to generate an overall polarity to the cell population (Theveneau and Mayor, 2012). During cancer metastasis, a macrophage-tumor cell paracrine loop, that involves secretion of growth factors from the two different cell types, allows for collective cell streaming in one specific direction on collagen fibrils (Roussos et al., 2011). Although this was proposed to involve chemotaxis, it is conceivable that chemokinesis might be sufficient to induce directional cell movement on the highly asymmetric collagen fiber. In both cases, the ability of a chemokinetic stimulus to hardwire directionality of pre-polarized cells might therefore provide a mean for generation of persistent, directional cell migration.

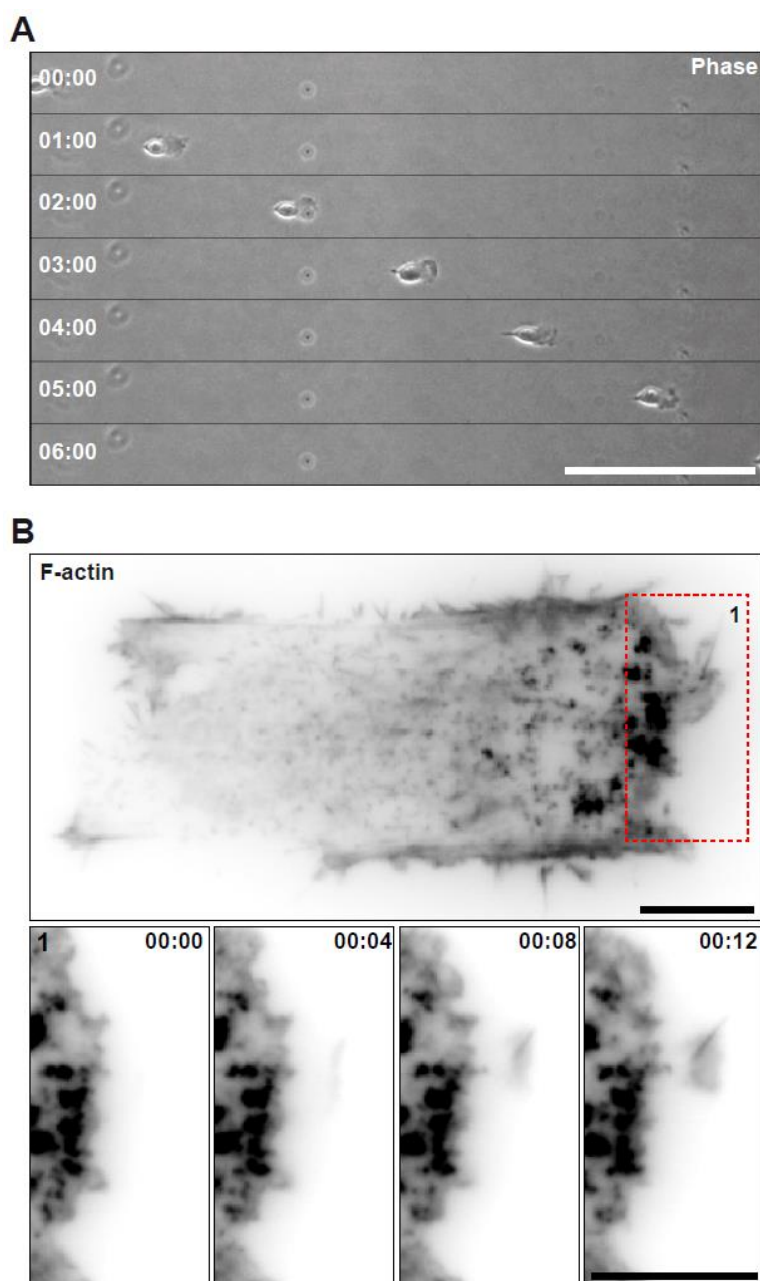


Figure 47: Unidirectional and persistent migrating chemo cells on LSs imaged in different spatial and temporal resolution. (A) Phase contrast time series of persistently migrating chemo cell on LS. Time indicated in hours: minutes. Scale bar = 100 μ m (B) Lifeact-GFP expressing chemo cell on LS imaged using TIRF microscopy; Whole cell micrograph and time series shown in ibw contrast. Time indicated in minutes: seconds. Scale bar = 10 μ m

So far, processes happening in different temporal and spatial resolutions demanded the use of different cell systems. Global migration dynamics are widely studied in small and fast migrating cells such as neutrophils or *dictiostelium* (Figure 48A) (Arriemerlou & Meyer 2005) precluding observations of fine cytoskeletal and signaling dynamics due to cell size. On the other hand large mesenchymal cells exhibiting flat morphologies are used to study fine cytoskeletal dynamics (Figure 48B, C) (Gupton & Waterman-Storer 2006) with the drawback of poor directional and persistent migration dynamics. There, random cell migration is caused by transient cell polarization and hinders drawing inferences from fine dynamics about global migration dynamics impossible.

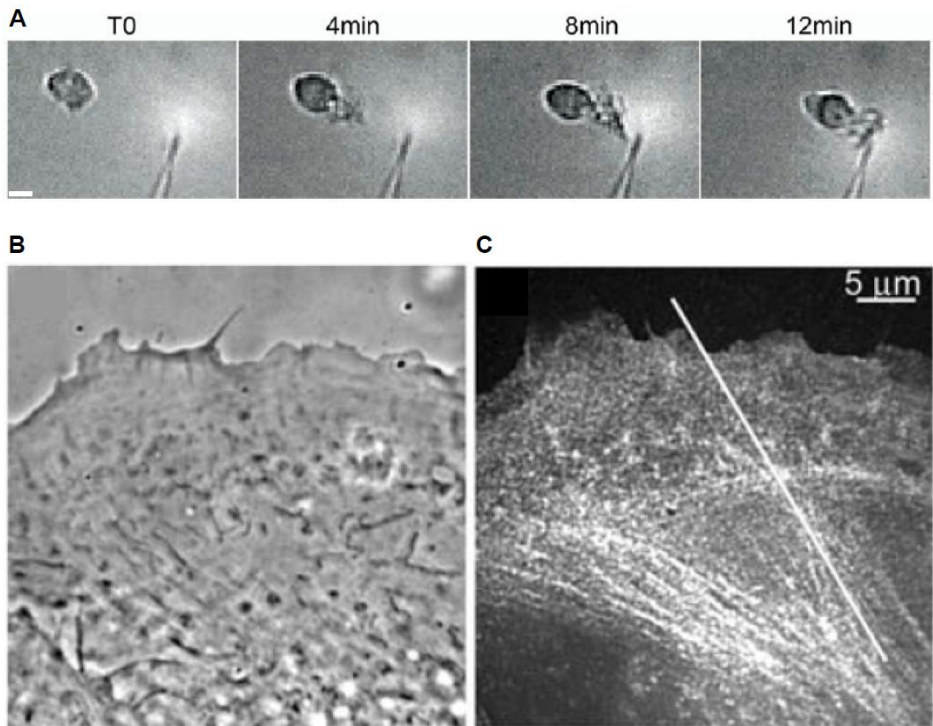


Figure 48: Different time and spatial scales. (A) Persistent migration of a *Dictiostelium* toward a micropipette filled with C5a (0.45 μM). Scale bar, 10 μm (Arriemerlou & Meyer 2005) **(B, C)** Leading edge of a PtK₁ cell. Scale bar, 5μm. (Gupton & Waterman-Storer 2006) **(B)** phase contrast **(C)** actin FSM

Working Model

We found in our study that persistent cell migration can be achieved by long term stimulation of fibroblasts with a uniform concentration of PDGF when cells were seeded on line substrates. Upon growth-factor stimulation in combination with topological confinements of the ECM we observed that cells remodel their cytoskeleton and migrate rapidly and unidirectionally for many hours. However, this exquisite migration mode requires in contrast to neutrophil chemokinesis several hours to implement morphogenetic changes leading to a steady state cell motion.

In order to explain this process of highly persistent cell migration we studied cytoskeletal and RhoA signaling dynamics as well as cell migration dynamics on a global scale. We were finally able to explain how fine dynamics happening within single micrometers and seconds impact on global migration behavior (observed within hours and tens of micrometers) of cells by applying a multi scale approach based on standardization of cell migration.

Chemo cells develop two functionally distinct modules

Cross-correlation analysis of cell front and back motion showed that leading and trailing edges of chemo cells move asynchronously. This result indicated that front and back motion did not depend on each other, which led us to the hypothesis of mechanical uncoupling of cell front and back. Further analyses demonstrated that chemo cells indeed develop two functionally distinct modules, which are mechanically uncoupled and crucial to maintain migration persistency in absence of gradient stimulation (Figure 49). A front module pushes the leading edge in direction of cell migration and a back module exerting tensile forces pulls at the tail to allow for tail retraction. Motion of both front and back module point towards direction of cell migration and presumably, this leads to a synergistic effect promoting unidirectional movement.

Cross-correlation analysis as well as drug perturbation experiments were used to formally proof the hypothesis of mechanical front/back uncoupling and provided valuable insights in functional modalities of these modules. These two functional modules differ in cytoskeletal organization and dynamics tremendously but cooperate during cell migration while showing minimal cross-talk.

The front module is characterized by a protrusive lamellipodium and non-contractile zone of PLSs with intermixed FCs. Surprisingly, we found, that this PLS zone functions as mechanical insulator of cell front and back and surrogates for the lamella precluding actin retrograde flow. PLSs as prevent as mechanical insulator the direct connection of cell front and back by acto-myosin filaments, which is usually the case in non-stimulated cells. Abolishment of this physical connection is reflected in a higher protrusive activity observed in fine leading edge dynamics. This leads further to an increased velocity of cell migration in combination with lower adhesiveness of chemo cells. Another hallmark of the PLS zone are FCs formed at the very leading edge, which never mature into focal adhesions due to the lack of stress fiber connection and actin retrograde flow. During cell migration the PLS zone maintains unchanged size because of constant PLS lifetime and unvaried positioning referred to the leading edge. Moreover, PLSs locally inhibit RhoA activity at the leading edge and confine a narrow RhoA activation zone at the lamellipodium.

In direct vicinity to the non-contractile front module a contractile module emerges allowing for tail retraction. We found there a cluster of myosin IIA activity co-localizing with actin filaments arranged in cross-like manner. These filaments emerge from the cell proximity and reach out to lateral and posterior FAs. Presumably, myosin IIA associates at that point also with cortical actin. During tail retraction sliding FAs at the cell rear disassemble coinciding with activation of RhoA at the very trailing cell edge. Rapidly, persistently migrating neutrophils (Pestonjamasp et al., 2006) and fish keratocytes (Svitkina et al., 1997) show similar myosin clusters at the cell rear, but not at the front. This leads us to the speculation, that a rear-concentrated myosin module may be a general feature of rapid persistent migration.

Breaking of the front/back mechanical insulation leads to non-persistent cell migration and impacts on RhoA signaling dynamics

By drug perturbation experiments we confirmed in addition to previous described observations our hypothesis of mechanical front/back uncoupling.

We either perturbed the mechanical insulator – the PLS zone – by using the ARP2/3 inhibitor CK666, which caused rapid disassembly of PLSs. Or, we specifically inhibited the contractile back module by the use of the myosin IIA inhibitor blebbistatin.

Performing again cross-correlation analysis on front/back motion of acutely inhibited cells, we found that inhibition of the PLS zone restores immediately mechanical coupling of cell front and back. This result was then confirmed on level of adhesion and cytoskeletal dynamics. There, we observed during live cell imaging experiments and acute drug perturbation that FCs at the leading edge mature immediately after disruption of the PLS zone into FAs. Perturbation of the PLS zone abolishes mechanical insulation and enables stress fibers to connect again front and back adhesions and further to apply tensile forces so that the cell front pulls at the cell back.

As already previously mentioned, chemo cells show altered RhoA signaling characteristics. While contractile hapto cells display a broad RhoA activation zone at the leading edge, in chemo cells RhoA activity is confined to the lamellipodium. By acute perturbation of the PLS zone and FRET imaging using a RhoA biosensor (Fritz et al., 2013) we could show, that restoring the mechanical connection of cell front and back leads again to a broadening of the RhoA activation zone. This experiment showed that the PLS zone locally inhibits RhoA activity.

Also acute perturbation of the back module by inhibiting myosin IIA activity was in line with previous findings. Cross-correlation analysis of front/back motion showed, that hapto cells perform asynchronous movement when contractility is inhibited. Inhibition of myosin IIA mediated contractility resulted in a severe tail retraction defect. Expectedly, chemo cells remained mechanically uncoupled upon blebbistatin treatment. Astonishing here was that a defect in tail retraction did not affect the front module, where we observed persistent edge progression until the cell was reaching a critical length. During cell stretching the cortex gets under tension which at one point induces again retraction. While the leading edge of blebbistatin treated chemo cells progressed, the PLS zone was maintained, although its localization was destabilized by time. Finally, these experiments strengthen again the hypothesis of mechanical front/back uncoupling of chemo cells on line substrate by the fact, that a defect in tail retraction did not disturb leading edge progression. However, apart from a non-contractile

front module an intact contractile back module might be crucial to persistently localize the PLS zone at the leading edge.

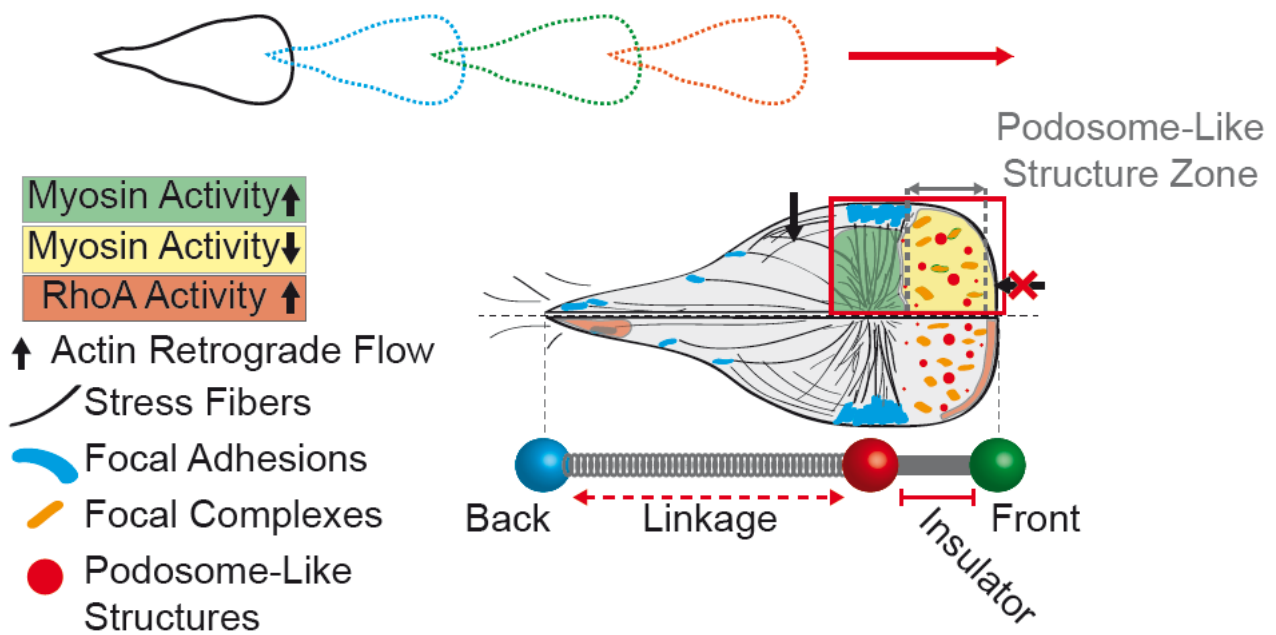


Figure 49: Working model: Mechanical front/back uncoupling mediates unidirectional and persistent cell migration in growth factor stimulated cells on line substrates.

PLSs locally inhibit Rac1 and Cdc42

Besides several live cell imaging experiments using fluorescently tagged markers we started to establish a procedure to monitor Cdc42 and Rac1 activity using FRET based biosensors.

First we aimed to generate stable cell lines using a lentiviral system similar as it was done for the RhoA biosensor. This approach failed because cells did not tolerate the construct leading to inhibited growth of expressing cells, severe morphological defects or loss of the construct.

To overcome these problems, we decided to transiently transduce cells using an adenoviral system. This enabled us to easily generate cells expressing the biosensor at low levels, although we still faced morphological aberrations. Live cell imaging experiments were performed, while Lifeact-mCherry was co-expressed to relate Rac1 and Cdc42 signaling patterns to F-actin dynamics. These data sets should be considered as preliminary and further experiments under optimized conditions are necessary to state any definite conclusions. However, in the meanwhile we managed to optimize experimental conditions, but the work on these data sets goes beyond the work of my PhD thesis and is not finalized yet.

Preliminary results show Cdc42 activity at the leading and trailing edge of haptotactic and chemotactic cells. Unexpectedly, Cdc42 activity does not co-localize with PLSs. Before these experiments were performed we hypothesized, that Cdc42 might be active at PLSs in order to drive actin polymerization

executed by the Arp2/3 complex via WASP. But obviously Cdc42 does not contribute to Arp2/3 activation.

However, proposed by kymograph analysis, we suspect that Cdc42 activation correlates with actin retrograde flow in hapto and chemo cells. Strongest Cdc42 activation occurs at the cell edge where actin turns over rapidly at the lamellipodium.

Results from the Rac1 biosensor were not clear for hapto, where Rac1 activity was elevated before protrusion onset instead of being delayed by 40 seconds to the protrusion maximum as it was stated by Machacek et al., 2009. Definitely there have to be more cells analyzed to draw any conclusion and therefore I would not consider this result.

Nevertheless, chemo cells showed robust Rac1 signaling dynamics related to F-actin dynamics. Rac1 activity is clearly reduced at PLSs, but elevated behind. Concerning Rac1 activity at the lamellipodium in chemo cells we obtained different results, although these differences might be explicable by cytoskeletal architecture: Once Rac1 activity is elevated in at the first 2 μm of cell edge within a broad lamellipodium, followed by a PLS zone with low Rac1 activity. Presumably, at the outer edge of this wide lamellipodium actin polymerization is regulated similarly to hapto cells. On the other hand chemo cells with a narrow lamellipodium, directly followed by a PLS zone, lack Rac1 activity at the lamellipodium pointing at different regulation of actin polymerization. Interestingly, in both cases, Rac1 activity is not dropping suddenly at PLSs, but decreases rather gradually.

Summarizing, we find Rac1 activity elevated at the first 2 μm of cell edge within a wide lamellipodium unlike in a narrow lamellipodium followed by a PLS zone.

By immunofluorescence stainings of the RAC1 GEFs βPIX and TIAM1, we confirmed Rac1 signaling patterns. The Rac1 GEF βPIX was found to be located along the lamella and stress fibers of hapto cells as well at the lamellipodium of chemo cells, if the PLS zone is not in direct vicinity to the cell edge. βPIX did not co-localize with PLSs, but was enriched again behind the PLS zone of chemo cells on plane substrate, however enrichment of βPIX behind the PLS zone on LSs is not obvious. The reason therefore might be stronger adhesiveness of cells on plane substrate. Resembling data was derived from immunofluorescence stainings of the Rac1GEF TIAM1. Although TIAM1 enrichment at the leading cell edge was more pronounced excluding the PLS zones.

TIAM1 was reported to accumulate at large tensile adhesions, but is depleted upon myosin inhibition by blebbistatin. Furthermore, TIAM1 was identified to enforce cell polarity via the PAR complexes 3 and 6 (Wang et al. 2012). Considering that TIAM1 accumulation goes hand in hand with traction force application, the absence of TIAM1 at non-contractile PLSs would coincide with these findings. Considerably, low contractile and low adherent chemo cells use alternative signaling mechanisms to maintain cell polarity.

Conclusively, we found Rac1 activated at the lamellipodium and often behind PLS zones consistent with localization of RAC1 GEFs. However PLS zones itself were lacking Rac1 activity as well as Rac1 GEFs. Therefore we propose Rac1 is not directly involved in activation of the Arp2/3 complex via WAVE complex at PLSs.

Static and dynamic imaging of cytoskeleton, adhesion structures and plasma membrane deepened our understanding of persistent fibroblast cell migration

Immunofluorescence stainings of Arp2, a component of the Arp2/3 complex revealed enrichment of this actin nucleator at the lamella and lamellipodium of hapto and chemo cells. We also found prominent co-localization of Arp2 and PLSs confirming additionally to CK666 drug perturbation experiments the role of the Arp2/3 complex in actin nucleation at PLSs.

In order to visualize new assembled adhesion structures we stained cells with a phosphor tyrosine specific antibody. FCs and FAs show strong signals, but also PLSs contained phospho tyrosine. In general, phospho tyrosine signal gradually decreased from the leading edge towards cell rear. This pattern is consistent with formation of new adhesions from at the leading edge to drive cell migration.

Similar to talin, the first and mechanosensitive protein interacting with a new formed integrin cluster, the adhesion component vinculin and paxillin were enriched at FCs and FAs. PLSs contained talin, but no vinculin and paxillin was detected. One could hypothesize that due to lack of contractility at the PLS zones, talin is not able to recruit any other adhesion components.

Concerning microtubule organization and orientation immunofluorescence stainings provided valuable information:

We observed enrichment of microtubules and +end marker EB3 at the ventral part of the leading edge of hapto cells, indicating that microtubule assembly preferentially occurs at the cell front similar to new assembled FCs. Furthermore, we realized microtubule filaments align with F-actin stress fibers alternately at the plasma membrane. Surprisingly, we encountered absence of microtubules from the ventral part of PLS zones. However, epifluorescence microscopy revealed that microtubules proceeded above PLSs and touched the plasma membrane again in their vicinity. Similarly, EB3 appeared adjacent to the PLS zone at the ventral part of the leading edge, indicating places of microtubule assembly.

Thus, microtubules and their +ends were absent from PLS zones suggest that no physical interaction takes place. Considering, that PLSs are non-contractile structures unlike FAs, this might explain the absence of microtubules.

In the beginning of this project we evaluated a variety of fluorescently tagged adhesion markers. We faced the fact, that our system is very sensitive to any perturbations, especially when cells are migrating on LSs. This sensitivity is characterized by not-wild type like morphology or poor cell health. The best performing adhesion marker in our hands is VASP-GFP, which gave us insights in adhesion dynamics during cell migration. Although except VASP-GFP all other tested adhesion markers did not allow to acquire comprehensive data sets with satisfying quality, we though obtained some information:

In life cell imaging experiments using the adhesion marker β_3 integrin-GFP we observed high endocytotic activity in chemo cells. β_3 integrin-GFP, enriched in lateral FAs, appeared after adhesion disassembly in endocytotic vesicles travelling from the leading edge towards the golgi. This

observation allowed the assumption that chemo cells effectively recycle their receptors to promote rapid cell migration.

Cells expressing β_1 integrin-GFP showed strong morphological defects. However, we detected β_1 integrin at PLS zones at low levels.

Caveolin-1 (Y14F) was used as marker for ventral membrane dynamics in hapto and chemo cells migrating on LSs. In hapto cells we observed membrane motion following actin retrograde flow, but anterograde membrane flow at lateral regions of the cell body and at the trailing edge. Surprisingly, proximal membrane regions of hapto cells showed vortical dynamics, reminiscent of turbulences in fluidic systems. Differently, chemo cells showed unidirectional, anterograde flow of membrane during rapid and directional cell migration. It was shown in *Drosophila* S2R+ cells that cortex rigidity increased upon rounding up of cells entering mitosis (Kunda et al. 2008). Therefore one could hypothesize, that the cell cortex might be stiffer in compact shaped and fast migrating chemo cells compared to hapto cells.

I want to draw an analogy to fluidic systems where flow properties are dependent on diameter and viscosity: Keeping the diameter of flow constant, viscosity would be the decision-making parameter for laminar or turbulent flow. Given, that chemo cells had a stiffer cortex, they would behave like highly viscose fluids and stream in laminar fashion, while hapto cells would correspond to fluids with lower viscosity and exhibit therefore turbulent flow characteristics. One could further hypothesize, that "laminar" and unidirectional membrane flow characteristics contribute as well to efficient and rapid cell migration such as found in chemo cells on line substrates.

Concluding remarks

Our findings provide novel insights into mechanistics and regulation of persistent fibroblast migration. Unidirectional migration for many hours is mediated by establishment of two spatially and functionally distinct modules. These modules are mechanically isolated from each other by a zone of PLSs. We suggest that organization of defined front and back module might be a common strategy for fast migrating cells to achieve robust persistent migration in absence of chemotactic gradients.

6. References

- Albiges-Rizo, C. et al., 2009. Actin machinery and mechanosensitivity in invadopodia, podosomes and focal adhesions. *Journal of cell science*, 122(Pt 17), pp.3037–49. Available at: <http://www.pubmedcentral.nih.gov/articlerender.fcgi?artid=2767377&tool=pmcentrez&rendertype=abstract> [Accessed August 9, 2013].
- Ang, S.-F. et al., 2010. DAAM1 is a formin required for centrosome re-orientation during cell migration. *PLoS one*, 5(9). Available at: <http://www.pubmedcentral.nih.gov/articlerender.fcgi?artid=2947498&tool=pmcentrez&rendertype=abstract> [Accessed September 3, 2013].
- Arriuermerlou, C. & Meyer, T., 2005. A local coupling model and compass parameter for eukaryotic chemotaxis. *Developmental cell*, 8(2), pp.215–27. Available at: <http://www.ncbi.nlm.nih.gov/pubmed/15691763> [Accessed August 8, 2013].
- Barton, W. a et al., 2006. Crystal structures of the Tie2 receptor ectodomain and the angiopoietin-2-Tie2 complex. *Nature structural & molecular biology*, 13(6), pp.524–32. Available at: <http://www.ncbi.nlm.nih.gov/pubmed/16732286>.
- Benink, H. a & Bement, W.M., 2005. Concentric zones of active RhoA and Cdc42 around single cell wounds. *The Journal of cell biology*, 168(3), pp.429–39. Available at: <http://www.pubmedcentral.nih.gov/articlerender.fcgi?artid=2171735&tool=pmcentrez&rendertype=abstract> [Accessed August 15, 2013].
- Benard, V., Bohl, B. P. and Bokoch, G. M. (1999). Characterization of rac and cdc42 activation in chemoattractant-stimulated human neutrophils using a novel assay for active
- Bernstein, B.W. & Bamberg, J.R., 2010. ADF/cofilin: a functional node in cell biology. *Trends in cell biology*, 20(4), pp.187–95. Available at: <http://www.pubmedcentral.nih.gov/articlerender.fcgi?artid=2849908&tool=pmcentrez&rendertype=abstract> [Accessed September 17, 2013].
- Bindschadler, M. & McGrath, J.L., 2004. Formin' new ideas about actin filament generation. *Proceedings of the National Academy of Sciences of the United States of America*, 101(41), pp.14685–6. Available at: <http://www.pubmedcentral.nih.gov/articlerender.fcgi?artid=522045&tool=pmcentrez&rendertype=abstract>.
- Bokoch, G.M., 2003. Biology of the p21-activated kinases. *Annual review of biochemistry*, 72, pp.743–81. Available at: <http://www.ncbi.nlm.nih.gov/pubmed/12676796> [Accessed August 7, 2013].
- Broussard, J. a, Webb, D.J. & Kaverina, I., 2008. Asymmetric focal adhesion disassembly in motile cells. *Current opinion in cell biology*, 20(1), pp.85–90. Available at: <http://www.ncbi.nlm.nih.gov/pubmed/18083360> [Accessed August 19, 2013].
- Buccione, R., Caldieri, G. & Ayala, I., 2009. Invadopodia: specialized tumor cell structures for the focal degradation of the extracellular matrix. *Cancer metastasis reviews*, 28(1-2), pp.137–49. Available at: <http://www.ncbi.nlm.nih.gov/pubmed/19153671> [Accessed August 7, 2013].
- Buccione, R., Orth, J.D. & McNiven, M. a, 2004. Foot and mouth: podosomes, invadopodia and circular dorsal ruffles. *Nature reviews. Molecular cell biology*, 5(8), pp.647–57. Available at: <http://www.ncbi.nlm.nih.gov/pubmed/15366708> [Accessed August 27, 2013].
- Buchsbaum, R.J., 2007. Rho activation at a glance. *Journal of cell science*, 120(Pt 7), pp.1149–52. Available at: <http://www.ncbi.nlm.nih.gov/pubmed/17376960> [Accessed March 11, 2013].
- Burnette, D.T. et al., 2011. A role for actin arcs in the leading-edge advance of migrating cells. *Nature cell biology*, 13(4), pp.371–81. Available at: <http://www.pubmedcentral.nih.gov/articlerender.fcgi?artid=3646481&tool=pmcentrez&rendertype=abstract> [Accessed August 16, 2013].
- Burridge, K. et al., 2004. Rho and Rac Take Center Stage Review. , 116, pp.167–179.
- Burridge, K., Turner, C.E. & Romer, L.H., 1992. Tyrosine phosphorylation of paxillin and pp125FAK accompanies cell adhesion to extracellular matrix: a role in cytoskeletal assembly. *The Journal of cell biology*, 119(4), pp.893–903. Available at: <http://www.pubmedcentral.nih.gov/articlerender.fcgi?artid=2289706&tool=pmcentrez&rendertype=abstract>.
- Cai, L. et al., 2009. NIH Public Access. , 134(5), pp.828–842.
- Calderwood, D. a., 1999. The Talin Head Domain Binds to Integrin beta Subunit Cytoplasmic Tails and Regulates Integrin Activation. *Journal of Biological Chemistry*, 274(40), pp.28071–28074. Available at: <http://www.jbc.org/cgi/doi/10.1074/jbc.274.40.28071> [Accessed August 21, 2013].
- Carlsson, A.E., 2010. Actin Dynamics : From Nanoscale to Microscale. , pp.91–110.

- Carman, C. V et al., 2007. Transcellular diapedesis is initiated by invasive podosomes. *Immunity*, 26(6), pp.784–97. Available at: <http://www.pubmedcentral.nih.gov/articlerender.fcgi?artid=2094044&tool=pmcentrez&rendertype=abstract> [Accessed August 12, 2013].
- Carman, C. V & Springer, T. a, 2003. Integrin avidity regulation: are changes in affinity and conformation underemphasized? *Current Opinion in Cell Biology*, 15(5), pp.547–556. Available at: <http://linkinghub.elsevier.com/retrieve/pii/S0955067403001121> [Accessed August 22, 2013].
- Caswell, P.T. & Norman, J.C., 2006. Integrin trafficking and the control of cell migration. *Traffic (Copenhagen, Denmark)*, 7(1), pp.14–21. Available at: <http://www.ncbi.nlm.nih.gov/pubmed/16445683> [Accessed August 13, 2013].
- Choi, C.K. et al., 2008. Actin and alpha-actinin orchestrate the assembly and maturation of nascent adhesions in a myosin II motor-independent manner. *Nature cell biology*, 10(9), pp.1039–50. Available at: <http://www.pubmedcentral.nih.gov/articlerender.fcgi?artid=2827253&tool=pmcentrez&rendertype=abstract> [Accessed August 7, 2013].
- Chrzanowska-Wodnicka, M. & Burridge, K., 1996. Rho-stimulated contractility drives the formation of stress fibers and focal adhesions. *The Journal of cell biology*, 133(6), pp.1403–15. Available at: <http://www.pubmedcentral.nih.gov/articlerender.fcgi?artid=2120895&tool=pmcentrez&rendertype=abstract>.
- Chung, I. et al., 2010. Spatial control of EGF receptor activation by reversible dimerization on living cells. *Nature*, 464(7289), pp.783–7. Available at: <http://www.ncbi.nlm.nih.gov/pubmed/20208517> [Accessed August 9, 2013].
- Cramer, L.P., Siebert, M. & Mitchison, T.J., 1997. Identification of novel graded polarity actin filament bundles in locomoting heart fibroblasts: implications for the generation of motile force. *The Journal of cell biology*, 136(6), pp.1287–305. Available at: <http://www.pubmedcentral.nih.gov/articlerender.fcgi?artid=2132518&tool=pmcentrez&rendertype=abstract>.
- Critchley, D.R., 2009. Biochemical and structural properties of the integrin-associated cytoskeletal protein talin. *Annual review of biophysics*, 38, pp.235–54. Available at: <http://www.ncbi.nlm.nih.gov/pubmed/19416068> [Accessed August 9, 2013].
- Cukierman, E. et al., 2001. Taking cell-matrix adhesions to the third dimension. *Science (New York, N.Y.)*, 294(5547), pp.1708–12. Available at: <http://www.ncbi.nlm.nih.gov/pubmed/11721053> [Accessed August 7, 2013].
- Desai, B., Ma, T. & Chellaiah, M. a, 2008. Invadopodia and matrix degradation, a new property of prostate cancer cells during migration and invasion. *The Journal of biological chemistry*, 283(20), pp.13856–66. Available at: <http://www.pubmedcentral.nih.gov/articlerender.fcgi?artid=2376228&tool=pmcentrez&rendertype=abstract> [Accessed August 27, 2013].
- Diaz, B. et al., 2009. Tks5-dependent, nox-mediated generation of reactive oxygen species is necessary for invadopodia formation. *Science signaling*, 2(88), p.ra53. Available at: <http://www.pubmedcentral.nih.gov/articlerender.fcgi?artid=2810640&tool=pmcentrez&rendertype=abstract> [Accessed September 13, 2013].
- Doyle, A.D. et al., 2009. One-dimensional topography underlies three-dimensional fibrillar cell migration. *The Journal of cell biology*, 184(4), pp.481–90. Available at: <http://www.pubmedcentral.nih.gov/articlerender.fcgi?artid=2654121&tool=pmcentrez&rendertype=abstract> [Accessed August 9, 2013].
- Du, X. et al., 1991. Ligands 'Activate' Integrin CQ, & (Platelet GPIIb-IIIa). , 65(Figure 16), pp.409–416.
- Eden, S. et al., 2002. Mechanism of regulation of WAVE1-induced actin nucleation by Rac1 and Nck. *Nature*, 418(6899), pp.790–3. Available at: <http://www.ncbi.nlm.nih.gov/pubmed/12181570>.
- Edwards, D.C. et al., 1999. Activation of LIM-kinase by Pak1 couples Rac/Cdc42 GTPase signalling to actin cytoskeletal dynamics. *Nature cell biology*, 1(5), pp.253–9. Available at: <http://www.ncbi.nlm.nih.gov/pubmed/10559936>.
- Etienne-Manneville, S. & Hall, A., 2002. Rho GTPases in cell biology. *Nature*, 420(6916), pp.629–35. Available at: <http://www.ncbi.nlm.nih.gov/pubmed/18460342>.
- Franco, S.J. et al., 2004. Calpain-mediated proteolysis of talin regulates adhesion dynamics. *Nature cell biology*, 6(10), pp.977–83. Available at: <http://www.ncbi.nlm.nih.gov/pubmed/15448700> [Accessed August 16, 2013].
- Friedl, P. et al., 1995. Migration of Coordinated Cell Clusters in Mesenchymal and Epithelial Cancer Explants in Vitro Advances in Brief Migration of Coordinated Cell Clusters in Mesenchymal and Epithelial Cancer in Vitro . *Cancer Res* 1995;55:4557-4560. Updated, pp.4557–4560.

- Friedl, P., 2004. Prespecification and plasticity: shifting mechanisms of cell migration. *Current opinion in cell biology*, 16(1), pp.14–23. Available at: <http://www.ncbi.nlm.nih.gov/pubmed/15037300> [Accessed August 15, 2013].
- Friedl, P. & Wolf, K., 2010. Plasticity of cell migration: a multiscale tuning model. *The Journal of cell biology*, 188(1), pp.11–9. Available at: <http://www.pubmedcentral.nih.gov/articlerender.fcgi?artid=2812848&tool=pmcentrez&rendertype=abstract> [Accessed August 8, 2013].
- Fritz, R.D. et al., 2013. A Versatile Toolkit to Produce Sensitive FRET Biosensors to Visualize Signaling in Time and Space. *Science signaling*, 6(285), p.rs12. Available at: <http://www.ncbi.nlm.nih.gov/pubmed/23882122> [Accessed August 7, 2013].
- Gandhi, M. et al., 2010. GMF is a cofilin homolog that binds Arp2/3 complex to stimulate filament debranching and inhibit actin nucleation. *Current biology : CB*, 20(9), pp.861–7. Available at: <http://www.pubmedcentral.nih.gov/articlerender.fcgi?artid=2869398&tool=pmcentrez&rendertype=abstract> [Accessed September 3, 2013].
- Geiger, T. & Zaidel-Bar, R., 2012. Opening the floodgates: proteomics and the integrin adhesome. *Current opinion in cell biology*, 24(5), pp.562–8. Available at: <http://www.ncbi.nlm.nih.gov/pubmed/22728062> [Accessed September 3, 2013].
- Giancotti, F.G., 1999. Integrin Signaling. *Science*, 285(5430), pp.1028–1033. Available at: <http://www.sciencemag.org/cgi/doi/10.1126/science.285.5430.1028> [Accessed August 7, 2013].
- Gianni, D. et al., 2008. The Involvement of the Tyrosine Kinase c-Src in the Regulation of Reactive Oxygen Species Generation Mediated by NADPH Oxidase-1. , 19(July), pp.2984–2994.
- Giannone, G. et al., 2007. Lamellipodial actin mechanically links myosin activity with adhesion-site formation. *Cell*, 128(3), pp.561–75. Available at: <http://www.ncbi.nlm.nih.gov/pubmed/17289574> [Accessed August 19, 2013].
- Gingras, A.R. et al., 2010. Central region of talin has a unique fold that binds vinculin and actin. *The Journal of biological chemistry*, 285(38), pp.29577–87. Available at: <http://www.pubmedcentral.nih.gov/articlerender.fcgi?artid=2937989&tool=pmcentrez&rendertype=abstract> [Accessed September 3, 2013].
- Gingras, A.R. et al., 2008. The structure of the C-terminal actin-binding domain of talin. *The EMBO journal*, 27(2), pp.458–69. Available at: <http://www.pubmedcentral.nih.gov/articlerender.fcgi?artid=2168396&tool=pmcentrez&rendertype=abstract> [Accessed August 26, 2013].
- Glotzer, M., 2005. The molecular requirements for cytokinesis. *Science (New York, N.Y.)*, 307(5716), pp.1735–9. Available at: <http://www.ncbi.nlm.nih.gov/pubmed/15774750> [Accessed August 7, 2013].
- Goode, B.L. & Eck, M.J., 2007. Mechanism and function of formins in the control of actin assembly. *Annual review of biochemistry*, 76, pp.593–627. Available at: <http://www.ncbi.nlm.nih.gov/pubmed/17373907> [Accessed August 9, 2013].
- Griffith, L.G. & Swartz, M. a, 2006. Capturing complex 3D tissue physiology in vitro. *Nature reviews. Molecular cell biology*, 7(3), pp.211–24. Available at: <http://www.ncbi.nlm.nih.gov/pubmed/16496023> [Accessed August 11, 2013].
- Grinnell, F. & Petroll, W.M., 2010. Cell motility and mechanics in three-dimensional collagen matrices. *Annual review of cell and developmental biology*, 26, pp.335–61. Available at: <http://www.ncbi.nlm.nih.gov/pubmed/19575667> [Accessed August 13, 2013].
- Gupton, S.L. & Waterman-Storer, C.M., 2006. Spatiotemporal feedback between actomyosin and focal-adhesion systems optimizes rapid cell migration. *Cell*, 125(7), pp.1361–74. Available at: <http://www.ncbi.nlm.nih.gov/pubmed/16814721> [Accessed August 9, 2013].
- Harburger, D.S., Bouaouina, M. & Calderwood, D. a, 2009. Kindlin-1 and -2 directly bind the C-terminal region of beta integrin cytoplasmic tails and exert integrin-specific activation effects. *The Journal of biological chemistry*, 284(17), pp.11485–97. Available at: <http://www.pubmedcentral.nih.gov/articlerender.fcgi?artid=2670154&tool=pmcentrez&rendertype=abstract> [Accessed September 3, 2013].
- Harris, E.S., Li, F. & Higgs, H.N., 2004. The mouse formin, FRLalpha, slows actin filament barbed end elongation, competes with capping protein, accelerates polymerization from monomers, and severs filaments. *The Journal of biological chemistry*, 279(19), pp.20076–87. Available at: <http://www.ncbi.nlm.nih.gov/pubmed/14990563> [Accessed August 19, 2013].
- Hemmings, L. et al., 1996. Talin contains three actin-binding sites each of which is adjacent to a vinculin-binding site. *Journal of cell science*, 109 (Pt 1, pp.2715–26. Available at: <http://www.ncbi.nlm.nih.gov/pubmed/8937989>.

- Himanen, J.-P. & Nikolov, D.B., 2003. Eph signaling: a structural view. *Trends in neurosciences*, 26(1), pp.46–51. Available at: <http://www.ncbi.nlm.nih.gov/pubmed/12495863>.
- Hoppe, A.D. & Swanson, J.A., 2004. Activation during Phagocytosis □. , 15(August), pp.3509–3519.
- Hotulainen, P. & Lappalainen, P., 2006. Stress fibers are generated by two distinct actin assembly mechanisms in motile cells. *The Journal of cell biology*, 173(3), pp.383–94. Available at: <http://www.pubmedcentral.nih.gov/articlerender.fcgi?artid=2063839&tool=pmcentrez&rendertype=abstract> [Accessed August 14, 2013].
- Humphries, J.D., Byron, A. & Humphries, M.J., 2006. Integrin ligands at a glance. *Journal of cell science*, 119(Pt 19), pp.3901–3. Available at: <http://www.pubmedcentral.nih.gov/articlerender.fcgi?artid=3380273&tool=pmcentrez&rendertype=abstract> [Accessed August 8, 2013].
- Hunter, T., 2007. The age of crosstalk: phosphorylation, ubiquitination, and beyond. *Molecular cell*, 28(5), pp.730–8. Available at: <http://www.ncbi.nlm.nih.gov/pubmed/18082598> [Accessed August 13, 2013].
- Hunter, T., 1998. The Croonian Lecture 1997. The phosphorylation of proteins on tyrosine: its role in cell growth and disease. *Philosophical transactions of the Royal Society of London. Series B, Biological sciences*, 353(1368), pp.583–605. Available at: <http://www.pubmedcentral.nih.gov/articlerender.fcgi?artid=1692245&tool=pmcentrez&rendertype=abstract>.
- Hynes, R.O., 2002. Integrins : Bidirectional , Allosteric Signaling Machines In their roles as major adhesion receptors , integrins. , 110(Table 1), pp.673–687.
- Kanchanawong, P. et al., 2010. Nanoscale architecture of integrin-based cell adhesions. *Nature*, 468(7323), pp.580–4. Available at: <http://www.pubmedcentral.nih.gov/articlerender.fcgi?artid=3046339&tool=pmcentrez&rendertype=abstract> [Accessed August 8, 2013].
- Kaverina, I., Krylyshkina, O. & Small, J.V., 2002. Regulation of substrate adhesion dynamics during cell motility. *The international journal of biochemistry & cell biology*, 34(7), pp.746–61. Available at: <http://www.ncbi.nlm.nih.gov/pubmed/11950592>.
- Kim, C., Ye, F. & Ginsberg, M.H., 2011. Regulation of integrin activation. *Annual review of cell and developmental biology*, 27, pp.321–45. Available at: <http://www.ncbi.nlm.nih.gov/pubmed/21663444> [Accessed August 8, 2013].
- Kirby, J.R., 2009. Chemotaxis-like regulatory systems: unique roles in diverse bacteria. *Annual review of microbiology*, 63, pp.45–59. Available at: <http://www.ncbi.nlm.nih.gov/pubmed/19379070> [Accessed August 7, 2013].
- Kloeker, S. et al., 2004. The Kindler syndrome protein is regulated by transforming growth factor-beta and involved in integrin-mediated adhesion. *The Journal of biological chemistry*, 279(8), pp.6824–33. Available at: <http://www.ncbi.nlm.nih.gov/pubmed/14634021> [Accessed September 3, 2013].
- Koestler, S. a et al., 2008. Differentially oriented populations of actin filaments generated in lamellipodia collaborate in pushing and pausing at the cell front. *Nature cell biology*, 10(3), pp.306–13. Available at: <http://www.ncbi.nlm.nih.gov/pubmed/18278037> [Accessed August 7, 2013].
- Komarova, Y. et al., 2009. Mammalian end binding proteins control persistent microtubule growth. *The Journal of cell biology*, 184(5), pp.691–706. Available at: <http://www.pubmedcentral.nih.gov/articlerender.fcgi?artid=2686402&tool=pmcentrez&rendertype=abstract> [Accessed August 10, 2013].
- Kovács, M. et al., 2003. Functional divergence of human cytoplasmic myosin II: kinetic characterization of the non-muscle IIA isoform. *The Journal of biological chemistry*, 278(40), pp.38132–40. Available at: <http://www.ncbi.nlm.nih.gov/pubmed/12847096> [Accessed September 18, 2013].
- Kovar, D.R. et al., 2006. Control of the assembly of ATP- and ADP-actin by formins and profilin. *Cell*, 124(2), pp.423–35. Available at: <http://www.ncbi.nlm.nih.gov/pubmed/16439214> [Accessed August 14, 2013].
- Kozma, R. et al., 1995. The Ras-related protein Cdc42Hs and bradykinin promote formation of peripheral actin microspikes and filopodia in Swiss 3T3 fibroblasts. *Molecular and cellular biology*, 15(4), pp.1942–52. Available at: <http://www.pubmedcentral.nih.gov/articlerender.fcgi?artid=230420&tool=pmcentrez&rendertype=abstract>.
- Kreis, T.E., 1960. Stress Fiber Sarcomeres Are Contractile of Fibroblasts. , 22(November).
- Kunda, P. et al., 2008. Moesin controls cortical rigidity, cell rounding, and spindle morphogenesis during mitosis. *Current biology : CB*, 18(2), pp.91–101. Available at: <http://www.ncbi.nlm.nih.gov/pubmed/18207738> [Accessed September 3, 2013].

- Kuo, J.-C. et al., 2011. Analysis of the myosin-II-responsive focal adhesion proteome reveals a role for β -Pix in negative regulation of focal adhesion maturation. *Nature cell biology*, 13(4), pp.383–93. Available at: <http://www.pubmedcentral.nih.gov/articlerender.fcgi?artid=3279191&tool=pmcentrez&rendertype=abstract> [Accessed August 6, 2013].
- Lammers, M. et al., 2005. The regulation of mDia1 by autoinhibition and its release by Rho*GTP. *The EMBO journal*, 24(23), pp.4176–87. Available at: <http://www.pubmedcentral.nih.gov/articlerender.fcgi?artid=1356318&tool=pmcentrez&rendertype=abstract> [Accessed August 19, 2013].
- Lee, C.-S. et al., 2010. Myosin II directly binds and inhibits Dbl family guanine nucleotide exchange factors: a possible link to Rho family GTPases. *The Journal of cell biology*, 190(4), pp.663–74. Available at: <http://www.pubmedcentral.nih.gov/articlerender.fcgi?artid=2928003&tool=pmcentrez&rendertype=abstract> [Accessed August 9, 2013].
- Leiss, M. et al., 2008. The role of integrin binding sites in fibronectin matrix assembly in vivo. *Current opinion in cell biology*, 20(5), pp.502–7. Available at: <http://www.ncbi.nlm.nih.gov/pubmed/18586094> [Accessed August 6, 2013].
- Lemmon, M. a & Schlessinger, J., 2010. Cell signaling by receptor tyrosine kinases. *Cell*, 141(7), pp.1117–34. Available at: <http://www.pubmedcentral.nih.gov/articlerender.fcgi?artid=2914105&tool=pmcentrez&rendertype=abstract> [Accessed August 7, 2013].
- Lo, C. et al., 2004. Nonmuscle Myosin IIB Is Involved in the Guidance of Fibroblast Migration □. , 15(March), pp.982–989.
- Lowery, L.A. & Van Vactor, D., 2009. The trip of the tip: understanding the growth cone machinery. *Nature reviews. Molecular cell biology*, 10(5), pp.332–43. Available at: <http://www.pubmedcentral.nih.gov/articlerender.fcgi?artid=2714171&tool=pmcentrez&rendertype=abstract> [Accessed August 8, 2013].
- Kimura .K. et al., 1996. Regulation of Myosin Phosphatase by Rho and Rho-Associated Kinase (Rho-Kinase) Science, 273 (July)
- Machacek, M. et al., 2009. Coordination of Rho GTPase activities during cell protrusion. *Nature*, 461(7260), pp.99–103. Available at: <http://www.pubmedcentral.nih.gov/articlerender.fcgi?artid=2885353&tool=pmcentrez&rendertype=abstract> [Accessed August 10, 2013].
- Maekawa, M., 1999. Signaling from Rho to the Actin Cytoskeleton Through Protein Kinases ROCK and LIM-kinase. *Science*, 285(5429), pp.895–898. Available at: <http://www.sciencemag.org/cgi/doi/10.1126/science.285.5429.895> [Accessed August 12, 2013].
- Maritzen, T. et al., 2012. Gadkin negatively regulates cell spreading and motility via sequestration of the actin-nucleating ARP2/3 complex. *Proceedings of the National Academy of Sciences of the United States of America*, 109(26), pp.10382–7. Available at: <http://www.pubmedcentral.nih.gov/articlerender.fcgi?artid=3387086&tool=pmcentrez&rendertype=abstract> [Accessed August 19, 2013].
- Meshel, A.S. et al., 2005. Basic mechanism of three-dimensional collagen fibre transport by fibroblasts. *Nature cell biology*, 7(2), pp.157–64. Available at: <http://www.ncbi.nlm.nih.gov/pubmed/15654332> [Accessed August 19, 2013].
- Miki, H. et al., 2000. IRSp53 is an essential intermediate between Rac and WAVE in the regulation of membrane ruffling. *Nature*, 408(6813), pp.732–5. Available at: <http://www.ncbi.nlm.nih.gov/pubmed/11130076>.
- Mimori-Kiyosue, Y., Shiina, N. & Tsukita, S., 2000. The dynamic behavior of the APC-binding protein EB1 on the distal ends of microtubules. *Current biology : CB*, 10(14), pp.865–8. Available at: <http://www.ncbi.nlm.nih.gov/pubmed/10899006>.
- Miyamoto, S., Akiyama, S.K. & Yamada, K.M., 1995. Synergistic roles for receptor occupancy and aggregation in integrin transmembrane function. *Science (New York, N.Y.)*, 267(5199), pp.883–5. Available at: <http://www.ncbi.nlm.nih.gov/pubmed/7846531>.
- Mogilner, A., 2006. On the edge: modeling protrusion. *Current opinion in cell biology*, 18(1), pp.32–9. Available at: <http://www.ncbi.nlm.nih.gov/pubmed/16318917> [Accessed August 8, 2013].
- Moser, M. et al., 2009. The tail of integrins, talin, and kindlins. *Science (New York, N.Y.)*, 324(5929), pp.895–9. Available at: <http://www.ncbi.nlm.nih.gov/pubmed/19443776> [Accessed August 7, 2013].
- Murphy, D. a & Courtneidge, S. a, 2011. The “ins” and “outs” of podosomes and invadopodia: characteristics, formation and function. *Nature reviews. Molecular cell biology*, 12(7), pp.413–26. Available at: <http://www.pubmedcentral.nih.gov/articlerender.fcgi?artid=3423958&tool=pmcentrez&rendertype=abstract> [Accessed August 20, 2013].

- Naumanen, P., Lappalainen, P. & Hotulainen, P., 2008. Mechanisms of actin stress fibre assembly. *Journal of microscopy*, 231(3), pp.446–54. Available at: <http://www.ncbi.nlm.nih.gov/pubmed/18755000>.
- Nelson, C.M. & Bissell, M.J., 2006. Of extracellular matrix, scaffolds, and signaling: tissue architecture regulates development, homeostasis, and cancer. *Annual review of cell and developmental biology*, 22, pp.287–309. Available at: <http://www.pubmedcentral.nih.gov/articlerender.fcgi?artid=2933192&tool=pmcentrez&rendertype=abstract> [Accessed August 18, 2013].
- Nobes, C.D. & Hall, a, 1995. Rho, rac, and cdc42 GTPases regulate the assembly of multimolecular focal complexes associated with actin stress fibers, lamellipodia, and filopodia. *Cell*, 81(1), pp.53–62. Available at: <http://www.ncbi.nlm.nih.gov/pubmed/7536630>.
- Nogales, E. & Wang, H.-W., 2006. Structural mechanisms underlying nucleotide-dependent self-assembly of tubulin and its relatives. *Current opinion in structural biology*, 16(2), pp.221–9. Available at: <http://www.ncbi.nlm.nih.gov/pubmed/16549346> [Accessed September 3, 2013].
- Oakes, P.W. et al., 2012. Tension is required but not sufficient for focal adhesion maturation without a stress fiber template. *The Journal of cell biology*, 196(3), pp.363–74. Available at: <http://www.pubmedcentral.nih.gov/articlerender.fcgi?artid=3275371&tool=pmcentrez&rendertype=abstract> [Accessed August 7, 2013].
- Ohta, Y., Hartwig, J.H. & Stossel, T.P., 2006. FilGAP, a Rho- and ROCK-regulated GAP for Rac binds filamin A to control actin remodelling. *Nature cell biology*, 8(8), pp.803–14. Available at: <http://www.ncbi.nlm.nih.gov/pubmed/16862148> [Accessed September 3, 2013].
- Ono, S., 2010. Dynamic regulation of sarcomeric actin filaments in striated muscle. *Cytoskeleton (Hoboken, N.J.)*, 67(11), pp.677–92. Available at: <http://www.pubmedcentral.nih.gov/articlerender.fcgi?artid=2963174&tool=pmcentrez&rendertype=abstract> [Accessed September 3, 2013].
- Palecek, S.P. et al., 1998. Physical and biochemical regulation of integrin release during rear detachment of migrating cells. *Journal of cell science*, 111 (Pt 7, pp.929–40. Available at: <http://www.ncbi.nlm.nih.gov/pubmed/9490637>.
- Parat, M., Anand-apte, B. & Fox, P.L., 2003. Differential Caveolin-1 Polarization in Endothelial Cells during Migration in Two and Three Dimensions. , 14(August), pp.3156–3168.
- Parsons, J.T., Horwitz, A.R. & Schwartz, M. a, 2010. Cell adhesion: integrating cytoskeletal dynamics and cellular tension. *Nature reviews. Molecular cell biology*, 11(9), pp.633–43. Available at: <http://www.pubmedcentral.nih.gov/articlerender.fcgi?artid=2992881&tool=pmcentrez&rendertype=abstract> [Accessed August 6, 2013].
- Parsons, M. et al., 2005. Spatially Distinct Binding of Cdc42 to PAK1 and N-WASP in Breast Carcinoma Cells Spatially Distinct Binding of Cdc42 to PAK1 and N-WASP in Breast Carcinoma Cells †.
- Pavalko, F.M. & Otey, C.A., 1991. a-Actinin : a direct link between actin and integrins Focal adhesions are a model for studying actin-membrane interactions In vitro identification of an a-actinin-.
- Pawson, T., 2004. Specificity in signal transduction: from phosphotyrosine-SH2 domain interactions to complex cellular systems. *Cell*, 116(2), pp.191–203. Available at: <http://www.ncbi.nlm.nih.gov/pubmed/14744431>.
- Pellegrin, S. & Mellor, H., 2007. Actin stress fibres. *Journal of cell science*, 120(Pt 20), pp.3491–9. Available at: <http://www.ncbi.nlm.nih.gov/pubmed/17928305> [Accessed August 8, 2013].
- Perentes, J.Y. et al., 2009. In vivo imaging of extracellular matrix remodeling by tumor- associated fibroblasts. *Nature methods*, 6(2), pp.2008–2010.
- Pertz, O. et al., 2006. Spatiotemporal dynamics of RhoA activity in migrating cells. *Nature*, 440(7087), pp.1069–72. Available at: <http://www.ncbi.nlm.nih.gov/pubmed/16547516> [Accessed August 8, 2013].
- Petrie, R.J., Doyle, A.D. & Yamada, K.M., 2009. Random versus directionally persistent cell migration. *Nature reviews. Molecular cell biology*, 10(8), pp.538–49. Available at: <http://www.pubmedcentral.nih.gov/articlerender.fcgi?artid=2752299&tool=pmcentrez&rendertype=abstract> [Accessed August 7, 2013].
- Plotnikov, S. V et al., 2012. Force fluctuations within focal adhesions mediate ECM-rigidity sensing to guide directed cell migration. *Cell*, 151(7), pp.1513–27. Available at: <http://www.ncbi.nlm.nih.gov/pubmed/23260139> [Accessed August 7, 2013].

- Pollard, T.D. & Borisy, G.G., 2003. Cellular motility driven by assembly and disassembly of actin filaments. *Cell*, 112(4), pp.453–65. Available at: <http://www.ncbi.nlm.nih.gov/pubmed/12600310>.
- Ponti, a et al., 2004. Two distinct actin networks drive the protrusion of migrating cells. *Science (New York, N.Y.)*, 305(5691), pp.1782–6. Available at: <http://www.ncbi.nlm.nih.gov/pubmed/15375270> [Accessed August 8, 2013].
- Puklin-Faucher, E. & Sheetz, M.P., 2009. The mechanical integrin cycle. *Journal of Cell Science*, 122(4), pp.575–575. Available at: <http://jcs.biologists.org/cgi/doi/10.1242/jcs.049544> [Accessed August 15, 2013].
- Dos Remedios, C.G. et al., 2003. Actin binding proteins: regulation of cytoskeletal microfilaments. *Physiological reviews*, 83(2), pp.433–73. Available at: <http://www.ncbi.nlm.nih.gov/pubmed/12663865>.
- Ren, X. D., Kiosses, W. B. and Schwartz, M. A. (1999). Regulation of the small GTP- binding protein Rho by cell adhesion and the cytoskeleton. *EMBO J.* 18, 578-585.
- Renkawitz, J. et al., 2009. Adaptive force transmission in amoeboid cell migration. *Nature cell biology*, 11(12), pp.1438–43. Available at: <http://www.ncbi.nlm.nih.gov/pubmed/19915557> [Accessed September 3, 2013].
- Ridley, a J. et al., 1992. The small GTP-binding protein rac regulates growth factor-induced membrane ruffling. *Cell*, 70(3), pp.401–10. Available at: <http://www.ncbi.nlm.nih.gov/pubmed/1643658>.
- Rio, A. et al., 2009. Stretching Single Talin Rod. , 323(January), pp.638–641.
- Roca-Cusachs, P. et al., 2013. Integrin-dependent force transmission to the extracellular matrix by α -actinin triggers adhesion maturation. *Proceedings of the National Academy of Sciences of the United States of America*, 110(15), pp.E1361–70. Available at: <http://www.ncbi.nlm.nih.gov/pubmed/23515331> [Accessed August 13, 2013].
- Rocca, D.L. et al., 2008. Inhibition of Arp2/3-mediated actin polymerization by PICK1 regulates neuronal morphology and AMPA receptor endocytosis. *Nature cell biology*, 10(3), pp.259–71. Available at: <http://www.pubmedcentral.nih.gov/articlerender.fcgi?artid=2664613&tool=pmcentrez&rendertype=abstract> [Accessed August 12, 2013].
- Roussos, E.T., Condeelis, J.S., and Patsialou, A. (2011). Chemotaxis in cancer. *Nature reviews Cancer* 11, 573-587
- Sahai, E. & Marshall, C.J., 2002. ROCK and Dia have opposing effects on adherens junctions downstream of Rho. *Nature cell biology*, 4(6), pp.408–15. Available at: <http://www.ncbi.nlm.nih.gov/pubmed/11992112> [Accessed August 14, 2013].
- Sandquist, J.C. et al., 2006. Rho Kinase Differentially Regulates Phosphorylation of Nonmuscle Myosin II Isoforms A and B during Cell Rounding.
- Schiller, H.B. et al., 2013. β 1- and α v-class integrins cooperate to regulate myosin II during rigidity sensing of fibronectin-based microenvironments. *Nature cell biology*, 15(6), pp.625–36. Available at: <http://www.ncbi.nlm.nih.gov/pubmed/23708002> [Accessed September 18, 2013].
- Schlessinger, J., 2000. Cell Signaling by Receptor Tyrosine Kinases A large group of genes in all eukaryotes encode for. , 103, pp.211–225.
- Schlessinger, J. & Lemmon, M. a., 2003. SH2 and PTB Domains in Tyrosine Kinase Signaling. *Science Signaling*, 2003(191), pp.re12–re12. Available at: <http://stke.sciencemag.org/cgi/doi/10.1126/scisignal.1912003re12> [Accessed September 18, 2013].
- Schneider, I.C. & Haugh, J.M., 2006. Mechanisms of Gradient Sensing and Chemotaxis ES SC. , 5(11), pp.1130–1134.
- Schuyler, S.C. & Pellman, D., 2001. Proteins ”: The End Is Just the Beginning. , 105, pp.421–424.
- Schwartz, M., 2004. Rho signalling at a glance. *Journal of cell science*, 117(Pt 23), pp.5457–8. Available at: <http://www.ncbi.nlm.nih.gov/pubmed/15509861> [Accessed April 9, 2013].
- Shattil, S.J., Kim, C. & Ginsberg, M.H., 2010a. The final steps of integrin activation: the end game. *Nature reviews. Molecular cell biology*, 11(4), pp.288–300. Available at: <http://www.ncbi.nlm.nih.gov/pubmed/20308986> [Accessed August 7, 2013].
- Shattil, S.J., Kim, C. & Ginsberg, M.H., 2010b. The final steps of integrin activation: the end game. *Nature reviews. Molecular cell biology*, 11(4), pp.288–300. Available at: <http://www.ncbi.nlm.nih.gov/pubmed/20308986> [Accessed August 7, 2013].

- Shatz, M. et al., 2010. Caveolin-1 mutants P132L and Y14F are dominant negative regulators of invasion, migration and aggregation in H1299 lung cancer cells. *Experimental cell research*, 316(10), pp.1748–62. Available at: <http://www.ncbi.nlm.nih.gov/pubmed/20153318> [Accessed September 3, 2013].
- Sjöblom, B., Salmazo, a & Djinić-Carugo, K., 2008. Alpha-actinin structure and regulation. *Cellular and molecular life sciences : CMLS*, 65(17), pp.2688–701. Available at: <http://www.ncbi.nlm.nih.gov/pubmed/18488141> [Accessed August 12, 2013].
- Smilenov, L.B., 1999. Focal Adhesion Motility Revealed in Stationary Fibroblasts. *Science*, 286(5442), pp.1172–1174. Available at: <http://www.sciencemag.org/cgi/doi/10.1126/science.286.5442.1172> [Accessed August 11, 2013].
- Soranno, T. & Bell, E., 1982. Cytostructural Dynamics of Spreading and Translocating Cells Immunofluorescence : Cell Preparation. , (Imr 90), pp.127–136.
- Stehbens, S. & Wittmann, T., 2012. Targeting and transport: how microtubules control focal adhesion dynamics. *The Journal of cell biology*, 198(4), pp.481–9. Available at: <http://www.pubmedcentral.nih.gov/articlerender.fcgi?artid=3514042&tool=pmcentrez&rendertype=abstract> [Accessed August 7, 2013].
- Stephens, L., Milne, L. & Hawkins, P., 2008. Moving towards a better understanding of chemotaxis. *Current biology : CB*, 18(11), pp.R485–94. Available at: <http://www.ncbi.nlm.nih.gov/pubmed/18522824> [Accessed August 15, 2013].
- Straight, A.F. et al., 2003. Dissecting temporal and spatial control of cytokinesis with a myosin II Inhibitor. *Science (New York, N. Y.)*, 299(5613), pp.1743–7. Available at: <http://www.ncbi.nlm.nih.gov/pubmed/12637748> [Accessed August 22, 2013].
- Suetsugu, S. et al., 2003. Differential roles of WAVE1 and WAVE2 in dorsal and peripheral ruffle formation for fibroblast cell migration. *Developmental cell*, 5(4), pp.595–609. Available at: <http://www.ncbi.nlm.nih.gov/pubmed/14536061>.
- Sun, G. et al., 2012. Protein tyrosine phosphatase α phosphotyrosyl-789 binds BCAR3 to position Cas for activation at integrin-mediated focal adhesions. *Molecular and cellular biology*, 32(18), pp.3776–89. Available at: <http://www.pubmedcentral.nih.gov/articlerender.fcgi?artid=3430204&tool=pmcentrez&rendertype=abstract> [Accessed August 19, 2013].
- Taylor, A.M. et al., 2005. A microfluidic culture platform for CNS axonal injury , regeneration and transport. , 2(8), pp.599–605.
- Teddy, J.M. & Kulesa, P.M., 2004. In vivo evidence for short- and long-range cell communication in cranial neural crest cells. *Development (Cambridge, England)*, 131(24), pp.6141–51. Available at: <http://www.ncbi.nlm.nih.gov/pubmed/15548586> [Accessed September 3, 2013].
- Theveneau, E., and Mayor, R. (2012). Neural crest delamination and migration: from epithelium-to-mesenchyme transition to collective cell migration. *Developmental biology* 366, 34-54
- Tojkander, S. et al., 2011. A molecular pathway for myosin II recruitment to stress fibers. *Current biology : CB*, 21(7), pp.539–50. Available at: <http://www.ncbi.nlm.nih.gov/pubmed/21458264> [Accessed August 19, 2013].
- Turner, C.E., West, K. a & Brown, M.C., 2001. Paxillin-ARF GAP signaling and the cytoskeleton. *Current opinion in cell biology*, 13(5), pp.593–9. Available at: <http://www.ncbi.nlm.nih.gov/pubmed/11544028>.
- Vadlamudi, R.K. et al., 2002. Filamin is essential in actin cytoskeletal assembly mediated by p21-activated kinase 1. *Nature cell biology*, 4(9), pp.681–90. Available at: <http://www.ncbi.nlm.nih.gov/pubmed/12198493> [Accessed August 13, 2013].
- Vallénius, T., 2013. Actin stress fibre subtypes in.
- Vicente-Manzanares, M. et al., 2008. Segregation and activation of myosin IIB creates a rear in migrating cells. *The Journal of cell biology*, 183(3), pp.543–54. Available at: <http://www.pubmedcentral.nih.gov/articlerender.fcgi?artid=2575793&tool=pmcentrez&rendertype=abstract> [Accessed August 15, 2013].
- Wang, S. et al., 2012. Tiam1 interaction with the PAR complex promotes talin-mediated Rac1 activation during polarized cell migration. *The Journal of cell biology*, 199(2), pp.331–45. Available at: <http://www.pubmedcentral.nih.gov/articlerender.fcgi?artid=3471226&tool=pmcentrez&rendertype=abstract> [Accessed August 9, 2013].
- Wang, W. et al., 2002. Single Cell Behavior in Metastatic Primary Mammary Tumors Correlated with Gene Expression Patterns Revealed by Molecular Profiling Single Cell Behavior in Metastatic Primary Mammary Tumors Correlated with Gene Expression Patterns Revealed by Molecular Pro. , pp.6278–6288.

- Ward, C.W. et al., 2007. The insulin and EGF receptor structures: new insights into ligand-induced receptor activation. *Trends in biochemical sciences*, 32(3), pp.129–37. Available at: <http://www.ncbi.nlm.nih.gov/pubmed/17280834> [Accessed August 7, 2013].
- Watanabe, N. et al., 1999. Cooperation between mDia1 and ROCK in Rho-induced actin reorganization. *Nature cell biology*, 1(3), pp.136–43. Available at: <http://www.ncbi.nlm.nih.gov/pubmed/10559899>.
- Weaver, a M. et al., 2001. Cortactin promotes and stabilizes Arp2/3-induced actin filament network formation. *Current biology : CB*, 11(5), pp.370–4. Available at: <http://www.ncbi.nlm.nih.gov/pubmed/11267876>.
- Weber, M. et al., 2013. Interstitial dendritic cell guidance by haptotactic chemokine gradients. *Science (New York, N.Y.)*, 339(6117), pp.328–32. Available at: <http://www.ncbi.nlm.nih.gov/pubmed/23329049> [Accessed August 8, 2013].
- Zaidel-Bar, R. et al., 2007. Functional atlas of the integrin adhesome. *Nature cell biology*, 9(8), pp.858–67. Available at: <http://www.pubmedcentral.nih.gov/articlerender.fcgi?artid=2735470&tool=pmcentrez&rendertype=abstract>.
- Zhu, J. et al., 2007. Requirement of alpha and beta subunit transmembrane helix separation for integrin outside-in signaling. *Blood*, 110(7), pp.2475–83. Available at: <http://www.pubmedcentral.nih.gov/articlerender.fcgi?artid=1988953&tool=pmcentrez&rendertype=abstract> [Accessed August 8, 2013].
- Zimerman, B., Volberg, T. & Geiger, B., 2004. Early molecular events in the assembly of the focal adhesion-stress fiber complex during fibroblast spreading. *Cell motility and the cytoskeleton*, 58(3), pp.143–59. Available at: <http://www.ncbi.nlm.nih.gov/pubmed/15146534> [Accessed August 19, 2013].

7.Acknowledgements

I want to thank my supervisor Prof. Olivier Pertz very much giving me the opportunity to do my PhD thesis in his lab and for his great support. During the time in his lab I learned a lot from a scientific point of view, to think out of the box and I gained a lot of confidence concerning my work. I'm very grateful for that! Thank you a lot, Olivier!

I am very thankful to our collaborators Prof. Gaudenz Danuser and Marco Vilela from Harvard Medical School for their great work on the paper and their inspiring input. Gaudenz helped us a lot conceptually and put a lot of effort in editing the paper, while Marco was handling bioinformatics in an expertly and creative manner. Thank you so much Gaudenz and Marco!

Thanks also to our collaborator Prof. Noo Li Jeon from Seoul National University who introduced microfabrication techniques to us and supported us with custom made material.

As well I want to thank especially my colleague Rafael a lot for having very inspiring discussions and good collaborations. Also special thanks to Ludovico for interesting and motivating conversations.

The time Daniel and Michel were still in the lab, especially at the beginning of my PhD thesis we shared a lot of funny and constructive moments. Thanks for this time Michel and Daniel!

I also want to thank Andreas, who I was working with after he finished his masters as well as my other lab mates joining the group more recently.

Very special thanks to Erika. She was technician in our lab, taking care about everyone and everything around the lab. When I freshly entered the lab she was immediately welcoming me warmly and this made the start far easier. Erika, ganz herzlichen Dank für Alles!

I want to acknowledge Prof. Gerhard Christofori and Prof. Markus Affolter as members of my PhD thesis committee.

Vielen Dank an meine Eltern und meinen „kleinen“ Bruder Manuel. Danke, dass Ihr immer für mich da wart und mich Unterstützt habt!

Danke an meine Oma bei ihr habe ich als Kind viel Zeit verbracht und sie hat mir immer viel Aufmerksamkeit und Zuwendung gegeben.

Ganz besonderen Dank an meinen Mann Gregor Martin. Danke Gregor, dass du immer für mich da warst, auch in ganz besonders schwierigen Zeiten und nie an mir gezweifelt hast. Ohne dich hätte ich das alles nicht geschafft!

8. Curriculum Vitae

Katrin Martin

Unmarried surname: Benakovitsch
Date and place of Birth: 12.11.1981, in Vienna

Address: Bachlettenstrasse 29, CH-4054 Basel, Switzerland
E-mail: katrin.martin@unibas.ch
Phone: +41 (0) 76 30 90 783
Nationality: Austrian
Swiss driving licence B
Swiss living permit B (until 31.12.2013)

EDUCATION:

January 2009 - Expected: October 2013

Center of Biomedicine, Institute of Biochemistry and Genetics, University Basel,
PhD program in Cell Biology
Research Project: Growth Factor Induced Fibroblast Migration Requires a Front/Back Mechanical Insulation Module
Supervisor: Prof. Olivier Pertz

January 2007 - November 2008

Institute of Applied Microbiology, University of Natural Resources and Applied Life Sciences, Vienna
Research Project: PhD program in Microbiology discontinued
Improvement of Protein Secretion in *P. pastoris*
Supervisor: Prof. Diethard Mattanovich

June 2006 - January 2007

Institute of Applied Microbiology, University of Natural Resources and Applied Life Sciences, Vienna
Master thesis
Research Project: Development of a Screening System to Identify High Protein Secreting *P.pastoris* Strains Using Flow Cytometry
Supervisor: Prof. Diethard Mattanovich

October 2002 - January 2007

University of Natural Resources and Applied Life Sciences, Vienna
Graduated in Food Science and Biotechnology

October 2002 - January 2007

Institute of Applied Microbiology, University of Natural Resources and Applied Life Sciences, Vienna
Half time work as technician in a microbiological lab

October 2001 - October 2002

Institute of Applied Microbiology, University of Natural Resources and Applied Life Sciences, Vienna
Full time work as technician in a microbiological lab

September 1996 - June 2001

Secondary College for Chemocal Technology, Vienna
Specialization: Biochemistry and Biochemical Technology
Graduated with excellence

Working experiences:

October 2002 - January 2007

Half time work as technician in a microbiological lab
Institute of Applied Microbiology, University of Natural Resources and Applied Life Sciences, Vienna

October 2001 - October 2002

Full time work as technician in a microbiological lab
Institute of Applied Microbiology, University of Natural Resources and Applied Life Sciences, Vienna

July 2000

Internship as technician in a microbiological lab
Vöslauer Mineralwasser AG; 2540 Bad Vöslau, Paitzriegelgasse 2, Austria

July 1999

Internship as technician in a microbiological lab
Vöslauer Mineralwasser AG; 2540 Bad Vöslau, Paitzriegelgasse 2, Austria

July 1998

Internship as technician in an analytical lab; Messer Austria; 2352 Gumpoldskirchen, Industriestrasse 5

Languages:

German (native language), English (fluent)

IT Skills:

Excellent use of MS Word, MS Excel and MS Powerpoint, statistical software (Origin, Prism), Adobe Illustrator, Adobe Indesign, Analysis software (Metamorph)

Publications:

- **Martin K**, Vilela M, Jeon NL, Danuser G, Pertz O, GROWTH-FACTOR-INDUCED, PERSISTENT FIBROBLAST MIGRATION IS MEDIATED BY MECHANICAL INSULATION OF CELL FRONT AND BACK, 2013, [submitted to Dev Cell](#)
- Fritz RD, Letzelter M, Reimann A, **Martin K**, Fusco L, Ritsma L, Ponsioen B, Fluri E, Schulte-Merker S, van Rheenen J, Pertz O., A VERSATILE TOOLKIT TO PRODUCE SENSITIVE FRET BIOSENSORS TO VISUALIZE SIGNALING IN TIME AND SPACE, 2013, Sci Signal
- Feltrin D, Fusco L, Witte H, Moretti F, **Martin K**, Letzelter M, Fluri E, Scheiffele P, Pertz O, GROWTH CONE MKK7 MRNA TARGETING REGULATES MAP1B-DEPENDENT MICROTUBULE BUNDLING TO CONTROL NEURITE ELONGATION., 2012, PLoS Biol.
- Stadlmayr G, **Benakovitsch K**, Gasser B, Mattanovich D, Sauer M., GENOME-SCALE ANALYSIS OF LIBRARY SORTING (GALIBSO): ISOLATION OF SECRETION ENHANCING FACTORS FOR RECOMBINANT PROTEIN PRODUCTION IN PICHIA PASTORIS, 2010, Biotechnol Bioeng.

Awards:

2009 BioValley Poster Award for the poster entitled: NEW TOOLS FOR SYSTEMS BIOLOGY ANALYSIS OF SPATIO-TEMPORAL SIGNALING DURING POLARIZED CELL MIGRATION. Basel, Switzerland. 1500 CHF

Attendance at courses and conferences:

Cell Migration an Invasion in Physiology and Disease, The Invadosome Consortium, 13th - 17th October 2013, Radboud University Nijmegen Medical Centre, Nijmegen, The Netherlands, **oral presentation**.

The Future of Membrane Biology, EuroMEMBRANE, 28th October - 1st November 2012, San Siro, Lago di Como, Italy, **oral presentation**

Membrane Dynamics in Physiology and Disease, EuroMEMBRANE 5th - 8th June 2012, ZLF, University of Basel, Basel, Switzerland

International SystemsX.CH Conference on Systems Biology, 24th - 26th October 2011, Congress Center Basel, Basel, Switzerland, **poster presentation**

Gradient Sensing & Directed Cell Migration (This meeting is currently known as "Directed Cell Migration"), Gordon's Research Conferences, 5th - 10th June 2011, Les Diablerets Conference Center, Switzerland, **poster presentation**

Cytomeet, 22nd January 2010, University of Bern, Bern, Switzerland

BioValley Life Sciences Week, 21st - 23th September, 2010 Basel, Switzerland, **poster presentiaon**

Cytomeet, 26th January 2010, Bern, Switzerland

Biological Image Processing Summer School, Friedrich Miescher Institute for Biomedical research (FMI), Swiss Federal Institute of Technology Zurich (ETH), 29th August - 3rd September 2010, Maennedorf, Switzerland

FEBS Advanced Lecture Course: Cytoskeleton, Contractility and Motility, Pierre-Gilles de Gennes Winter School 2010, 22th - 27th February 2010, Institut d'Études Scientifiques de Cargèse, Corsica, France, **poster presentation**

BioValley Life Sciences Week, 13th - 16th October 2009 Basel, Switzerland, **poster presentation**

Cytomeet, 26th January 2009, University of Bern, Bern, Switzerland, **oral presentation**

Advanced Microscopy Course, Friedrich Miescher Institute for Biomedical research (FMI), Leica AG, 7th - 11th September 2009, Basel, Switzerland

Interests, Activities & other Information:

Since 10 years me and my husband travel every year to malaysia to improve our skills in the local martial art, called Pencak Silat. In the meanwhile, we found very good friends there, who almost became brothers and sisters to us. I love sports like climbing, horse riding, swimming or skiing. Apart from sports I enjoy any creative activity starting from drawing until grafting. My guinea pigs are very precious to me and I indulge interacting with them.